



**Design and Manufacturing Methods for Fused  
Deposition Modelling in Additive Manufacturing for  
the South African Railway Industry**

**Submitted By:**

**Ashley Dillon Toth (BScEng, UKZN) – 212502090**

**Supervisor:**

**Dr Jared Padayachee**

**July 2022**

Submitted in fulfilment of the degree of:

**Master of Science in Engineering (Mechanical Engineering);**

College of Agriculture, Engineering and Science; University of KwaZulu-Natal

# DECLARATION 1: SUBMISSION AND ORIGINALITY

## **Supervisor**

As the Candidate's Supervisor, I agree with the submission of this dissertation.

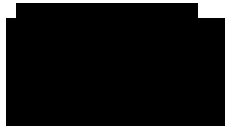
Signed: .....

Date: .....

Dr Jared Padayachee

## **Student**

I declare this dissertation has not previously been submitted for any degree in this or any other university, and it is the student's (MSc Eng Candidate Ashley Dillon Toth's) own original work.



Signed: .....

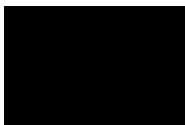
Date: 21-06-2022

Mr Ashley Dillon Toth

## DECLARATION 2: PLAGIARISM

I, Ashley Dillon Toth (212502090), declare that:

1. The research reported in this dissertation, except where otherwise indicated, is my original research.
2. This dissertation has not been submitted for any degree or examination at any other university.
3. This dissertation does not contain other persons' data, pictures, graphs or other information unless expressly acknowledged as being sourced from others.
4. This dissertation does not contain other persons' writing unless expressly acknowledged as being sourced from other researchers. Where other written sources have been quoted, then:
  - a. Their words have been re-written, but the general information attributed to them has been referenced
  - b. Where their exact words have been used, then their writing has been placed in italics and inside quotation marks and referenced.
5. This dissertation does not contain text, graphics or tables copied and pasted from the internet unless expressly acknowledged, and the source is detailed in the dissertation and the References section.



Signed: .....

Date: 21-06-2022

Mr Ashley Dillon Toth

## **DECLARATION 3: PUBLICATIONS**

Details of contribution to peer-reviewed publications that include research presented in this dissertation. The undersigned agrees that the following submissions were made and accepted as described and that the content therein is contained in this research.

### **Published: SAHHA 2021/2022 Conference**

A.D Toth, J. Padayachee and S. Vilakazi

“Digital Maintenance Centre for Additive Manufacturing and 3D Printing in the Railway Industry” in the conference of the "South African Heavy Haul Association of 2021", 254 - 261, ISBN: 978-0-620-97887-3.

The paper was published on 26 July 2021 in Johannesburg, South Africa.

Ashley Dillon Toth was the lead author for this paper and conducted all research and experimentation under the academic authors' supervision.

### **Submitted for Publication: IHHA 2021/2022/2023 Conference**

Under review

A.D Toth, J. Padayachee and S. Vilakazi

"Additive Manufacturing: Producing functional parts for the South African railway industry" in the conference of the "International Heavy Haul Association of 2021."

The paper was published on 26 October 2021 in Beijing, China. Due to Covid 19 regulations, international travel was suspended, and the conference in China was forwarded to be held in Brazil. The expected date for the presentation is August 2023.

Ashley Dillon Toth was the lead author for this paper and conducted all research and experimentation under the academic authors' supervision.

### **Published: Scientific African Journal 2022**

Toth AD, Padayachee J, Mahlatiji T, Vilakazi S

“A Report on Case Studies of Additive Manufacturing in the South African Railway Industry” in the Elsevier Journal Special Issue: Scientific African. <https://doi.org/10.1016/j.sciaf.2022.e01219>.

The paper was published on 28th May 2022.



Ashley Dillon Toth was the lead author for this paper and conducted all research and experimentation under the other two authors' supervision.

**Submitted for Publication: SAIMEchE R&D Journal 2022**

Under Review

A.D Toth and J. Padayachee

“Using topology optimisation to influence the infill placement of fused deposition modelled parts.” In South African Institute of Mechanical Engineers Research & Development Journal, 2022

The paper was submitted for review on 11 April 2022 in South Africa.

Ashley Dillon Toth was the lead author for this paper and conducted all research and experimentation under the other two authors' supervision.

**Published: Proceedings of the Institution of Mechanical Engineers, Part F: Journal of Rail and Rapid Transit**

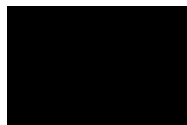
Published

A.D Toth, J. Padayachee, V. Matjeke, S. Vilakazi,

“Analytic Hierarchy Process Methodology for Part Selection for Fused Deposition Modelling in the South African Railway Industry.” In Part F: Journal of Rail and Rapid Transit, 2022

The paper was submitted for review on 28 May 2022.

Ashley Dillon Toth was the lead author for this paper and conducted all research and experimentation under the other two authors' supervision.



Signed: .....

Date: 21-06-2022

Mr Ashley Dillon Toth

# ACKNOWLEDGEMENTS

First and foremost, I would like to thank God for giving me the courage to pursue this research and the ability to complete it.

I want to thank my supervisor, Dr Jared Padayachee, for his supervision, guidance and mentorship during the entirety of this research. He went beyond what was expected of him, for which I am very grateful. His constructive feedback on my publications and dissertation structure allowed me to improve my academic contributions and structure the research more concisely and meaningfully.

I want to thank my fiancé Christine Evette Reddy for all the support, motivation and encouragement during my research study.

I want to acknowledge Transnet Freight Rail (TFR) for providing a platform to conduct research in an innovative field and be able to apply it for the benefit of the organisation within my assigned responsibilities. I would also like to thank Transnet Engineering (TE) and the materials and manufacturing department colleagues for providing laboratory facilities for this research.

I want to thank Mr Siboniso Vilakazi for providing a platform to expand the Additive Manufacturing field for the technical division at Transnet Freight Rail.

Lastly, I would like to thank my family for their support, encouragement, and assistance throughout the research trials and tribulations.

*Intentionally Left Blank*

# ABSTRACT

Additive Manufacturing, commonly known as 3D printing, is a transformative technology that has seen rapid adoption in well-established industrial environments due to its increasing reliability and associated economic value. Its adoption within the South African industry has been driven by the biotechnical/medical, aerospace and automotive industries, with limited adoption in the railway industry. The rolling stock and rail infrastructure consists of numerous systems and components that may benefit from the technology within the railway environment. This study explores utilizing additive manufacturing technology as an additional technique to create functional railway-related components. The study aims to develop tools, methods, and processes for designing and manufacturing functional end-use railway parts, ultimately allowing the industry to derive the economic benefits of additive manufacturing.

The study is limited to using the Fused Deposition Modelling technique and polymer materials. Firstly, the available physical and digital manufacturing workflow techniques are identified through literature with recommendations for best practices. Secondly, the research proposes a Multi-Criteria Decision-Making methodology based on the Analytic Hierarchy Process to identify potential railway-related parts that may benefit from the Fused Deposition Modelling additive manufacturing process. The methodology is validated through case studies found in literature. Thirdly, a novel method to optimise the infill design is presented for improving the strength of the 3D printed parts, thereby making the parts more suitable for the railway environment. The method is based on combining Finite Element Analysis and Bi-directional Structural Optimisation Topology Optimisation. Lastly, the study presents a custom-developed application built using Visual Basic and Excel. The application is built upon a generic design process to aid railway design engineers in effectively using the Fused Deposition Modelling technology to create functional 3D printed parts.

The research concludes with a case study of a roof scoop and air vent, which was identified, redesigned, optimised, and manufactured using Fused Deposition Modelling. The part was used as a replacement component on a railway inspection vehicle. Compared to the existing design, an 18,7 % reduction in shear stress was achieved for the 3D printed design.

**Keywords:** *Additive Manufacturing, Fused Deposition Modelling, Railway Infrastructure, Rolling Stock, Analytic Hierarchy Process, Bi-directional Evolutionary Structural Optimisation.*

# TABLE OF CONTENTS

DECLARATION 1: SUBMISSION AND ORIGINALITY .....	ii
DECLARATION 2: PLAGIARISM.....	iii
DECLARATION 3: PUBLICATIONS .....	iv
ACKNOWLEDGEMENTS .....	vi
ABSTRACT.....	viii
TABLE OF CONTENTS.....	ix
ABBREVIATIONS .....	xv
NOMENCLATURE .....	xvii
LIST OF FIGURES .....	xviii
LIST OF TABLES .....	xxii
CHAPTER 1: INTRODUCTION .....	1
Abstract.....	1
1.1    Introduction.....	1
1.2    Background and Motivation.....	2
1.3    Existing Research and Research Gap.....	3
1.4    Research Aims and Research Objective .....	4
1.5    Research Methodology .....	5
1.6    Dissertation Overview.....	6
1.7    Chapter Summary .....	6
CHAPTER 2: ADDITIVE MANUFACTURING LITERATURE.....	7
Abstract.....	7
2.1    Introduction to Additive Manufacturing .....	8
2.2    Physical Manufacturing Workflow .....	9
2.2.1    Mechanical Properties of Fused Deposition Modelling Printed Parts .....	9
2.3    Digital Manufacturing Workflow .....	11
2.3.1    Computer-Aided Design Technology .....	12
2.3.2    Finite Element Analysis .....	13
2.3.3    Tool-Path Generator (Slicing Software) .....	13

2.4	Multi-Criteria Decision Analysis .....	15
2.4.1	Multi-Criterial Decision Analysis in Additive Manufacturing a State-of-the-Art .....	15
2.4.2	Selection Criteria for AM Parts in the Railway Environment .....	19
2.5	Types of Structural Optimisation .....	20
2.5.1	Shape Optimisation .....	20
2.5.2	Size Optimisation .....	20
2.5.3	Topology Optimisation .....	20
2.6	Custom Infill Placement .....	21
2.3.4	Bi-directional Evolutionary Structural Optimisation (BESO) .....	22
2.3.5	Smoothing Technique for Post-Processing .....	25
2.7	Design for Additive Manufacturing .....	26
2.8	Chapter Summary .....	28
CHAPTER 3: PART SELECTION: DECISION MODEL FOR ADDITIVELY MANUFACTURING PARTS FOR THE RAILWAY ENVIRONMENT .....		29
Abstract .....		29
3.1	Introduction .....	30
3.2	The Analytic Hierarchy Process .....	30
3.2.1	First Principles .....	30
3.2.2	Application: Weights, Criteria and Decision Matrix .....	34
3.2.3	AHP Model Verification and Validation .....	34
3.2.4	Application: Part Identification .....	34
3.3	Functional End-Use 3D Printed Railway Parts Case Studies .....	35
3.3.1	Maintenance Tooling .....	36
3.3.2	Maintenance Measuring .....	38
3.3.3	Rolling Stock .....	39
3.3.4	Prototypes .....	40
3.4	Chapter Summary .....	41
CHAPTER 4: CUSTOM INFILL PLACEMENT USING TOPOLOGY OPTIMISATION AND FINITE ELEMENT ANALYSIS .....		43

Abstract.....	43
4.1 Introduction.....	44
4.2 Influencing the Infill Design Using BESO .....	44
4.2.1 Model Construction (Stage 1) .....	46
4.2.2 Mesh Generation (Stage 2) .....	46
4.2.3 Finite Element Analysis (Stage 3).....	48
4.2.4 Topology Optimisation using BESO (Stage 4).....	48
4.2.5 Post-Processing Topology Optimised Mesh (Stage 5).....	51
4.2.6 Infill Design (Stage 6).....	52
4.3 Mechanical Testing: Flexural Response .....	53
4.3.1 Test Specimen Preparation.....	53
4.3.2 Test Results .....	55
4.3.3 Discussion .....	60
4.4 Chapter Summary .....	63
CHAPTER 5: RAILWAY APPLICATION: DESIGN OF A FUNCTIONAL 3D PRINTABLE COMPONENT.....	64
Abstract.....	64
5.1 Background.....	65
5.1.1 Case Study: Roof Scoop and Air Vent.....	65
5.1.2 FDM Functional Part Workflow .....	66
5.1.3 MCDM AHP Model Evaluation .....	67
5.2 Digital Manufacturing Workflow .....	68
5.2.1 Reverse Engineering .....	68
5.2.2 Conceptual Designs.....	69
5.2.3 Design Selection .....	70
5.2.4 Railway Engineering Standards .....	72
5.2.5 Computational Fluid Dynamics Simulations .....	72
5.2.6 Finite Element Analysis .....	75
5.3 Physical Manufacturing Workflow .....	78

5.3.1	Material Selection .....	78
5.3.2	Process Parameters.....	79
5.3.3	Support Material Optimisation.....	79
5.3.4	Infill Material Optimisation .....	80
5.3.5	AM Printing Process .....	81
5.4	Installation.....	84
5.4.1	Visual Inspection.....	84
5.4.2	Print Accuracy.....	84
5.4.3	Final Assembly .....	85
5.5	Chapter Summary .....	86
CHAPTER 6: DISCUSSION.....		87
6.1	Introduction.....	87
6.2	Discussion .....	87
6.3	Design Contributions .....	90
6.4	Practicable Contributions.....	91
CHAPTER 7: CONCLUSIONS & RECOMMENDATIONS.....		92
7.1	Introduction.....	92
7.2	Achievement of Project Objectives.....	92
7.3	Research Question Conclusion .....	94
7.3.1	Research Study Conclusion .....	94
7.3.2	Application-Specific Conclusion .....	94
7.4	Recommendations and Future Work.....	95
REFERENCES .....		97
Appendix A: Fused Deposition Modelling .....		112
8.1	Fused Deposition Modelling in Additive Manufacturing .....	112
8.2	FDM 3D Printing Materials .....	113
8.2.1	FDM Material Properties .....	113
Appendix B: Additive Manufacturing in the Railway Industry.....		114
9.1	The South African Additive Manufacturing Strategy .....	114



9.2	Additive Manufacturing in International Railway Industries .....	114
9.3	AM Challenges for the South African Railway Environment .....	115
Appendix C: Part Selection.....		116
10.1	Application: Weights, Criteria and Decision Matrix .....	116
10.2	AHP Model Verification and Validation .....	119
10.2.1	Case Study 1: Sheet Metal Forming .....	119
10.2.2	Case Study 2: 3D Printed Moulds.....	119
10.2.3	Case Study 3: 3D Printed Metal Brake Pedal .....	119
10.2.4	Case Study 4: 3D Printed Racing Wheel and Automotive Control Arm .....	119
10.3	Functional End-Use 3D Printed Railway Parts.....	121
10.3.1	Maintenance Tooling .....	121
10.3.2	Maintenance Measuring.....	121
10.3.3	Rolling Stock .....	122
10.3.4	Prototypes & Light-Weighting.....	122
Appendix D: Custom Infill Placement.....		124
11.1	Material Properties.....	124
11.2	Custom Infill Placement.....	124
11.2.1	Model Construction (Stage 1) .....	124
11.2.2	Mesh Generation (Stage 2) .....	125
11.2.3	Finite Element Analysis (Stage 3).....	126
11.2.4	Topology Optimisation using BESO (Stage 4).....	128
11.2.5	Post-Processing Topology Optimised Mesh (Stage 5).....	129
11.2.6	Infill Design (Stage 6).....	129
11.3	3D Printed Test Specimens .....	130
11.3.1	Experimental Test Setup and Printing Parameters.....	132
11.3.2	First Test Comparison.....	132
11.3.3	Second Test Comparison .....	133
11.4	Print Accuracy .....	133
11.4.1	First Test Comparison.....	133

11.4.2	Second Test Comparison .....	134
11.5	Test Results.....	136
Appendix E: Custom Design Guide.....		139
Abstract.....		139
12.1	Introduction.....	140
12.2	Custom Design Guide .....	140
12.2.1	Clearance and Interference Guide .....	141
12.2.2	Layer Height and Print Orientation Guide .....	142
12.2.3	Wall Thickness Guide .....	143
12.2.4	Holes and Overhangs Guide .....	143
12.2.5	Infill Density Guide .....	145
12.3	Advanced Design for Fused Deposition Modelling.....	145
12.3.1	Self-Supporting Structures .....	145
12.3.2	Design of Interlocking Joints .....	148
12.3.3	Hardware Embedment: Fasteners .....	149
12.4	Railway Application .....	153
12.4.1	Case Study 1 – Weather Station Prototype .....	153
12.5	Chapter Summary .....	155
Appendix F: Application Tool.....		156
14.4	Introduction.....	156
14.5	Generic Design Process .....	156
14.5.1	Conceptual Design .....	158
14.5.2	Embodiment Design.....	158
14.5.3	Detailed Design.....	158

# ABBREVIATIONS

---

1D	One-Dimensional
2D	Two-Dimensional
3D	Three-Dimensional
ABS	Acrylonitrile Butadiene Styrene
AHP	Analytic Hierarchy Process
AM	Additive Manufacturing
AMPRSP	Additive Manufacturing Process and Resource Selection Problem
ANN	Artificial Neural Network
ANOVA	Analysis of Variance
ASA	Acrylic Styrene
ASCII	American Standard Code for Information Interchange
ASTM	American Standard for Testing Materials
BESO	Bi-directional Evolutionary Structural Optimisation
BSI	British Standard Institution
CAD	Computer-Aided Design
CAE	Computer Assisted Engineering
CSIR	Council for Scientific and Industrial Research
CFD	Computational Fluid Dynamics
CLT	Classical Laminate Theory
CVN	Charpy V-Notch
DB	Deutsche Bahn
DfMA	Design for Manufacturing and Assembly
DfAM	Design for Additive Manufacturing
DMA	Dynamic Mechanical Analysis
DOF	Degrees of Freedom
DST	Department of Science and Technology
DTI	Department of Trade and Industry
ESO	Evolutionary Structural Optimisation
ELECTRE	Elimination ET Choix Traduisant la Realité
FDM	Fused Deposition Modelling
FEA	Finite Element Analysis
FEM	Finite Element Method
GUI	Graphical User Interface
HIPS	High Impact Polystyrene

---

---

ISR	Increate in Strength Ratio
MADM	Multi-Attribute Decision-Making
MCDA	Multi-Criteria Decision-Analysis
MCDM	Multi-Criteria Decision-Making
MCES	Multi-Criteria Evaluation System
PC	Polycarbonate
PEEK	Polyaryletherkethone
PETG	Polyethylene Terephthalate
PLA	Polylactic Acid
PM	Pugh Matrix
PP	Polypropylene
PRASA	Passenger Rail Agency of South Africa
PROMOTHEE	Preference Ranking Organisation Method for Enrichment Evaluations
PVA	Polyvinyl Alcohol
RAPDASA	Rapid Product Development Association of South Africa
SAW	Simple Additive Weighting
SIMP	Solid Isotropic Material and Penalisation
SMR	Strength to Mass Ratio
SMART	Simple Multi-Attribute Rating Technique
STL	Standard Tessellation Language
SU	Stellenbosch University
TFR	Transnet Freight Rail
TLIU	Technology Localisation Implementation Unit
TOPSIS	Technique for Order of Preference by Similarity to Ideal Solution
TPU	Polyurethane
TRIZ	Theory of Inventive Problem Solving
TSCA	Two-Step Cluster Analysis
UTS	Ultimate Tensile Strength
UV	Ultraviolet
.VTK	Visualisation Tool Kit

---

# NOMENCLATURE

---

$C$	Product Weight/ Criteria Weight
$CI$	Consistency Measurement
$m$	Number of Criteria
$PM$	Pairwise Comparison Matrix/ Normalised Matrix
$R$	Total Criteria Weight
$RI$	Random Index
$j$	Rating Scale
$f$	Applied Load
$u$	Displacement Vector
$C$	Mean Compliance
$V_i$	Individual Element Volume
$V^*$	Total Structural Volume
$N$	Total Number of Elements
$x_i$	Design Variable
$u_i$	Nodal Displacement of $i^{th}$ element
$k_i$	Element Stiffness Matrix
$M$	Total Number of Elements Connected to the $j$ th Node
$w_i$	Weight Factor of $i$ th Element
$r_{ij}$	Distance Between the Centre of the $i$ th Element and the $j$ th Node
$\Omega_i$	Sub-domain
$r_{min}$	Radius of Sub-domain
$K$	Total Number of Nodes in Sub-domain
$w(r_{ij})$	Linear Weight Factor
$ER$	Evolutionary Ratio
$V^k$	Current Structural Volume
$V^{k+1}$	Next Volume Iteration
$\alpha_{th}$	Threshold
$[k]$	Stiffness Matrix
$\{f\}$	Nodal Force of a Single Element
$\{d\}$	Nodal Displacement
$[K]$	Global Stiffness Matrix
$\{F\}$	Global Force Vector

# LIST OF FIGURES

Figure 1 - 1 3D Printed Parts Produced by Application by 1504 Engineering Businesses [4] .....	1
Figure 2 - 1 Additive Manufacturing Technologies [24] .....	8
Figure 2 - 2 Impact of Process Parameters on Part Characteristics [28] .....	10
Figure 2 - 3 Several Railway-Related CAD Models.....	12
Figure 2 - 4 Example of Railway-Related Replacement Parts Sliced and Prepared for 3D Printing Using Cura.....	14
Figure 2 - 5 3D Printed Letters Test with Corresponding G-code from Different Slicers [57] .....	14
Figure 3 - 1 Decision Hierarchy for Evaluating Part Candidates for Additive Manufacturing .....	30
Figure 3 - 2 Process Flow Diagram to Identify Potential AM Parts .....	35
Figure 3 - 3 3D Printed Replacement Parts for the Lubricator Equipment [10] .....	36
Figure 3 - 4 3D Printed Grease Place Brackets and Custom 3D Printed Gauges [3], [10] .....	37
Figure 3 - 5 Custom 3D Printed Wheel Lateral Displacement Measuring Device for Calibrating Wayside Lubricators [10] .....	38
Figure 3 - 6 3D Printed Mounting Brackets and Injection Moulded Plastic Cover [10] .....	40
Figure 3 - 7 3D Printable Low-Cost Weather Station for Track-Specific Measurements [10].....	41
Figure 4 - 1 Custom Infill Placement Workflow .....	45
Figure 4 - 2 Stages used to achieve a Custom Infill Placement .....	45
Figure 4 - 3 Digital Models of the Grease Plate Bracket .....	46
Figure 4 - 4 Combination of 2D and 3D Mesh Algorithms on Grease Plate Bracket.....	47
Figure 4 - 5 Finite Element Analysis Results for the Grease Plate Bracket.....	48
Figure 4 - 6 BESO Mesh Results for the Grease Plate Bracket .....	50
Figure 4 - 7 Flow Diagram Representing the Steps to Convert the FEM Mesh into a 3D Model .....	51
Figure 4 - 8 Post-Processing the BESO Optimised Mesh of the Grease Plate Bracket .....	51
Figure 4 - 9 Infill Design Flow Steps.....	52
Figure 4 - 10 Graphical Representation of Infill Design.....	52
Figure 4 - 11 Sketch of the Intended Flexural Test Specimen with Dimensions in mm [142].....	53
Figure 4 - 12 Illustration of the Test Cases .....	54
Figure 4 - 13 Solid Infill on BESO Optimised Rectangular Test Specimens .....	55

Figure 4 - 14 Multi-Infill Geometry Design on BESO Optimised Rectangular Test Specimens .....	55
Figure 4 - 15 Bottom Surface Defect on Test Specimens .....	56
Figure 4 - 16 Universal Tensile Testing Machine Used in this Investigative Study .....	56
Figure 4 - 17 Test Specimens Fractured using the Three-Point Bending Tests .....	57
Figure 4 - 18 Failed Test Specimens During the Bending Test Campaign.....	57
Figure 4 - 19 Flexural Stress-Strain Curves for Solid Infill Specimens Testing Using the Three-Point Bending .....	58
Figure 4 - 20 Flexural Stress-Strain Curves for Multi-Infill Geometry Test Specimens Using the Three-Point Bending.....	58
Figure 4 - 21 Flexural Stress-Strain Curves for Solid Infill Specimens Testing Using the Three-Point Offset Bending .....	59
Figure 4 - 22 Flexural Stress-Strain Curves for Multi-Infill Geometry Test Specimens Using the Three-Point Offset Bending.....	59
Figure 4 - 23 Relative Performance Improvement of the Multi-Infill Geometry Specimens in Three-Point Bending.....	62
Figure 4 - 24 Relative Performance Improvement of the Multi-Infill Geometry Specimens in Three-Point Offset Bending.....	62
Figure 5 - 1 Railway Inspection Vehicle .....	65
Figure 5 - 2 Failed Roof Scoop and Air Vent .....	65
Figure 5 - 3 Workflow to Select, Redesign, Optimise and Manufacture of Functional 3D Printable Roof Scoop and Air Vent.....	66
Figure 5 - 4 Original Roof Scoop and Air Vent Dimensions.....	68
Figure 5 - 5 Reverse Engineered Original Roof Scoop and Air Vent.....	68
Figure 5 - 6 Concept 1 Isometric View (A), Front View (B), Right View (C), Cross-Section View (D), Top View (E) .....	69
Figure 5 - 7 Concept 2 Isometric View (A), Front View (B), Right View (C), Cross-Section View (D), Exploded View (E) .....	69
Figure 5 - 8 Concept 3 Isometric View (A), Front View (B), Right View (C), Cross-Section View (D), Exploded View (E) .....	70
Figure 5 - 9 Selected Design Isometric View (A), Front View (B), Right View (C), Cross-Section View (D), Exploded View (E) [143] .....	71
Figure 5 - 10 CFD Mesh Generation for the Inspection Trolley.....	73
Figure 5 - 11 Wind Flow Experienced at the Roof Scoop Region for the Original Design [143] .....	74

Figure 5 - 12 Wind Flow Experienced at the Roof Scoop Region for the New Design [143].....	74
Figure 5 - 13 Wind Flow Inside the Roof Scoop Air Vent Isometric View (A), Front View (B), Rear Isometric View (C), Sectioned Left View (D).....	75
Figure 5 - 14 Loading Applied to Surface Regions .....	76
Figure 5 - 15 Structural Simulation Boundary Conditions .....	76
Figure 5 - 16 Expected Von Mises Stress on the Roof Scoop (A), the Air Vent (B) and the Rivets (C) .....	77
Figure 5 - 17 Expected Displacement on the Roof Scoop (A), the Air Vent (B) and the Rivets (C) ...	77
Figure 5 - 18 Expected Principal Stress on the Roof Scoop (A) and the Air Vent (B).....	78
Figure 5 - 19 Print Orientation and Support Material for Air Vent .....	79
Figure 5 - 20 Print Orientation and Support Material for Roof Scoop .....	80
Figure 5 - 21 Custom Infill Placement (A) for Improved Strength on the Air Vent in Slicer Software at layer 10 (B) .....	80
Figure 5 - 22 Custom Infill Placement (A) for Improved Strength on the Roof Scoop in Slicer Software at layer 10 (B) .....	81
Figure 5 - 23 3D Printed Custom Infill on the Air Vent at layer 5 of the 3D Print .....	81
Figure 5 - 24 Process illustrates the Stages used to Realise a Final 3D Printed Functional Part .....	83
Figure 5 - 25 Side View of the 3D Printed Roof Scoop with the Stair-Stepping Artifact [143].....	84
Figure 5 - 26 Reference Measuring Points for the Digital and 3D Printed Parts .....	84
Figure 5 - 27 The Functional 3D Printed Roof Scoop Air Vent Installed [143].....	85
Figure A - 1 Schematic of a Fused Deposition Modelling 3D Printer (A) and the Creality CR10 S Pro 3D Printer (B) [13], [150] .....	112
Figure A - 2 illustrates the material types and their respective categories [153].....	113
Figure E - 1 Digital Design of the Design Cube .....	141
Figure E - 2 Digital Model and 3D Printed Square Tolerance Guide on the Design Cube .....	141
Figure E - 3 Digital Model and 3D Printed Circular Hole Tolerance Guide on the Design Cube.....	142
Figure E - 4 Digital Model and 3D printed Layer Height and Print Orientation Visual Guide on the Design Guide .....	142
Figure E - 5 Digital Model and 3D Printed Wall Thickness.....	143
Figure E - 6 3D Printed Versions for Supported Walls (A), Supported Walls with Chamfers (B), Unsupported Walls (C) and Unsupported Walls with Chamfers (D).....	143
Figure E - 7 Digital Model and 3D printed Hole Diameters and Printing Angles .....	144



Figure E - 8 3D Printed Versions of Self-Supporting Angles (A-C) and Embossed and Engraved Detail (D) and an Example Using the Emboss and Engrave Details (E) Designed into the Models.....	144
Figure E - 9 Digital Model and 3D printed Infill Density.....	145
Figure E - 10 Digital Design of a Stepper Motor Housing Using Sacrificial Bridging .....	146
Figure E - 11 Digital Design of Custom Support Tabs on Motor Housing .....	146
Figure E - 12 Digital Design of a Tear-Drop and Square through Holes .....	147
Figure E - 13 3D Printed Case using the Dovetail Joint (A-C) and 3D Printed Snap-Fit Joints (D-F) [177].....	148
Figure E - 14 3D Printed Fastener Insert Types.....	149
Figure E - 15 Digital Cross-Section and 3D Printed Slot Insert (A-C), Digital Cross-Section and 3D Printed Press-Fit Nut Insert (D-E), Digital Cross-Section and 3D Printed Embedded Nut Inserts (F-G), and Digital Cross-Section and 3D Printed Threaded Insert .....	150
Figure E - 16 Self-Threading and Self-Forming Screws .....	151
Figure E - 17 3D Printed Parts that Integrate with Bearings, Rubber Seals, Magnets, Shoulder Screws and Eyelets.....	152
Figure E - 18 Pe-Generated Support Material (A) Custom Designed in Supports (B) and the Final 3D Printed Version .....	153
Figure E - 19 Advanced Design Techniques Used to Embed, Fix and Mount Hardware Components to Assemble the Components of the 3D Printed Weather Station [10], [176] .....	154
 Figure F - 1 Fishbone Diagram of the Application Tools Structured to the Generic Design Process	157
Figure F - 2 The Main Interface Program Menu for the Application Tool.....	158
Figure F - 3 Conceptual Design Interface Windows (A-B), Embodiment Design Interface Windows (C-F), Detailed Design Interface Window (G) and Past Railway Projects Interface (H) .....	159

## LIST OF TABLES

Table 2 - 1 The Main Process Parameters for FDM 3D Printing and Their Definitions [28].....	9
Table 2 - 2 The Main Process Parameters for FDM 3D Printing and Their Definitions Continued [28] .....	10
Table 2 - 3 Process Parameter Settings for Optimum Flexural Strength [28], [46], [47], [48], [49], [50] .....	11
Table 2 - 4 Part Selection Criteria for the Railway Environment .....	19
Table 2 - 5 Part Selection Criteria for the Railway Environment Continued .....	20
Table 3 - 1 Decision Hierarchy Levels with Identified Criteria.....	31
Table 3 - 2 Pairwise Comparison Scale [131].....	31
Table 3 - 3 Random Indices [132] .....	33
Table 3 - 4 Consistency Ratio .....	34
Table 3 - 5 Total Weight and Overall Priority for the Case Study.....	37
Table 3 - 6 Total Weight and Overall Priority for the Case Study.....	38
Table 3 - 7 Total Weight and Overall Priority for the Case Study.....	39
Table 3 - 8 Total Weight and Overall Priority for the Case Study.....	40
Table 4 - 1 Gmsh Mesh Element Shapes [136].....	47
Table 4 - 2 Gmsh 2D Mesh Algorithms [136] .....	47
Table 4 - 3 Gmsh 3D Mesh Algorithms [136] .....	47
Table 4 - 4 Boundary Conditions for Grease Plate Bracket Simulation .....	48
Table 4 - 5 BESO Graphical User Interface Options and Definitions [139].....	49
Table 5 - 1 Qualitative Evaluation of Part Candidate Case Studies.....	67
Table 5 - 2 Quantitative Evaluation of Part Candidate Case Studies.....	67
Table 5 - 3 Total Weight and Overall Priority for the Case Study.....	67
Table 5 - 4 Features of the Original Roof Scoop and Air Vent .....	68
Table 5 - 5 Strengths and Weaknesses Associated with the Conceptual Designs .....	70
Table 5 - 6 Design Criteria used in the Pugh Matrix [143].....	70
Table 5 - 7 Pugh Decision Matrix for the Conceptual Designs .....	71
Table 5 - 8 Railway Standards Used in Study [143].....	72
Table 5 - 9 CFD Simulation Details [143] .....	73

Table 5 - 10 Final Summarised CFD Results for the Roof Scoop and Air Vent .....	74
Table 5 - 11 Summarised Results for the Internal Roof Scoop and Air Vent.....	75
Table 5 - 12 Structural Surface Region Loading Forces.....	76
Table 5 - 13 Structural Simulation Details.....	76
Table 5 - 14 Final Summarised Results for Roof Scoop.....	77
Table 5 - 15 Material Properties for PETG [146], [143].....	78
Table 5 - 16 Selected Optimal Process Parameters.....	79
Table 5 - 17 The Generic Stages of the Additive Manufacturing Process .....	82
Table 5 - 18 Print Time and Material Mass of the Roof Scoop and Air Vent [143].....	82
Table 5 - 19 Dimensional Accuracy between Digital Model and 3D Print [143].....	85
Table B - 1 AM Challenges for the South African Railway Industry [10] .....	115
Table C - 1 Pairwise Comparison Matrix .....	116
Table C - 2 Normalized Matrix.....	116
Table C - 3 Criteria Weights and Consistency Measures .....	117
Table C - 4 Decision Matrix for Selection Potential Railway Parts for AM .....	118
Table C - 5 Qualitative Evaluation of Part Candidate Case Studies .....	120
Table C - 6 Quantitative Evaluation of Part Candidate Case Studies .....	120
Table C - 7 Total Weight and Overall Priority for the Case Study [128] .....	120
Table C - 8 Qualitative Evaluation of Part Candidate Case Studies .....	121
Table C - 9 Quantitative Evaluation of Part Candidate Case Studies .....	121
Table C - 10 Qualitative Evaluation of Part Candidate Case Studies .....	121
Table C - 11 Quantitative Evaluation of Part Candidate Case Studies .....	122
Table C - 12 Qualitative Evaluation of Part Candidate Case Studies .....	122
Table C - 13 Quantitative Evaluation of Part Candidate Case Studies .....	122
Table C - 14 Qualitative Evaluation of Part Candidate Case Studies .....	122
Table C - 15 Quantitative Evaluation of Part Candidate Case Studies .....	123
Table D - 1 Polymer Filament Properties Used in the Study [146] .....	124
Table D - 2 Finite Element Mesh Settings for the Rectangular Test Specimens [134] .....	125
Table D - 3 Boundary Conditions for Simulation.....	126
Table D - 4 FEA results for the different test cases [134] .....	126
Table D - 5 BESO Properties for the Rectangular Test Specimens.....	128

Table D - 6 3D Printed Test Specimen Details for the First Test Comparison [134] .....	130
Table D - 7 3D Printed Test Specimen Details for the Second Test Comparison [134].....	130
Table D - 8 Printer Parameters Used to 3D Print the Test Specimens for First Test Comparison .....	132
Table D - 9 Printer Parameters Used to 3D Print the Test Specimens for Second Comparison.....	133
Table D - 10 Dimensional Accuracy between Digital Model and 3D Print First Test Comparison...	134
Table D - 11 Dimensional Accuracy between Digital Model and 3D Print First Case of Second Test Comparison .....	134
Table D - 12 Dimensional Accuracy between Digital Model and 3D Print Second Case Cubic Infill of Second Test Comparison .....	135
Table D - 13 Dimensional Accuracy between Digital Model and 3D Print Second Case Gyroid Infill of Second Test Comparison .....	135
Table D - 14 Dimensional Accuracy between Digital Model and 3D Print Second Case Octet Infill of Second Test Comparison .....	135
Table D - 15 Dimensional Accuracy between Digital Model and 3D Print Second Case Lines Infill of Second Test Comparison .....	136
Table D - 16 Relative Performance Improvement Over Rectilinear Infill Geometry Using Three-Point Bending Test .....	136
Table D - 17 Summary of Test Results for Three-Point Bending Testing Campaign [134].....	136
Table D - 18 Summary of Test Results for Three-Point Offset Bending Testing Campaign [134]....	137
Table D - 19 Relative Performance Improvement Over Rectilinear Infill Geometry Using Three-Point Offset Bending Test .....	137
Table D - 20 Simulation Results of the 3D Printed Test Specimen for Three-Point Bending.....	137
Table E - 1 Recommended Single Layer Thickness for PETG Material .....	146
Table E - 2 Recommended Single Tab Wall Thickness for PETG Material .....	147
Table E - 3 Recommended Tear-Drop Height for PETG Models with a 0.4 mm Nozzle .....	147
Table E - 4 Recommended Clearance Values for Several Components Using PETG.....	152

# CHAPTER 1: INTRODUCTION

## Abstract

This chapter describes the motivation behind this MSc project and gives an overview of how the research is conducted and documented. The explanations for this study can be found in the background and research gap section, whereas the remaining sections describe the research approach and the study's contribution.

## 1.1 Introduction

Application, utilisation, and development of transformative technology in well-established industrial environments are gaining adoption due to modernisation. The acceptance of new technology by the industrial sector depends on the new technology's certainty, reliability, and economic value. In most cases, a significant gap exists between transformative technology for industrial applications and the technology's research stages. Innovative advances may never achieve their expected potential due to a lack of knowledge, skill, market access and understanding of the economic advantage these technologies will provide to the industrial and commercial markets [1]. Additive Manufacturing is one of these transformative technologies and is defined as the process of joining materials in a bottom-up approach layer-by-layer to make parts directly from digital 3D model data [2]. However, this process relies heavily on digital and physical workflows for the prints to succeed in their expected applications [3]. In recent years, Additive Manufacturing technologies have rapidly evolved within various mainstream manufacturing sectors, including biotechnical/medical, aerospace, automotive and consumer products [1]. This evolution and rapid adoption within these manufacturing sectors are due to the increasing number of companies utilising this technique for commercial end-use part production using newer cost-efficient production machines. This is supported by the additive manufacturing trend report produced by Hubs [4], illustrated in Figure 1 - 1, which looked at the international trends and uses for AM based on responses from 1504 engineering businesses.

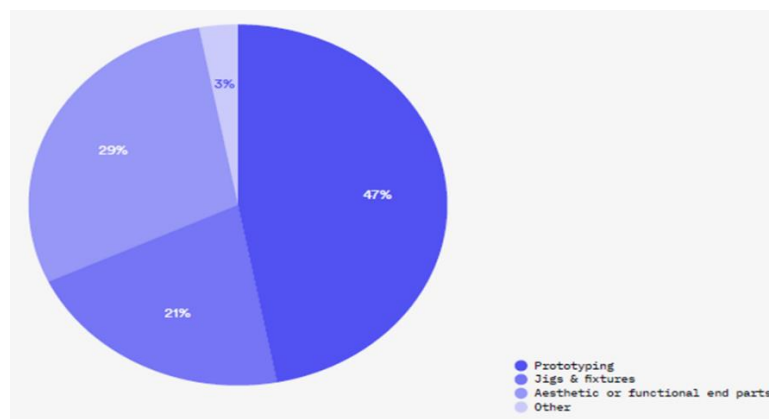


Figure 1 - 1 3D Printed Parts Produced by Application by 1504 Engineering Businesses [4]

## 1.2 Background and Motivation

Functional components, parts, assemblies, structures, and prototype systems used in industry undergo various manufacturing processes. Manufacturing advances in recent years in all technology domains have enabled these functional systems to be fabricated from design perspectives through to being production-ready and recycled when the product reaches its end of life. These significant developments are made by utilising advanced digital tools, including computer-aided design systems, non-destructive testing in the form of finite element analysis (FEA), and testing iterative designs for a subsystem or part. These processes form conventional designing practices for manufacturing and assembly (DfMA) [5]. “Advanced technology and digital tools play a significant role in producing functional grade 3D printed parts [6]. Because of this, AM technologies have seen rapid adoption in various industries. This growth in adoption results from the increased freedom afforded to the external model's design and the internal structure of 3D printable parts. It presents more significant opportunities in optimising a part's mechanical properties to enhance its performance specific to its application [7]. The benefits of additive manufacturing are an attractive addition to the South African railway industry compared to traditional manufacturing methods [8]; however, a knowledge gap exists in integrating this technology into the railway industry to assist rail design engineers and operators [9]. The design knowledge and methodologies are substantially different when Designing for Additive Manufacturing (DfAM), which relies on the digital processes to create various functional parts compared to the conventional DfMA approach [5].” [10]

The AM process involves creating substantial parts in a bottom-up process. Material is additively applied one layer at a time until the final part is built. This process relies extensively on digital and physical workflows for the prints to succeed [6]. The digital process utilises computer-aided-design technology, computer simulations, and machine code and tools to produce specifically designed models capable of being 3D printed. The physical workflow utilises AM technology and relies on the materials, the printer capabilities, and post-processing techniques to create suitable components [3]. Optimally merging these two processes results in 3D printed parts suitable for real-world applications. In the railway industry, specific design approaches must be identified to utilise additive manufacturing techniques. Conventional design methods must be changed and adapted for the additive manufacturing process [11]. Once the design approach is adopted and an understanding of the printing process is developed, railway-related components will benefit from the AM process [3]. The South African Department of Science and Technology (DST) commissioned a South African Additive Manufacturing Technology roadmap in 2016. The roadmap intends to guide the South African private and public sectors in adopting additive manufacturing through identified gaps and opportunities between 2016 – 2023 [12]. However, the roadmap primarily targets high-value components in the military, biotechnical/medical, automotive, and aerospace industries with little to no focus on the railway environment. With limited research in additive manufacturing within the locomotive industry and rail

infrastructure, it is essential to fill this research need and expand the South African Department of Science and Technology's AM roadmap to the South African railway industry. Therefore, it is essential to understand the technical limitations and design methods needed for creating functional railway parts using AM. This will form the basis for developing future complex 3D printable railway-related parts.

### **1.3 Existing Research and Research Gap**

Additive Manufacturing (AM) offers several advantages to the railway environment. As AM becomes more mainstream within the railway industry, it is essential to have a structured method to select railway-related parts that will benefit from the technology at the conceptual design stage. The current approach to determining suitable part candidates for railway-related applications is based on prototyping and testing, which is not an efficient method for selecting parts [13]. “Feasibility studies have shown that 3D printing technologies can be used within the railway environment to help reduce manufacturing costs and lead time for spare part fabrication for legacy designed systems, lightweight structures through assembly-part consolidation, topology optimisation and material change. In addition, by utilising the full benefits of additive manufacturing, newly designed tooling such as measuring gauges, embedded electronics, and IoT systems for customised complex track measuring devices and new, improved designs for jigs and fixtures and functional end-use parts further reduce repair lead times and improves railway track measuring capabilities [3], [8], [13], [14], [15]. In order to incorporate these technologies within the industry and produce functional systems, the design methodology for 3D printed parts must be determined for their respective application following strict railway standards.” [10] To truly capitalise on AM processes, a streamlined technical and logical process must be in place to determine the potential benefits of selecting appropriate railway-related parts and components for AM applications before the prototyping and testing stages are initiated. Once a streamlined technical process is developed, it can be applied by railway engineers in selecting and identifying appropriate railway-related parts to capitalise on the AM process fully.

Achieving the optimised mechanical performance of as-printed parts is to dynamically change the infill density and pattern based on applied loading conditions for the FDM process. Given the limitations of extruding material layer-upon-layer, internal structures (infill) of 3D printed parts are built based on two-dimensional repeating patterns. In contrast, the repeating patterns' density is scaled linearly regardless of the loading conditions [7]. Topology optimisation techniques could change the infill pattern dynamically, density and redistribute the internal structure within the parts boundary regions experiencing increased stress based on FEA results. This will result in reducing the overall weight and strengthen the load-affected regions [16].

In the Additive Manufacturing sector, topology optimisation techniques and algorithms are standard methods manufacturers use to improve strength-to-weight performance and reduce costs of additively manufactured parts typically manufactured using powder-based technologies [17], [18], [19]. In

comparison, the use of topology optimisation techniques for the FDM technology for internal (infill) and external structures remains relatively immature and not fully adopted [7], [14], [16], [20], [21]. This is more evident in generating the internal structures (infill) of a 3D printable part using the FDM technology. Commercial and open-source slicing software packages use traditional infill geometries and infill density scaling to create infill within the part without applying custom infill structures influenced by the parts stress profiles for the FDM technology. The three most applied topology optimisation techniques include Solid Isotropic Material and Penalisation (SIMP), Evolutionary Structural Optimisation (ESO) and Bi-directional ESO (BESO) [16]. Researchers have attempted various methods of trying to change the infill pattern dynamically, and density based on FEA stress results using topology optimisation techniques for the FDM process, such as [7], [14], and [20]. However, these methods have resulted in case-specific custom-developed software to integrate stress profiles with topology optimisation techniques for desktop studies instead of repeatable manufacturing methods. Given the extensive literature on topology optimisation and the ability to manipulate FDM parts' internal structure, translating the optimised geometry into a manufacturable component remains challenging [7]. Bracket et al. [22] presented an overview of two critical issues regarding topology optimisation. These included the resolution achieved using topology optimisation and the modifications required between the topology and manufacturing stages. The method to generate topology-optimised structures uses ideal numerical algorithms to automatically determine optimal external contour shapes without considering the manufacturing process [23]. In most commercial software, the optimised structure requires further refinements to the surfaces and regions to be manufacturable for the specific AM technology [23]. By utilising this technique of optimising FDM 3D printed parts' internal structure, benefits of strength-to-weight performance, improved mechanical performance, improved predictability of failure modes, and the ability of multi-material printing could see further developments in FDM printed parts.

## **1.4 Research Aims and Research Objective**

The research aims to develop methodologies and tools to identify and select potential railway part candidates that will benefit from the Fused Deposition Modelling process and to assist rail design engineers in applying design techniques to manufacture functional, additively manufacturable products suitable for the railway environment. The current approach to identifying, selecting, and manufacturing railway-related parts using AM technology is through trial-and-error. The research scope is limited to designing and manufacturing techniques for the material extrusion AM technology, Fused Deposition Modelling, and polymer materials to develop functional end-use parts. Thus, the main research question is formulated as follows:

*What design tools and techniques are needed by the rail industry to support the development of functional Fused Deposition Modelled 3D printed parts?*



To answer the main research question, the following Project Objectives (PO) need to be achieved to guide the research study:

1. To develop a decision-making model to identify and evaluate potential railway-related parts that will benefit from the Fused Deposition Modelling process at the conceptual design stage.
2. To develop a method to optimise the internal (infill) structure of additively manufactured Fused Deposition Modelled parts by allocating material at specific locations based on the parts' stress profile for a given application.
3. To analyse the mechanical performance through experimental testing between traditional infill structures and the custom-developed infill placement method for a specific material and process parameters identified through literature.
4. To develop a custom design guide to assist novice rail design engineers in applying the design features and advanced techniques available to the Fused Deposition Modelling process to functional 3D printable components to ensure manufacturing repeatability.
5. To apply the design techniques, tools, and methodologies to produce a functional 3D printable roof scoop and air vent rolling stock replacement part.

## **1.5 Research Methodology**

A systematic methodology is adopted to achieve the research aim. The Research Methodology (RM) contains the following steps:

1. Identify and evaluate the state-of-the-art multi-criteria decision-making processes in literature with a specific criterion for railway requirements and the Fused Deposition Modelling process.
2. Evaluate and validate the proposed decision-making process using qualitative and quantitative data from published case studies on Fused Deposition Modelling found in literature and apply the model to past railway-related case studies.
3. Identify the state-of-the-art structural optimisation techniques and software in literature to achieve an optimised internal (infill) structure based on part stress.
4. Carry out experimental testing to compare the mechanical performance of 3D printed test specimens using traditional infill structures and the proposed internal (infill) optimised technique.
5. Apply the design techniques to identify, select, redesign, optimise, and manufacture a functional 3D printable replacement part using the Fused Deposition Modelling process.

## 1.6 Dissertation Overview

The study is divided into chapters based on the project objectives, research question, and methodology. An overview of the chapters in this dissertation is as follows:

**Chapter 2** – A literature review on the physical and digital manufacturing workflow, state-of-the-art multi-criteria decision-making tools, structural optimisation techniques and design for additive manufacturing methods is performed.

**Chapter 3** – A Multi-Criteria Decision-Making methodology is proposed using the Analytic Hierarchy Process. The method is validated using qualitative and quantitative data from published case studies on Fused Deposition Modelling. The validated model is then applied to past railway case studies.

**Chapter 4** – A method to optimise and improve the internal (infill) structures of FDM 3D printable components using the Bi-directional Evolutionary Structural Optimisation (BESO) technique and Finite Element Analysis is proposed. Experimental testing is performed on 3D printed test specimens to determine their mechanical characteristics of flexural responses. The experimental results are reviewed and evaluated.

**Chapter 5** – A case study is presented of an additively manufactured functional roof scoop and air vent for a railway inspection vehicle using the fused deposition modelling technology and the techniques presented in this dissertation.

**Chapter 6** - Presents an overall discussion of the various dissertation chapters.

**Chapter 7** – The dissertation conclusion and recommendations are presented.

## 1.7 Chapter Summary

This chapter introduces the existing literature and motivation for performing the MSc project. Firstly, the research gaps for structured decision-making, design tools and structural optimisation of FDM 3D printable parts for the South African railway environment are presented. Secondly, the aims and objectives of the study are highlighted with a brief discussion on the methodology used to answer the proposed research question. Lastly, a summary overview of the chapters that make up the dissertation are presented.

# CHAPTER 2:

## ADDITIVE MANUFACTURING

### LITERATURE <sup>1,2</sup>

#### Abstract

This chapter presents a literature review on the physical and digital manufacturing workflow associated with the Fused Deposition Modelling process. Secondly, the state-of-the-art in Multi-Criteria Decision-Making methodologies for the Fused Deposition Modelling process are reviewed with identified selection criteria for the railway environment. Lastly, the state-of-the-art structural optimisation techniques, software, and custom infill optimisation methods focused on the Fused Deposition Modelling Process are reviewed. Finally, a review of the design for Additive Manufacturing methods is performed.

---

<sup>1</sup>Elements of this chapter are based on [3]: Toth AD, Padayachee J and Vilakazi S, 2021, Digital Maintenance Centre for Additive Manufacturing and 3D Printing in the Railway Industry, South African International Heavy Haul Association, Johannesburg, 254 – 261, ISBN: 978-0-620-97887-3 and in [10]: <sup>2</sup>Toth AD, Padayachee J, Mahlatiji T, Vilakazi S, 2021, A Report of Case Studies of Additive Manufacturing in the South African Railway Industry. Elsevier, Scientific African Journal, 1 – 16, ISSN 2468-2276.

## 2.1 Introduction to Additive Manufacturing

Additive Manufacturing (commonly known as 3D printing) is a collective term representing various technologies that join material to produce physical products from blueprint digital model data [24]. In this process, unlike the traditional manufacturing methods, parts are built gradually from the bottom-up layer-by-layer [25]. The British Standards Institution (BSI) has classified the various AM systems with specific industry manufacturing applications into one of the seven leading technologies represented by additive manufacturing [24]. Figure 2 - 1 illustrates the seven AM technologies with their corresponding printing systems. This research will focus on the Fused Deposition Modelling (FDM) additive manufacturing technology under material extrusion. A summary of the FDM technology, the material types, and the material properties are presented in Appendix A.

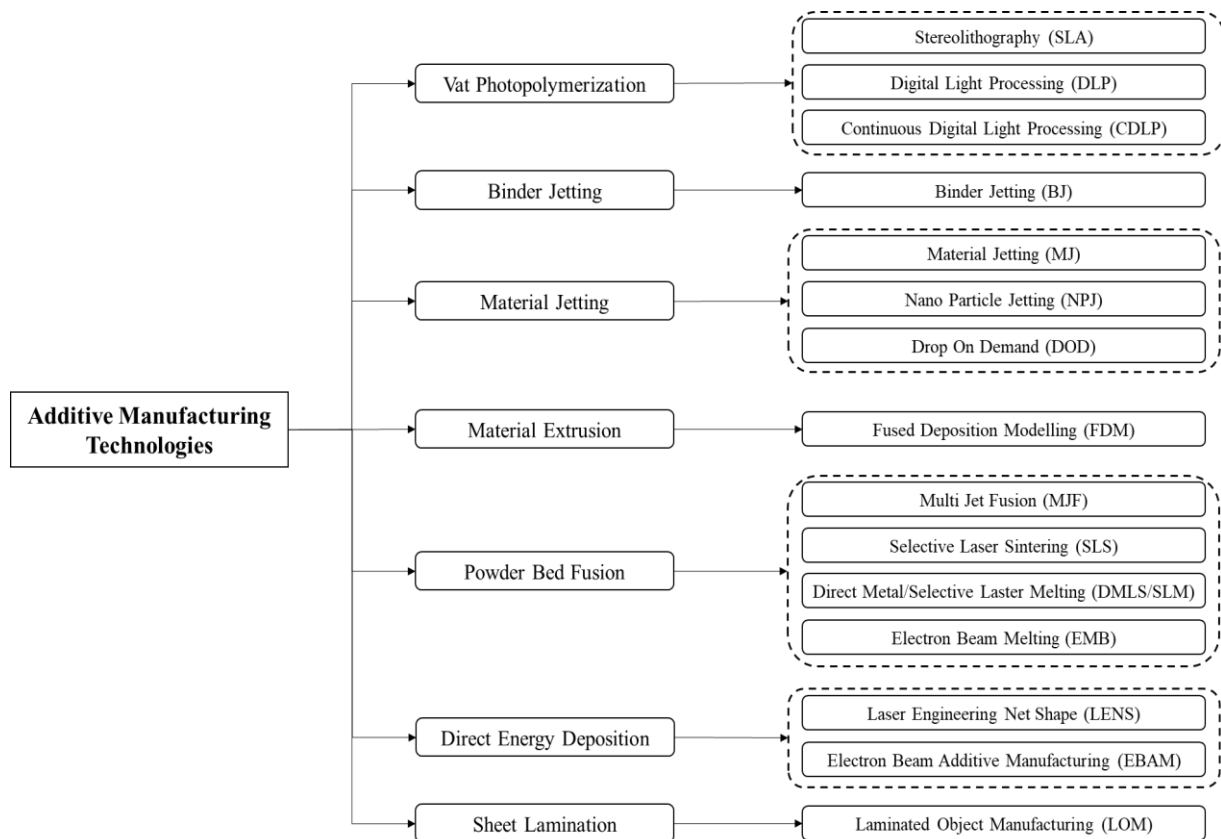


Figure 2 - 1 Additive Manufacturing Technologies [24]

## 2.2 Physical Manufacturing Workflow

### 2.2.1 Mechanical Properties of Fused Deposition Modelling Printed Parts

Fused deposition modelling (FDM) is considered the most popular additive manufacturing technology due to its ease of use, economic accessibility, and variety of commercially available materials [26]. This type of technology has shown several use cases and benefits of being applied within the railway environment [3], [13], [14], [15]. As a result, developing a detailed understanding of the structural behaviour of 3D printed parts and components using the FDM technology under different loading conditions is critical for railway design engineers. This aids in accelerating the adoption of this manufacturing process within the railway environment by allowing railway design engineers to evaluate better, design and implement 3D printable end-use parts. Current methods of studying the mechanical properties of additively manufactured components using the FDM technology have been restricted primarily to experimental characterisation with little work in computational failure predictions and testing [27]. Literature has shown [28], [29], [30], that structural parameters such as layer thickness, infill density, perimeters, infill orientation, infill pattern, air gaps and raster width have a more significant influence on the mechanical properties of FDM 3D printed components than the printer parameters such as build platform temperature, extruder temperature and printing speed. All these parameters can be modified within the tool-path generator software, directly influencing the mechanical properties of 3D-printed parts. It is, therefore, essential to develop a baseline result of influential parameters based on available literature. The FDM process has several process parameters that significantly impact part characteristics and production efficiency [28], [31]. Table 2 - 1 and Table 2 - 2 illustrate the main process parameters with their descriptions.

**Table 2 - 1 The Main Process Parameters for FDM 3D Printing and Their Definitions [28]**

Process Parameters	Description
Layer Height/ Thickness	Specifies the height of each deposited filament layer along the Z-axis, generally the vertical axis of an FDM machine.
Infill Density	Refers to the density percentage volume of material allocated to the structure inside the outer shell of an object. The strength and mass of FDM parts depend on the infill density.
Print Speed	This is the distance the extruder travels along the XY plane of the FDM machine per unit of time while it extrudes filament. The printing time depends on the print speed measured in mm/s.
Extrusion Temperature	The temperature at which the polymer filament is extruded.
Infill Orientation/Raster Orientation	Infill orientation or raster orientation is the angle at which the material bead is extruded. It can range from 0° – 180°.

**Table 2 - 2 The Main Process Parameters for FDM 3D Printing and Their Definitions Continued [28]**

Process Parameters	Description
Infill Pattern	Refers to the geometry or pattern that is printed inside a model. Several infill patterns have advantages and disadvantages between print time, strength, and material usage.
Air Gap	The gap between two adjacent rasters on a deposited layer.
Raster Width	Raster width is defined as the width of the deposition beads. It depends on the extrusion nozzle diameter.
Perimeters (Shells & Walls)	The number of times the 3D printer traces the outer walls of the model contour before starting the infill section.

A survey compiled by Dey and Yodo [28], investigated FDM process parameters' impact on dimensional accuracy, surface roughness, build time and mechanical properties. The survey screened 100 research articles from 2005 to 2019 to quantify the process parameters of 3D printed part characteristics. Figure 2 - 2 illustrates the summarised fishbone diagram as a visual representation of the quantified results obtained.

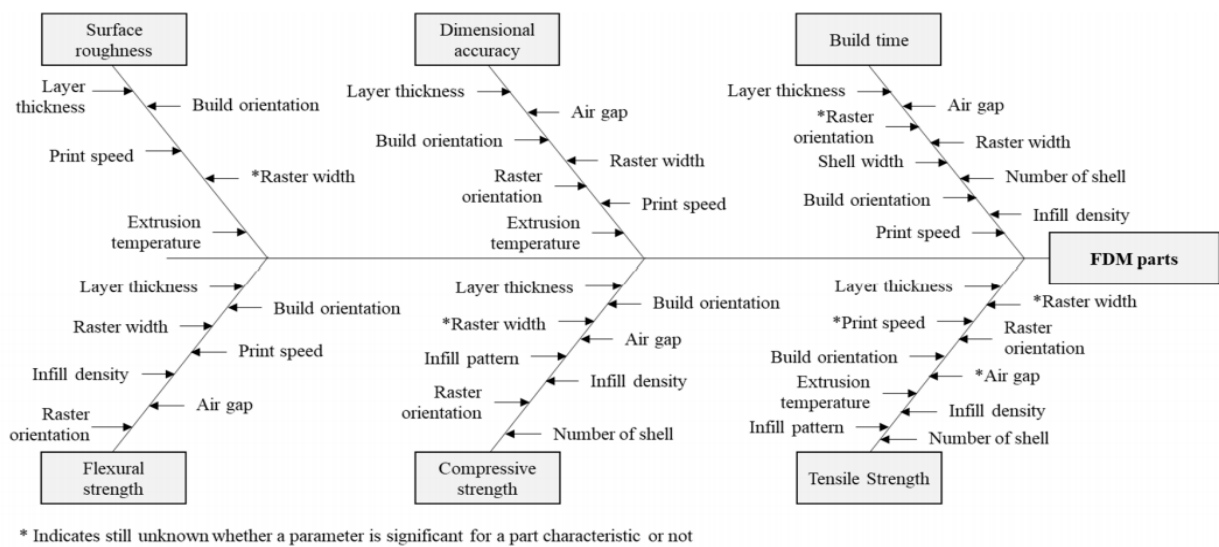


**Figure 2 - 2 Impact of Process Parameters on Part Characteristics [28]**

The mechanical performance of 3D printed test specimens in tensile response is well documented in the literature and will not be presented in this dissertation [28], [32], [33], [34], [35], [36]. The mechanical performance of 3D printed test specimens in compressive response is also well documented and will not be discussed [28], [37], [38], [39], [40], [41]. This section of the study will evaluate the mechanical performance of 3D printed specimens in flexural response [28], [42], [43], [44], [45], [46].

### 2.2.1.1 Flexural Response

The flexural strength of functional parts is an essential mechanical property like tensile and compressive strength. Despite this, little research has been done on characterising 3D-printed FDM beams' flexural properties. International standards, such as ASTM D790 and ISO 178, are used to test thermoplastics' flexural properties, where a three-point bend test is typically used to determine flexural strength. This section summarises the existing literature on determining the influence of process parameters on the flexural strength of FDM 3D printed parts. Based on the existing literature [28], [42], [43], [44], [45], [46], flexural strength is one of the least analysed mechanical properties compared to tensile and compressive strength. The available research mainly focused on build orientation while the impact of some parameters such as infill geometry, infill density, extrusion temperature, layer thickness, raster orientation, print speed and air gap on flexural properties are not widely analysed.

Further research is required to quantify the flexural properties of the different process parameters, as this will be valuable to know the impact of printed parts on flexural strength. Based on the research survey, a baseline recommendation of process parameter settings can be summarised. Table 2 - 3 illustrates the recommended process parameter settings for parts intended to experience bending loading conditions.

**Table 2 - 3 Process Parameter Settings for Optimum Flexural Strength [28], [42], [43], [44], [45], [46]**

Process Parameters	Settings
Build Orientation	XY Plane (lying flat perpendicular to loading or 0° build orientation)
Layer Heights/Thickness	$\geq 0.2$ mm
Infill Density	50 – 90 %
Perimeter Walls/Shells	$\geq 5$
Wall Thickness	1.6 mm
Printing Temperature	5 °C > Recommended manufacturing temperature
Raster Orientation	0°/90°

## 2.3 Digital Manufacturing Workflow

“The additive manufacturing process relies heavily on digital and physical workflows to produce functional parts. This process usually starts with a product idea, a 2D image, sketches, or a physical 3D object like a prototype or a reference part for reverse engineering. These are transformed into digital models using state-of-the-art digital design technologies. The most critical factors related to the digital additive technology process are detailed in [5].” [3] The additive manufacturing process depends mainly on the digital tools available. A 3D printed part is only created based on the digital model. This is due to the required data a 3D printer needs to print the part. In most cases, the 3D printer only needs the

external geometrical representations of a digital model. Due to this process, software tools for the additive manufacturing method are separated into different process applications. These applications include 1) converting CAD data, 2) STL file viewers, 3) support structure optimisation, 4) process simulation, 5) data repair and 6) topology optimisation. Commercial software providers have also become more active in providing specialised software tools specific to AM applications, but this is limited [47]. Only software tools that contribute to the research are examined for this study.

### 2.3.1 Computer-Aided Design Technology

“Computer-Aided Design (CAD) model is a computer-generated 2D and 3D model file used to analyse, optimise, simulate, and modify in a digital environment. The CAD model usually represents a real-world part, component, or subsystem, containing geometrical shapes and dimensions, material properties, and tolerances in either two or three dimensions. Figure 2 - 3 presents examples of CAD models representing railway-related systems. In mechanical design, these files form the basis for pre-manufacturing processes by allowing Computer-Aided Engineering (CAE) tasks such as structural and dynamic FEA to be performed. These simulations determine whether the CAD model is correctly designed for its intended application. Similar operations are used in AM and 3D Printing, where CAD files are created as the base to which alterations and additions can be made [48]. The most common file used to represent a part's dimension and tolerance for 3D printing is a Stereolithography (STL) file generated from the original CAD model without the extra information.” [3]

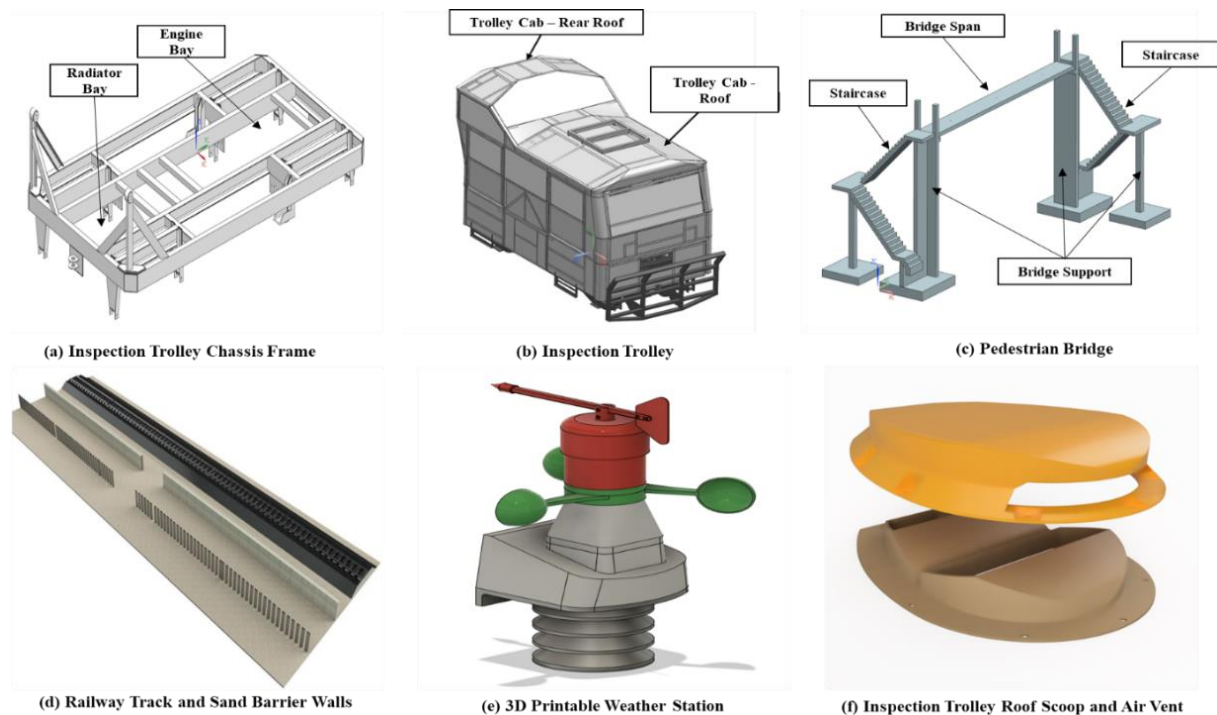


Figure 2 - 3 Several Railway-Related CAD Models



### **2.3.2 Finite Element Analysis**

In this study, the focus is directed toward structural simulations for solutions to the elastic problem. All Finite Element Analyses (FEA's) are conducted on computational software packages due to the large equation sets that approximate the physics problems. The FEM discretises a model into equally distributed element bodies containing material properties and is interconnected at various node points, boundary lines and surfaces that make up the structure of the digital model. Elements used in these analyses vary from 1D, 2D or 3D, and first or second order depending on the complexity of the problem [49]. Each nodal point is associated with a set of governing equations with six degrees of freedom (DOF), three translational and three rotational equations. There are two methods for structural analysis, the force or flexibility method and the stiffness or displacement method [49]. This research will use the stiffness method since it is simpler to implement using available computational tools [49].

### **2.3.3 Tool-Path Generator (Slicing Software)**

“3D printers are not capable of reading or 3D printing native STL file formats on their own [50], [51]. The digital STL file needs to be discretised and converted into machine code for the 3D printer to understand [52], [53]. The machine code, known as G-Code, is used as instructions to a 3D printer and is created by specialised slicing or tool-path generator software [54], [55]. The software uses an explicit slicing method to generate two-dimensional contours in the XY plane representing the digital model [56], [57]. These contours are then stacked along the Z-plane to represent the height of the digital model [58]. The parallel planes and layers are converted into G-code for the printer to follow and 3D print the intended part [52], [59], [60]. Figure 2 - 4 illustrates the slicing and stacking layers generated in the Cura slicing software.” [3] Several slicing software tools are available for the FDM AM process and are usually sub-categorised into free, paid, and open-source versions. Free and paid slicing software usually operates with specific printer brands, while open-source software can be used for any printer. A detailed list of available AM slicing software tools is presented in [61]. A team of researchers [53] investigated the dimensional accuracy and print quality of different slicing tools for 3D printers. The study showed that different software produced different results even though the input parameters were the same. This is due to each software's slicing algorithms and path planning. Figure 2 - 5 illustrates how the same 3D printed letters' results would be constructed using various slicing software and G-code variants [53]. There is currently only two open-source slicing software considered state-of-the-art. These include Cura, which Ultimaker develops, and Slic3r. These packages have accessible source code, which can be modified and improved based on the required AM tasks. Due to this and the results obtained in [53] and [62], the Cura slicer will be the selected tool-path generator software used in this study. The slicing software generally allows the designer to select and input a range of printing parameters based on the part's intended application and the material used [52]. The standard printing parameter feature setting available on the Cura slicer is detailed in [3], [63]. To produce a 3D printed

part that closely represents the digital model and is functional, the combination of print parameters found on the slicing software must be correctly selected.

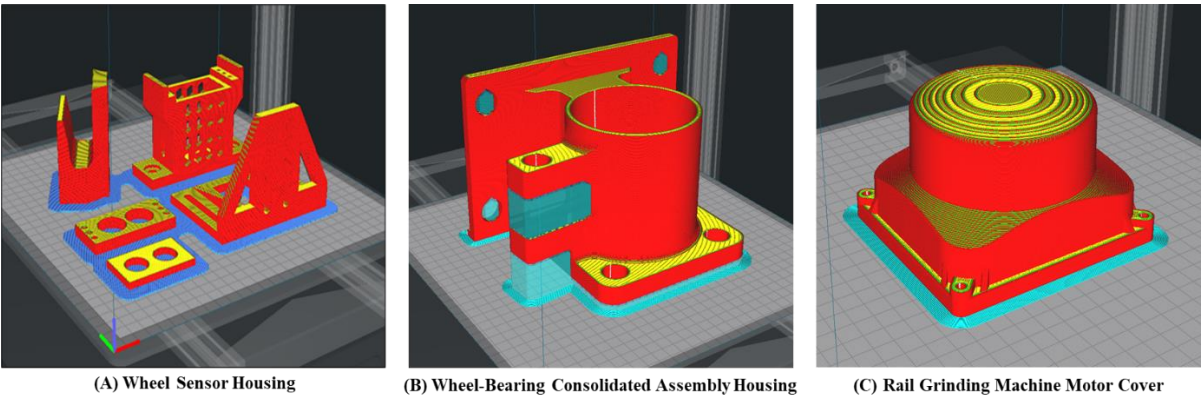


Figure 2 - 4 Example of Railway-Related Replacement Parts Sliced and Prepared for 3D Printing Using Cura

































							
Cura	KISS	Skein	Slic3r	Cura	KISS	Skein	Slic3r
							
Cura	KISS	Skein	Slic3r	Cura	KISS	Skein	Slic3r
							
Cura	KISS	Skein	Slic3r	Cura	KISS	Skein	Slic3r
							
Cura	KISS	Skein	Slic3r	Cura	KISS	Skein	Slic3r

Figure 2 - 5 3D Printed Letters Test with Corresponding G-code from Different Slicers [53]

## 2.4 Multi-Criteria Decision Analysis

Multi-Criteria Decision Analysis (MCDA) is a logical analysis support tool in the decision-making of complex, conflicting criteria that apply to solving problems where a choice is required based on several available alternatives [64], [65]. Several types of MCDA tools and their application exist in the literature and are beyond this research's scope to evaluate every type of MCDA method available. A critical comparison and evaluation of published literature on the most common models were performed by Sabaei et al [66]. A total of 394 articles between 2013 – 2015 identified the five most common decision-making methods, namely; 1) Analytic Hierarchy Process (AHP), 2) PROMOTHEE (Preference Ranking Organisation Method for Enrichment Evaluations), 3) ELECTRE (Elimination ET Choix Traduisant la Realite), 4) SMART (Simple Multi-Attribute Rating Technique), and 5) TOPSIS (Technique for Order of Preference by Similarity to Ideal Solution). The researchers determined that the AHP method provides decision-makers with a robust solution for maintenance management decisions [66]. This chapter focuses on the extended work of the AHP method with considerations of the Fused Deposition Modelling Additive Manufacturing technology to support better decisions in identifying and selecting appropriate complex parts and product designs specific to the railway infrastructure environment.

### 2.4.1 Multi-Criterial Decision Analysis in Additive Manufacturing a State-of-the-Art

Multi-Criteria Decision-Making (MCDM) analyses or Multi-Criteria Decision Analysis (MCDA) tools are commonly applied to a variety of applications to support decision-makers in selecting optimal solutions to complex decision problems [67]. The application of MCDM or MCDA in additive manufacturing, particularly the selection of potential railway-related parts for the FDM technology, is limited [68]. A brief review of the methods used to perform decision-making for AM applications, specifically the FDM technology, is performed.

Sapkal and Warule [69] investigated the application of different Multi-Attribute Decision-Making (MADM) methods for evaluating process parameters and dimensional accuracy of 3D printed specimens using the Fused Deposition Modelling technology. The study showed that the Simple Additive Weighting (SAW) and the Weighted Product Method (WPM) are well suited for small, qualitative datasets. In applications with large, qualitative and quantitative datasets, PROMETHEE is more suited. Yao et al. [70] presented a hybrid machine learning algorithm based on the hierarchical clustering technique to assist inexperienced designers by recommending design features based on geometric complexity for AM potential parts at the conceptual design phase. The study evaluated several existing industrial design applications using the hybrid machine learning model and grouped similarities of complex design features for AM [70]. Bikas et al. [71] presented a framework and method to assist novice designers in additive manufacturing. The framework is based on evaluating questionnaires for three different levels using the SAW and WPM techniques. The first level evaluates

the AM technologies, the second level evaluates the feasibility of applying the AM technology, and the third level evaluates the manufacturability issues based on design features. The proposed framework and method provided a structured approach to identifying the effectiveness of AM within the different levels [71]. Ransikarbum and Kim [67] developed a robust MCDM framework to analyse alternative 3D printing orientations based on economic and mechanical desire. The framework incorporates the AHP model, which evaluates and considers the multiple criteria the decision-maker sets for the FDM technology. The criteria's used in the study included; 1) build time, 2) build cost, 3) surface quality, 4) part accuracy, 5) mechanical properties, and 6) support volume. Finally, based on the framework, the ideal print orientation was determined.

Tavcar and Nordin [72] proposed an MCDM model based on the SAW and WPM methods for AM functions. The model is intended to help compare selected AM technologies and product design at the conceptual design phase, influencing the expected product cost. The product design is initially evaluated by recommended Design for Additive Manufacturing (DFAM) guidelines. The economic criteria used in the model are based on; 1) part volume, 2) material type, 3) material strength, 4) product quality, 5) part quantity, 6) pre-and post-processing time, and 7) operator costs. The technical criteria are based on; 1) material temperature, 2) material strength, 3) material weight, 4) material cost, 5) processing time, and 6) AM processing cost. Finally, a case study using the model investigated the cost estimate for printing a Raspberry Pi enclosure using the FDM and SLS process. The model determined that the FDM process was more economical for low quantities.

Lui et al. [73] developed an MCDM methodology to facilitate AM process selection and assist designers at the initial product design stages. The methodology enables designers to 1) determine whether AM is an economical and technically viable process to produce a product based on the design requirements, 2) modify and design the part specific to the AM process and 3) identify and select the AM technology for producing the part. The model is developed based on a logical decision-making process achieved using the AHP technique based on four elements; 1) part screening, 2) technical evaluation and AM process selection, 3) re-evaluating the AM process, and 4) AM technology selection. The AHP criteria used in the model include; 1) material availability, 2) tensile strength, 3) build volume, 4) dimensional accuracy, and 5) multiple colour printability. Finally, the developed MCDM methodology is applied to an industrial case study, particularly the design and manufacturing of an exhaust gas duct using the SLM process.

Kadkhoda-Ahmadi et al. [74] developed an integrated Additive Manufacturing Process and Resource Selection Problem (AMPRSP), which determines the most suitable AM processes and manufacturing resources based on different criteria. This is achieved by the proposed Multi-Criteria Evaluation System (MCES) to solve the AMPRSP by performing manufacturability analysis, material selection and process technique during concurrent engineering using an integrated design approach. The most suitable alternatives are selected by using the AHP technique. The criteria used in the proposed MCES include;

1) build time, 2) performance accuracy and 3) cost. Finally, the methodology is applied to an industrial case study, particularly a car vehicle fog light bezel, which verified the proposed approach of the MCES. Muvunzi et al. [75] proposed a generalised methodology to evaluate the sustainability of using AM technologies to produce parts for transport equipment. The study reviewed the literature to identify potential parameters for selecting parts and presented an MCDM matrix based on the AHP technique. The criteria used in the methodology include; 1) geometric complexity, 2) value of the part, 3) production volume, 4) design improvement, 5) material removal, 6) function of the part, and 7) time to manufacture. The proposed methodology is developed using case studies for parts produced using the SLM technology for metals. Lastly, the authors proposed that more work is required to fill the identified gap as a limited amount of literature exists when identifying and selecting potential part candidates specific to industrial environments for AM applications.

Mancanares et al [76] presented a methodology for selecting an appropriate AM process and technology based on the part's technical specification. A four-stage process is utilised to develop the selection process for the AM technology. The model relies on the AHP technique to rank the AM technologies and presents the appropriate machine to manufacture the specific part. The criteria used for the part selection included; 1) multi-colour part requirements, 2) print accuracy, 3) surface quality, 4) impact resistance, and 5) flexural strength. Finally, the proposed methodology is applied to three potential parts (a turbine blade, a bearing holder and an architectural scale house model), where specific AM processes and machines were identified and selected to manufacture the parts.

Ayala and Herrera [77] presented an MCDM methodology for evaluating the maintenance prevention of FDM 3D printer hardware components. The MCDM is based on the AHP technique, which is used to evaluate specifically identified hardware components such as; 1) stepper motors, 2) feeder material, 3) fans, 4) nozzle feeders, 5) nozzle air pressure, 6) temperature controllers, and 7) electronic controllers. Finally, the proposed AHP model is evaluated and verified using a case study which determined that the temperature controller is the most critical part of maintenance prevention measures for hardware components on FDM machines.

Wortmann et al [78] presented a four-stage process model to evaluate and select process parameters for AM to support designers at the initial product development phase in part selection. The first stage proposed using VITOSTRA (method for developing consistent strategy options) to evaluate and select part candidates based on eleven characteristics. The second and third stages investigated the cost estimate to manufacture the part based on the manufacturing process, while the fourth stage presented the selection of the process parameters for the AM technology. The process model is evaluated using an industrial case study, particularly an impeller blade. It was determined that the FDM process was the most economical method to produce the selected part compared to SLS, STL and milling processes.

Renjith et al [79] developed a design framework for AM using the integration of axiomatic design and the theory of inventive problem-solving (TRIZ) technique. The framework is developed to assist

designers in the initial design phase, which comprises three stages of development; 1) conceptual design phase, 2) embodiment design phase, and 3) detailed design phase. The TRIZ technique identifies design parameters corresponding to each design parameter, functional requirement and AM capabilities in an axiomatic design structure for the specific part. The framework is developed to integrate with a specifically designed AM database containing information on general AM capabilities corresponding to the design parameter. Lastly, an electronics housing-cover redesign case study demonstrates the proposed design framework. The proposed case study results showed that a traditionally manufactured part could be redesigned and manufactured using AM technologies.

Chaudhuri et al [68] performed and developed an extensive spare part selection methodology for AM using a structured design science approach. A four-phase design science approach is used to develop the methodology, which includes; 1) developing a solution incubation, 2) refining the solution, 3) explanation using substantive theory and 4) explanation using formal theory. The TOPSIS multi-criteria decision-making technique is first used to rank the large dataset of potential spare parts based on three criteria: 1) part lead time, 2) part demand, and 3) part overhead costs. Secondly, a Two-Step Cluster Analysis (TSCA) is performed to develop specific cluster sizes based on the large dataset. Lastly, the AHP and TOPSIS MCDM are applied to the cluster sizes to identify the appropriate spare parts. Finally, the authors presented a generalised approach to using the methodology for large datasets of spare parts. The authors proposed that more work is required to close the identified gap where limited literature exists when identifying and selecting potential spare parts suitable for AM. Frandsen et al [80] presented an extensive literature review on classifying and selecting suitable spare parts for AM. The review consulted 204 journal publications spanning from 1986 to 2017 related to categories in additive manufacturing, spare part selection and supply chain. The review found that limited research addresses an identification process for suitable spare parts for AM, with only two articles presenting methodologies for identifying suitable part candidates. Secondly, the authors identified seven areas for future research relating to suitable spare part selection methodologies. The areas include: 1) screening of spare parts for AM, 2) selecting suitable spare parts for AM using cross-functional processes, 3) developing specific methodologies for suitable spare part selections for AM, 4) understanding suitable spare part characteristics for AM, 5) DfAM and its impact on part selection, 6) product integrity and modularity and its impact on AM and 7) combination of conventional manufacturing and AM for spare part production. Lastly, the review showed a need for in-depth research and development of a framework and methodology for selecting suitable spare parts for AM specific to individual businesses and industrial environments. Finally, the literature review showed that multi-criteria methods could be used to classify suitable spare parts to assess their suitability for AM

## 2.4.2 Selection Criteria for AM Parts in the Railway Environment

Identifying and selecting parts that will benefit from the AM process, particularly the FDM process for the railway environment, depends on several factors considered at the conceptual design stage [3]. Part size and printer parameters, such as build volume, limit the production to specific parts and components. The influence of printing parameters and technical characteristics such as 1) layer height, 2) infill geometry, 3) infill density, 4) shell walls, 5) printing temperature, 6) surface quality, 7) dimensional accuracy, 8) build time, 9) material shrinkage, 10) strength-to-weight ratio, and 11) stiffness-to-weight ratios affect the mechanical performance of as-printed parts [14], [28], [29], [30]. In the case of material properties, the FDM process is limited to selecting polymer and metal materials, which are dependent on the printer's capabilities and needs to be factored into the decision-making process at the conceptual design stage [1], [5], [81]. Finally, environmental characteristics for as-printed parts to operate in the railway environments include 1) temperature resistance, 2) chemical resistance, 3) moisture and water resistance, 4) Ultra-Violet resistance, and 5) material interaction needs to be considered [5]. Appropriate parts need to be selected to ensure that these benefits are achieved. The selection of existing railway parts for potential candidates in AM requires a specific criterion based on railway engineering requirements and literature. Table 2 - 4 illustrates the recommended selection criteria for railway parts.

**Table 2 - 4 Part Selection Criteria for the Railway Environment**

<b>Selection Criteria</b>	<b>Description</b>
Material Removal [79], [82]	Existing railway parts that can be manufactured without requiring any material to be removed, require a limited amount of material to be removed or requires a substantial amount of material to be removed need to be evaluated at the initial design phase.
Part Function [75], [82]	Understanding the intended part's function within the railway environment will determine whether it forms part of a critical system or a stand-alone non-critical system. Railway design engineers will need to determine the importance of the identified part.
Part Size	Most parts within the railway rolling stock environment are huge, while supporting infrastructure may present smaller components within assemblies. The identified part must be within the print volume of the 3D printer.
Material	Several types of materials parts are manufactured from within the railway environment. In this case, existing polymer components or potential material change components need to be determined. The selected material needs to comply with the recommended railway engineering design requirements.
Manufacturing Time [68], [83]	Depending on the type of part, component, subsystem or assembly, the influence of manufacturing time between conventional manufacturing techniques and the AM technology needs to be determined and if there are any advantages or disadvantages.
Geometric Complexity [82], [84], [83]	The type of part or component needs to be evaluated against its complexity and the capability of manufacturing it using traditional methods.

**Table 2 - 5 Part Selection Criteria for the Railway Environment Continued**

<b>Selection Criteria</b>	<b>Description</b>
Design Optimisation [79], [73], [84], [83]	Many systems and components within the railway environment are considered legacy systems. Spares parts to legacy systems may present opportunities for redesign using optimisation techniques such as light-weighting, assembly-part consolidation or material change from metals to high-performance polymers. These need to be determined at the initial design phase.
Production Volume [72], [68]	Parts, components, and assemblies produced for the rail infrastructure and rolling stock environment are in low-quantity batches. This is due to the preventative and corrective maintenance philosophy used in the railway environment.
Part Benefit [80], [83]	The identified railway-related part provides a specific role to railway operations, and the level of importance needs to be determined.

## 2.5 Types of Structural Optimisation

Structural topology optimisation is considered a procedure for optimising the topological material arrangement of a part within the design domain. This is achieved by eliminating the material volume that does not contribute to the structure's integrity, while the optimised shape is generated based on the material volume that experiences loading and specific boundary conditions [85]. The types of structural optimisation can be classified into three categories: 1) Shape optimisation, 2) size optimisation, and 3) topology optimisation.

### 2.5.1 Shape Optimisation

The boundaries of the initial continuum structure are modified to search for an optimal shape based on the structure's intended service conditions and the initial boundary conditions [86].

### 2.5.2 Size Optimisation

Size optimisation is used to find an optimal design by changing the size variables, such as the cross-sectional dimensions of trusses and frames or the thickness of the plate. This is the earliest and most straightforward approach to improving structural performance [87].

### 2.5.3 Topology Optimisation

An optimised parameter is set for each discretised element within the design domain. These parameters determine the material properties of the element, allowing to set empty spaces or gaps in the design domain. The objective of the optimisation method is to find a parameter configuration that defines an optimal material distribution over the domain. Several methodologies have been used to solve the topology optimisation problem; these include methods using knowledge of the elastic mechanic



problem to meta-heuristics capable of solving optimisation problems with only the objective function. The two commonly used methodologies for topology optimisation include: 1) Evolutionary Structural Optimisation (ESO) [16], [88] and 2) Bi-directional Evolutionary Structural Optimisation (BESO) [16]. Other methods available for solving topology optimisation problems include: 1) Homogenisation methods [16], [89], [90], [91], 2) Level set method [92], [93], 3) Phase-field methods [94], and 4) Meta-heuristic [95]. In this research, the bi-directional evolutionary optimisation technique will be used to develop and create custom infill placements for FDM 3D printed parts.

## **2.6 Custom Infill Placement**

To date, most of the research concerning the optimisation of FDM parts has focused on dimensional accuracy, surface roughness and build time compared to the digitally designed model or the strength of a part based on process parameter changes made in standard slicers such as infill percentage, infill orientation and layer thickness.

J.A. Gopsill et al. [7] investigated and validated a five-stage method to create topology-optimised infill structures for FDM parts. The methodology used finite element analysis data obtained from Autodesk simulation mechanical and a weighted stress criterion based on the evolutionary structural optimisation (ESO) method. A custom python script was developed based on graph theory to generate 2D linear infill structures due to the applied ESO method to the FDM printed parts. The procedure was validated using three-point bending tests and showed a three and half times increase in strength. This process, however, is restricted to 2D loading conditions and structures. Due to the scripting method employed, the infill structure is limited to a predefined infill geometry, infill orientation and does not consider using multi-infill geometry within the 3D printed part. It also does not consider the material in the case of multi-material optimisation. Xiong et al. [96] presented a method to design a highly efficient structure using the Bi-directional Evolutionary Structural Optimisation (BESO) technique. The BESO method was used to produce a conceptual design of a hinge arm based on a set of loading conditions, and smoothing algorithms were used to post-process the conceptual design into a manufacturable part with the objective of mass reduction. The method was developed around the stereolithography additive manufacturing technology due to the ease of manufacturing complex structures. The optimised hinge design was mechanically tested on an experimental hinge compression machine. The experimental results showed that the optimised hinge design achieved a peak force of 1.920 kN before failure. This BESO-optimised hinge design achieved the highest peak force before failure compared to 17 other design types. Nager et al. [23] presented an extensive review of the market availability of software packages with topology optimisation features. The study presented practical, real-world applications of topology-optimised structures using available software. The software packages investigated included ANSYS, ABAQUS, CREO, NASTRAN and COSMOS, where different topology optimisation methods and algorithms are used. The study showed that optimisation tasks could be easily

accomplished using the appropriate methodology, and final component designs were manufactured using additive manufacturing technologies.

Reddy et al. [97] extensively reviewed the current state of topology optimisation software packages and their capabilities, focusing on manufacturing considerations important to additive manufacturing. A total of twenty different commercial and educational software tools were investigated and categorised. All commercially available topology optimisation software packages offered similar capabilities and considerably more functionality than educational software, with none of the tools providing adequate manufacturing constraints specifically for AM. Many commercially available tools utilised the Solid Isotropic Material with Penalisation (SIMP) density-based topology optimisation method, which resulted in similar capabilities. Toth and Vilakazi [14] presented a method of creating custom infill geometry placements for FDM printed parts using the shape optimisation and finite element analysis methods available in a commercial software package, Fusion 360. The study also investigated the relationships between the various print parameters and tensile-tested specimens' mechanical performance. The study results showed a two-and-a-half times increase in strength and a 27 % mass reduction for the optimised specimens while maintaining the original test specimen's shape. Lastly, a case study is presented to demonstrate the application of designing a railway component using the presented method of creating a custom reinforced infill geometry for the FDM 3D printed part. For topology optimisation methods to create custom infill structures with the FDM technology, the manufacturing constraints and the process parameters must be fully defined, as the mechanical performance depends on them [28].

#### **2.3.4 Bi-directional Evolutionary Structural Optimisation (BESO)**

The Bi-directional Evolutionary Structural Optimisation (BESO) method allows the material to be removed and added simultaneously. The initial research on BESO was conducted by [98] for stiffness optimisation. In their study, the sensitivity numbers of the void elements are estimated through a linear extrapolation of the displacement field after a finite element analysis. Then, the solid elements with the highest sensitivity numbers are changed into solid elements. Two unrelated parameters determine the number of added and removed elements in each iteration; the rejection ratio (RR) and the inclusion ratio (IR). The BESO algorithm has also been applied to a 'full stress design' using the von Mises stress criterion [99]. This algorithm removes the elements with the lowest von Mises stresses, and void elements near the highest von Mises stress regions are switched on as solid elements.

Similarly, the number of elements to be removed and added are treated separately with rejection and inclusion ratios, respectively [100]. The new bi-directional evolutionary structural optimisation (BESO) algorithm for stiffness optimisation [16] addresses many issues related to the topology optimisation of continuum structures. In the BESO method, a part or structure is optimised by removing and adding elements simultaneously based on an initial finite element analysis (FEA). The elements represented by

the FEA mesh are treated as the design variable rather than the associated physical or material parameters. The optimisation problem with the volume constraint is stated as [16]:

$$\text{Minimize:} \quad C = \frac{1}{2} \mathbf{f}^T \mathbf{u} \quad 2 - 1$$

$$\text{Subject to:} \quad V^* - \sum_{i=1}^N V_i x_i = 0 \quad 2 - 2$$

$$x_i = 0 \text{ or } 1 \quad 2 - 3$$

Where  $\mathbf{f}$  and  $\mathbf{u}$  are the applied load and displacement vectors, and  $C$  is the mean compliance.  $V_i$  is the individual element volume and  $V^*$  is the total structural volume prescribed.  $N$  is the total number of elements in the system. The binary design variable  $x_i$  declares the absence (0) or presence (1) of an element [100]. When a solid element is removed from a structure, the mean compliance or total strain energy change equals the elemental strain energy. This change is defined as the elemental sensitivity number [16]:

$$\alpha_i^e = \Delta C_i = \frac{1}{2} \mathbf{u}_i^T \mathbf{K}_i \mathbf{u}_i \quad 2 - 4$$

Where  $\mathbf{u}_i$  is the nodal displacement vector of the  $i^{\text{th}}$  element,  $\mathbf{K}_i$  is the element stiffness matrix. When a non-uniform mesh is assigned, the sensitivity number should consider the effect of the volume of the element. In such a case, the sensitivity number can be replaced with the elemental strain energy density as [16]:

$$\alpha_i^e = \Delta e_i = \frac{\frac{1}{2} \mathbf{u}_i^T \mathbf{K}_i \mathbf{u}_i}{V_i} \quad 2 - 5$$

A filtering scheme will be used to obtain the sensitivity number for the void elements and smooth the sensitivity number in the whole design domain to add material to the design domain. Nodal sensitivity numbers which do not carry any physical meaning on their own are defined by averaging the elemental sensitivity numbers as follows [16]:

$$\alpha_j^n = \sum_{i=1}^M w_i \alpha_i^e \quad 2 - 6$$

Where  $M$  denotes the total number of elements connected to the  $j$ th node.  $w_i$  is the weight factor of the  $i$ th element and  $\sum_{i=1}^M w_i = 1$ .  $w_i$  can be defined by [16]:

$$w_i = \frac{1}{M-1} \left( 1 - \frac{r_{ij}}{\sum_{i=1}^M r_{ij}} \right) \quad 2 - 7$$

Where  $r_{ij}$  is the distance between the centre of the  $i$ th element and the  $j$ th node. The above weight factor indicates that the elemental sensitivity number has a more significant effect on the nodal sensitivity number when it is close to the node. Nodes located inside a sub-domain  $\Omega_i$  centred at the centroid of the  $i$ th element with a radius of  $r_{\min}$  contribute to the computation of the improved sensitivity number of the  $i$ th element by [16]:

$$\alpha_i = \frac{\sum_{j=1}^K w(r_{ij}) \alpha_j^n}{\sum_{j=1}^K w(r_{ij})} \quad 2 - 8$$

Where  $K$  is the total number of nodes in the sub-domain  $\Omega_i$ ,  $w(r_{ij})$  is the linear weight factor defined as [16]:

$$w(r_{ij}) = r_{\min} - r_{ij} \quad (j = 1, 2, \dots, K) \quad 2 - 9$$

BESO updates the design from the initial complete design and gradually reduces the structural volume in each iteration. The volume of the next iteration  $V^{K+1}$  is determined by an evolutionary ratio  $ER$  and the current structural volume  $V^K$  as follows [16]:

$$V^{K+1} = V^K (1 \pm ER) \quad (K = 1, 2, 3 \dots) \quad 2 - 10$$

Once the volume constraint is satisfied, the volume of the structure will be kept constant for the remaining iterations as [16]:

$$V^{K+1} = V^* \quad 2 - 11$$

A threshold  $\alpha_{th}$  is used for updating the design variables according to the  $V^{K+1}$  and their sensitives. The update scheme of BESO is defined as [16]:

$$x_i^{K+1} = \begin{cases} x_{min} & \text{if } \alpha_i \leq \alpha_{del}^{th} \\ 1 & \text{if } \alpha_i > \alpha_{add}^{th} \\ x_i^K & \text{otherwise} \end{cases} \quad 2 - 12$$

### 2.3.5 Smoothing Technique for Post-Processing

The BESO technique introduces complicated and intricate shapes with peaks or spikes due to adding and removing elements that experience less stress. These shapes result in manufacturing limitations for the FDM process. Producing manufacturable parts using the FDM process using the BESO technique performed on STL files requires post-processing to create printable objects. These routines usually include analyzing and repairing non-manifold edges, peaks, and spikes generated during the topology optimisation method. There are several approaches to surface smoothing of 3D meshes based on literature [101], [102] which involve; 1) using local curvature of neighbour faces, 2) using filters based on patch normal, 3) using the position of vertices and 4) by filtering the surface with a frequency-based approach. Several advantages and disadvantages are associated with each technique; however, the method based on using the position of vertices is considered the most straightforward and fastest approach for smoothing meshes [103]. Surface smoothing is achieved by manipulating STL models' vertices, triangular facets, and normal vectors for each facet. The commonly available techniques [101], [102], [103] to smooth meshes based on the position of vertices include 1) HC Laplacian smooth, 2) Laplacian smooth, 3) scale-dependent Laplacian smooth, 4) Taubih smooth and 5) two-step smooth. The Laplacian smooth technique will be used for this study for smoothing topology optimised meshes [103], [104].

### 2.6.3.3 Laplacian Mesh Smoothing

The optimised model using the BESO technique contains boundary contours that are not streamlined and are usually rough due to mesh elements. This is due to the element's shape and the BESO method of element removal. The optimised model (with zig-zag boundaries) may reduce structure performance and present FDM technology manufacturing difficulties. A smoothing technique is proposed for reconstructing the element-based model [105]. The Laplacian mesh processing technique [104] makes the optimised structure smooth enough to enable manufacturing using the FDM technology. The Laplacian mesh processing technique encodes the iso-surface vertices from Euclidean coordinates to Lagrange coordinates. It then averages each vertex position with even weighted positions with neighbour vertices while preserving the geometric details. Thus, the structural topology would not be changed during surface editing. The Laplacian coordinate of a vertex  $v_i$  is defined as follows [104]:

$$\delta_i = v_i - \sum_{j \in N(i)} \frac{v_j}{d_i} \quad 2 - 13$$

Where  $v_j$  and  $N(i)$  represent the neighbours of the vertex  $v_i$  and neighbour set, respectively, and  $d_i$  is the number of neighbours of  $v_i$ . Surface editing operations can be efficiently and robustly applied to surface mesh with Laplacian coordinates [104].

Laplacian smoothing is one of the most common algorithms for mesh denoising. It repeatedly and simultaneously adjusts the coordinates of each vertex in the mesh to the geometric centre of its neighbours. Although the Laplacian smoothing algorithm is efficient and straightforward, it may produce an over-smoothened result where small features might be lost during the process. An optimal way is to convert the triangular mesh into a quadrilateral mesh before Laplacian smoothing [104]. Quadrilateral meshes could snap the sharp details, which is more suitable for mechanical models than triangular meshes. In this work, the remeshing process will convert the triangular meshes into a quadrilateral mesh by applying a 4-8 subdivision scheme. It introduces only a single vertex for each triangle instead of four [106].

## 2.7 Design for Additive Manufacturing

Design for Additive Manufacturing (DfAM) is the process and methodology design engineers use to create a product that takes advantage of the unique capabilities of the Additive Manufacturing (AM) technology. The DfAM process goes beyond re-designing existing components for AM, which may yield material reduction and assembly-part consolidation benefits. Effective use of the DfAM process is considering the additional benefits associated with the AM technology [107]. Improvements to an entire component or product in form, fit and function (FFF) can be realised when conscious design decisions are made instead of blindly following a set of design rules [108], [131]. A distinct hierarchy of different design types for the AM process of products is usually categorised into Modifying the AM printing process parameters, modifying the form of the part, and complete redesign of a part based on its intended function. Generally, these three design approaches are: 1) direct part replacement, 2) adapt for AM and 3) design for AM [109]. Within the railway environment, these design approaches can be applied to create new 3D printable components for different assets by leveraging the benefits of AM technology and understanding DfAM guidelines. Tangible benefits of the technology for the railway industry will be seen by applying these design types for part consolidation, material change, design optimisation techniques for lightweight structures, customised measuring and monitoring railway device housings, replacement parts for obsolete or legacy designed systems, new complex designs,

custom jigs, fixtures and tooling and not in replicating existing railway products without capitalising on the advantages of AM [3], [5], [13], [14], [110], [111], [112]. Booth et al. [113] presented a single-page visual DfAM worksheet to assist AM novice and intermittent users at the conceptual design stage. The worksheet assists designers by evaluating the conceptual design of a part based on part complexity, part function, material removal, unsupported features, thin features, stress concentration, part tolerance and geometric exactness. The goal of the worksheet is to reduce potential print failures, improve AM understanding and present recommendations for conceptual designs. Pradel et al. [114] proposed a conceptual framework which organised the growing literature on DfAM principles. The proposed framework is based on the generic design process model, including 1) conceptual design, 2) embodiment design, 3) detailed design, 4) process planning and 5) process selection. A total of 81 articles on DfAM are used to develop the framework to provide a clear summary of the current state-of-the-art. Diegel et al. [109] formulated a general seven-rule guideline to determine whether a part will benefit from the AM process and if it will genuinely add value to the final product. Mechanical design features of functional parts are limited by the manufacturing technology the parts are designed for. Features on parts designed for the FDM technology are limited to specific dimensions and design techniques to be successfully printed [115], [116], [117], [118]. Redwood et al. [115] and e3D [116] identified ten common feature types and presented design recommendations. The ten features include; 1) supported walls, 2) unsupported walls, 3) support material, 4) embossed & engraved details, 5) horizontal bridges, 6) holes, 7) overhangs, 8) minimum features, 9) pin diameter and 10) tolerance.

## 2.8 Chapter Summary

The study in this chapter presented the physical and digital manufacturing workflow associated with the FDM method. Firstly, the material properties, the process parameters and their influence on the mechanical performance of 3D prints are identified. A set of recommended print process parameters are determined through literature for as-printed parts in flexural responses. It must be noted that based on the literature, the mechanical responses for dynamic, fracture and fatigue are limited, and more research is required to understand 3D printed parts better using the FDM process. Secondly, a detailed review of the state-of-the-art Multi-Criteria Decision-Making techniques in AM is reviewed and presented. Lastly, a literature review on the different types of structural optimisation techniques and custom infill placement methods is reviewed with a clear focus on the Bidirectional Evolutionary Structural Optimisation method. Finally, design for AM techniques and methods are reviewed, focusing on the common design feature types and the generic design process for the FDM process. For this study, Siemens NX is selected for all CAD-related tasks, Siemens NX Advanced Simulation and the CalculiX solver are selected for structural finite element analysis, FlowEFD is selected for computational fluid dynamic exercises and Cura version 4.11 is selected as the slicing software (tool-path generator). The STL file format will also be used as the selected 3D printing file format. The Analytic Hierarchy Process is selected as the Multi-Criteria Decision-Making model for evaluating and selecting potential railway-related parts that may benefit from the FDM process. Lastly, the Bidirectional Evolutionary Structural Optimisation technique is selected as the structural optimisation technique to create custom infill placements. Finally, a summary of the FDM technology, the material types, and the material properties are presented in Appendix A, while specific slicing software features and specific slicing software parameters used for Cura are presented in Appendix C. The printing profile presented in Appendix C is specifically for an FDM 3D printer with a 0.4 mm nozzle to print PETG materials.



# **CHAPTER 3: PART SELECTION: DECISION MODEL FOR ADDITIVELY MANUFACTURING PARTS FOR THE RAILWAY ENVIRONMENT <sup>1,2</sup>**

## **Abstract**

The study presented in this chapter proposes a method to evaluate and select parts and components within the railway environment that will benefit from the Fused Deposition Modelling Additive Manufacturing technology at the conceptual design stage. A detailed literature review on the state-of-the-art in Multi-Criteria Decision-Making models is performed with a clear focus on the Fused Deposition Modelling Additive Manufacturing process. Secondly, the criteria identified in the literature are summarised for part selection, focusing on the Analytic Hierarchy Process. Furthermore, the identified criteria are used to develop a custom evaluation model for railway maintenance applications verified using case studies published in the literature. Finally, the evaluation model is applied to potential railway case studies to determine its benefit using the Fused Deposition Modelling technology. The case studies present functional end-use 3D printed railway-related parts and products for maintenance tooling and measuring activities, rolling stock replacement parts, a prototype environmental monitoring system for sand sedimentation, design optimisation techniques and light-weighting of rolling stock components through assembly-part consolidation.

---

<sup>1</sup> Elements of this chapter are presented in [119]: Toth AD, Padayachee J, Vilakazi S, Matjeke V, 2022, Multi-Criteria Decision-Making Methodology in Part Selection for Fused Deposition Modelling in the Railway Industry, Proceedings of the Institution of Mechanical Engineers, Part F: Journal of Rail and Rapid Transit, 1 – 12, and in [10]: <sup>2</sup> Toth AD, Padayachee J, Mahlatiji T, Vilakazi S, 2021, A Report of Case Studies of Additive Manufacturing in the South African Railway Industry, Elsevier, Scientific African Journal, 1 – 16, ISSN 2468-2276.

### 3.1 Introduction

Additive manufacturing (AM) offers several advantages to the railway environment. As additive manufacturing becomes more mainstream within the railway industry, it is essential to have a structured method to select railway-related parts that will benefit from the technology at the conceptual design stage. The current approach to determining suitable part candidates for railway-related applications is based on prototyping and testing, which is not an efficient method for selecting parts [13]. To truly capitalise on the additive manufacturing process, a streamlined technical and logical process needs to be in place to determine the potential benefits of selecting appropriate railway-related parts and components for additive manufacturing applications before the prototyping, and testing stages are initiated. Once a streamlined technical process is developed, concrete guidance to railway engineers in selecting and identifying appropriate railway-related parts can be done to fully capitalise on the AM process.

### 3.2 The Analytic Hierarchy Process

The Analytic Hierarchy Process (AHP) was developed by Saaty [120] and is considered one of the most popular MCDA tools. The AHP model is developed to assist decision-makers in effectively comparing multiple complex alternatives in a structured approach. Alternatives are compared based on their performance for each assigned criterion, including the assigned weights by the decision-makers, where a priority is identified based on a final decision [120], [121].

#### 3.2.1 First Principles

The first step in applying the AHP is to derive the decision hierarchy levels to evaluate potential railway-related part candidates for additive manufacturing. Table 3 - 1 illustrates the decision hierarchy levels used in this study. Figure 3 - 1 illustrates the decision hierarchy flow diagram used for the AHP evaluation method.

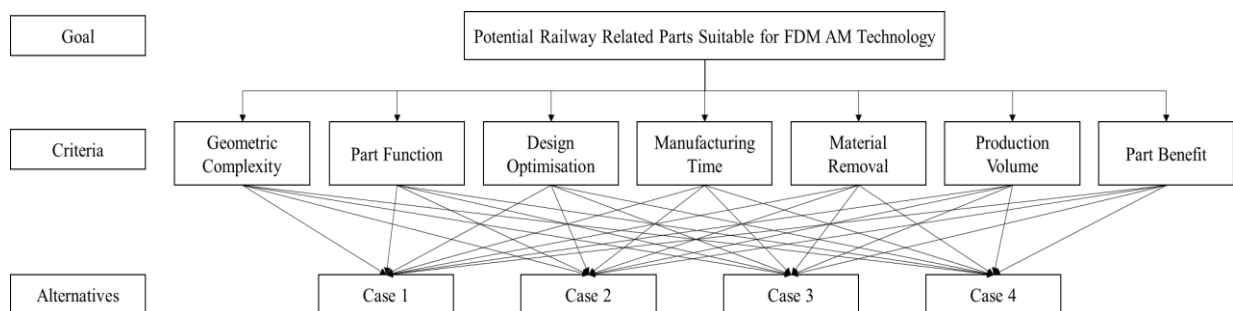


**Figure 3 - 1 Decision Hierarchy for Evaluating Part Candidates for Additive Manufacturing**

**Table 3 - 1 Decision Hierarchy Levels with Identified Criteria**

<b>Goal</b>	
To identify potential railway-related parts suitable for the FDM AM technology	
<b>Criteria</b>	
Geometric Complexity [82], [84], [83]	Based on existing railway parts, components, or products.
Part Function [75], [82]	The function and operation of the railway part.
Design Optimisation [79], [73], [84], [83]	Optimisation techniques such as lightweight, assembly-part consolidation or material change are required for the existing railway part.
Manufacturing Time [68], [83]	Time taken to manufacture the existing part using traditional manufacturing techniques compared to AM methods.
Material Removal [79], [82]	Time and requirement to remove material from feedstock material to produce railway-related parts using traditional manufacturing techniques
Production Volume [72], [68]	The number of parts currently being produced.
Part Benefit [80], [83]	The importance of the existing railway-related part to the overall system.
<b>Alternatives</b>	
Based on the number of parts identified	

The criteria (level 2 hierarchy) are evaluated based on a level of importance using a pairwise rating scale. The criterion is evaluated in pairs [122], as shown in Table 3 - 2.

**Table 3 - 2 Pairwise Comparison Scale [122]**

<b>Level of Importance</b>	<b>Rating</b>
Extreme Importance	9
Very Strong Importance	7
Moderate Importance	5
Equal Importance	3
Equal Importance	1
Compromise between the above values	2, 4, 6, 8

A matrix is populated using Equation 3 - 1 and values from the assigned rating scale [122]:

$$PM = \begin{bmatrix} a_{11} & a_{12} & \dots & a_{1m} \\ a_{21} & a_{22} & \dots & a_{2m} \\ \vdots & \vdots & \ddots & \vdots \\ a_{m1} & a_{m2} & \dots & a_{mm} \end{bmatrix} \quad 3 - 1$$

Using Equation 3 - 2, the matrix elements are normalised by the column sum [122].

$$PM = \begin{bmatrix} \frac{a_{11}}{\sum_{i=1}^m a_{i1}} & \frac{a_{12}}{\sum_{i=1}^m a_{i2}} & \dots & \frac{a_{1m}}{\sum_{i=1}^m a_{im}} \\ \frac{a_{21}}{\sum_{i=1}^m a_{i1}} & \frac{a_{22}}{\sum_{i=1}^m a_{i2}} & \dots & \frac{a_{2m}}{\sum_{i=1}^m a_{im}} \\ \vdots & \vdots & \ddots & \vdots \\ \frac{a_{m1}}{\sum_{i=1}^m a_{i1}} & \frac{a_{m2}}{\sum_{i=1}^m a_{i2}} & \dots & \frac{a_{mm}}{\sum_{i=1}^m a_{im}} \end{bmatrix} \quad 3 - 2$$

Once the matrix is normalised, the criteria weights C are calculated using Equation 3 - 3 [122].

$$C = \begin{bmatrix} C_1 \\ \vdots \\ C_m \end{bmatrix} = \begin{bmatrix} \frac{\frac{a_{11}}{\sum_{i=1}^m a_{i1}} + \frac{a_{12}}{\sum_{i=1}^m a_{i2}} + \dots + \frac{a_{1m}}{\sum_{i=1}^m a_{im}}}{m} \\ \vdots \\ \frac{\frac{a_{m1}}{\sum_{i=1}^m a_{i1}} + \frac{a_{m2}}{\sum_{i=1}^m a_{i2}} + \dots + \frac{a_{mm}}{\sum_{i=1}^m a_{im}}}{m} \end{bmatrix} \quad 3 - 3$$

Using Equation 3 - 4, the product of PM and C is calculated to determine the consistency of the weights [122].

$$PM.C = \begin{bmatrix} a_{11} & a_{12} & \dots & a_{1m} \\ a_{21} & a_{22} & \dots & a_{2m} \\ \vdots & \vdots & \ddots & \vdots \\ a_{m1} & a_{m2} & \dots & a_{mm} \end{bmatrix} \begin{bmatrix} C_1 \\ \vdots \\ C_m \end{bmatrix} = \begin{bmatrix} x_1 \\ x_2 \\ \vdots \\ x_m \end{bmatrix} \quad 3 - 4$$

The principal eigenvalue ( $\delta_a$ ) using Equation 3 - 5 [122].

$$\delta_a = \frac{1}{m} \sum_{i=1}^m \frac{\text{ith entry in } PM.C}{\text{ith entry in } C} \quad 3 - 5$$

Using Equation 3 - 6, the consistency measurement (CI) is determined [122]:

$$CI = \frac{\delta_a - m}{m - 1} \quad 3 - 6$$

The weights of the consistency measurement is evaluated by the ratio CI/RI [123]. The random index (RI) is represented in Table 3 - 3.

**Table 3 - 3 Random Indices [123]**

<b>n</b>	<b>1</b>	<b>2</b>	<b>3</b>	<b>4</b>	<b>5</b>	<b>6</b>	<b>7</b>	<b>8</b>	<b>9</b>	<b>10</b>
RI	0	0	0.58	0.9	1.12	1.24	1.32	1.41	1.45	1.49

The following conditions apply when evaluating the calculated weights:

The calculated criteria weights are considered consistent  $\frac{CI}{RI} \leq 0.1$

The calculated criteria weights are considered inconsistent  $\frac{CI}{RI} > 0.1$

The weights of the consistency measurement are evaluated by a ratio of the consistency measure and the random index. A rating scale (k) is developed based on group evaluations [122]. Each criterion is then evaluated independently of the other. The total weight of each criterion is calculated by multiplying (C) by the rating scale (k). Using Equation 3 - 7, the total criteria weight is calculated. [122]. Table C - 4 illustrates the assigned rating scales for each criterion.

$$R = \sum_{i=1}^7 a_{ik} c_i \quad 3 - 7$$

Where criteria  $i = 1 \dots 7$  and rating scale  $k = 1, 2, 3$

The following part criteria range limits apply when using the total rating scale weight R obtained from Equation 3 – 7 [75], [122]:

Not suitable for AM application  $R \leq 1.5$

Design revision is required to be acceptable for AM  $1.5 > R \leq 2.5$

No design revision is required to be acceptable for AM  $2.5 > R < 3$

### 3.2.2 Application: Weights, Criteria and Decision Matrix

For the proposed decision-making model, part size and material type are considered the most critical factors in the initial screening of potential railway-related part candidates and product designs. The rest of the identified parameters are used in formulating the evaluation model. Using Equation 3 - 1, the pairwise matrix is generated, illustrated in Table C - 1 in Appendix C, based on the level of importance rating presented in Table 3 - 2, while Table C - 2 in Appendix C illustrates the normalised matrix using Equation 3 - 2. The consistency values and criteria weights' degree of importance are calculated using Equation 3 - 3 and Equation 3 - 4. Table C - 3 in Appendix C presents the criteria weights and consistency measure. Using Equation 3 - 5, Equation 3 - 6 and Equation 3 - 7, the consistency ratio is determined. Table 3 - 4 illustrates the principal eigenvalue, the random indices, and the consistency ratio.

**Table 3 - 4 Consistency Ratio**

$\delta_a$	Consistency Index (CI)	Random Indices (RI)	Consistency Ratio
7.568	0.0947	1.32	0.07175

The calculated consistency ratio, 0.07175, is less than the recommended 0.1 value. This implies that the obtained criteria weights are considered consistent and can be applied in the final decision matrix presented in Table C - 4 in Appendix C.

### 3.2.3 AHP Model Verification and Validation

The proposed AHP model is verified and validated using FDM case studies published in the literature. Section 10.2 in Appendix C details the four case studies selected for the verification. The proposed AHP model is validated and can be used for other FDM cases, particularly in the railway environment. Since the total weights for each case study are calculated, these values are compared to the part candidate criteria range. The total weight values calculated fall within the respective range limit based on each case study. The weight values within the respective range limits match the outcomes of the case studies. This proves that the proposed evaluation model is valid and can be used for other applications, specifically for the FDM process in identifying potential parts in the railway environment.

### 3.2.4 Application: Part Identification

Table C - 4 in Appendix C presents the final decision matrix for selecting candidate parts for the FDM additive manufacturing technology in the railway environment. The most critical factors for evaluating railway parts for AM applications are part size and material compatibility. Considering the FDM 3D printer presented in Appendix A with a build volume of 300 x 300 x 300 mm, it is necessary to determine whether the potential part can be printed as a single object. The existing material profile is polymer

FDM filaments for material compatibility due to the available printer. Once the part size and material compatibility are established, the AHP model evaluates whether the identified part will benefit from the AM process. Figure 3 - 2 illustrates a process flow diagram for identifying potential parts.

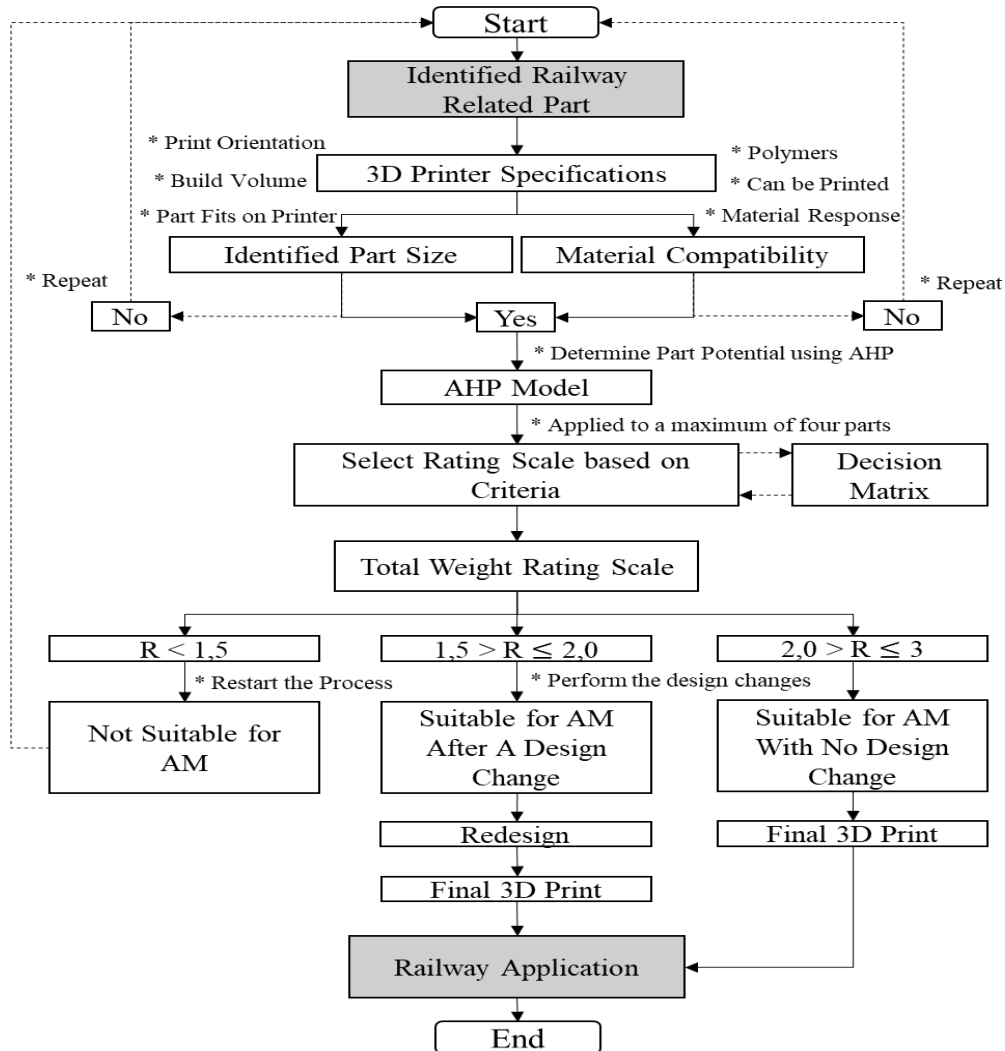


Figure 3 - 2 Process Flow Diagram to Identify Potential AM Parts

### 3.3 Functional End-Use 3D Printed Railway Parts Case Studies

The proposed MCDM AHP model evaluates potential part candidates for the FDM AM process within the railway environment. The case studies in sections 3.3.1 – 3.3.4 present functional end-use 3D printed railway-related parts and products for maintenance tooling and measuring activities, rolling stock replacement parts, a prototype environmental monitoring system for sand sedimentation, design optimisation techniques and light-weighting of rolling stock components through assembly-part consolidation. The application of the AHP MCDM model is applied to each case study.

### 3.3.1 Maintenance Tooling

#### 3.3.1.1 Case Study 1: Wayside Lubricator Tools

Toth et al. [10] presented the development of custom 3D printable tools and replacement parts specific to trackside lubricators. Trackside lubricators help reduce excessive wheel-rail wear by applying a layer of grease on the rail when trains pass through. One thousand six hundred eighty-nine wayside lubricators are installed across TFR's rail network [10]. The proposed parts, illustrated in Figure 3 - 3, are considered non-critical, have low volumes, require no design optimisation, and material removal with simplistic geometric complexity. The overall benefit of the parts is limited to maintenance operations and is beneficial when existing spares are not accessible.

#### 3.3.1.2 Case Study 2: Wayside Lubricator Grease Plate Bracket

Toth and Vilakazi [124] investigated the feasibility of using the FDM process to 3D print design optimised grease plate brackets. These brackets are used to support the grease plates to the rail gauge, and a material change was investigated due to theft and vandalism. The brackets are considered simplistic in geometry but require material removal due to the rail profile. The bracket is considered for medium volumes, manufacturing time, and part benefit; however, it has the critical function of ensuring the grease plates are supported [3], [14], [10]. Figure 3 - 4-A illustrates the metal grease plate bracket, and Figure 3 - 4-C illustrates the 3D printed version.

#### 3.3.1.3 Case Study 3: Thermite Welding Gauges

“Calibration gauges are commonly used within the rail infrastructure when maintenance activities are performed. In rail wear, particularly on turnouts, custom gauges are used to monitor the wear rate on the turnout frog. The gauge informs track personnel if grinding interventions are required to restore the profile. Custom gauges are also used to ensure the correct rail gap is left for the thermite weld based on the rail type when rails are thermite welded. Additive manufacturing allows design engineers to reproduce these gauges on demand to aid in tracking maintenance activities. Figure 3 - 4-D and Figure 3 - 4-E illustrate the rail wear gauges, while Figure 3 - 4-F illustrates the thermite welding gauge.” [10]

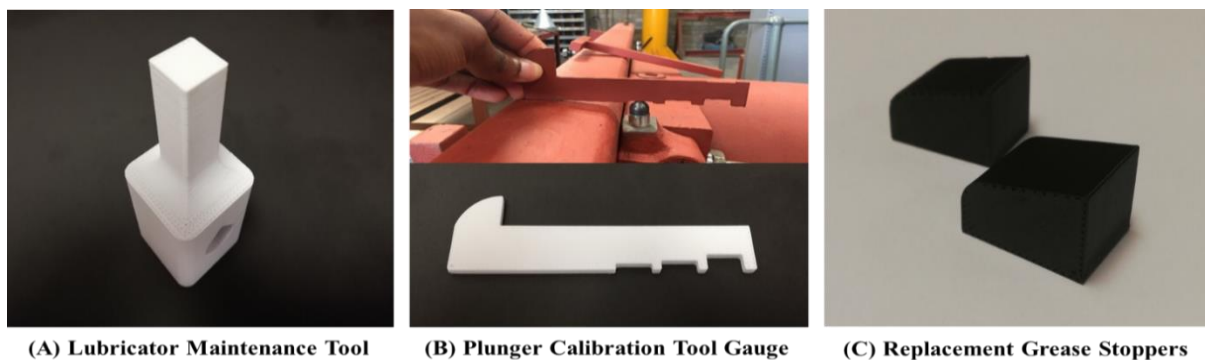


Figure 3 - 3 3D Printed Replacement Parts for the Lubricator Equipment [10]





(A) 3D Printed Bracket Comparison



(B) 3D Printed Brackets



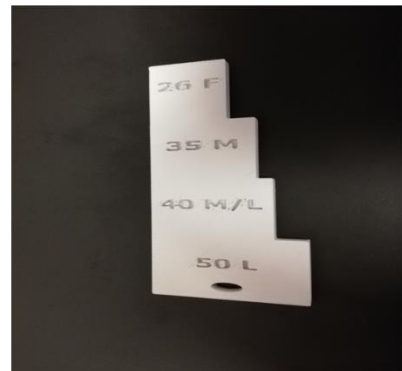
(C) Rail Tested



(D) Rail Profile Gauge



(E) Turnout Rail Profile Gauge



(F) Thermite Welding Calibration Gauge

Figure 3 - 4 3D Printed Grease Place Brackets and Custom 3D Printed Gauges [3], [10]

Table C - 8 in Appendix C illustrates the qualitative evaluation performed on the three case studies, while Table C - 9 in Appendix C illustrates the quantitative evaluation. Table 3 - 5 presents the total weight (R) for each case study and the overall priority by applying the rating scale method and the criteria weights for each criterion.

Table 3 - 5 Total Weight and Overall Priority for the Case Study

Case Studies	Total Weight (R)	Overall Priority	Potential
1	1.815	0,360	Suitable for AM after a design change.
2	2.221	0,441	Suitable with no design change.
3	1,001	0,199	Not suitable for AM.

The total weight, priority, and part potential for three rail infrastructure case studies are determined. Based on the criterion, the third case study showed no benefit from the FDM AM technology. This outcome is due to the simplistic geometry of the proposed wayside lubricator tools. Traditional manufacturing techniques and generic feedstock material can replicate the tooling.

### 3.3.2 Maintenance Measuring

#### 3.3.2.1 Case Study 1: Trackside Measuring Tools

“A custom non-contact wheel lateral displacement measuring device was developed to calibrate wayside lubricators using off-the-shelf electronics, with the housing and mounting clamps being 3D printed using the FDM technology. The rail network consists of three rail types (48 kg/m, 57 kg/m and UIC 60 kg/m), each with unique rail profiles depending on the freight transported. To accommodate the different rail profiles and ensure the measuring device is cost-effective, the non-contact wheel sensor housing is designed to be 3D printed without supports matching the different rail profiles. Further design optimisation techniques were performed on the housing components to allow the sensors and embedded nuts to press-fit into place and ensure low manufacturing time. The geometric complexity of the proposed one-off measuring tool is considered medium but has a high production value with a critical function. Figure 3 - 5-A illustrates the 3D printed housing parts, Figure 3 - 5-B and Figure 3 - 5-C illustrates the instrumented railway track..” [10]



**Figure 3 - 5 Custom 3D Printed Wheel Lateral Displacement Measuring Device for Calibrating Wayside Lubricators**  
[10]

Table C - 10 in Appendix C presents the qualitative evaluation applied to the measuring tool case study, while Table C - 11 in Appendix C presents the quantitative evaluation. Table 3 - 6 presents the total weight (R) for each case study and the overall priority by applying the rating scale method and the criteria weights for each criterion.

**Table 3 - 6 Total Weight and Overall Priority for the Case Study**

Case Studies	Total Weight (R)	Overall Priority	Potential
1	1.908	1.000	Suitable after a design change

The total weight, priority, and part potential for the case study are determined. Based on the criterion, the case study benefited from the FDM AM technology after applying the design optimisation techniques.

### 3.3.3 Rolling Stock

#### 3.3.3.1 Case Study 1: Inspection Trolley Radiator Cooling Pipe Brackets

“Toth [15] investigated the feasibility of designing and 3D printing additional radiator cooling pipe brackets installed on the chassis of the inspection trolley. The railway vehicles were designed and manufactured by Transnet between 1994 and 1998. Due to the legacy design, spare parts and replacement components have become limited and difficult to procure. This is due to discontinued service parts, company closures and extremely long lead times for parts not locally manufactured. The brackets are printed with polypropylene but with a simplistic geometry and limited material removal. The part volume, benefit and function are considered medium due to the requirement. The brackets are shown in Figure 3 - 6” [10]

#### 3.3.3.2 Case Study 2: Hydraulic Injection Moulded Cover

“A vital feature of the inspection vehicle is the hydraulic turntable installed at the centre of the chassis. The turntable allows the inspection vehicle to rotate 360 degrees on track while stationary in cases where the vehicle needs to travel in the opposite direction.” [10]. Toth et al. [10] proposed a new design of a single injection-moulded hydraulic cover for the turntable on the inspection trolley. The cover's design easily incorporates design techniques commonly used on injection-moulded parts. Using traditional manufacturing methods, replacement parts will be time-intensive and costly. Figure 3 - 6-D illustrates the injection moulded part. Figure 3 - 6-E illustrates the internal mechanism, and Figure 3 - 6-F illustrates the 3D printed replacement.

Table C - 12 in Appendix C presents the qualitative evaluation of the two case studies, while Table C - 13 in Appendix C presents the quantitative evaluation. Table 3 - 7 presents the total weight (R) for each case study and the overall priority by applying the rating scale method and the criteria weights for each criterion.

**Table 3 - 7 Total Weight and Overall Priority for the Case Study**

Case Studies	Total Weight (R)	Overall Priority	Potential
1	1,904	0,462	Suitable after a design change.
2	2.221	0,538	Suitable with no design change.

The total weight, priority, and part potential for both case studies are determined. Based on the criterion, the case studies benefited from the FDM AM technology after applying the design optimisation techniques.



Figure 3 - 6 3D Printed Mounting Brackets and Injection Moulded Plastic Cover [10]

### 3.3.4 Prototypes

#### 3.3.4.1 Case Study 1: 3D Printable Weather Station

“Different parts of South Africa experience high wind speeds. Railway tracks that run adjacent to coastal environments, such as the iron ore heavy haul line, are prone to sand build-up and sand sedimentation on the track superstructure due to these winds.” [10]. Toth et al. [10] proposed a new design of a low-cost weather station to track wind speeds and direction printed using the FDM process to inform wind barrier wall placements. The weather station incorporates several design optimisation techniques to ensure the assembly parts have a medium geometric complexity. The function of the weather station is critical to identifying suitable locations for wind barrier walls along the heavy haul railway line. Figure 3 - 7-A illustrates the sand sedimentation on the heavy haul railway line, while Figure 3 - 7-C illustrates the 3D printed version of the proposed weather station prototype. Table C - 14 in Appendix C presents the qualitative evaluation of the case study, while Table C - 15 in Appendix C presents the quantitative evaluation. Table 3 - 8 presents the total weight (R) for the case study and the overall priority by applying the rating scale method and the criteria weights for each criterion.

Table 3 - 8 Total Weight and Overall Priority for the Case Study

Case Studies	Total Weight (R)	Overall Priority	Potential
1	2,381	1,000	Suitable with no design change

The total weight, priority, and part potential are determined. Based on the criterion, the case study benefited from the FDM AM technology, with no design changes required for the first case study.

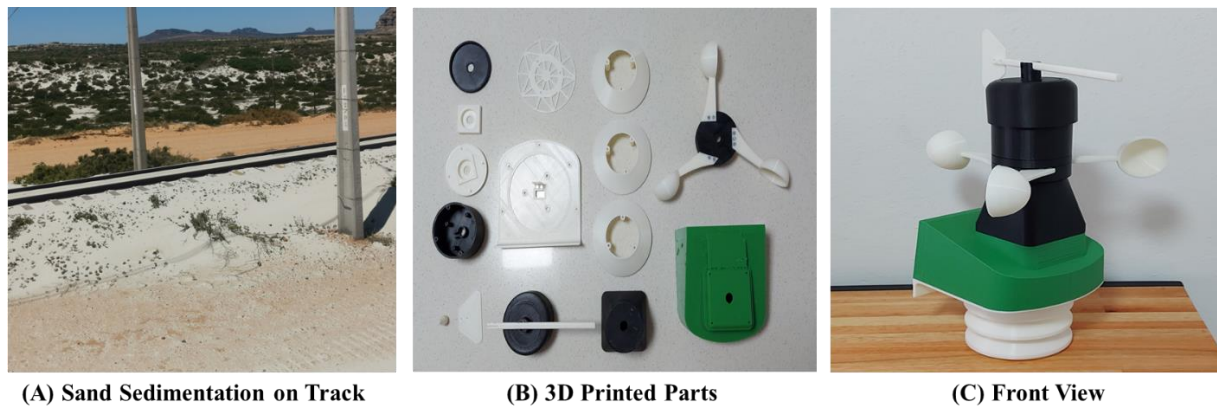


**Figure 3 - 7 3D Printable Low-Cost Weather Station for Track-Specific Measurements [10]**

### 3.4 Chapter Summary

The study presents a new structured technical process to select potential railway-related parts that benefit from FDM AM technology. The Analytic Hierarchy Process evaluates potential parts based on commonly applied criteria identified through literature. The criteria identified through literature include 1) geometric complexity, 2) production volume, 3) part function, 4) part benefit, 5) design optimisation, 6) manufacturing time, and 7) material removal. Weights are assigned to each criterion based on the decision maker's preferences and requirements for the railway environment. The assigned criteria weights are tested by determining the consistency ratio. A consistency ratio of 0.07175 is calculated and is less than the 0.1 criteria. Based on the calculated consistency ratio, the assigned weights are considered consistent. Secondly, the proposed AHP decision model is validated using FDM case studies reviewed by experts and published in the literature. The results showed that the proposed AHP model accurately evaluated the case studies proving its correctness. Lastly, the proposed AHP model evaluates past railway-related parts, components, and products printed using the FDM process for the railway infrastructure and rolling stock equipment. All case studies except the custom tooling and replacement parts for the wayside lubricators were suitable for 3D printing and showed benefits. Finally, based on the proposed model, potential railway-related parts and components can be evaluated and selected in a structured technical approach instead of trial and error.

The AHP methodology uses a single value for the pairwise comparison scale to evaluate two factors simultaneously. In real-world applications, since the level of uncertainty and weight of expert opinion is the main characteristics of the problem, the potential for human error is possible when using the AHP method. To overcome this limitation and allow for more criteria, the fuzzy AHP technique can be used,

which deals with a triangular scale to evaluate the criteria factors. Based on the study, further work in improving the proposed model includes:

- Using the Fuzzy AHP technique to select potential railway-related parts.
- Expand the selection criteria by introducing the part cost and mechanical characteristics of as-printed parts.

# **CHAPTER 4:**

## **CUSTOM INFILL PLACEMENT USING**

### **TOPOLOGY OPTIMISATION AND FINITE**

#### **ELEMENT ANALYSIS <sup>1</sup>**

#### **Abstract**

The study presented in this chapter proposes a method to optimise and improve the internal (infill) structures of FDM 3D printable components. Creating custom infill placements is based on the Bi-directional Evolutionary Structural Optimisation (BESO) technique for topology optimisation. The BESO technique uses a stress criterion from Finite Element Analysis (FEA) results to remove material that experiences non-critical stress due to the loading conditions. The relation between Fused Deposition Modelling (FDM) print parameters, mechanical performance, manufacturability and the BESO technique is established by merging the results using state-of-the-art slicing tools. This allows the generation of custom infill placements, which BESO and FEA influence. Experimental testing is performed on 3D printed test specimens to determine their mechanical characteristics of tensile and flexural responses, compared between test specimens with traditional internal structures to the proposed method of optimised internal structures.

---

<sup>1</sup>Elements of this chapter are based on [125]: Toth AD and Padayachee J, (2022). Using topology optimisation to influence the infill placement of fused deposition modelled parts. Journal of the South African Mechanical Engineers Institution, 1-13



## 4.1 Introduction

Products manufactured using the FDM process builds parts in a layer-by-layer method. The external contours of a 3D printed part are based on the digital model's external contours, while the internal structure (infill) is based on a preselected geometrical pattern available in slicing tools. The infill geometry is traditionally generated using the infill profiles from slicing tools, and its density is linearly increased or decreased depending on the parts application. This limits the ability to dynamically apply infill structures in locations that would experience internal loading. The study in this chapter proposes a methodology to improve the internal material allocation of as-printed parts based on the expected loading the part will experience. This is achieved using FEA and the BESO topology optimisation techniques to dynamically apply infill structures to sections that will experience internal loading conditions. Most research in optimising FDM parts has focused on dimensional accuracy, surface roughness and build time compared to the digitally designed model or the strength of a part based on process parameter changes made in standard slicers such as infill percentage, infill orientation and layer thickness [31], [32], [44], [46]. Creating custom infill placement for FDM 3D printed parts is an advanced design optimisation method. Several studies have investigated potential methods of using topology optimisation and shape optimisation techniques to influence the infill placement of FDM printed parts based on the part's stress [96], [126].

## 4.2 Influencing the Infill Design Using BESO

The objective is to use FEA results to influence the infill placement while ensuring that the external geometry is not altered; it takes the manufacturing constraints of FDM into account, applicable to different types of components, allowing for multi-infill geometry and applying it to different material types.

The method comprises the following stages to achieve an optimised infill geometry placement: 1) model construction, 2) mesh generation, 3) FEA, 4) topology optimisation using BESO, 5) post-processing topology optimised mesh, 6) infill design, and 7) validation. The workflow for creating a custom infill geometry placement for FDM parts is presented in Figure 4 - 1. Figure 4 - 2 illustrates the stages required to achieve the custom infill placement.



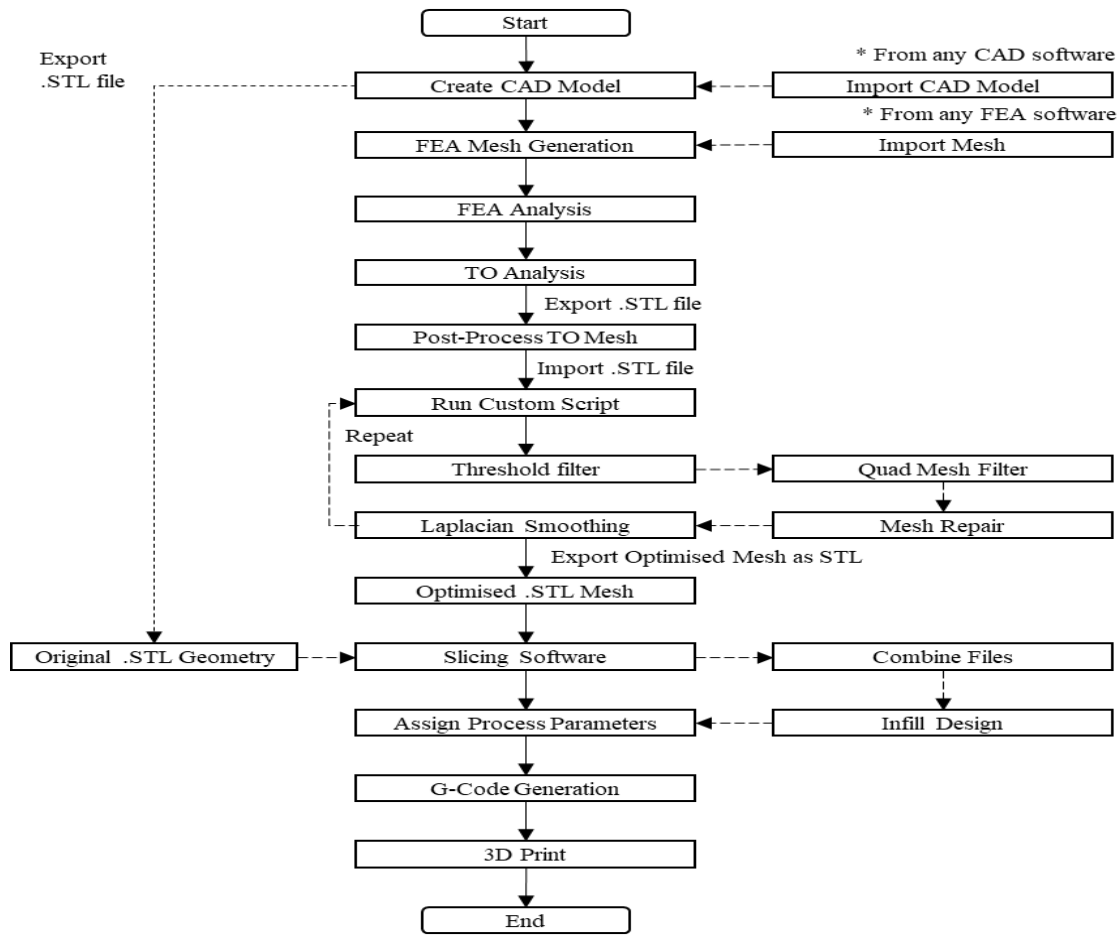


Figure 4 - 1 Custom Infill Placement Workflow

Sections 4.2.1 to 4.2.6 detail the steps proposed to create a custom infill placement using the BESO technique with FEA results and the capabilities of the slicing software (tool-path generator). A grease plate bracket found on wayside rail lubricators is used as an example component to illustrate the proposed methodology.

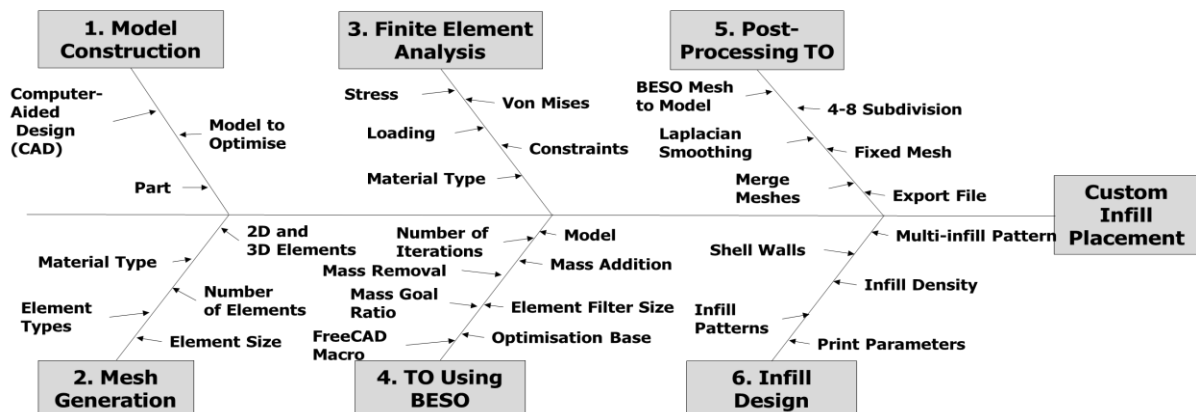


Figure 4 - 2 Stages used to achieve a Custom Infill Placement

### 4.2.1 Model Construction (Stage 1)

The first step in achieving a custom infill placement for a 3D printable part is creating the digital blueprint model representing the part. The computer-aided design (CAD) model is saved in two formats: an STL file and a STEP file. The STL file, which represents the part, is created to preserve the original external shape of the CAD model, which is used during the infill design stage. The STEP file is created to perform structural finite element analyses to determine the expected stresses the part will experience due to the loading conditions. The FEA results are then used to perform the Bi-directional Evolutionary Structural Optimisation (BESO) technique that will remove material from the model which does not experience high stresses. In this study, Siemens NX is used to design and export the required file formats of the CAD model. The .STEP file is then imported into FreeCAD, where the FEA is performed using the native CalculiX solver. Figure 4 - 3 illustrates the different 3D digital file formats of a railway trackside lubricator grease plate bracket.

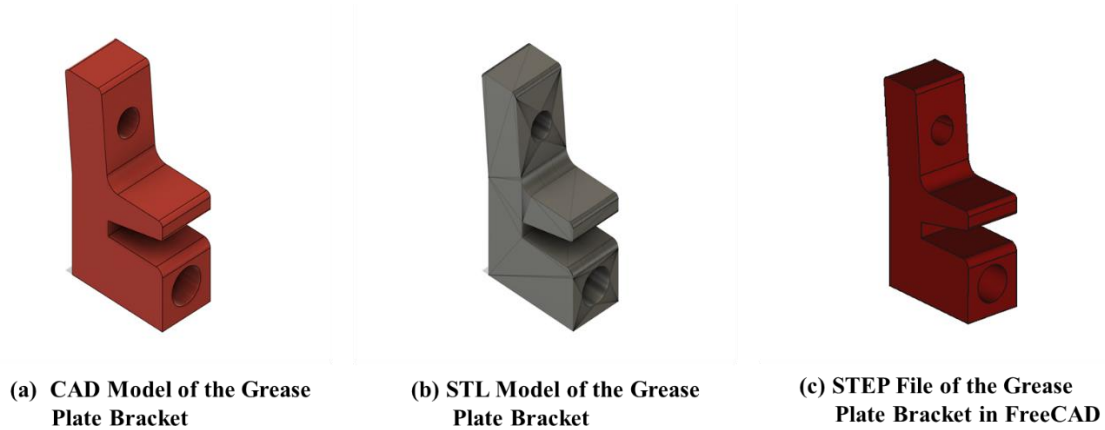


Figure 4 - 3 Digital Models of the Grease Plate Bracket

### 4.2.2 Mesh Generation (Stage 2)

The finite element mesh is created within FreeCAD's FEM workbench using Gmsh [127]. Since the BESO method adds and removes elements based on a stress criterion, the mesh element size and shape determines the final shape of the optimised structure. The Gmsh module can generate 1D, 2D and 3D mesh elements that are either structured or unstructured grids containing lines, triangles, quadrangles, tetrahedra, prisms, hexahedra, and pyramids. Table 4 - 1 illustrates the mesh element shapes associated with structured or unstructured grids. Table 4 - 2 illustrates the 2D mesh algorithms available in Gmsh and FreeCAD, while Table 4 - 3 illustrates the 3D mesh algorithms available in Gmsh and FreeCAD. Figure 4 - 4 illustrates a graphical representation of the 2D and 3D mesh algorithms.

**Table 4 - 1 Gmsh Mesh Element Shapes [127]**

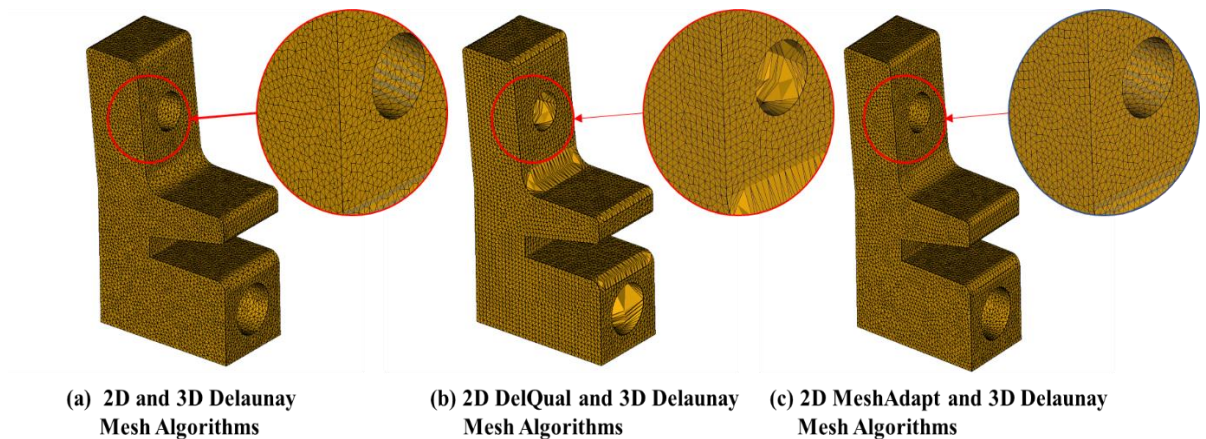
	Unstructured Grid	Structured Grid
2D	Triangles and Quadrangles	Triangles and Quadrangles
3D	Tetrahedra and Pyramids	Tetrahedra and Fully Hexahedral

**Table 4 - 2 Gmsh 2D Mesh Algorithms [127]**

2D Mesh Algorithms	Definitions
MeshAdapt	Makes use of edge swaps, splits, and collapses long edges. The MeshAdapt algorithm is best used with very complex curved surfaces.
Delaunay	New points are inserted sequentially at the circumcenter of the element that has the largest adimensional circumradius. The Delaunay algorithm is best used for large planar surfaces as it is fast and efficient.
Frontal	The Frontal algorithm is best used when a high element quality is required.
BAMG	The BAMG is an experimental algorithm that allows the generation of anisotropic triangulation.
DelQuad	The DelQuad is an indirect algorithm where a triangular mesh is generated first, followed by a merging procedure to produce quadrilaterals. It can quickly generate quadrangles when the triangular elements are merged.

**Table 4 - 3 Gmsh 3D Mesh Algorithms [127]**

3D Mesh Algorithms	Definitions
Delaunay	This is a 3D version of the 2D Delaunay algorithm and functions similarly.
New Delaunay	This is a 3D version of the 2D Delaunay algorithm with additional points inserted.
Frontal	The algorithm is based on the Netgen meshing technique.
Frontal Delaunay	This is a 3D version of the 2D Frontal algorithm and functions similarly.
Frontal Hex	A new efficient algorithm with a parallel reimplementation of the Delaunay algorithm.
MMG3D	An experimental algorithm that generates anisotropic tetrahedralizations.

**Figure 4 - 4 Combination of 2D and 3D Mesh Algorithms on Grease Plate Bracket**

### 4.2.3 Finite Element Analysis (Stage 3)

The finite element analysis is done using the CalculiX solver, which determines a part's Von Mises stress profile to the applied loading condition [128]. The Von Mises stress is used in the BESO technique to add and remove elements that do not experience high-stress levels and are based on a mass ratio. The CalculiX tool can solve linear and non-linear calculations for static, dynamic, and thermal problems. The solver uses the Abaqus input format, which allows it to work with commercial pre-processors. Some of these commercial pre-processors include Nastran, Abaqus and Code-Aster. Table 4 - 4 illustrates the loading and boundary conditions used to determine the structural integrity of the lubricator grease plate bracket, while Figure 4 - 5 illustrates a graphical representation of the FEA results from the simulation.

**Table 4 - 4 Boundary Conditions for Grease Plate Bracket Simulation**

Applied Force	1000 N
Fixed Constraints	0° freedom at the through-holes and slot surface
Material	CalculiX-Steel

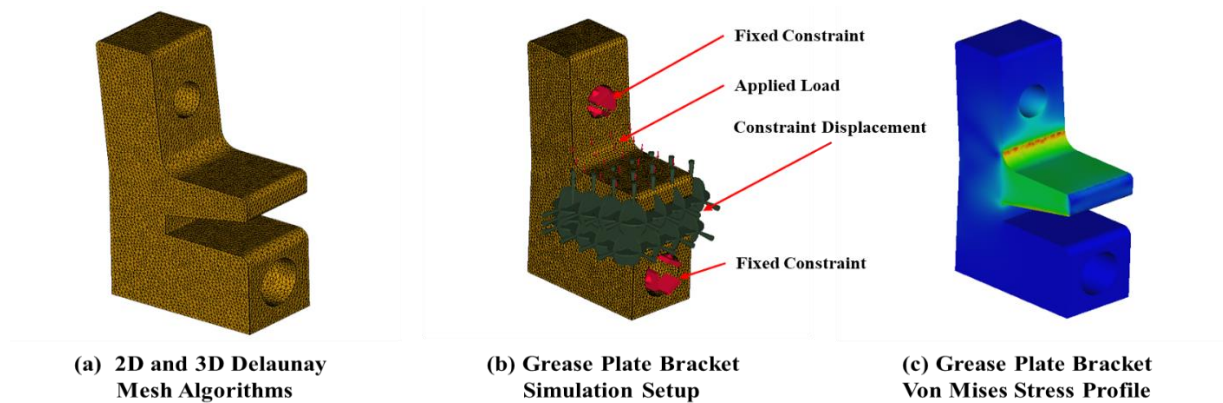


**Figure 4 - 5 Finite Element Analysis Results for the Grease Plate Bracket**

### 4.2.4 Topology Optimisation using BESO (Stage 4)

The software package used for this research study will be the BESO macro available for the FreeCAD software. This tool has been selected due to limitations in commercial software licenses and in accessing the topology optimisation code from commercial packages. Furthermore, the use of the BESO macro illustrates the use of the topology optimisation technique in creating optimised custom infill placements due to FEA results. Future work will apply commercial software tools for railway industry applications [23], [97]. The BESO technique functions by adding and removing the least effective elements in a finite element model (FEM) through several iterative steps. Since the BESO technique is a heuristic method, there is no certainty that the final iteration is the real optimum, i.e. the best result. Given this limitation of validating the BESO technique, the given solution serves as an initial design stage that

informs where material should be removed and where material should be placed to create an efficient and optimised part [129]. A custom-developed python script and graphical user interface (GUI), inspired by the algorithms described in [100], which interfaces with FreeCAD, is used in this study [130]. The script interfaces into FreeCAD's workbench macros which performs the BESO method using the FEM created by Gmsh and the FEA results from the CalculiX solver. The macro performs the BESO method by iterating the removal of elements until the specified stress and mass criterion is achieved. The program's goal is to create lightweight optimal structures using the BESO technique [131]. The custom script, when executed, switches elements from initial high states to lower element states based on a sensitivity number. The element sensitivity number is represented by Equation 4 – 1.

$$\frac{\text{Failure Index}}{\text{Effective Density}} \quad 4 - 1$$

Where the *Failure Index* is equal to the actual stress divided by the allowable stress, which is extracted from the CalculiX solver. The element switching is stopped once the goal mass is achieved. Finally, the results from the tool creates a native FreeCAD FEM graphical file and a .vtk file format for use in visualisation tool kits. Further steps are required to create an STL model from the results file [129]. Table 4 - 5 illustrates the properties of the GUI macro used to perform the BESO technique on the grease plate brackets. Figure 4 - 6 illustrates the BESO technique applied to the grease plate bracket using the custom macro at different iterations.

**Table 4 - 5 BESO Graphical User Interface Options and Definitions [130]**

<b>GUI Options</b>	<b>Description</b>
Select Analysis File	.inp file generated by FreeCAD and CalculiX. The simulation results are used as inputs for the BESO algorithm to work.
Thickness Object	Generated by FreeCAD and Gmsh, mainly when the domain contains 2D shell elements. In this simulation, none is used.
Stress Limit	Adding a specific stress value will stop the BESO iteration process of material removal once the stress limit is reached. In this simulation, no stress limit is added. The full extent of the iterations is generated.
Filter Range	Used to filter the mesh elements and is recommended to be twice the size of the element size used in the FEM.
Optimisation Range	The BESO technique can be used for stiffness and heat problems. In this simulation, the stiffness is selected.
Mass Goal Ratio	The percentage of mass to remain unless the stress limit is reached. A 0.4 mass goal is used.
Generate Conf.	Begins the optimisation process

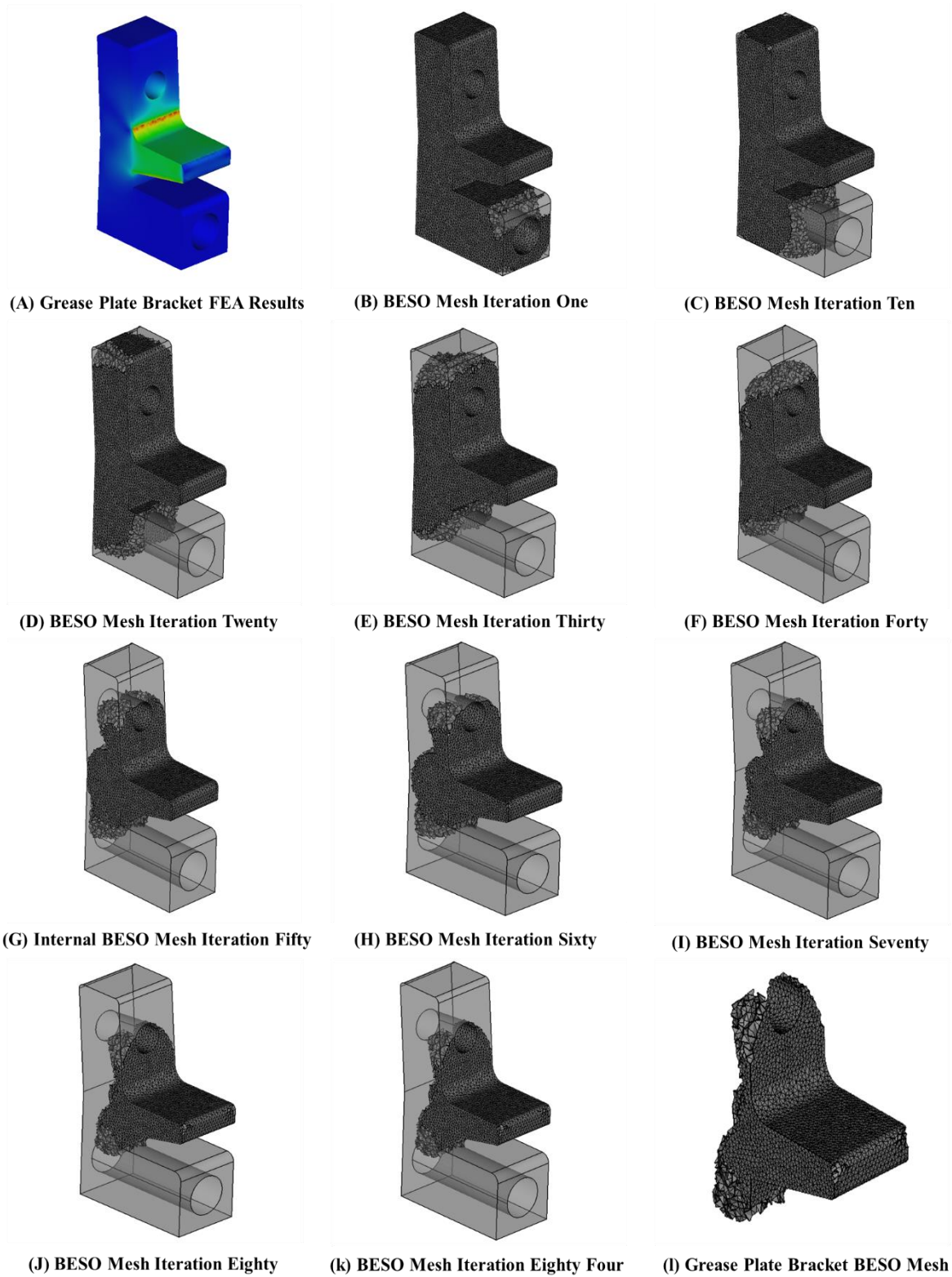


**Figure 4 - 6 BESO Mesh Results for the Grease Plate Bracket**

Several iterations are generated when using the BESO technique. The final BESO-generated mesh is based on the 0.4 mass goal ratio selected for the iteration process. Due to adding and removing mesh elements during the iteration steps, earlier iterations resulted in geometry that is not 3D printable.



#### 4.2.5 Post-Processing Topology Optimised Mesh (Stage 5)

Since the BESO technique provides a final iteration that might not be the real optimum and has other limitations, such as not having a final 3D model, a final manufacturable part, and a solution that is not natively optimised for AM. Additional post-processing techniques are required when using the FDM process to 3D print a topology optimised model. The post-processing stage presents a seamless method to create a manufacturable part using the FDM technology from the visualisation tool kit results generated by the BESO macro. MeshLab [132] is used to post-process the BESO mesh to ensure that the final model is 3D printable using the FDM process. This involves four main steps.

1. Convert the FEM mesh into a tessellated mesh.
2. Convert the tessellated mesh into a geometry mesh.
3. Modify the geometry mesh by changing the mesh elements to quadrilateral elements.
4. Modify the quadrant mesh into a smooth contour profile without reducing the original model's mass or shape.

Figure 4 - 7 presents a basic flow diagram of steps to produce FDM 3D printable parts, while Figure 4 - 8 illustrates a graphical representation of the BESO grease plate bracket mesh being converted into a 3D printable model using the FDM technology.

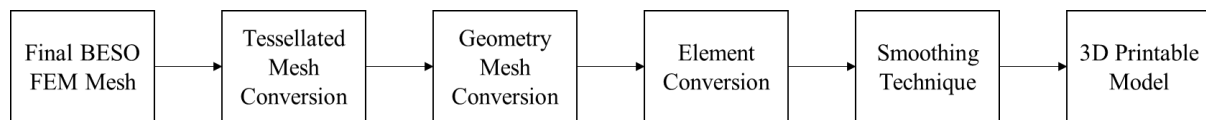


**Figure 4 - 7 Flow Diagram Representing the Steps to Convert the FEM Mesh into a 3D Model**

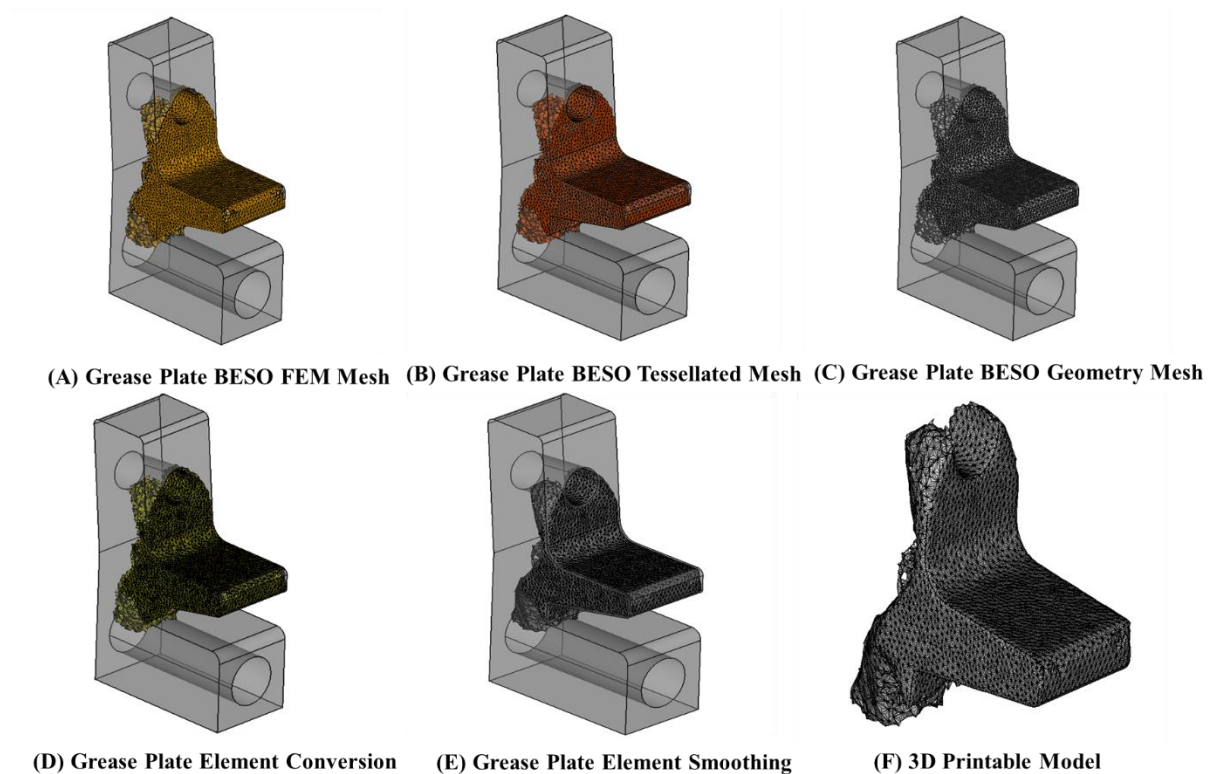


**Figure 4 - 8 Post-Processing the BESO Optimised Mesh of the Grease Plate Bracket**

#### 4.2.6 Infill Design (Stage 6)

The sixth stage involves generating the infill structure and related 3D printing process parameters. To start, both the original CAD model and the BESO structure are imported into the slicer software. In the case of this study, both models are imported into Cura 4.11 as STL files. The process parameters are then assigned for each model. Finally, both models are merged, and the print G-code is created. Using this approach, the BESO structure is assigned a 100 % infill density, while the bracket is assigned a 20 % infill geometry. This combination resulted in a final 3D printed bracket with a weight of 163 g compared to a bracket printed with a 100 % infill density with a weight of 279 g. Using the custom infill placement technique resulted in an optimised bracket that is 58.42 % lighter and a part that is 68.7 % faster to print. Figure 4 - 9 illustrates the flow diagram detailing the steps to perform the infill design, while Figure 4 - 10 illustrates the graphical steps to merge the grease plate bracket models.

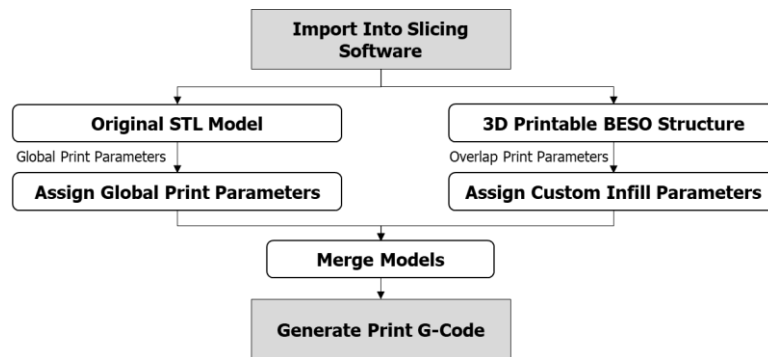


Figure 4 - 9 Infill Design Flow Steps

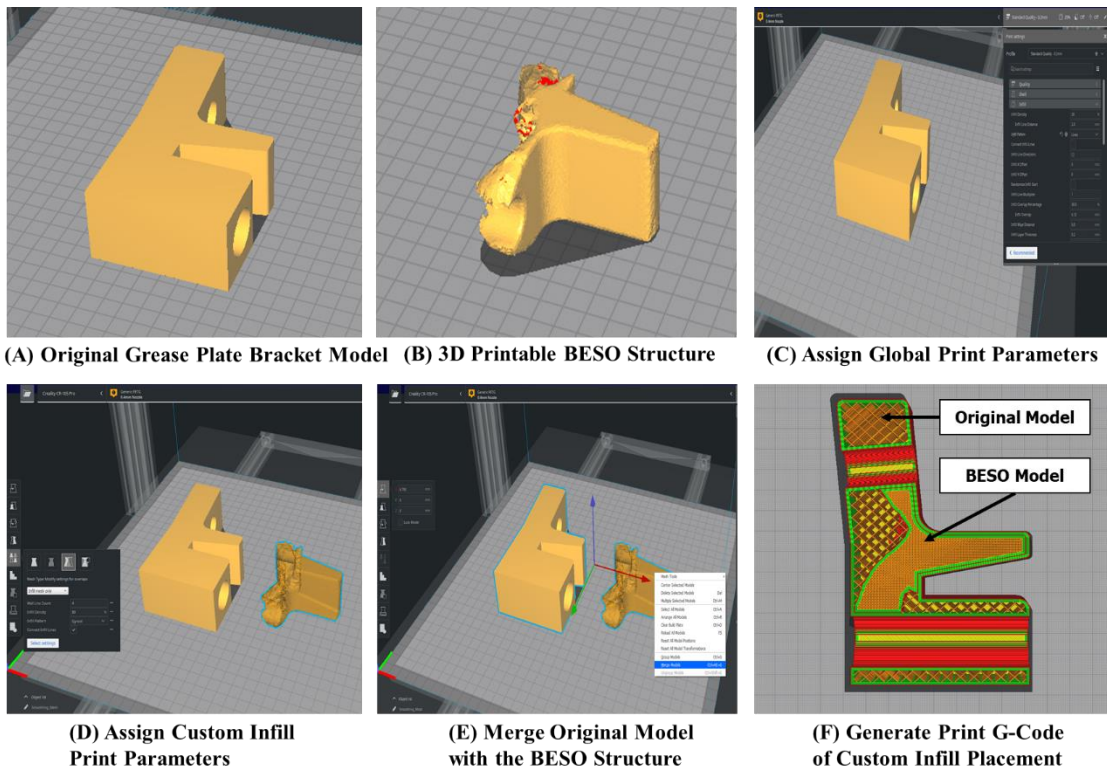


Figure 4 - 10 Graphical Representation of Infill Design



### 4.3 Mechanical Testing: Flexural Response

The BESO technique is used to optimise bending test specimens to determine opportunities in creating a custom infill placement due to a parts stress profile. The experimental study details test setups for three-point bending, three-point offset bending, four-point bending and inverted four-point bending to develop a deeper understanding of the material behaviour. Only the three-point bending and three-point offset bending were performed from the four different test setups. This is due to Covid-19 restrictions, and limited testing capability within Transnet Freight Rail and the University of Kwa-Zulu Natal to perform the four-point bending tests. In determining the flexural response, process parameters match tests guided by research performed by [42], [43], [44], [45], [46] and presented in Chapter 2 of this dissertation. Further, the BESO optimised test specimens have varying infill patterns specific to 3D infill patterns. The results are compared to determine differences between traditional infill structures and the presented custom infill placement method. The steps taken to assign a custom infill placement on the test specimens with internal representations are detailed in Appendix D.

#### 4.3.1 Test Specimen Preparation

The test specimens used in this research study will comply with [7] test methods for flexural properties of unreinforced and reinforced plastics [133]. Two sets of test specimens complying with the recommended standard will be 3D printed. The first set of specimens are printed using the industry-standard infill geometry (rectilinear) with printing parameters based on literature summarised in Chapter 2 of this dissertation [7], [21], [42], [43], [44], [45], [46]. The second set of test specimens will have the custom-generated infill placement based on FEA and the BESO technique. These test specimens will have a multi-infill geometry configuration with all the BESO structures containing 3D infill patterns, and the outer regions will have the rectilinear pattern matching the baseline specimens. Figure 4 - 11 illustrates the sketch and related dimensions of the test specimens.

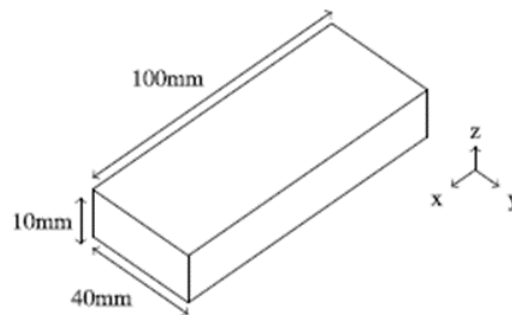


**Figure 4 - 11 Sketch of the Intended Flexural Test Specimen with Dimensions in mm [133]**

A beam undergoing two different loading scenarios is tested to investigate the potential affordance of optimising the infill design using FEA and the BESO method. The three-point bending and offset three-point bending tests are performed with further details presented in Figure 4 - 12.

For this experiment, 100 mm x 10 mm x 40 mm (length x depth x height) beams are tested on a 25 kN Instron machine. The Instron machine is set to provide a linear constraint displacement of  $0.02 \text{ mms}^{-1}$  in the compression direction until the specimen either fails or interferes with the testing equipment. The test specimens are tested to their stress-strain limits to determine comparisons across the full extent of their structural behaviour. The tests are repeated for each case to determine an average set of results. The infill density controls the conditions of the tests, and specimen mass remained constant at 20% and 26 g for all optimised test specimens, respectively. Table D - 8 details the process parameters selected for printing the test specimens, and Table D - 5 provides the amount of deposited material used to 3D print the test specimens. Figure 4 - 14 illustrates the optimised infill structure for each test case.

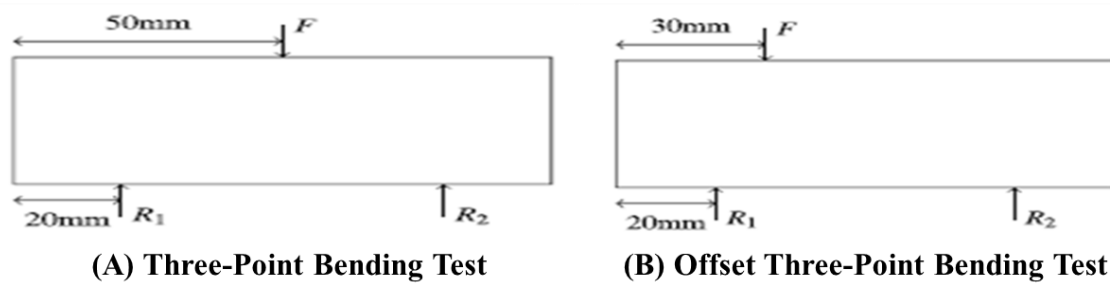
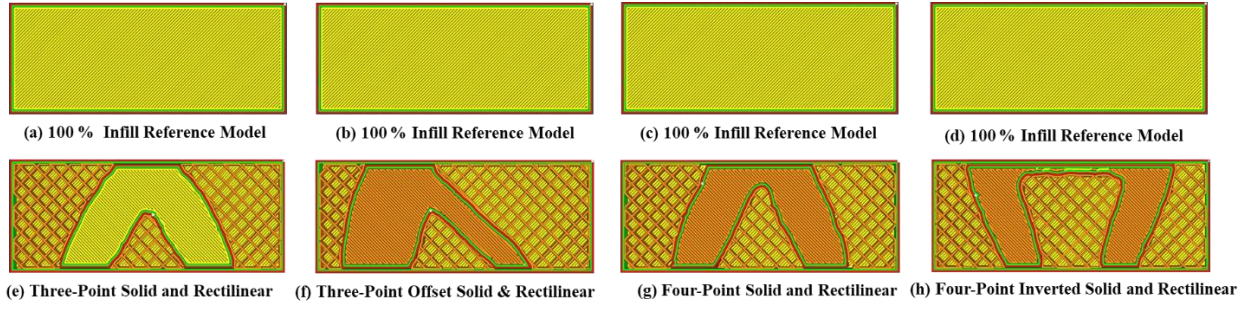


Figure 4 - 12 Illustration of the Test Cases

Table D - 10 through to Table D - 15 in Appendix D printing accuracy of the 3D printed test specimens to the digital models.

#### 4.3.1.1 Infill Design

Figure 4 - 13 illustrates the graphical representation of the first test comparison where the reference test specimen is 3D printed with 100 % infill density and a total mass of 51 grams. In comparison, the BESO optimised infill is printed in 100 % density with a 20 % infill density for the global rectilinear pattern and a total mass of 35 grams. Table D - 6 in Appendix D illustrates the printing parameters for the first test comparison. Figure 4 - 14 illustrates the graphical representation of the second test comparison where the reference test specimen is 3D printed with a 33 % infill density using the rectilinear infill geometry while the BESO optimised structures are printed with a multi-infill geometry combination. All test specimens are printed with a constant mass of 28 grams. Table D - 7 in Appendix D illustrates the printing parameters and infill patterns used to print the test specimens for the second test comparison, while Figure 4 - 14 presents the graphical representation of the various infill geometry configurations.



**Figure 4 - 13 Solid Infill on BESO Optimised Rectangular Test Specimens**

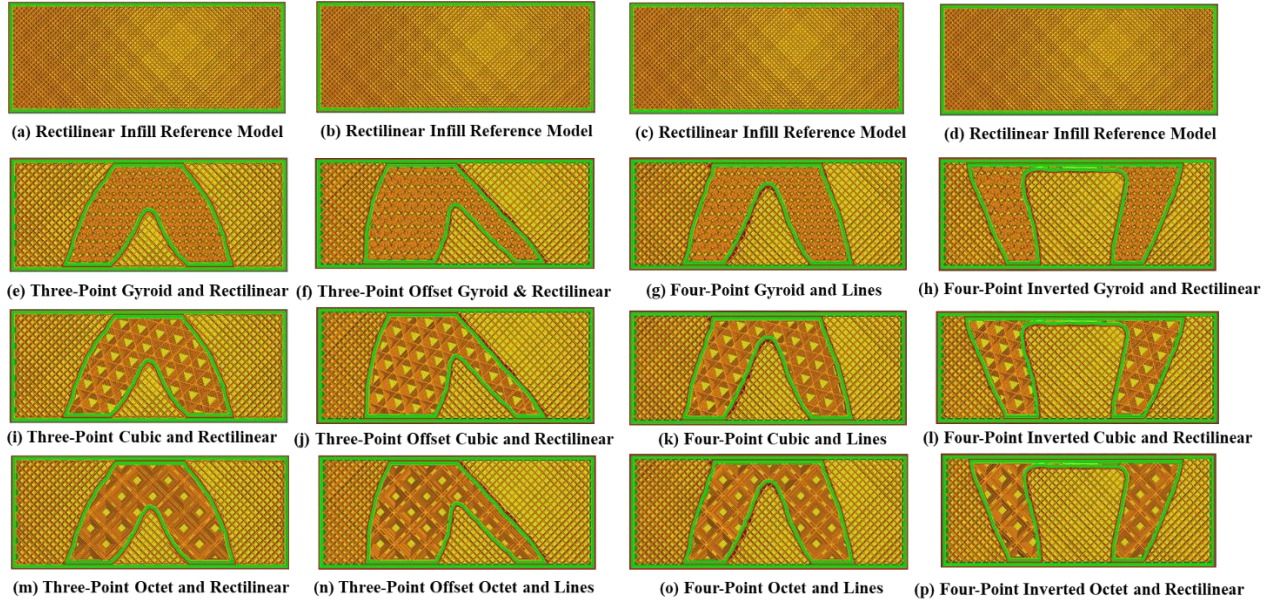


**Figure 4 - 14 Multi-Infill Geometry Design on BESO Optimised Rectangular Test Specimens**

### 4.3.2 Test Results

All flexural test specimens were printed in PETG. Each specimen was inspected for print defects and dimensional correctness. The print accuracy between the digital model and the 3D printed test specimens is presented in Table D - 10 to Table D - 15 in Appendix D. The only print defects visible on the test specimen were the bottom surface, illustrated in Figure 4 - 15. This defect is due to the surface of the 3D printer's bed platform. The identified surface defect was acceptable as it did not show any signs of affecting the test results.



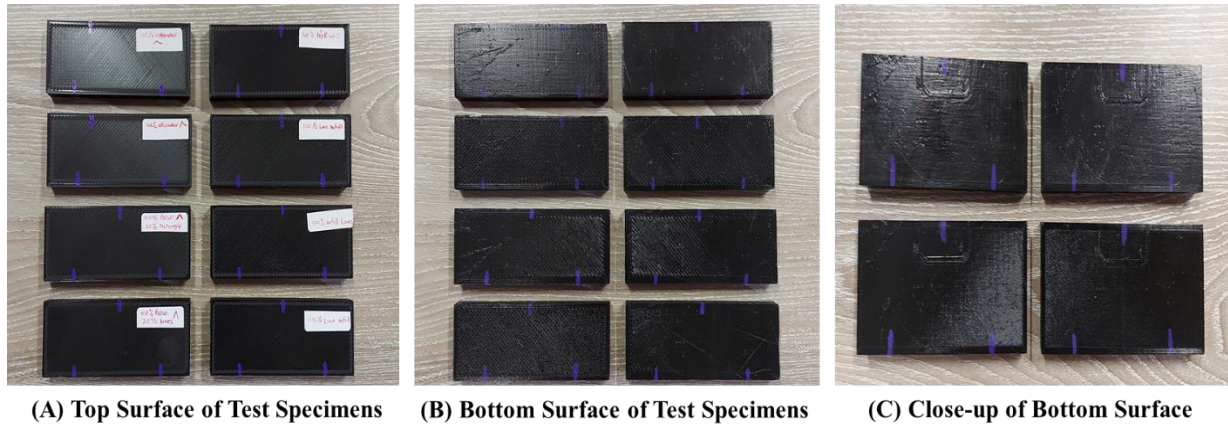


**Figure 4 - 15 Bottom Surface Defect on Test Specimens**

The MTS Criterion Model C45.105 universal tensile tester illustrated in Figure 4 - 16 performed all bending tests in a humidity and temperature-controlled room. The 3D printing material used in the experiment has a high glass transition temperature and low moisture absorptivity. Due to this, the effects of environmental humidity and temperature on the test specimens were assumed negligible when the experiments were performed. Figure 4 - 17 illustrates the fractured test specimens printed solid and optimised using the BESO technique.

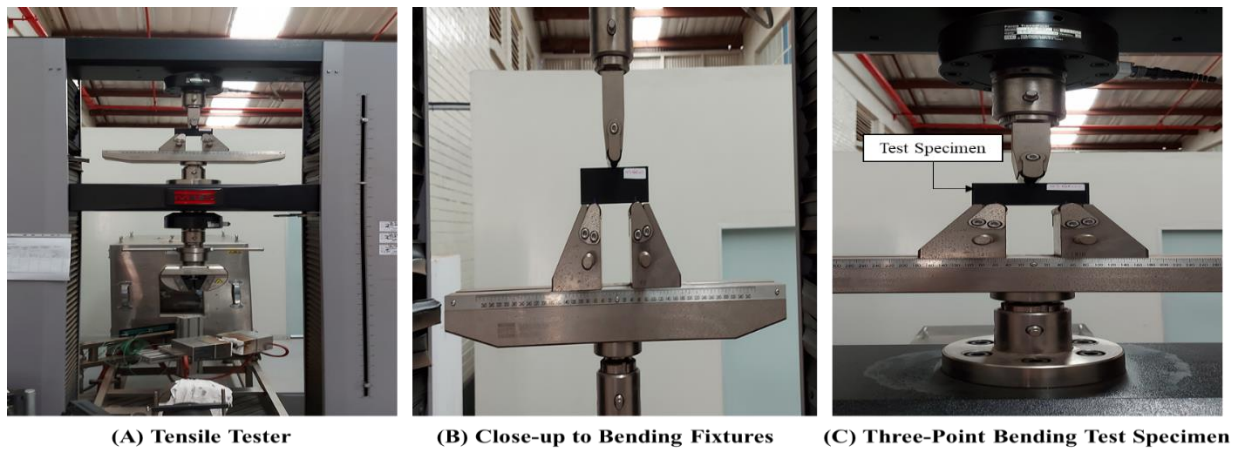


**Figure 4 - 16 Universal Tensile Testing Machine Used in this Investigative Study**

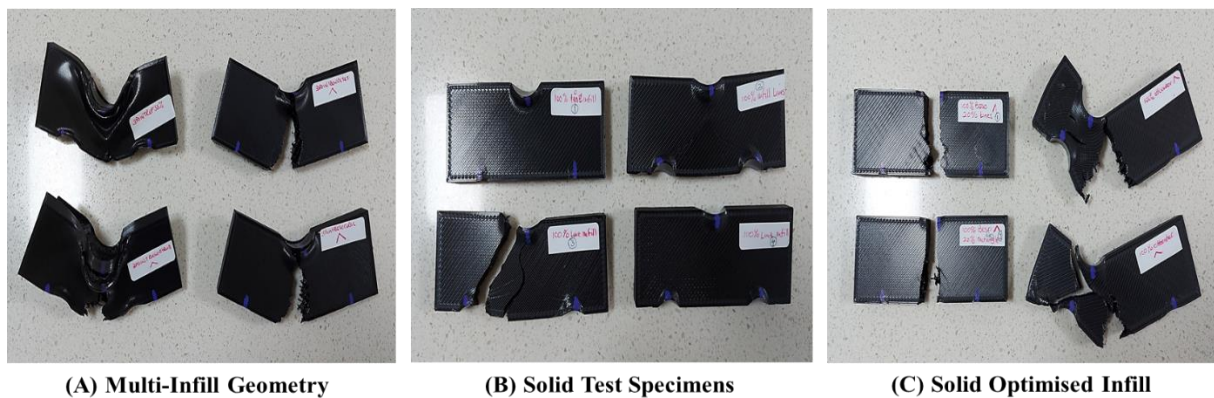


**Figure 4 - 17 Test Specimens Fractured using the Three-Point Bending Tests**

During the bending test, two specimens printed with 100 % infill failed during the three-point bending test. These specimens are noted as “Reference Specimen 1” and “Reference Specimen 4”, which are not included in the results presented. Figure 4 - 18 illustrates the type of failure experienced by these specimens during the testing campaign.

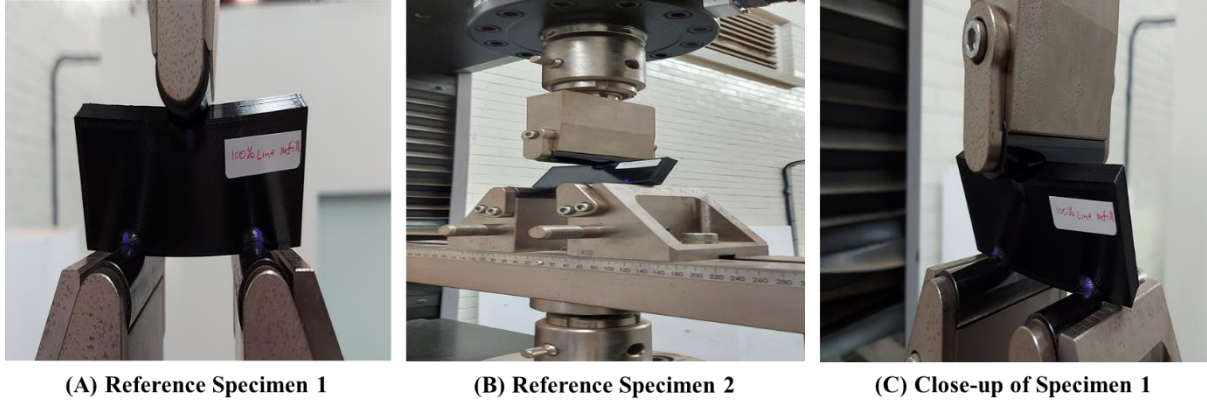


**Figure 4 - 18 Failed Test Specimens During the Bending Test Campaign**

Table D - 17 and Table D - 18 in Appendix D illustrates the summarised results for the three-point bending tests, while Table D - 19 in Appendix D illustrates the relative performance improvement for the optimised infill placement over the rectilinear infill geometry.

#### **4.3.2.1 Force vs Extension Curves**

Two comparative tests have been conducted. The first test compared solid (100 % infill density) rectangular test samples to test samples with a solid infill density based on the BESO optimisation technique. The second test compared test specimens with a multi-infill geometry for the optimised specimens with a specimen with standard rectilinear infill. Both test comparisons were conducted for 3-point bending and 3-point offset bending. Figure 4 - 19 and Figure 4 - 20 illustrate the force-extension results for the three-point bending test comparisons, while Figure 4 - 21 and Figure 4 - 22 illustrates the force-extension results for the three-point offset bending tests.

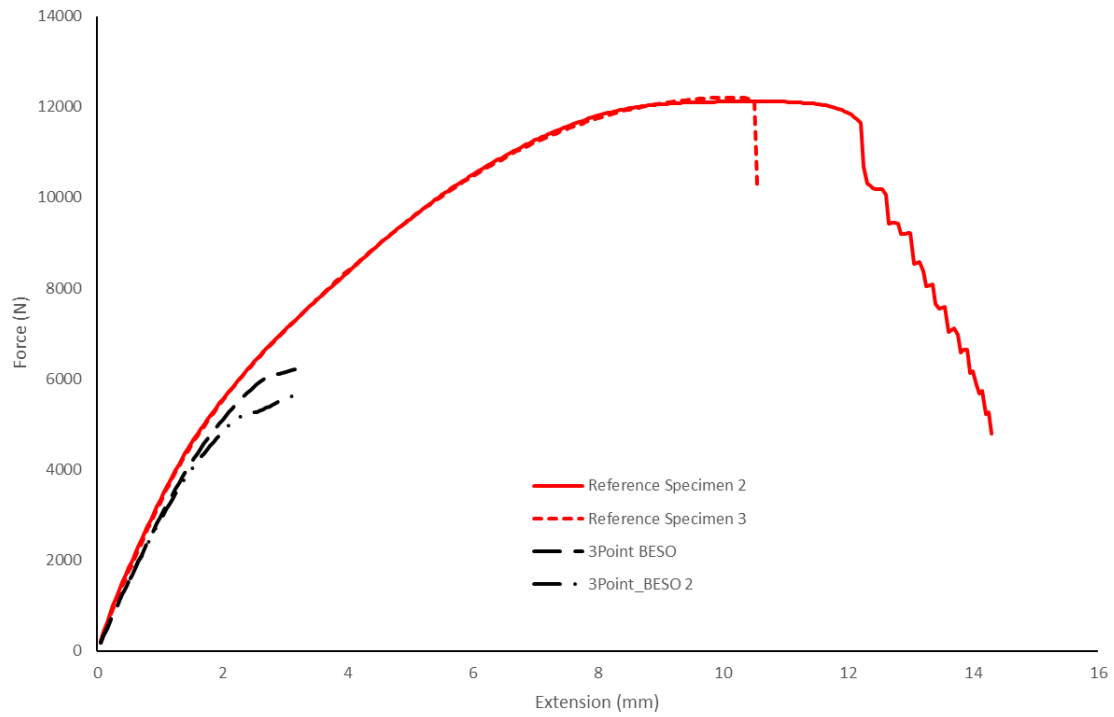


**Figure 4 - 19 Flexural Stress-Strain Curves for Solid Infill Specimens Testing Using the Three-Point Bending**

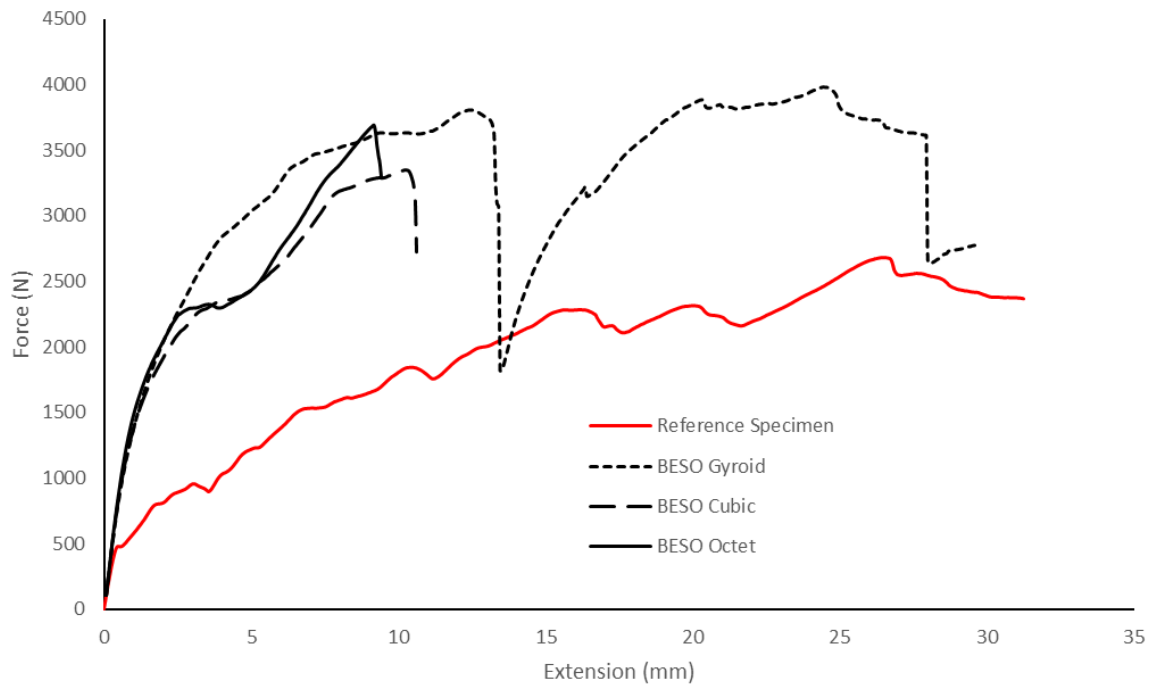


**Figure 4 - 20 Flexural Stress-Strain Curves for Multi-Infill Geometry Test Specimens Using the Three-Point Bending**

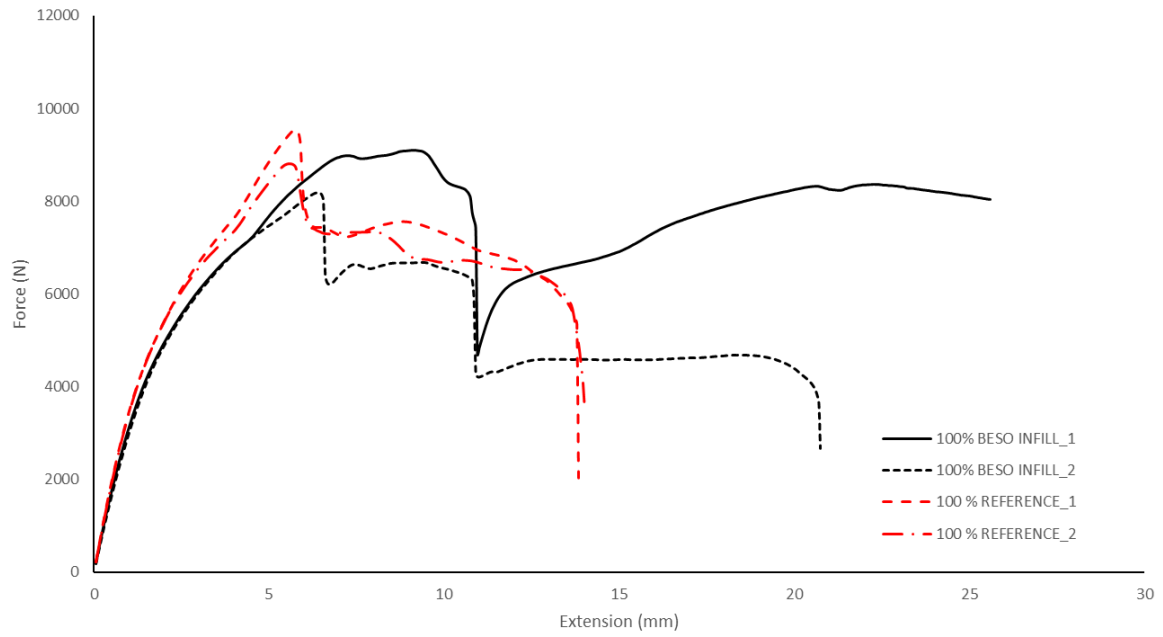


**Figure 4 - 21 Flexural Stress-Strain Curves for Solid Infill Specimens Testing Using the Three-Point Offset Bending**

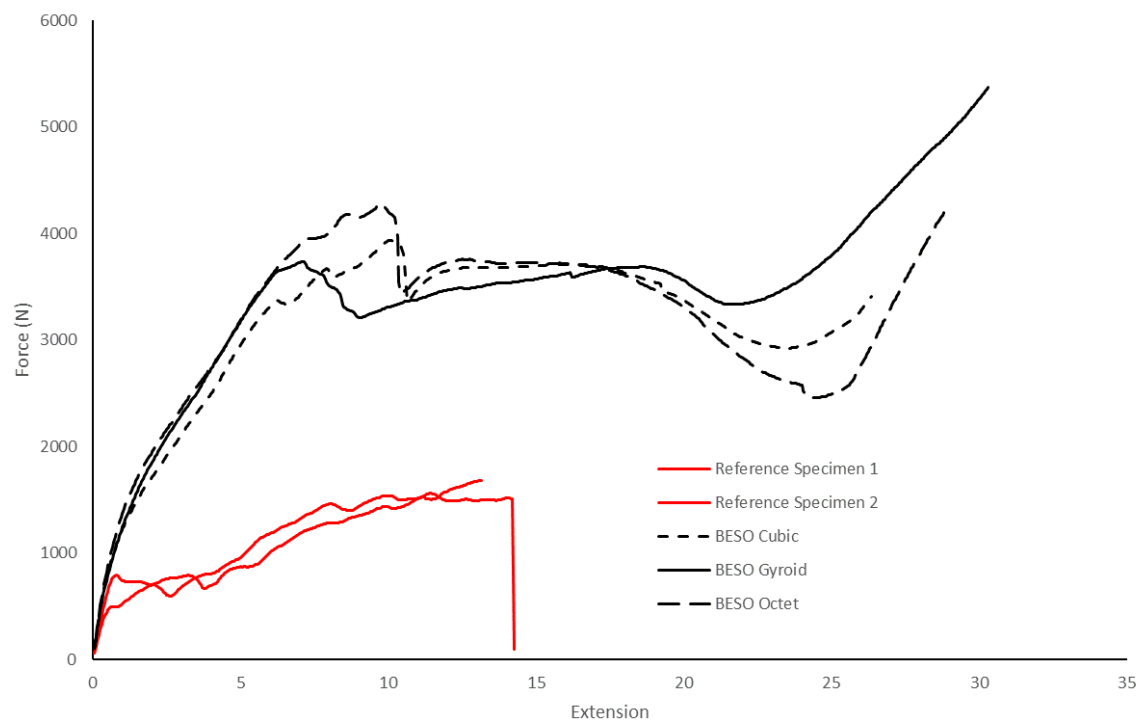


**Figure 4 - 22 Flexural Stress-Strain Curves for Multi-Infill Geometry Test Specimens Using the Three-Point Offset Bending**

### **4.3.3 Discussion**

#### **4.3.3.1 Maximum Loading Capacity**

Based on the first test comparison, it is evident that the solid (100% infill density) test specimens could withstand a larger loading capacity than the BESO optimised infill for three-point bending. The BESO optimised specimens failed before yielding compared to the reference specimens. This is primarily due to the solid and porous infill density configuration. In the case of the three-point offset bending, the solid (100% infill density) BESO test specimens experienced a reduced loading capacity of 6 % with a mass reduction of 32 % compared to the reference solid (100% infill density) test specimen. Based on the second test comparison, it is evident that the custom infill placement using multi-infill geometry produced test specimens capable of withstanding a large loading capacity compared to the traditional rectilinear infill pattern.

#### **4.3.3.2 Maximum Force Extension**

Considering the maximum specimen extension at which the peak force occurs, it can be seen in Table D - 17, and Table D - 18 show that the peak force occurs at a lower strain for all the BESO-influenced infill placements compared to the reference test specimens. The second test comparison, the BESO-influenced infill placement, sees the most significant reduction in the strain at increased peak forces compared to the reference test specimens. The results show that the BESO infill placement with a gyroid pattern tested using the three-point bending experienced a 49 % increase in peak force with a 53 % reduction in strain compared to the reference rectilinear infill specimen. In all cases of the BESO multi-infill geometry, the peak forces are increased with a reduction in strain. This is an essential factor in utilising multi-infill geometry patterns for particular failure modes when a component requires to fail at a particular strain. This allows using multi-infill geometry to design functional components that may require specific operating strains.

#### **4.3.3.3 Beam Stiffness**

In the first test comparison, it is evident that the solid test specimens performed better than the BESO optimised solid infill. Although the BESO optimised solid infill specimens did not match or surpass the reference test specimens, it is essential to note that a stiffness reduction of 11 % was achieved for test specimens which are 42 % lighter compared to the solid reference test specimens. In the case of the second test comparisons, it is evident that the BESO optimised multi-infill geometry specimens outperformed the traditional rectilinear test specimens. The most significant stiffness increase (46 %) is achieved by the BESO Octet infill geometry tested under three-point bending. This highlights the significance of loading scenarios when applying the BESO topology optimisation. The most significant changes in peak loading, strain at peak loading and stiffness can be influenced by applying specific infill geometries and more material at these locations.



#### **4.3.3.4 Energy Absorption**

The BESO optimised test specimens decreased strain energy in all test comparisons. In the case of the three-point offset bending tests, all the BESO optimised test specimens did not experience catastrophic failure but instead began to experience compression. This is due to the placement of the BESO internal structure and the fixture rollers. This confirms that models with a well-defined loading profile might benefit from an FEA-influenced infill design.

#### **4.3.3.5 Failure Modes of Structure**

When considering the failure modes of the specimens tested, some interesting buckling phenomena are experienced across both the BESO optimised and the traditional infill specimens. With the increase in stiffness of the BESO optimised specimens, an increase in brittleness is also experienced. This is evident in the first test comparison between the solid test specimens and the solid BESO test specimens, which is clearly captured in the stress-strain curves illustrated in Figure 4 - 19 and Figure 4 - 21. In the case of the solid test specimens in three-point bending, it must be noted that 'Reference Specimen 1' and 'Reference Specimen 4' failed to be tested correctly on the tensile tester. During the testing process, these specimens slipped off the bending fixture. The solid test specimens that were correctly tested to failure showed ductile bending instead of complete fracture compared to the BESO optimised specimens. The reference rectilinear infill test specimens gradually failed during the testing process. This is illustrated in Figure 4 - 20, Figure 4 - 21 and Figure 4 - 22 by the interruptions in the stress-strain curves, which presents a fail-safe mechanism realising high internal stresses before the whole part fails due to the infill geometry.

In contrast, the BESO multi-infill geometry optimised test specimens presented buckling events in the early stages of the testing process. These illustrate the internal failures where the shell walls, BESO infill geometry and the rectilinear infill patterns connect. The fixtures then settle within the optimised infill structure, where the loading capacity increases once again (Figure 4 - 20, Figure 4 - 21 and Figure 4 - 22). This is evident by the stress-strain curves for the BESO Gyroid test specimens. The consistency of the buckling points for the BESO optimised specimens could support planned and predictable failure modes for parts, which could also assist in the post-failure analysis

#### **4.3.3.6 Summary**

Six key findings were determined from the two test comparisons, with Figure 4 - 23 and Figure 4 - 24 highlighting the key results. All solid test specimens outperformed the BESO infill optimised test specimens in the first test comparison. Secondly, the solid test specimens exhibited ductile material behaviour, while the BESO infill optimised test specimens exhibited brittle behaviour. This result may assist designers in creating functional parts to fail at specific loading and strains. In the second test

comparison, all the BESO infill optimised test specimens outperformed the reference rectilinear infill geometry by supporting larger loads before failure. The BESO infill optimised test specimens provided increased strength based on the topology optimisation and finite element analysis generated by the stress profile. In addition, the peak loading extension for all the BESO infill optimised test specimens were reduced. All BESO optimised infill geometry were stiffer than the rectilinear specimens. Lastly, the combination of gyroid–rectilinear infill geometry withstood the highest loading before failure under three-point bending, while the cubic–rectilinear infill geometry configuration withstood the highest loading under three-point offset bending.

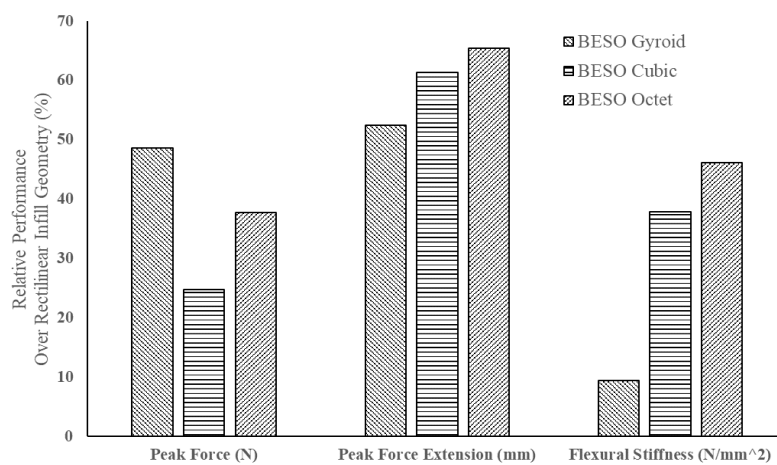


**Figure 4 - 23 Relative Performance Improvement of the Multi-Infill Geometry Specimens in Three-Point Bending**

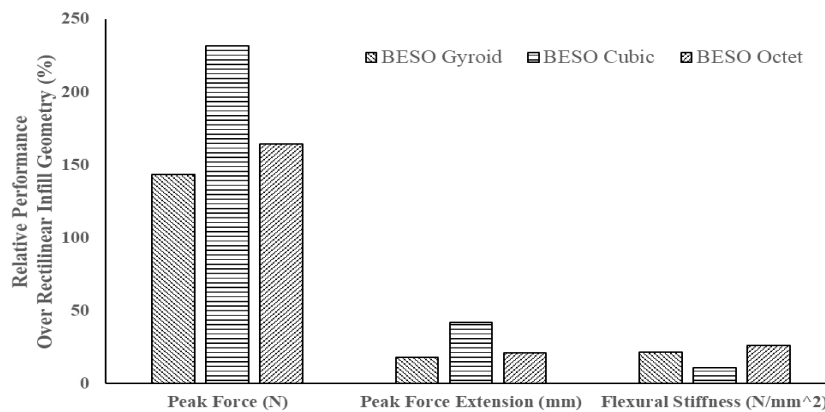


**Figure 4 - 24 Relative Performance Improvement of the Multi-Infill Geometry Specimens in Three-Point Offset Bending**

## 4.4 Chapter Summary

The study presented in this chapter proposed a method to optimise and improve the internal (infill) structures of FDM 3D printable parts based on finite element analysis (FEA) results and using the Bi-directional Evolutionary Structural Optimisation (BESO) technique. A six-stage methodology is presented to achieve a custom infill placement. The BESO technique uses a stress criterion from FEA results to remove material that experiences non-critical stress due to the loading conditions. Since the BESO technique provides a final iteration that might not be the real optimum and has other limitations, such as not having a final 3D model, a final manufacturable part, and a solution that is not natively optimised for 3D printing, using the FDM process, further post-processing techniques are required. The final BESO iteration solution is post-processed into a 3D printable structure using MeshLab. The chapter also presents the steps to apply the six-stage methodology to determine where material should be placed to create an efficient and optimised part. A trackside railway lubricator grease plate bracket is used as an example component to illustrate the methodology. Finally, creating custom infill placements for flexural test specimens is presented in this chapter in preparation for determining the mechanical performance of the custom infill placement methodology. The relation between FDM print parameters, mechanical performance, manufacturability, and the BESO technique is established by merging the results using state-of-the-art slicing tools that allow the generation of custom infill placements influenced by FEA results and the BESO technique. A vital feature of the custom infill placement based on the part's stress profiles is the ability to assign multi-infill geometry combinations, including three-dimensional infill geometries. The proposed process has been experimentally evaluated for rectangular beams under two loading cases, where the generated designs were compared to solid and rectilinear infill geometry. The test showed relative performance increases:

- 49 % increase in peak loading for the gyroid–rectilinear infill geometry combination compared to the standard rectilinear infill pattern under three-point bending tests.
- 66 % reduction in peak force extension for the octet-rectilinear infill geometry combination compared to the standard rectilinear infill geometry in three-point bending tests.
- 46 % increase in flexural stiffness for the octet-rectilinear infill geometry combination compared to the standard rectilinear infill geometry in three-point bending.
- 232 % increase in peak force for the cubic-rectilinear infill geometry compared to the standard rectilinear infill geometry in three-point offset bending tests.
- 143 % increase in peak force for the gyroid-rectilinear infill geometry combination compared to the standard rectilinear infill geometry in three-point offset bending tests.
- Brittle material behaviour for solid BESO infill optimised test specimens in three-point bending.
- More predictable buckling modes for FDM 3D printed parts under bending.

# **CHAPTER 5: RAILWAY APPLICATION: DESIGN OF A FUNCTIONAL 3D PRINTABLE COMPONENT<sup>1,2</sup>**

## **Abstract**

Feasibility studies have been done within the South African railway industry on design optimisation, lightweight structures, complex assembly consolidation, and re-designs for additively manufactured components. The studies have shown that AM can help railway designers create spare or new parts for legacy system designs, measuring gauges, jigs & fixtures, and straightforward tooling for railway infrastructure and rolling stock equipment. The study in this chapter details the selection, new design, manufacture and installation of an additively manufactured functional roof scoop and air vent for a railway inspection vehicle using the fused deposition modelling technology. The roof scoop is designed with an optimised aerofoil profile for streamlining airflow using additive manufacturing techniques. Computational Fluid Dynamic simulations influenced the design and verified the 3D printed roof scoop's improved efficiencies to the existing air vent. Stress plots generated by Finite Element Analysis were used to apply custom topology optimised infill placements to improve the part strength at the mounting regions and determine the optimal 3D printing material based on wind loading conditions and environmental conditions. Further optimisation was performed for the support structure placed on the roof scoop and air vent to reduce manufacturing lead times, tooling and part replacements.

---

<sup>1</sup> Elements of this chapter are presented in [134]: Toth AD, Padayachee J and Vilakazi S, 2021, Additive Manufacturing: Producing Functional Parts for the South African Railway Industry, International Heavy Haul Association, China, 1 – 9 and in [125]: <sup>2</sup>Toth AD and Padayachee J, (2022). Using topology optimisation to influence the infill placement of fused deposition modelled parts. Journal of the South African Mechanical Engineers Institution, 1-13,

## 5.1 Background

### 5.1.1 Case Study: Roof Scoop and Air Vent

The current railway passenger vehicles used by Transnet Freight Rail to perform infrastructure inspections and track-related maintenance activities are the inspection trolleys shown in Figure 5 - 1. Transnet designed, manufactured, and maintained these railway vehicles in the 1990s. “Due to the legacy design, spare parts and replacement components have become limited and difficult to source. This is due to company closures, discontinued service parts, and long lead times. The roof scoop and air vent installed on the inspection vehicles' roof is one such part. A recent mechanical failure of the roof scoop due to environmental conditions motivated the creation of a replacement part using additive manufacturing technology.” [10]

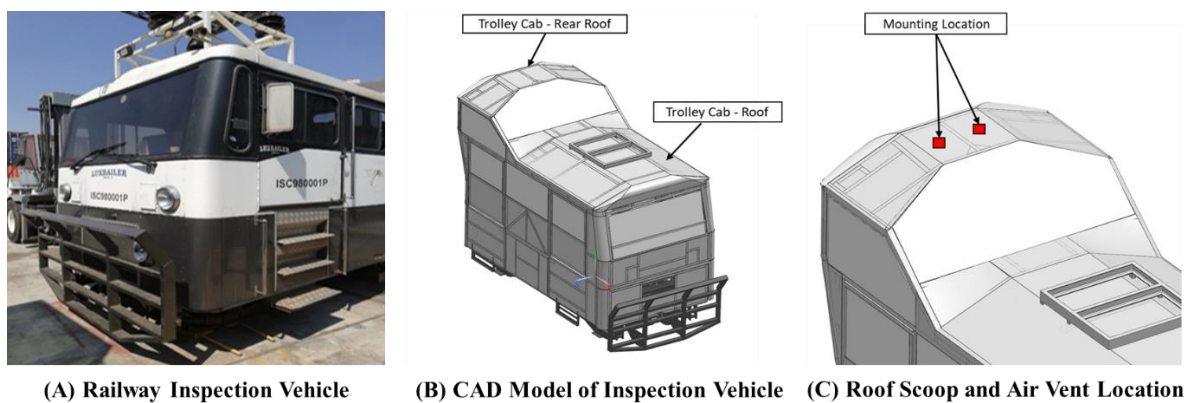


Figure 5 - 1 Railway Inspection Vehicle

The roof scoop and air vent unit are located at the rear end of the trolley's roof and were installed after the initial trolley design was approved. These vents were installed to improve ventilation and reduce heat within the passenger trolley cab. This is achieved by allowing hot air from the cab to exit while allowing cool air to enter. The design of the vent system also prevents dirt and dust from entering the cab. Figure 5 - 2-A illustrates the original air vent, and Figure 5 - 2-B illustrates the failed unit. Since no digital models existed, reverse engineering methods were used to create the original roof scoop. Reverse-engineered models of the original scoop were used with simulations to evaluate new design modifications.

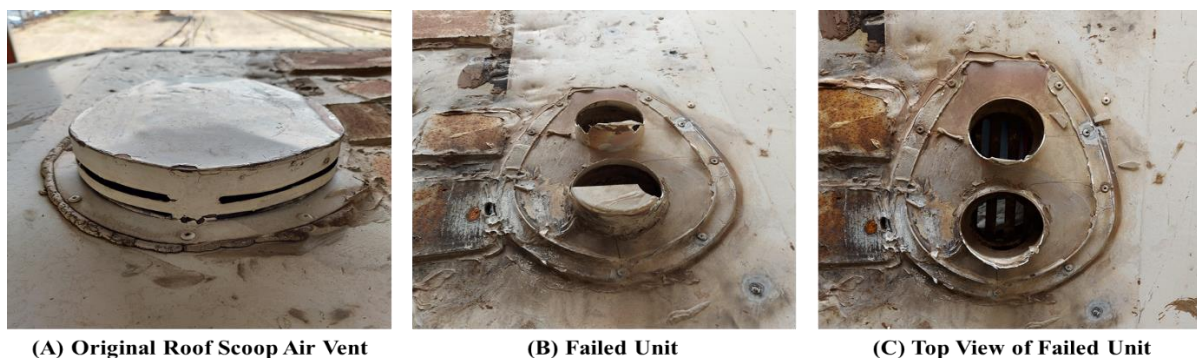


Figure 5 - 2 Failed Roof Scoop and Air Vent

### 5.1.2 FDM Functional Part Workflow

To realise a functional 3D printable roof scoop and air vent, the parts are evaluated through a design workflow presented in Figure 5 - 3. First, the parts are evaluated to determine whether they will benefit from the Fused Deposition Model (FDM) Additive Manufacturing (AM) technique. Once the parts are identified, the existing components are reverse-engineered, where three conceptual designs are produced. The conceptual designs are then evaluated using the Pugh matrix method to select a final design. Design optimisation methods are applied to the designed model based on the digital and physical manufacturing workflows. Further design optimisation methods are applied to support material and the custom infill design process. The roof scoop and air vent are manufactured using the FDM process, where the final parts are visually inspected and installed onto the railway inspection vehicle.

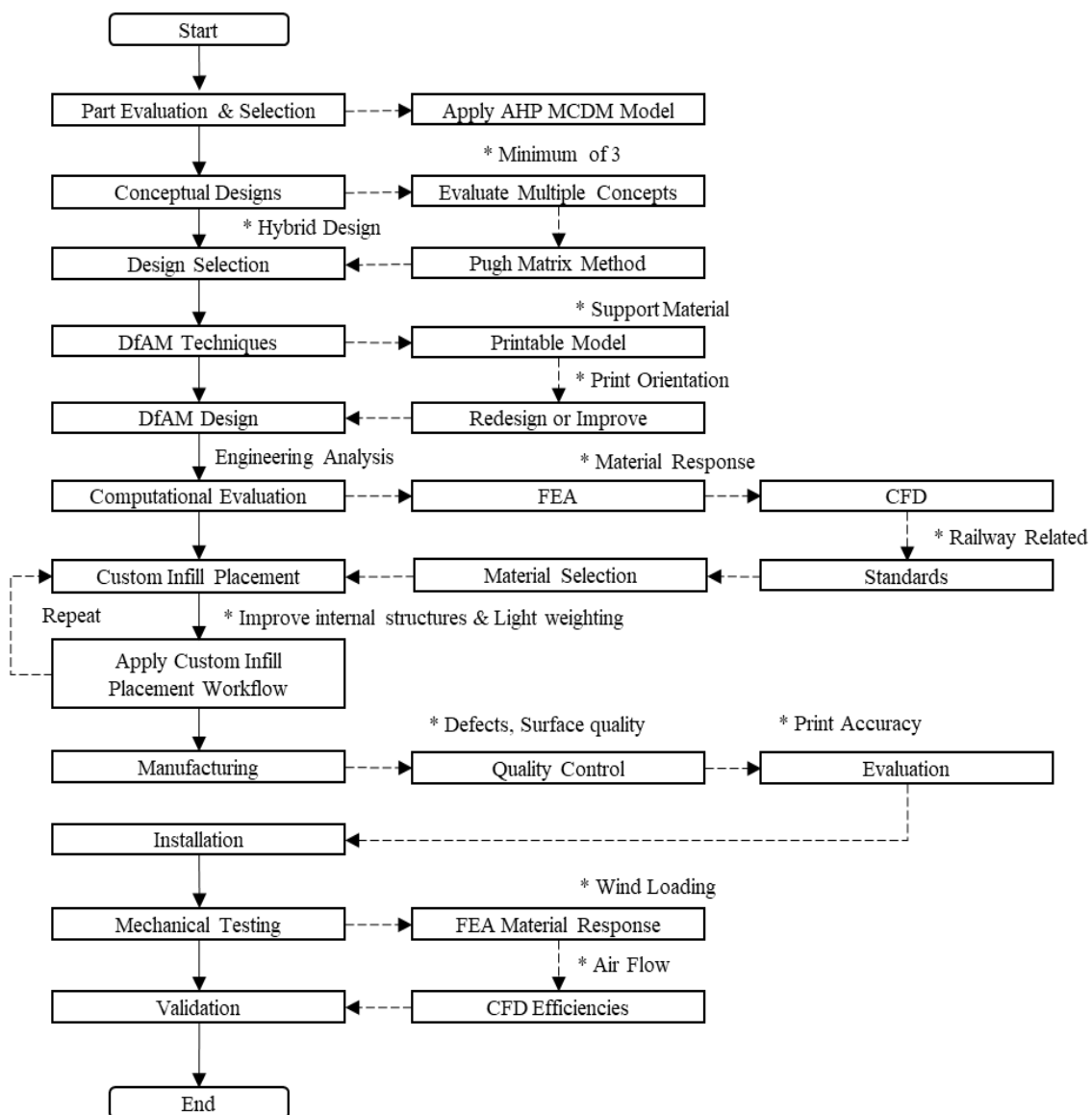


Figure 5 - 3 Workflow to Select, Redesign, Optimise and Manufacture of Functional 3D Printable Roof Scoop and Air Vent

### 5.1.3 MCDM AHP Model Evaluation

The proposed MCDM AHP model evaluates whether the roof scoop and air vent components are potential parts that will benefit from the FDM AM technology. Table 5 - 1 illustrates the qualitative evaluation of the existing roof scoop and air vent parts, while Table 5 - 2 illustrates the quantitative evaluation. Table 5 - 3 presents the total weight (R) for the roof scoop and air vent and the overall priority by applying the rating scale method and the criteria weights for each criterion.

**Table 5 - 1 Qualitative Evaluation of Part Candidate Case Studies**

	Geometric Complexity	Production Volume	Part Benefit	Function	Design Optimisation	Manufacturing Time	Material Removal
Criteria Weights	0,317	0,201	0,148	0,151	0,104	0,044	0,036
Case 1: Roof Scoop and Air Vent	Medium	Low	Medium	Critical	Medium	Medium	Low

**Table 5 - 2 Quantitative Evaluation of Part Candidate Case Studies**

	Geometric Complexity	Production Volume	Part Benefit	Function	Design Optimisation	Manufacturing Time	Material Removal
Criteria Weights	0,317	0,201	0,148	0,151	0,104	0,044	0,036
Case 1	2	1	2	3	2	2	1

**Table 5 - 3 Total Weight and Overall Priority for the Case Study**

Case Studies	Total Weight (R)	Overall Priority
1	1,916	1.000

Based on the total weight (R), the score is within the range that the part will benefit from the AM process but will require some design changes to ensure that the model is optimised for printing and the efficiencies are improved.

## 5.2 Digital Manufacturing Workflow

### 5.2.1 Reverse Engineering

The existing roof scoop and air vent installed on the inspection vehicle do not have a 3D model. Due to this, reverse engineering methods are performed to determine the basic dimensions used to create a CAD model. The existing roof scoop will be used as a template to design a new 3D model. Table 5 - 4 illustrates the existing roof scoop and air vent features, while Figure 5 - 4 illustrates the critical dimensions.

**Table 5 - 4 Features of the Original Roof Scoop and Air Vent**

Feature	Description
Vents	Two
Height	60 mm
Material Grade	Heavy-Duty Applications - ABS
Rivets	Around location

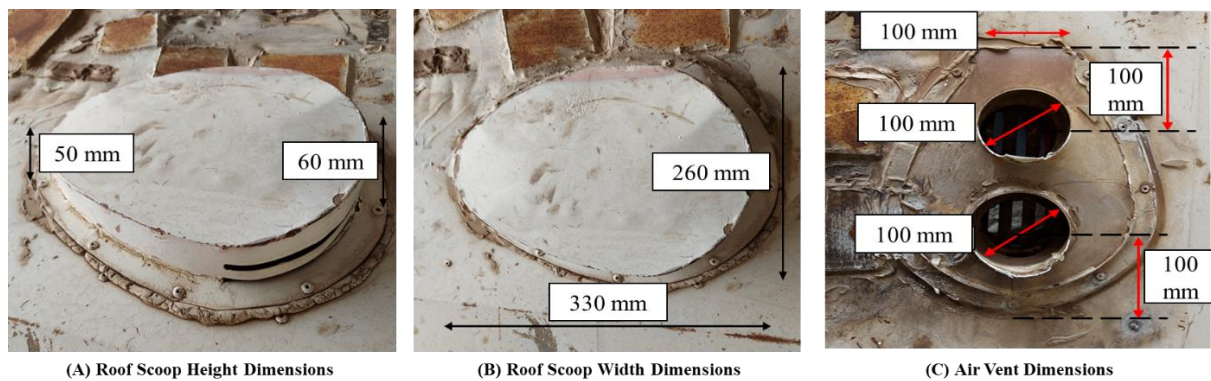


**Figure 5 - 4 Original Roof Scoop and Air Vent Dimensions**

A parametric roof scoop 3D model design is constructed using the dimensions in Figure 5 - 4. Figure 5 - 5. The CAD model will be used in developing conceptual designs for a new air vent design, and structural and CFD simulations will be applied to the selected conceptual design to optimise the design. Design for additive manufacturing techniques will then be applied to the finalised digital model to optimise the air vent for AM.

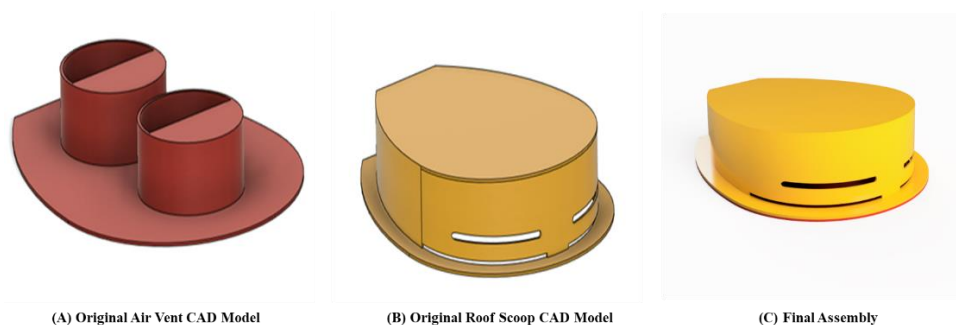


**Figure 5 - 5 Reverse Engineered Original Roof Scoop and Air Vent**



### 5.2.2 Conceptual Designs

Three conceptual ventilator designs (static, rotational and aerofoil) were developed for the intended replacement roof scoop and air vent. The static ventilator, illustrated in Figure 5 - 6, is a simple case cover vent with six inlet vents and a large rectangular base that allows air to flow into the cabin. The rotational ventilator, illustrated in Figure 5 - 7, was designed to capture wind and enter the cabin while spinning. Finally, the aerofoil ventilator, illustrated in Figure 5 - 8, was designed with a modified streamlined NACA 2414 aerofoil profile and a single channel opening to allow air to enter the cabin.

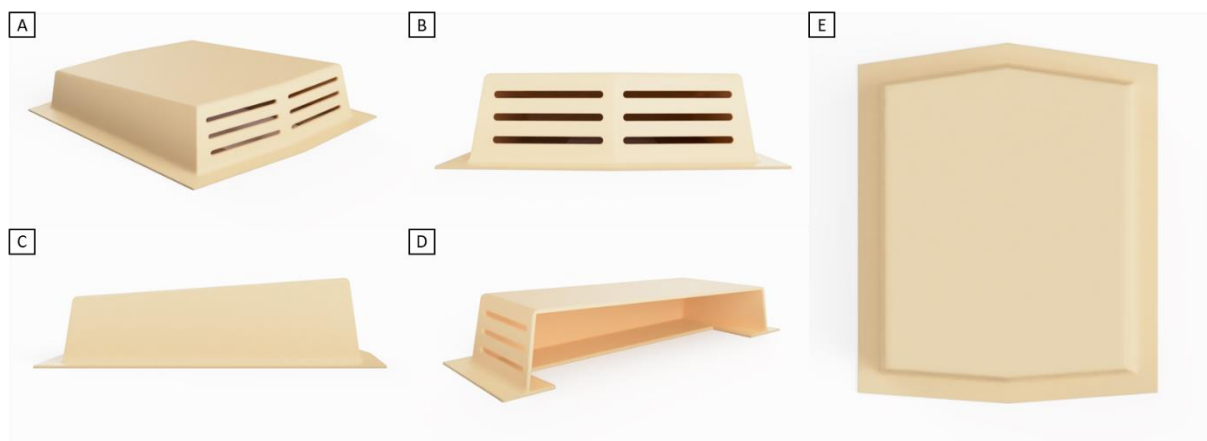


Figure 5 - 6 Concept 1 Isometric View (A), Front View (B), Right View (C), Cross-Section View (D), Top View (E)



Figure 5 - 7 Concept 2 Isometric View (A), Front View (B), Right View (C), Cross-Section View (D), Exploded View (E)



**Figure 5 - 8 Concept 3 Isometric View (A), Front View (B), Right View (C), Cross-Section View (D), Exploded View (E)**

Table 5 - 5 illustrates the strengths and weaknesses of the different conceptual designs.

**Table 5 - 5 Strengths and Weaknesses Associated with the Conceptual Designs**

Concept 1		Concept 2		Concept 3	
Strengths	Weaknesses	Strengths	Weaknesses	Strengths	Weaknesses
Compact	Aerodynamics	Compact	Multiple Components	Aerofoil Design	Complex Shape
Single Part	Air Intake & Exit	Small Form	Very Small	Compact	Printability
Large Form	Printability	Air Exchange	Wear	Simple Design	Insert Failure

### 5.2.3 Design Selection

The Pugh Matrix (PM) method assessed the conceptual designs. The Pugh Matrix is a decision tool that iteratively evaluates several design candidates, leading to the concept that best meets a set of criteria. The Pugh Matrix's additional benefits are its ability to qualitatively optimise alternative concepts by generating a final hybrid design [135]. The criteria for evaluating the ventilator concepts were based on the intended application's engineering requirements and specifications. Table 5 - 6 illustrates the criteria used.

**Table 5 - 6 Design Criteria used in the Pugh Matrix [134]**

Criteria	Requirement	Criteria	Requirement
Safety	Design of parts	Eco-friendly	Material type
Complexity	3D printing and manufacturing	Efficiency	Airflow
Durability	AM material	Ergonomics	Design of parts
Implementation	Installation and printing of design	Potential Wear	Design, material, and manufacturing
Printability	Design, material, and manufacturing	Cost	Material, manufacturing, and time

As illustrated in Table 5 - 7, a Pugh decision matrix determines the appropriate conceptual model based on the criteria. The matrix is designed with standard guidelines used in mechanical design for additive manufacturing. Each criterion is given a priority 1 to 5 (1 = low, 2 = standard, 3 = high, 4 = very high, and 5 = extremely high) as well as a quality rating on a scale 1 to 5 (1 = worst, 3 = fair, 5 = good, 8 = very good, and 10 = excellent). The weighted average is then multiplied by the priority weighting value by the quality rating, with these values summed to find the proposed design's total rating. Both concept one and concept three have equal score ratings. Due to this, the final design will incorporate the positive aspects of the conceptual designs together. This approach will generate a suitable product that will be printable and reliable.

**Table 5 - 7 Pugh Decision Matrix for the Conceptual Designs**

Criterion	Weighting	Concept 1	Concept 2	Concept 3
Safety	4	3(x4)	2(x4)	3(x4)
Complexity (Shape)	4	4(x4)	5(x4)	4(x4)
Durability	5	7(x5)	6(x5)	7(x5)
Implementation (Location)	4	4(x4)	3(x4)	4(x4)
Printability	4	4(x4)	5(x4)	4(x4)
Eco-friendly (Material)	3	5(x3)	6(x3)	5(x3)
Efficiency	5	7(x5)	5(x5)	7(x5)
Ergonomic Design	4	5(x4)	4(x4)	5(x4)
Potential Wear	4	5(x4)	7(x4)	5(x4)
Cost	4	5(x4)	4(x4)	5(x4)
<b>Total</b>	<b>350</b>	<b>196</b>	<b>184</b>	<b>196</b>

A final hybrid design using elements from each concept was selected based on the Pugh Matrix. The roof scoop design is a two-part system designed using design for additive manufacturing techniques [11]. The roof scoop and the air vents incorporate a modified NACA 2414 aerofoil profile [136], optimised for AM. Figure 5 - 9 illustrates the final design.

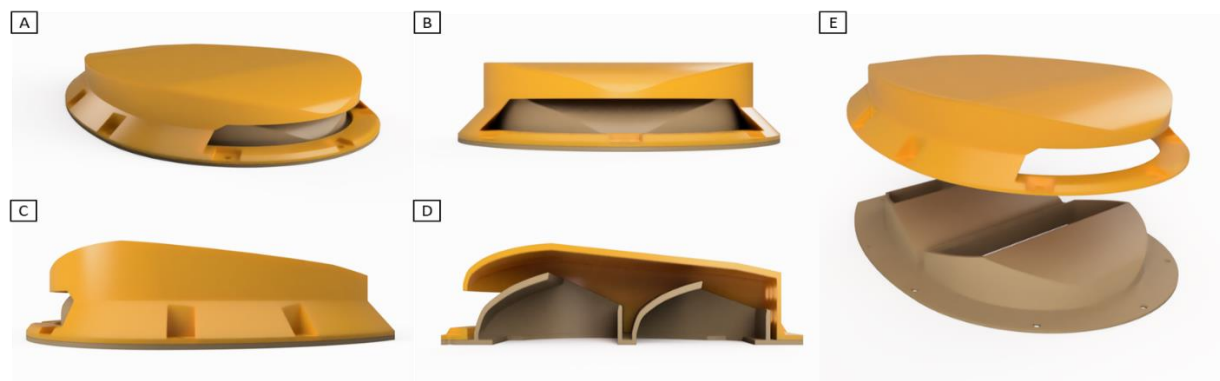


**Figure 5 - 9 Selected Design Isometric View (A), Front View (B), Right View (C), Cross-Section View (D), Exploded View (E) [134]**

### 5.2.4 Railway Engineering Standards

Designing new components for railway assets requires strict compliance with railway standards. Unfortunately, standards for 3D printable components are limited or only produced for specialised materials in industries such as aerospace or medical. In designing the 3D printable roof scoop and air vent, railway standards on traditional manufacturing and design methods were used with increased safety factors. Table 5 - 8 illustrates the railway standards that influenced the engineering analysis for the roof scoop and air vent design.

**Table 5 - 8 Railway Standards Used in Study [134]**

Standards	Title
BS EN 12663-1:2010	Railway Vehicle Coordinate System
BS EN 12663-1:2010	Structural Requirements of Railway Vehicle Bodies (part 1)
BS EN 14067:2003	Aerodynamics
Transnet Track Manual	Clearance for railway vehicles

Standard BS EN 12663-1:2010 recommends evaluating new designs by comparing existing and new products' performance efficiencies using computational software. This approach will evaluate the 3D printable roof scoop and air vent.

### 5.2.5 Computational Fluid Dynamics Simulations

Two Computational Fluid Dynamic (CFD) simulations using FlowEFD were conducted on the trolley with the roof scoop attached. The first simulation investigated the original design, while the second investigated the new 3D printable design. Figure 5 - 10 illustrates the 3D model mesh generated for the CFD simulation. A high refinement level is created at the roof scoop region to determine the appropriate flow region. The same mesh generation is used for both CFD simulations. The simulations were based on the recommended vehicle speed and the standards presented in Table 5 - 8 to determine the pressure, wind velocity and airflow on the roof scoops' geometrical designs. The results from the analysis were compared to determine differences. Table 5 - 9 presents the properties used in the simulations. Figure 5 - 11 and Figure 5 - 12 illustrate the CFD simulations for the original and 3D printable roof scoop, while Table 5 - 10 presents the final results from the analysis. The CFD simulation results show a clear difference in airflow patterns between the two designs. The new design illustrates improved streamlined flow due to the profile design and reduced shear stresses experienced on the body. It also allows a larger air volume to enter the cab via the air vents than the original design. Knowing the internal flow is essential in determining the efficiency of the new roof scoop and air vent design. A CFD simulation,

illustrated in Figure 5 - 13, was performed on the new roof scoop design's internal chamber based on the properties determined in Table 5 - 10, while Table 5 - 11 presents the results of the CFD analysis.

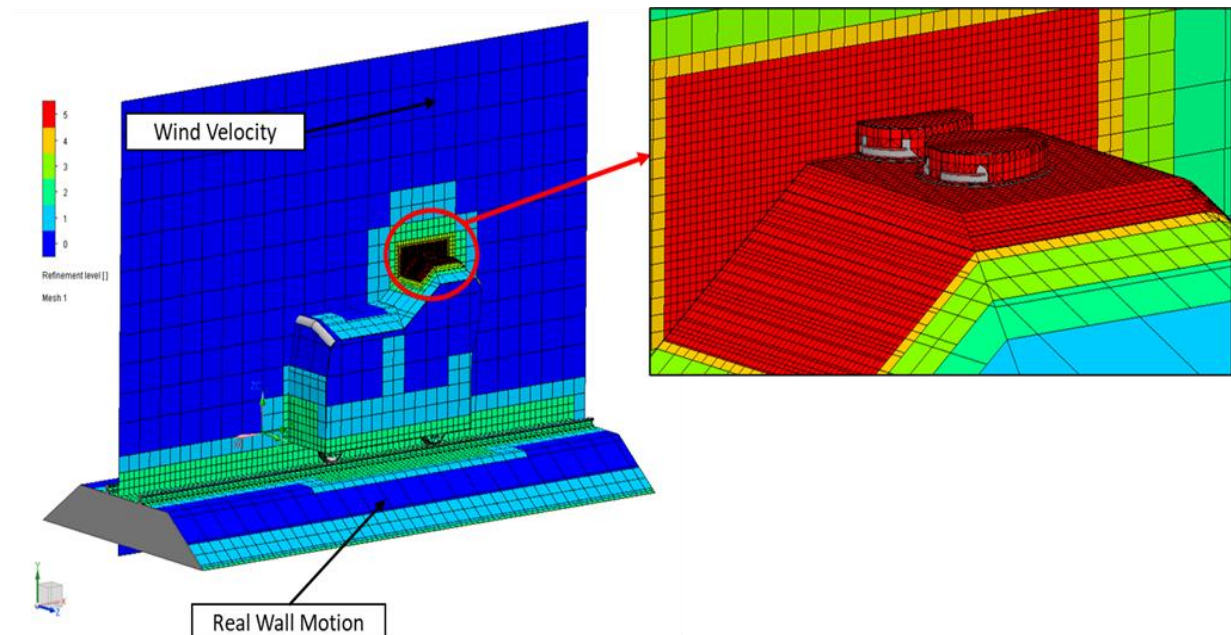


**Figure 5 - 10 CFD Mesh Generation for the Inspection Trolley**

**Table 5 - 9 CFD Simulation Details [134]**

Computational Domain	8 m <sup>3</sup>
Fluid	Air Gas
Flow Type	Laminar and Turbulent
Analysis	External Surface with Internal Space and Cavities
Wall Thermal Condition	Adiabatic
Wall Roughness	0 micrometres
Pressure	101325 Pa
Temperature	293.2 K
Wind Loading ((x-direction))	100 km/h or 33.33 m/s
Real Wall Motion	Applied to rails – Speed of 100 km/h or 33.33 m/s
Turbulence Intensity	0.1 %
Global Mesh Settings – Resolution Level	4
Local Mesh Settings – Small Solid Feature Refinement Level	3
Local Mesh Settings – Tolerance Level	2
Local Mesh Settings – Maximum Channel Refinement	2



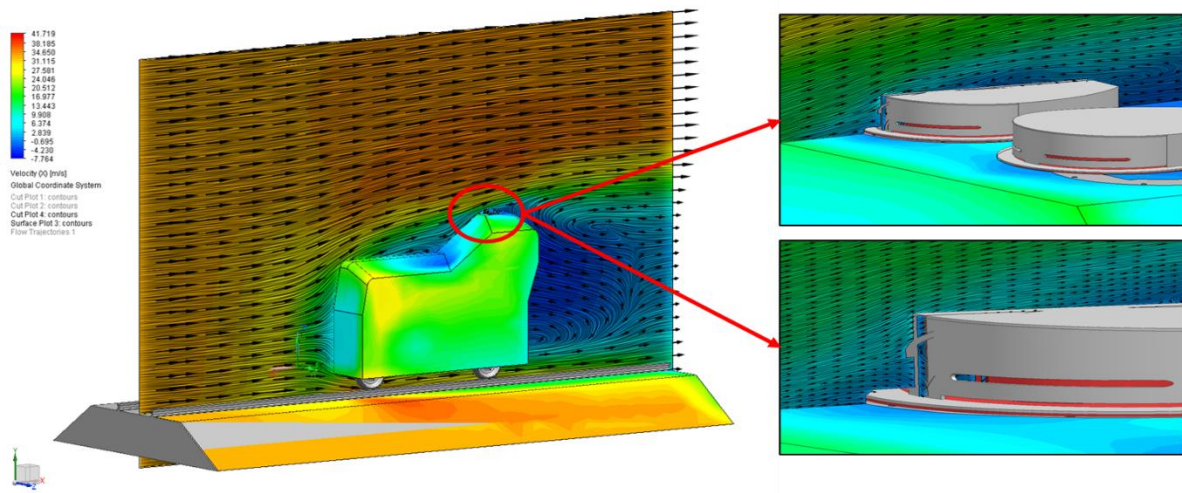


Figure 5 - 11 Wind Flow Experienced at the Roof Scoop Region for the Original Design [134]

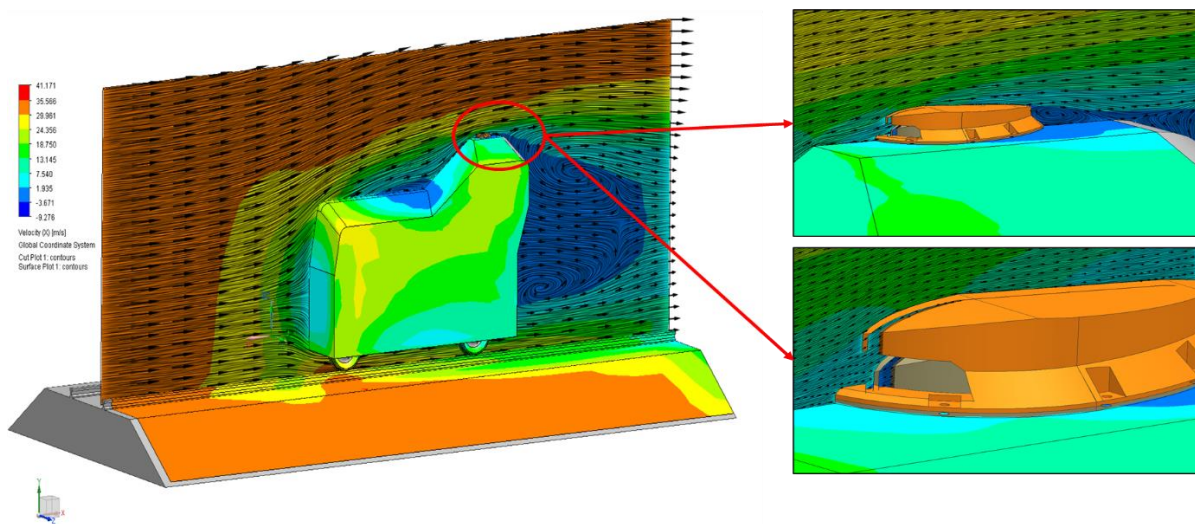
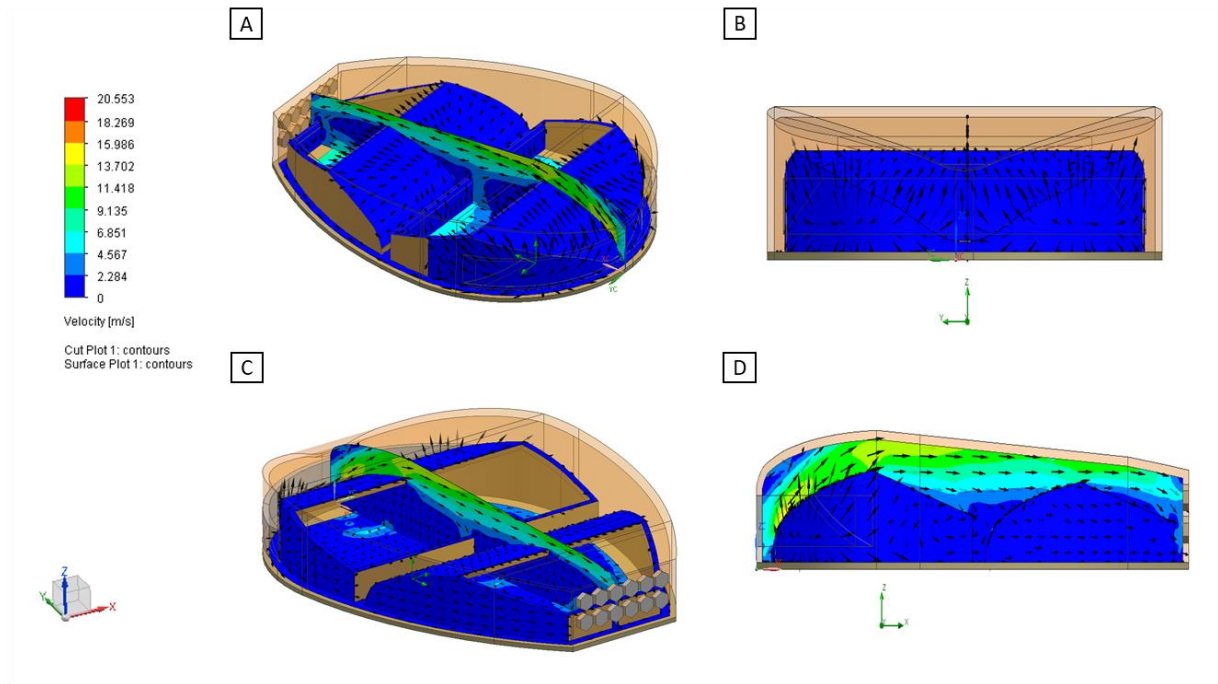


Figure 5 - 12 Wind Flow Experienced at the Roof Scoop Region for the New Design [134]

Table 5 - 10 Final Summarised CFD Results for the Roof Scoop and Air Vent

Final Results: Original Roof Scoop Design	
Force	38.226 N in the X direction at the surface of the Roof Scoop
Total Pressure	101.324 kPa Along the surface of the Roof Scoop
Shear Stress	8.21 Pa
Wind Velocity	4.52 m/s or 16.27 km/hr in the X direction
Final Results: New Roof Scoop Design	
Force	24.366 N in the X direction at the surface of the Roof Scoop
Total Pressure	101.668 kPa Along the surface of the Roof Scoop
Shear Stress	6.71 Pa
Wind Velocity	4.52 m/s or 16.27 km/hr in the X direction



**Figure 5 - 13 Wind Flow Inside the Roof Scoop Air Vent Isometric View (A), Front View (B), Rear Isometric View (C), Sectioned Left View (D)**

**Table 5 - 11 Summarised Results for the Internal Roof Scoop and Air Vent**

Combined Force	0.721 N
Torque	0.043 Nm
Total Pressure	101.539 kPa
Relative Pressure	186.59 Pa
Shear Stress (Z-direction)	5.82 Pa
Shear Stress (x-direction)	3.19 Pa
Internal Flow Velocity	2.28 m/s or 8.2 km/hr (Based on Trolley Travelling at 100 km/hr)

### 5.2.6 Finite Element Analysis

A Finite Element Analysis (FEA) was performed using the Siemens NX software package to determine the structural performance of the roof scoop and air vent based on the output from the CFD analyses. These simulations were performed to determine the expected stresses and critical regions based on the geometry of the air vent and the 3D printing material properties. Silicon adhesion was used to mount the underside of the roof scoop to the roof of the trolley, and standard 6.5 mm diameter pop rivets were used to fix the components to the roof permanently. Figure 5 - 14 illustrates the loading surfaces applied to the roof scoop, while Table 5 - 12 and Table 5 - 13 provide the loads with a safety factor (SF) of 5 and boundary conditions for the structural simulation. Figure 5 - 15 illustrates the boundary conditions applied to the roof scoop geometry. Table 5 - 14 provides the final results.

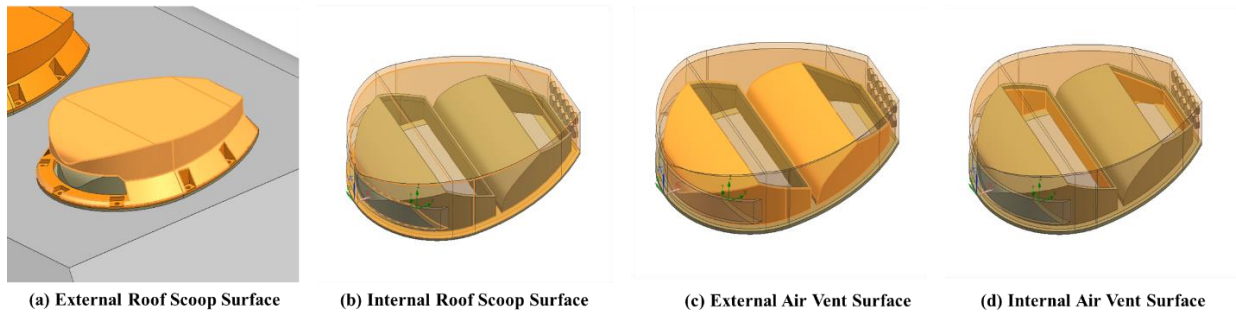


**Figure 5 - 14 Loading Applied to Surface Regions**

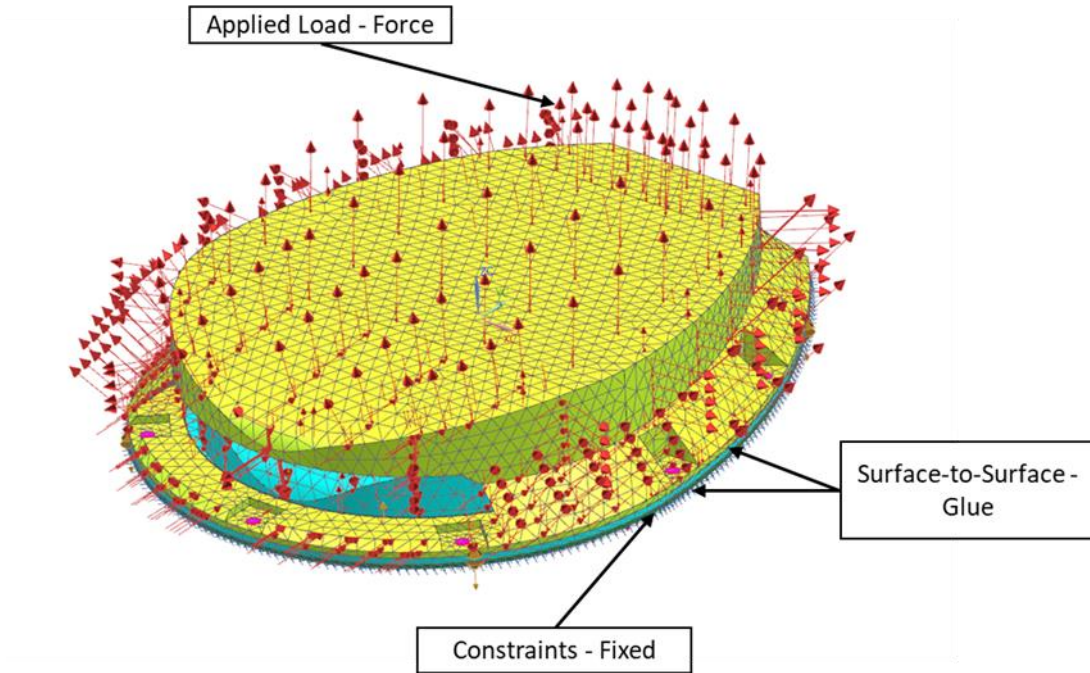


**Figure 5 - 15 Structural Simulation Boundary Conditions**

**Table 5 - 12 Structural Surface Region Loading Forces**

Surface Region	Measured Force (N)	SF Force (N)
External Roof Scoop (A)	23.607	118.04
Internal Roof Scoop (B)	0.430	2.15
External Air Vent (C)	0.467	2.38
Internal Air Vent (D)	0.008	0.4

**Table 5 - 13 Structural Simulation Details**

Element Used	CTetra(10)
Element Size	6 mm
Material	PETG
Applied Load	Table 7
Constraint	Fixed, Surface-to-Surface Gluing



**Table 5 - 14 Final Summarised Results for Roof Scoop**

Von Mises Stress (Roof Scoop)	1.009 MPa
Von Mises Stress (Air Vent)	0.0673 MPa
Von Mises Stress (Rivet Joints)	0.0083 MPa
Maximum Principal Stress (Roof Scoop)	0.915 MPa
Maximum Principal Stress (Air Vent)	0.0377 MPa
Displacement	0.660 mm

The simulation results showed that the geometry and material selection for the roof scoop and the rivets were adequate for the intended application. The results show that the stresses experienced by the roof scoop and the air vent while the inspection trolley travels at 100 km/hr are far below the material yield strength. It must be noted that all inspection trolleys are restricted to travel on the railway network at 80 km/h. Figure 5 - 16, Figure 5 - 17 and Figure 5 - 18 illustrate the expected Von Mises stress, displacement and the maximum principal stress on the roof scoop and air vent, respectively.

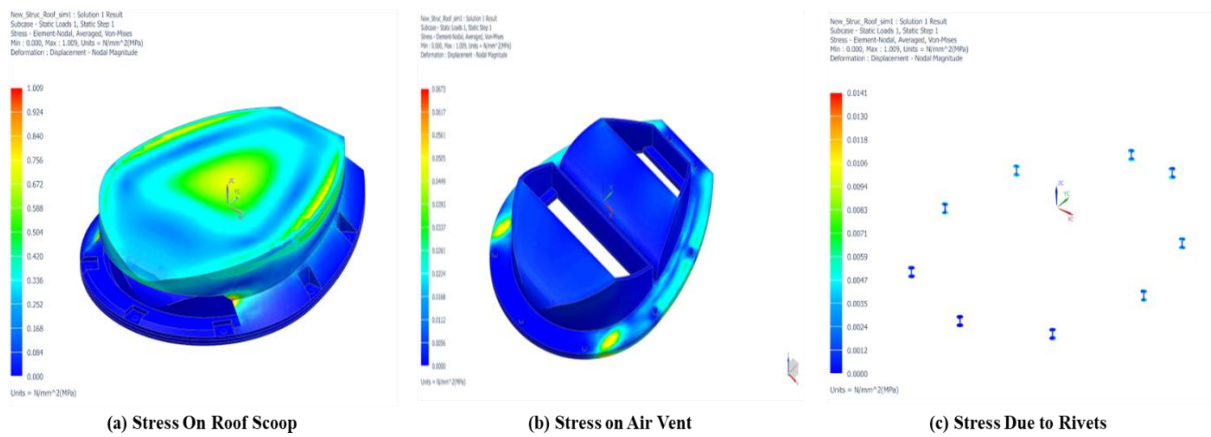


**Figure 5 - 16 Expected Von Mises Stress on the Roof Scoop (A), the Air Vent (B) and the Rivets (C)**

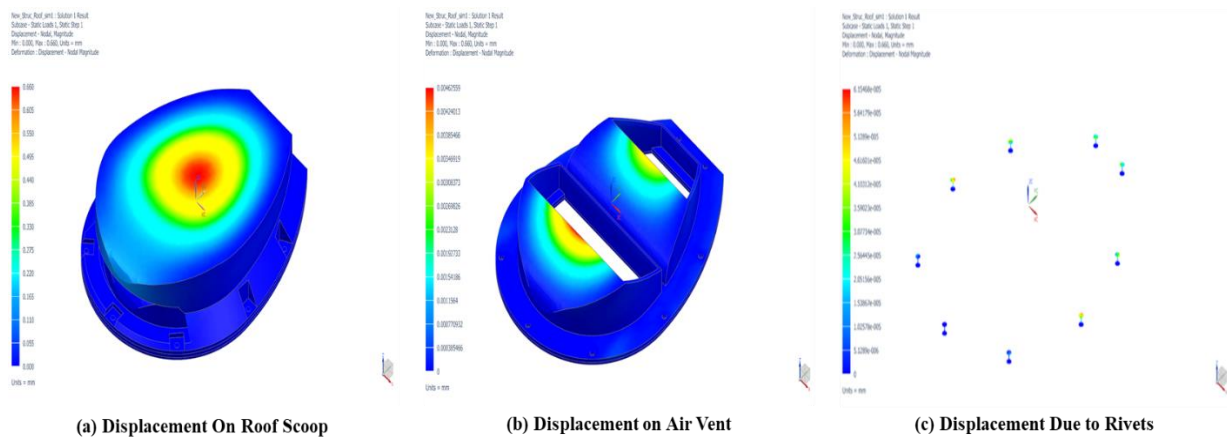


**Figure 5 - 17 Expected Displacement on the Roof Scoop (A), the Air Vent (B) and the Rivets (C)**

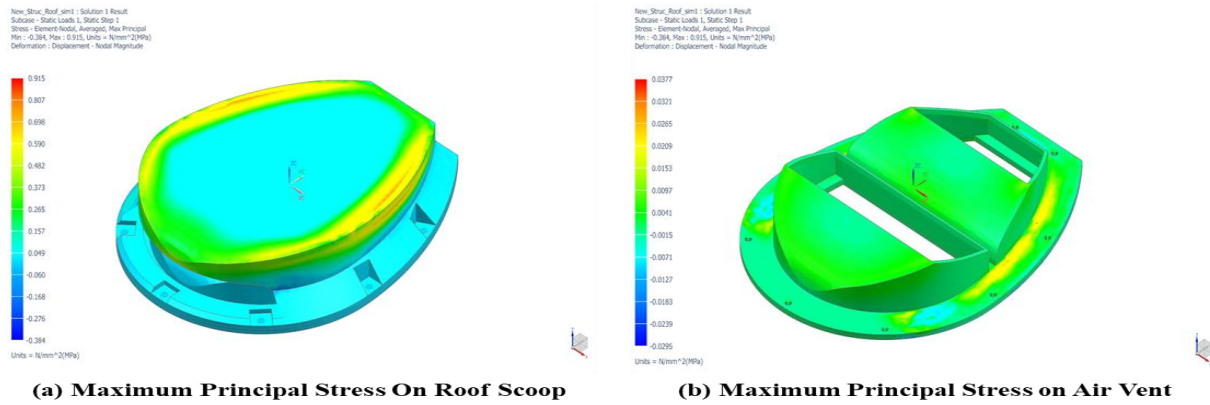


Figure 5 - 18 Expected Principal Stress on the Roof Scoop (A) and the Air Vent (B)

## 5.3 Physical Manufacturing Workflow

### 5.3.1 Material Selection

Material performance requirements for the roof scoop included UV stability, cost-effectiveness, ease of printing and mechanical performance. Based on a Pugh Matrix analysis, four polymer materials (ABS, ASA, PETG and PC) complied with the engineering specifications and requirements. Finally, a single polymer was selected. The material selected for 3D printing was Poly Ethylene-Glycol (PETG) [137]. Table 5 - 15 provides the properties of PETG.

Table 5 - 15 Material Properties for PETG [137], [134]

Description	Value	Unit
Shrinkage	1 - 3	%
Water Absorption 24 hours	0.13	%
Melting Temperature	81 - 91	°C
Flexibility (Flexural Modulus)	2.1	GPa
Strength at Break (Tensile)	28	MPa
Strength at Yield (Tensile)	50	MPa
Young Modulus	2.11	GPa
Density	1.27	g/cm3
UV Light Resistance	Good	

### 5.3.2 Process Parameters

Process parameters influence the mechanical properties and characteristics of FDM 3D printed parts [62]. For example, producing a functional 3D printed roof scoop and air vent requires selecting the optimal parameters for infill density, infill pattern, perimeters (shells) and the build orientation. Table 5 - 16 provides the optimal parameters selected for implementation based on literature and state-of-the-art methods. However, it must be noted that no Computer Assisted Engineering (CAE) tools currently exist to effectively quantify the mechanical behaviour of FDM 3D printed parts based on the various process parameters.

**Table 5 - 16 Selected Optimal Process Parameters**

Description	Value
Infill Pattern - Models	Rectilinear
Infill Density - Models	40 %
Perimeter Shells - Models	3
Infill Pattern – Strengthen Hole	Bi-directional Evolutionary Structural Optimisation
Infill Density - Strengthen Hole	100 %
Shells - Strengthen Hole	3
Build Orientation	XY plane - 45°

### 5.3.3 Support Material Optimisation

The support material provides a platform for regions of the 3D model with overhangs. Using support material affects the surface finish and print time of the 3D model. Support optimisation was performed on the roof scoop and air vent within the slicer software to reduce print time and material use. Figure 5 - 19 and Figure 5 - 20 illustrate the optimisation performed by the slicer software, Cura 4.11.

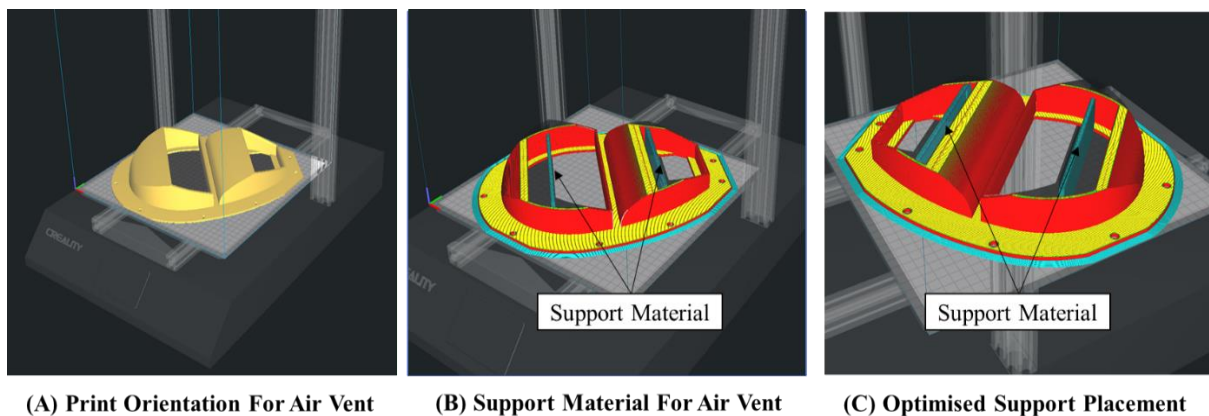
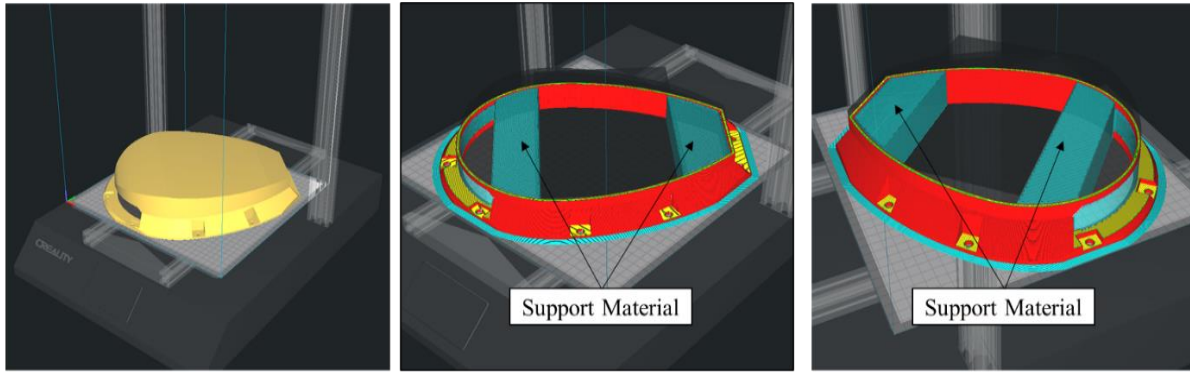


**Figure 5 - 19 Print Orientation and Support Material for Air Vent**



(A) Print Orientation For Roof Scoop (B) Support Material For Roof Scoop (C) Optimised Support Placement

Figure 5 - 20 Print Orientation and Support Material for Roof Scoop

### 5.3.4 Infill Material Optimisation

Infill geometry and density are the internal structures of the 3D model. The infill settings are presented in Table 5 - 16. Further infill optimisation involved creating a custom infill placement at the mounting regions for the pop rivets based on the expected stress the models would experience due to wind loading. The custom infill was created using the proposed method presented in chapter 5 of this dissertation, where solid bodies were created. The solid bodies were then merged within the slicer software to create the custom infill placement [14], [125]. Due to the anticipated compressive stresses, these regions were assigned different infill densities and geometries, as presented in Table 5 - 16. Figure 5 - 21 and Figure 5 - 22 illustrates the optimisation performed on the slicer software, while Figure 5 - 23 illustrates the 3D printed version.

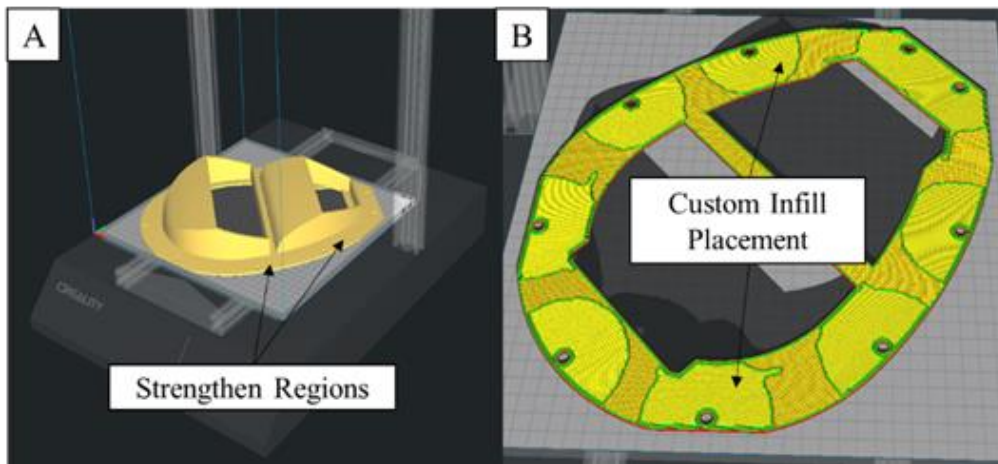


Figure 5 - 21 Custom Infill Placement (A) for Improved Strength on the Air Vent in Slicer Software at layer 10 (B)

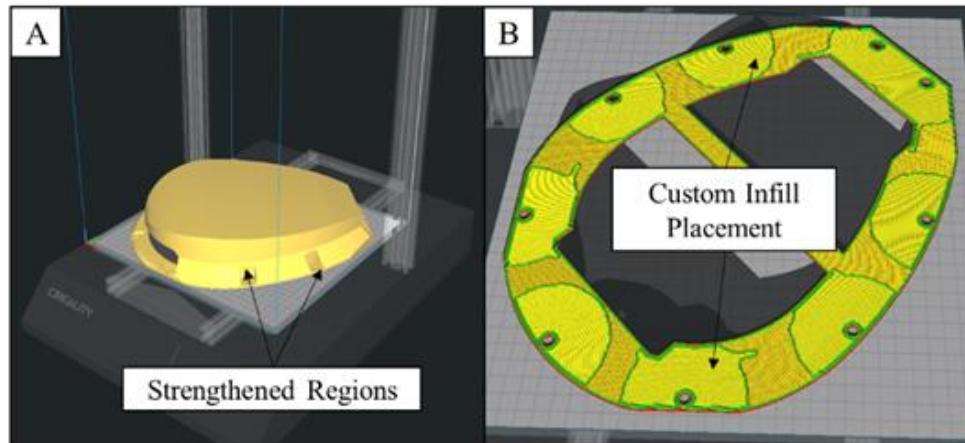


Figure 5 - 22 Custom Infill Placement (A) for Improved Strength on the Roof Scoop in Slicer Software at layer 10 (B)

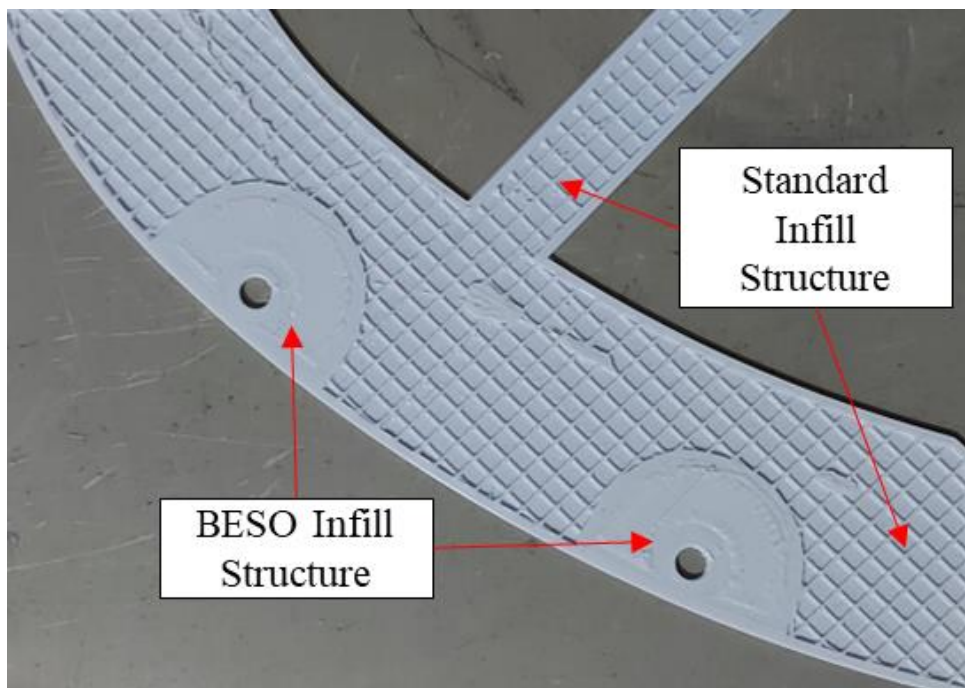


Figure 5 - 23 3D Printed Custom Infill on the Air Vent at layer 5 of the 3D Print

### 5.3.5 AM Printing Process

The AM process involves multiple steps to produce a physical object from a digital blueprint model. Generally, the AM process involves eight stages in producing a final functional part [138]. In this study, creating a custom infill placement is an additional stage to the generic AM printing process. The stages are presented in Table 5 - 17, and a visual presentation of the roof scoop following this process is shown in Figure 5 - 24. Table 5 - 18 illustrates the print time and material mass used to 3D print the roof scoop and air vent models. Further improvements in print time can be achieved by changing the nozzle diameter, which increases the raster width. This allows for more material to be printed at a faster rate as compared to the stock 0.4 mm nozzle used.

**Table 5 - 17 The Generic Stages of the Additive Manufacturing Process**

<b>Stages</b>	<b>Description</b>
1. Digital Blueprint	Create a digital 3D model
2. STL Conversion	Convert the 3D model into an STL file
3. Custom Infill Placement	Computation Evaluation – Finite Element Analysis
	Bi-directional Evolutionary Structural Optimisation Technique
	Mesh Modification – 4-8 Subdivision
4. File Transfer	FDM Manufacturability – Laplacian Mesh Smoothing
	Transfer the STL file to the printer software
	Select the appropriate process parameters to print the model based on its application
5. 3D Printing	3D prints the model layer-by-layer
6. Print Removal	Remove the print for the machine
7. Post-Processing	Clean the print
8. Installation	Install the final model for its application

**Table 5 - 18 Print Time and Material Mass of the Roof Scoop and Air Vent [134]**

Nozzle Diameter	0.4 mm
Print Time – Air Vent	29 hr 8 min
Print Time – Roof Scoop	33 hr 22 min
Print Mass – Air Vent	435 g
Print Mass – Roof Scoop	576 g



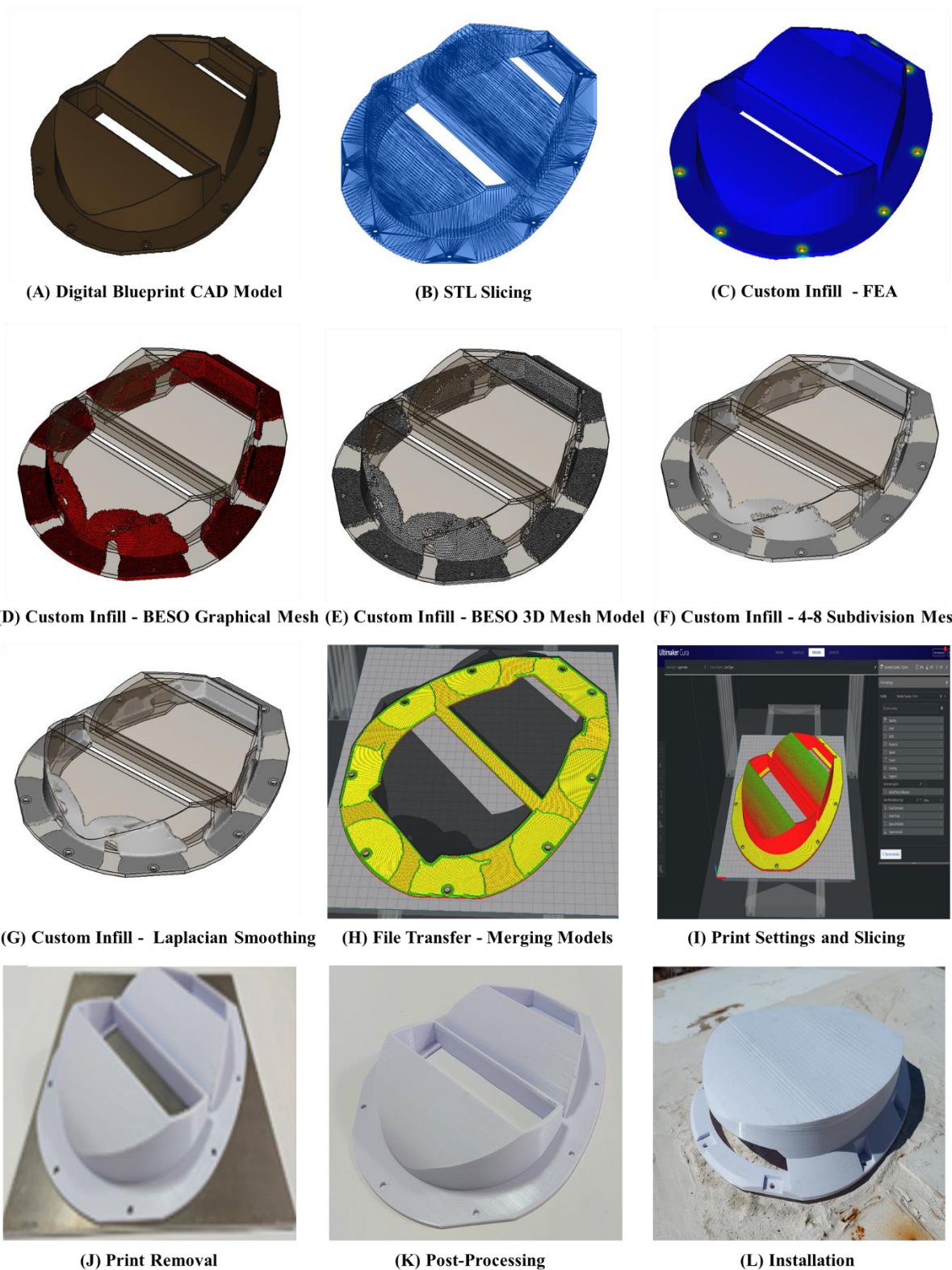


**Figure 5 - 24 Process illustrates the Stages used to Realise a Final 3D Printed Functional Part**

## 5.4 Installation

### 5.4.1 Visual Inspection

After the roof scoop and air vents were 3D printed, they were inspected for any defects or artefacts which could cause failure during operation. The only visible artefact is the stair-stepping effect on the contour surface of the roof scoop and air vents. This artefact is a standard limitation of the FDM technology. Non-planar surfaces all exhibit stair-stepping artefacts due to the deposition of molten plastic one layer at a time. This artefact does not negatively impact the structural performance of the roof scoop air vent. Figure 5 - 25 illustrates the artefacts.



Figure 5 - 25 Side View of the 3D Printed Roof Scoop with the Stair-Stepping Artifact [134]

### 5.4.2 Print Accuracy

The accuracy of the 3D print was compared to the digital 3D model. The most critical dimensions for the 3D print included the rivets' holes and the total width, height, and length of the roof scoop and air vent illustrated in Figure 5 - 26. The accuracy of all sections was  $\pm 0.1$  mm between the digital design and the 3D printed components. It must be noted that when parts are designed using DfAM techniques, the dimensions of the 3D printed components can be almost identical. Dimensional accuracy also depends on the 3D printer, process parameters and printer calibration [62]. Table 5 - 19 provides the sections compared for dimensional accuracy.

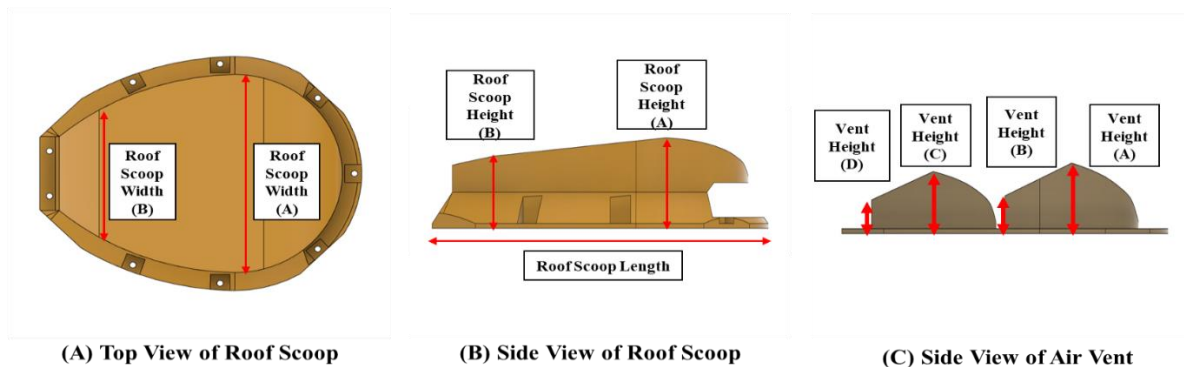


Figure 5 - 26 Reference Measuring Points for the Digital and 3D Printed Parts



**Table 5 - 19 Dimensional Accuracy between Digital Model and 3D Print [134]**

Reference	3D Model (mm)	3D Print (mm)	Error (mm)
Rivet Hole Diameter	6.5	6.42	0.08
Roof Scoop Width (A)	260	260	0
Roof Scoop Width (B)	166	166	0
Roof Scoop Length	330	329.93	0.07
Roof Scoop Height (A)	57.5	57.43	0.12
Roof Scoop Height (B)	45.8	45.68	0.12
Air Vent Height (A)	43	42.88	0.12
Air Vent Height (B)	23	22.89	0.11
Air Vent Height (C)	38	37.89	0.11
Air Vent Height (D)	20.5	20.38	0.12
Air Vent Width (A)	260	260	0
Air Vent Width (B)	166	166	0
Air Vent Length	330	329.93	0.07

### 5.4.3 Final Assembly

Once the manufacturing accuracy and quality assurance tests were completed, the roof scoop and air vent were installed onto the roof of the railway vehicle. Figure 5 - 27 illustrates the installed 3D printed functional roof scoop and air vent.



**Figure 5 - 27 The Functional 3D Printed Roof Scoop Air Vent Installed [134]**

## 5.5 Chapter Summary

The study in this chapter details the selection, redesign, manufacturing and installation of a functional 3D printable roof scoop and air vent. The design need and selected manufacturing process are based on the legacy component requiring replacement due to failure. The roof scoop and air vent's final design were achieved using the Pugh Matrix method, which evaluated three concepts and selected elements. The roof scoop and air vent 3D models were further optimised using DfAM techniques specific to the FDM printing technology to ensure that they would be 3D printable. Finally, CFD simulations were done to determine performance differences between the original roof scoop to the new design. FEA was further used to determine the material response due to the loading conditions. Optimisation techniques for support materials and infill placement have successfully reduced the print time and applied material at localised sections within the designed component using the FEA analysis. This study has shown that AM technology can create new and optimised spare parts for legacy components for railway-related applications. However, the applications and use cases are case-dependent, and rail design engineers must understand the interdependent relationships between the physical and digital workflows in creating functional 3D printable parts. Furthermore, with limited standards developed to effectively govern the design and manufacture of functional 3D printable parts within the railway industry using additive manufacturing technologies, experimental and critical knowledge is required.

# CHAPTER 6:

## DISCUSSION

### 6.1 Introduction

Additive Manufacturing in South Africa has been driven by the biotechnical/medical, aerospace and automotive industries due to a focus on research and high-value components. To date, there has been limited research involvement from the railway sector. Within the railway environment, the rolling stock and rail infrastructure consists of numerous systems and components that benefit from the technology in creating replacement spare parts, lightweight structures, improved jigs and fixtures, and new designs of consolidated part-assemblies. This research study aimed to further industrialise the additive manufacturing technology within the railway environment as an additional manufacturing method to produce improved functional end-use railway-related products. The proposed approach to achieving the objective was understanding the design and manufacturing methods available to the material extrusion AM technology in creating functional railway-related products. This chapter discusses the contribution of this dissertation by discussing the chapters and presenting contributions to both the design field and practical applications within the railway environment.

### 6.2 Discussion

Chapter 3 proposed a method to evaluate and select parts and components within the railway environment that will benefit from the FDM AM technology at the conceptual design stage. A detailed literature review on the state-of-the-art in Multi-Criteria Decision-Making models is performed, clearly focusing on the FDM AM process. Secondly, the criteria identified in the literature are summarised for part selection in the railway environment, focusing on the Analytic Hierarchy Process. The criterion used in the study included 1) geometric complexity, 2) part function, 3) design optimisation, 4) manufacturing time, 5) material removal, 6) production volume, and 7) part benefit. For the proposed decision-making model, part size and material type were considered the most critical factors in the initial screening of potential railway-related part candidates and product designs. This was due to the printing capabilities of the Creality CR10 Pro 3D printer used in the study. Applying the equations presented in Chapter 2 and the level of importance rating to each criterion, the consistency ratio, consistency index and principal eigenvalues were calculated. The consistency ratio of 0.07174 was less than the recommended 0.1 value. This proved that the obtained weights were considered consistent and could be applied to the final decision matrix, implying that each criterion's assigned level of importance concerning the railway environment was correctly given. In finalising the decision matrix, a rating scale between one and three was added to each criterion to allow users to perform group ratings for a set of

components. The finalised decision matrix was validated using FDM AM case studies published and reviewed by experts. The validation process involved applying the decision-making model to each case study and evaluating the study's outcome and the calculated results using the decision-making tool. The comparison showed consistency between the calculated results from the decision-making tool and the outcomes of the case studies. Finally, the evaluation model is applied to railway-specific case studies published and reviewed by experts to determine if the parts truly benefited from the FDM technology. The case studies presented functional end-use 3D-printed railway-related parts and products for maintenance tooling and measuring activities, rolling stock replacement parts, a prototype environmental monitoring system for sand sedimentation, and design optimisation techniques. After the decision-making tool was applied to the railway components, it was found that all parts benefited from the FDM process except the wayside lubricator tools due to their geometric simplicity. Lastly, the AHP methodology was hardcoded into an application using Visual Basic for Applications (VBA) on Microsoft Excel.

Chapter 4 proposed a method to optimise and improve the internal (infill) structures of FDM 3D printable parts based on FEA results and using the BESO technique. A six-stage methodology was presented to achieve a custom infill placement which included 1) model construction, 2) mesh generation, 3) FEA, 4) topology optimisation using BESO, 5) post-processing topology optimised model, and 6) infill design.

The model construction stage involved the 3D model design that needed to be optimised. Siemens NX was used to create the grease plate bracket and the bending test specimen. The 3D digital models are imported into the FEA package at the mesh generation stage, where a 3D mesh is assigned to the model. In the case of the bending test specimens, a 2D DelQuad mesh is applied to the surface of the rectangular model, while a 3D Delaunay mesh is generated through the entire body. An element size of 3 mm was used due to the size of the rectangular model. The third stage of the methodology required the structural FEA to be performed on the rectangular test specimen, where a vertical force of 5000 N was applied to the model in the three-point bending test procedure. The applied force was used as a worst-case for the PETG material to determine the full extent of the stress profile. In the fifth stage of the methodology, the FEA results were used to perform the BESO technique. The final optimised model was created using the BESO technique after 65 iterations. Since the BESO technique provides a final iteration with limitations such as not having a final 3D model, a final manufacturable part, and a solution that was not natively optimised for AM, using the FDM process, further post-processing techniques were required. The final BESO iteration solution was post-processed into a 3D printable structure using MeshLab in the sixth stage of the methodology. The mesh geometry represented by elements was converted into quadrilateral elements using the 4-8 subdivision method. Finally, Laplacian smoothing is applied to the

quadrant mesh to create a smooth FDM 3D printable model while maintaining the optimised structural shape.

Additionally, the sixth stage of the methodology presented the steps needed to merge the original 3D model with the BESO-optimised model, where the printing process parameters were assigned, and the final model was 3D printed using the Cura 4.11 slicing tool. A trackside railway lubricator grease plate bracket was used as an example component to illustrate the methodology. Finally, creating custom infill placements for flexural test specimens was presented in Appendix D in preparation to determine the mechanical performance of the custom infill placement methodology through an experimental study.

The experimental study detailed the required test setups for three-point bending, three-point offset bending, four-point bending and inverted four-point bending to develop a deeper understanding of the material behaviour. Unfortunately, only the three-point and three-point offset bending were performed from the four different test setups due to Covid-19 restrictions and limited testing capability within Transnet Freight Rail and the University of Kwa-Zulu Natal to perform the four-point bending tests. Two sets of test specimens complying with the recommended standard were 3D printed. The first set of specimens was printed using the industry-standard infill geometry (rectilinear) with printing parameters based on literature summarised in Chapter 2. The second set of test specimens had the custom-generated infill placement based on FEA and the BESO technique. These test specimens had a multi-infill geometry configuration, with all the BESO structures containing 3D infill patterns and the outer regions having the rectilinear pattern matching the baseline specimens. The first test comparison had reference test specimens 3D printed with 100 % infill density with a total mass of 51 grams, while the BESO optimised infill was printed in 100 % infill density with a 20 % infill density for the global rectilinear pattern and a total mass of 35 grams. The second test comparison had reference test specimens 3D printed with a 33 % infill density using the rectilinear infill geometry, while the BESO-optimised structures were printed with a multi-infill geometry combination. All test specimens are printed with a constant mass of 28 grams.

The final test results achieved by the experimental study included: 1) 49 % increase in peak loading for the gyroid – rectilinear infill geometry combination compared to the standard rectilinear infill pattern under three-point bending tests, 2) 66 % reduction in peak force-extension for the octet-rectilinear infill geometry combination compared to the standard rectilinear infill geometry in three-point bending tests, 3) 46 % increase in flexural stiffness for the octet-rectilinear infill geometry combination compared to the standard rectilinear infill geometry in three-point bending, 4) 232 % increase in peak force for the cubic-rectilinear infill geometry compared to the standard rectilinear infill geometry in three-point offset bending tests, 5) 143 % increase in peak force for the gyroid-rectilinear infill geometry combination compared to the standard rectilinear infill geometry in three-point offset bending tests, 6) brittle material behaviour for solid BESO infill optimised test specimens in three-point bending, and 7) more predictable buckling modes for FDM 3D printed parts under bending.

Chapter 5 detailed the selection, redesign, manufacturing and installation of a functional 3D printable roof scoop and air vent for a rolling stock vehicle. The design need and selected manufacturing process were based on the legacy component requiring replacement due to failure. The decision-making model was first applied to the roof scoop and air vent, which determined that the part would benefit from the FDM process. Secondly, the roof scoop and air vent's final design were achieved using the Pugh Matrix method, which evaluated three concepts and selected elements. The roof scoop and air vent 3D models were further optimised using DfAM techniques specific to the FDM printing technology to ensure that they would be 3D printable. Finally, CFD simulations were done to determine performance differences between the original roof scoop to the new design. Localized surface goals on the roof scoop were set up in the CFD package with an assigned direction along the x-axis as per the recommendations of the railway engineering standard. The location of the pressure is along the surface of the roof scoop. It was found that the optimised roof scoop was more efficient than the original design. FEA was further used to determine the material response due to the loading conditions generated from the CFD and recommendations from the railway engineering standard. Optimisation techniques for support materials and custom infill placement were applied to the model, successfully reducing the print time and applying material at localised sections within the designed component. Finally, the printed and digital models' accuracy had a  $\pm 0.2$  mm variation. Lastly, the functional 3D-printed roof scoop and air vent were installed on the inspection trolley in preparation for performing experimental tests to evaluate the efficiencies determined in the CFD analysis. Unfortunately, days after installing the roof scoop, the inspection trolley experienced a failure to the gearbox and the axle. Due to this, the vehicle has been placed at the depot for repairs with no confirmed lead time within this financial year to fix the vehicle.

### **6.3 Design Contributions**

This research project resulted in several design contributions, benefiting the South African academic society with new information and application methods for additive manufacturing within the railway environment (Chapter 3, Chapter 4, Chapter 5, Appendix B, Appendix C, Appendix E and Appendix F). Advanced design techniques based on common design features available to the FDM process have been proposed to overcome some manufacturing limitations (Appendix C and Appendix E). A Multi-Criteria Decision-Making methodology to select potential railway-related part candidates that would benefit from the FDM AM technology is proposed, validated and evaluated (Chapter 3). The MCDM tool presented a selection criterion based on the requirements of the railway environment and the FDM process. A novel method has been proposed to optimise the internal (infill) structures of FDM 3D printed parts based on the expected stress using the Bi-directional Evolutionary Structural Optimisation technique and stress-based Finite Element Analysis (Chapter 4, Appendix D and Chapter 5). In proposing the custom infill placement technique, coupling mesh refinement and smoothing scripts to

topology-optimised results provides manufacturability using the FDM technology (Chapter 4 and Appendix D).

## **6.4 Practicable Contributions**

A structured approach for rail design engineers intending to use Additive Manufacturing technologies to produce railway-related parts using the FDM (Chapter 3, Chapter 4, Chapter 5, Appendix C, Appendix D, Appendix E and Appendix F) has been presented. A technical approach to identifying and selecting potential railway-related part candidates that may benefit from the FDM AM technology removes the trial-and-error approach and reduces economic costs (Chapter 3). Advanced design techniques for self-supporting structures, design interlocking joints and design integration for fasteners and mechanical components, expanding the potential use case of the FDM technology for product designs (Appendix E). A custom design aid integrates all the common design features for practising rail design engineers to ensure the digital design meets real-world expectations (Appendix E). The internal structures of 3D printable railway-related components can be improved by strategically allocating material in regions where potentially high stress is expected (Chapter 4, Appendix D and Chapter 5). A custom application toolkit details the design recommendations, methodologies, and techniques in selecting, designing and manufacturing 3D printable components based on the generic design process. Using the FDM technology, the application toolkit can be easily installed onto any computer to assist practising railway design engineers in achieving a functional end-use component (Appendix F). Further expanding the centre of excellence for additive manufacturing technologies within the railway environment with structured and technical methods to select, design and manufacture potential railway-related parts (Chapter 3, Chapter 4 and Chapter 5).

# CHAPTER 7:

## CONCLUSIONS & RECOMMENDATIONS

### 7.1 Introduction

The conclusion to this research study is obtained by answering the main research question by achieving the project objectives. The work presented in this dissertation has answered the research question at two levels: 1) research study conclusion and 2) application-specific conclusion.

### 7.2 Achievement of Project Objectives

To answer the main research question for this study, the Project Objectives (PO) initially set out are answered first:

**PO 1:** To develop a decision-making model to identify and evaluate potential railway-related parts that will benefit from the Fused Deposition Modelling process at the conceptual design stage.

A Multi-Criteria Decision-Making methodology using the Analytic Hierarchy processes is proposed, evaluated, and validated to assist novice rail design engineers in identifying and select potential railway-related parts that will benefit from the FDM AM technology. The methodology is validated and verified through several published FDM case studies (Chapter 3).

**PO 2:** To develop a method to optimise the internal (infill) structure of 3D printed Fused Deposition Modelled parts by allocating material at specific locations based on the parts' stress profile for a given application.

Different structural optimisation techniques, such as size, shape and topology optimisation, and computational simulation packages, are reviewed in relation to the FDM manufacturing limitations and capabilities. A method to optimise and improve the internal (infill) structures of FDM 3D printable parts based on finite element analysis (FEA) results and using the Bi-directional Evolutionary Structural Optimisation (BESO) technique is proposed. A six-stage methodology is presented to achieve a custom infill placement. The BESO technique uses a stress criterion from FEA results to remove material that experiences non-critical stress due to the loading conditions. A trackside railway lubricator grease plate bracket is used as an example component to illustrate the methodology. Optimisation techniques such as the custom infill placement using the BESO method provides an additional approach to improve the internal (infill) structure, and the mechanical performance (stiffness, strength, and mass) of FDM 3D printed parts by adding more material to specifically stressed regions. The methodology is also applied



to developing the roof scoop and air vent replacement parts to allocate material internally based on the parts' stress profile (Chapter 4, Appendix D and Chapter 5).

**PO 3:** To analyse the mechanical performance through experimental testing between traditional infill structures and the custom-developed infill placement method for a specific material and process parameters identified through literature.

All solid test specimens outperformed the BESO infill optimised test specimens in the first test comparison. Secondly, the solid test specimens exhibited ductile material behaviour, while the BESO infill optimised test specimens exhibited brittle behaviour. This result may assist designers in creating functional parts to fail at specific loading and strains. In the second test comparison, all the BESO infill optimised test specimens outperformed the reference rectilinear infill geometry by supporting larger loads before failure. The BESO infill optimised test specimens provided increased strength based on the topology optimisation and finite element analysis generated by the stress profile. In addition, the peak loading extension for all the BESO infill optimised test specimens were reduced. All BESO-optimised infill geometry were stiffer than the rectilinear specimens. Lastly, the combination of gyroid–rectilinear infill geometry withstood the highest loading before failure under three-point bending, while the cubic–rectilinear infill geometry configuration withstood the highest loading under three-point offset bending (Chapter 3, Chapter 5 and Appendix D).

**PO 4:** To develop a custom design guide to assist novice rail design engineers in applying the design features and advanced techniques available to the Fused Deposition Modelling process to functional 3D printable components to ensure manufacturing repeatability.

A custom design guide is presented, integrating the common design features and considerations for rail design engineers to create functional parts. Since FDM technologies and material types are continuously advancing, the design guide considers the capabilities of a specific printer and material type. The illustrative guide and the DfAM strategies are intended to assist rail engineers with decision-making at the design stage to meet the functional needs of the part while ensuring manufacturability is repeatable and consistent using the FDM process. Moreover, the proposed design guide and advanced design strategies can be extended to other FDM printers, materials, and print process parameters. As a result, an advanced set of design strategies for features, self-supporting design techniques, interlocking methods and infill optimisation techniques have been proposed based on the main technical limitations of the FDM process (Appendix E).

**PO 5:** To apply the design techniques, tools, and methodologies to produce a functional 3D printable roof scoop and air vent rolling stock replacement part.

A custom-developed application toolkit is developed to assist railroad designer engineers in producing functional 3D printable parts using the FDM process by consolidating the design techniques, methods, and recommendations. The application is hardcoded using Visual Basic for Application in Microsoft Excel and presents recommendations in a structured generic design process. The generic design process contains three stages, 1) the conceptual design, 2) the embodiment design, and 3) the final design stages. The application toolkit containing the design tools and techniques is used to select, redesign, optimise and manufacture a functional 3D printable roof scoop and air vent for a railway inspection vehicle using the fused deposition modelling technology (Appendix F).

## **7.3 Research Question Conclusion**

### **7.3.1 Research Study Conclusion**

The process of using the Fused Deposition Modelling technique to create functional end-use 3D printable products for railway-related applications has been revealed. The required steps involve identifying a suitable railway-related product that benefits from the additive manufacturing process, determining the digital and physical workflows which affect the manufacturing of the product using the fused deposition modelling technique and finally, applying the BESO optimisation method to improve further the internal (infill) structure of the FDM printed part. The methods and techniques presented in this dissertation can be applied to other designs and prototypes in the railway industry or other manufacturing industries where the FDM technology will be used.

### **7.3.2 Application-Specific Conclusion**

Specific print process parameters (infill density, infill geometry, wall thickness, number of walls, raster angle, print orientation, material type, support material, and cooling) are selected to manufacture the roof scoop and air vent parts based on the physical and digital workflows. Design optimisation techniques for self-supporting structures are applied to the models to reduce manufacturing lead times. Internal structures (infill) optimisation is performed on the roof scoop and air vent based on the expected wind loading conditions and the predicted stress from finite element analysis results. The infill optimisation is performed to improve the strength of the parts without sacrificing the external profile and its efficiencies. These techniques and methodologies have been applied to several other railway-related products, resulting in functional 3D printed systems using the FDM technology.

Based on the previous chapters, a more specific conclusion can be made, particularly for the custom application program developed.

### **7.3.2.1 FDM Generic Design Process Application Tool**

The custom application tool is developed to assist practising railway design engineers to effectively capitalise on the benefits associated with the Fused Deposition Modelling technology. The program is structured according to the generic design process with recommendations, methodologies and techniques that can be used to identify, select, redesign, optimise and manufacture functional end-use products for the railway environment. The design stages include 1) the conceptual design stage, 2) the embodiment design stage, and 3) detailed design. At the conceptual design stage, the program presents an automated calculator to perform the Multi-Criteria Decision-Making methodology based on the Analytic Hierarchy Process to identify potential railway-related part candidates and an automated calculator to perform the conceptual design evaluations based on the Pugh Matrix method. At the embodiment design stage, the digital and physical manufacturing workflow is presented, recommended printing parameters, advanced design techniques for the Fused Deposition Modelling Process and design steps to perform custom infill design placements. The final design stage summarises the methods and recommendations to succeed in producing functional 3D printable parts, components and products using the Fused Deposition Modelling Process by presenting the case study of producing a functional 3D printable roof scoop and air vent parts for the rolling stock vehicle. Moreover, the proposed application tool can be extended to other FDM printers, materials, print process parameters, and industries using the FDM technology to produce functional end-use parts. This will ensure that manufacturability is repeatable and consistent. As the additive manufacturing technology continues to be industrialised within the railway environment, the proposed techniques and methodologies within the application tool will be a keystone to further advancements.

## **7.4 Recommendations and Future Work**

Based on the chapters in this dissertation, a summary of recommendations can be made. More railway-specific research in additive manufacturing is required as an apparent gap in the capability matrix developed under the South African Additive Manufacturing Strategy, and the proposed AMCoC framework is the railway industry involvement (Appendix B and Chapter 2). More research is needed in approving the different material types, technology tools, mass production capabilities, developing AM skills specific to railway engineering requirements, post-processing realities for FDM parts and specific railway engineering design standards and requirements to regulate functional end-use FDM products for the railway industry applications (Chapter 5 and Annexure B). Based on the literature review, the mechanical responses for dynamic, fracture and fatigue are limited and more research is required to understand 3D printed parts better using the FDM process (Chapter 2). By understanding the material performance under these loading conditions and having specific railway engineering design standards and requirements, further potential railway applications could be realised. Based on the literature review, research in quantifying the process parameters and developing a repeatable set of

parameters using artificial intelligence is required (Chapter 2). The design guide presented in this study focused on the PETG material printed with a 0.4 mm nozzle.

Further research in applying different FDM materials, printers and process parameters to the custom design guide (Chapter 2, Chapter 4 and Appendix E). This study focused on only three infill geometry configurations; more research should be done on applying the BESO technique for multi-material and multi-geometry infill optimisation of FDM parts (Chapter 4 and Appendix D). To develop a more robust decision-making tool and allow for more criteria to be added, the Fuzzy AHP method could be used to improve the Multi-Criteria Decision-Making process for railway-related part candidates. (Chapter 3 and Appendix C). The proposed AHP Decision-Making tool should be applied to other AM technologies to identify potential railway-related parts (Chapter 3 and Appendix C).

## REFERENCES

- [1] C. K. Chua, C. H. Wong and W. Y. Yeong, *Standards, Quality Control and Measurement Sciences in 3D Printing and Additive Manufacturing*, 1st ed., United Kingdom: Elsevier Academic Press, 2017.
- [2] ISO/TC 261 Additive Manufacturing Committee, “Additive Manufacturing - General Principles - Terminology,” *ISO/ASTM 52900:2015*, pp. 1 - 8, 2015.
- [3] A. D. Toth, J. Padayachee and S. Vilakazi, “Digital Maintenance Centre for Additive Manufacturing and 3D Printing in the Railway Industry,” in *South African Heavy Haul Association 2021*, Johannesburg, 2021.
- [4] Tess Roberts (Hubs), “Additive Manufacturing Trend Report 2021: 3D Printing Market Growth in the Year of the COVID-19,” HUBS: A Protolabs Company, USA, 2021.
- [5] M. K. Thompson, G. Moroni, T. Vaneker, G. Fadel, R. I. Campbell, I. Gibson, A. Bernard, J. Schulz, P. Graf, B. Ahuja and F. Martina, “Design for additive manufacturing: trends, opportunities, considerations and constraints,” *CIRP Annals Manufacturing Technology*, vol. 65, no. 2, pp. 737 - 760, 2016.
- [6] Y. Bar-Cohen, “Chapter 1: State-of-the-Art of Manufacturing and Processing Methods in the Digital Era,” in *Advances in Manufacturing and Processing of Materials and Structures*, T. & F. Group, Ed., New York City, CRC Press, 2019, p. 1.
- [7] J. A. Gopsill, J. Shindler and B. J. Hicks, “Using finite element analysis to influence the infill design of fused deposition modelled parts,” *Progress in Additive Manufacturing*, vol. 3, no. 2018, pp. 145 - 163, 2017.
- [8] S. Vilakazi, N. R. Mathe and L. C. Tshabalala, “Feasibility of Additive Manufacturing for the South African Rail Industry,” in *International Heavy Haul Association Conference June 2019*, Narvik, 2019.
- [9] Transnet Freight Rail, “Overview,” Transnet Freight Rail, 05 May 2010. [Online]. Available: <https://www.transnet.net/Divisions/Pages/FreightRail.aspx>. [Accessed 05 August 2021].
- [10] A. D. Toth, J. Padayachee, T. Mahlatji and S. Vilakazi, “Report on case studies of additive manufacturing in the South African railway industry,” *Scientific African*, vol. 16, no. e01219, pp. 1 - 12, 2022.

- [11] O. Diegel, A. Nordin and D. Motte, "Current Usage of Additive Manufacturing," in *A Practical Guide to Design for Additive Manufacturing*, D. T. Pham, Ed., Singapore, Springer, 2020, pp. 7 - 8.
- [12] W. B. du Preez and D. J. de Beer, "Implementing the South African Additive Manufacturing Technology Roadmap - The Role of an Additive Manufacturing Centre of Competence," *South African Journal of Industrial Engineering*, vol. 26, no. 2, pp. 85 - 92, August 2015.
- [13] A. D. Toth and L. Msibi, "A Conceptual Evaluation and Benefit of Additive Manufacturing Technology to Improve Maintenance Tasks in the Railway Industry," in *International Heavy Haul Association Conference June 2019*, Navik, 2019.
- [14] A. D. Toth and S. Vilakazi, "Benefits of reinforced meshing and materials testing of 3D printed parts to assist mechanical design in the railway infrastructure environment," in *Rapid Product Development Association of South Africa Conference Proceeding*, Bloemfontein, 2019.
- [15] A. D. Toth, "Design of an Additively Manufactured Inspection Trolley Water Cooling Pipe Clamp Bracket," Transnet Freight Rail, Johannesburg, 2020.
- [16] X. Huang and Y. M. Xie, "Evolutionary topology optimization of continuum structures including design-dependent self-weight loads," *Finite Elements in Analysis and Design*, vol. 47, no. 2011, pp. 942 - 948, 2011.
- [17] A. Moussa, D. Melancon, A. El Elmi and D. Pasini, "Topology optimization of imperfect lattice materials built with process-induced defects via Powder Bed Fusion," *Additive Manufacturing*, vol. 37, no. 101608, pp. 1 - 29, 2020.
- [18] L. Cheng, X. Liang, J. Bai, Q. Chen, J. Lemon and A. To, "On Utilizing Topology Optimization to Design Support Structure to Prevent Residual Stress Induced Build Failure in Laser Powder Bed Metal Additive Manufacturing," *Additive Manufacturing*, vol. 27, no. 1016, pp. 290 - 304, 2019.
- [19] Y. Saadlaoui, J.-L. Milan, J.-M. Rossi and P. Chabrand, "Topology optimization and additive manufacturing: Comparison of conception methods using industrial codes," *Journal of Manufacturing Systems*, vol. 43, no. 4, p. 178–186, 2017.
- [20] L. Lu, A. Sharf, H. Zhao, Y. Wei, Q. Fan, X. Chen, Y. Savoye, C. Tu, D. Cohen-Or and B. Chen, "Build-to-Last: Strength to Weight 3D Printed Objects," *ACM Transactions on Graphics*, vol. 33, no. 97, pp. 1 - 10, 2014.
- [21] J. A. Gopsill and B. J. Hicks, "Deriving infill design of fused deposition modelled parts from predicted stress profiles," in *Proceedings of the ASME 2016 International Design Engineering*

*Technical Conferences and Computers and Information in Engineering Conference IDETC/CIE 2016*, Charlotte, North Carolina, 2017.

- [22] D. Brackett, I. Ashcroft and R. Hague, "Topology optimization for additive manufacturing," *22nd Annual Solid Freeform Fabrication Symposium*, pp. 348 -362, 2011.
- [23] M. J. B. Nagera, P. H. Toniasso, G. M. Slaviero, C. E. de Souza and R. Q. Rodriguez, "Topological Optimization Software Tools: Literature Review and Real Application," in *Proceedings of the XL Ibero-Latin-American Congress on Computational Methods in Engineering, ABMEC*, Natal/RN, Brazil, 2019.
- [24] The British Standards Institution 2016, "BS ISO/ASTM 52900 Additive Manufacturing - General principles - Terminology," BSI Standards Limited 2016, UK, 2015.
- [25] T. Pereira, J. V. Kennedy and J. Potgieter, "A Comparison of Traditional Manufacturing vs Additive Manufacturing, the Best Method for the Job," in *14th Global Congress on Manufacturing and Management*, Auckland, 2019.
- [26] N. G. Tanikella, B. Wittbrodt and J. M., "Tensile Strength of Commercial Polymer Materials for Fused Filament Fabrication 3D Printing," *Additive Manufacturing*, vol. 15, pp. 40-47, 2017.
- [27] N. Dialami, M. Cervera, M. Chiumenti and R. Rossi, "Numerical and experimental analysis of the structural performance of AM components built by Fused Filament Fabrication," *International Journal of Mechanics and Materials in Design*, pp. 1-25, 2020.
- [28] A. Dey and N. Yodo, "A Systematic Survey of FDM Process Parameter Optimization and Their Influence on Part Characteristics," *Journal of Manufacturing and Materials Processing*, vol. 3, no. 3, pp. 1-30, 2019.
- [29] M. Somireddy and A. Czekanski, "CHARACTERIZATION OF MATERIAL BEHAVIOR OF THE FUSED DEPOSITION MODELING PROCESSED PARTS," in *Proceedings of the ASME 2017 12th International Manufacturing Science and Engineering Conference*, Los Angeles, CA, USA, 2017.
- [30] C. Tosto, L. Saitta, E. Pergolizzi, I. Blanco, G. Celano and G. Cicala, "Methods for the Characterization of Polyetherimide Based Materials Processed by Fused Deposition Modelling," *Applied Science*, vol. 10, no. 3195, pp. 1-15, 2020.
- [31] E. Cuan-Urquizo, E. Barocio, V. Tejada-Ortigoza, V. B. Pipes, C. A. Rodriguez and A. Roman-Flores, "Characterisation of Mechanical Properties of FFF Structures and Materials: A Review on the Experimental, Computational and Theoretical Approaches," *Multidisciplinary Digital Publishing Institute: Materials*, vol. 12, no. 895, pp. 1 - 25, 2019.

- [32] A. Pandzic, D. Hodzic and A. Milovanovic, "Effect of Infill Type and Density on Tensile Properties of PLA Material for FDM Process," in *Proceedings of the 30th DAAAM International Symposium*, Vienna, Austria, 2019.
- [33] N. G. Tanikella, B. Wittbrodt and J. M. Pearce, "Tensile Strength of Commercial Polymer Materials for Fused Filament Fabrication 3D Printing," *Additive Manufacturing*, vol. 15, pp. 40-47, 2017.
- [34] P. Vosynek, T. Navrat, A. Krejbychova and D. Palousek, "Influence of Process Parameters of Printing on Mechanical Properties of Plastic Parts Produced by FDM 3D Printing Technology," in *MATEC Web of Conferences*, 2018.
- [35] L. Bergonzi, M. Vettori, L. Stefanini and L. D'Alcamo, "Different infill geometry influence on mechanical properties of FDM produced PLA," in *IOP Conference Series: Materials Science and Engineering 1038*, 2021.
- [36] B. Goldschmidt, "The Best Cura Infill Pattern (for Your Needs)," ALL3DP, 01 April 2021. [Online]. Available: <https://all3dp.com/2/cura-infill-patterns-all-you-need-to-know/>. [Accessed 10 May 2021].
- [37] K. P. Motaparti, G. Taylor, M. C. Leu, K. Chandrashekhara, J. Castle and M. Matlack, "Effects of build parameters on compression properties for ULTEM 9085 parts by fused deposition modeling," in *Solid Freeform Fabrication 2016: Proceedings of the 26th Annual International Solid Freeform Fabrication Symposium – An Additive Manufacturing Conference*, Missouri, USA, 2016.
- [38] T. F. Abbas, F. M. Othman and H. B. Ali, "Effect of infill Parameter on compression property in FDM Process," *International Journal of Engineering Research and Application*, vol. 7, no. 10, pp. 16-19, 2017.
- [39] P. Yadav, A. Sahai and R. S. Sharma, "Strength and Surface Characteristics of FDM-Based 3D Printed PLA Parts for Multiple Infill Design Patterns," *Journal of The Institution of Engineers (India): Series C*, vol. 102, p. 197–207, 2021.
- [40] N. Vidakis, M. Petousis, A. Vairis, K. Savvakis and A. Maniadi, "On the compressive behavior of an FDM Steward Platform part," *Journal of Computational Design and Engineering*, vol. 4, no. 2017, pp. 339-346, 2017.
- [41] A. W. Gebisa and H. G. Lemu, "Effect of Process Parameters on Compressive Properties of ULTEM 9085 Produced By FDM Process," in *International Mechanical Engineering Congress and Exposition*, Pittsburgh, PA, USA, 2018.



- [42] O. Lužanin, D. Movrin and M. Plančak, "Effect of Layer Thickness, Deposition Angle, and Infill on Maximum Flexural Force in FDM-Built Specimens," *Journal of Technology of Plasticity*, vol. 39, no. 1, pp. 49 - 58, 2014.
- [43] J. M. Chacon, M. A. Caminero, E. Garcia-Plaza and P. J. Nunez, "Additive manufacturing of PLA structures using fused deposition modelling: effect of process parameters on mechanical properties and their optimal selection," *Materials & Design*, vol. 124, no. 15, pp. 143 - 157, 2017.
- [44] I. Durgun and R. Ertan, "Experimental investigation of FDM process for improvement of mechanical properties and production cost," *Rapid Prototyping Journal*, vol. 20, no. 3, pp. 228 - 235, 2014.
- [45] S. Raut, V. S. Jatti, N. K. Khedkar and T. P. Singh, "Investigation of the effect of built orientation on mechanical properties and total cost of FDM parts," *Procedia Materials Science*, vol. 6, no. 2014, pp. 1625 - 1630, 2014.
- [46] A. W. Gebisa and H. G. Lemu, "Investigating Effects of Fused-Deposition Modeling (FDM) Processing Parameters on Flexural Properties of ULTEM 9085 using Designed Experiment," *Materials MDPI*, vol. 11, no. 4, pp. 1 - 23, 2018.
- [47] I. Gibson, D. Rosen, B. Stucker and M. Khorasani, "Software for Additive Manufacturing," in *Additive Manufacturing Technologies Third Edition*, Switzerland, Springer, 2021, pp. 491 - 522.
- [48] Y. Bar-Cohen, "Chapter1: State-of-the-Art of Manufacturing and Processing Methods in the Digital Era," in *Advances in Manufacturing and Processing of Materials and Structures*, T. & F. Group, Ed., New York City, CRC Press, 2019, p. 1.
- [49] D. L. Logan, *A first course in the Finite Element Method Sixth Edition*, United States of America: Cengage Learning, 2015.
- [50] 3D Systems, "Stereolithography Interface Specification," 3D Systems, 1988.
- [51] AdditiveX, "What file formats are used in 3D printing?," AdditiveX, 10 January 2021. [Online]. Available: <https://www.additive-x.com/blog/file-formats-used-3d-printing/>. [Accessed 23 June 2021].
- [52] D. Ahlers, *3D Printing of Nonplanar Layers for Smooth Surface Generation*, Rotherbaum: Universitat Hamburg, 2018, pp. 7-9.
- [53] F. Baumann, H. Buydayci, J. Grunert, F. Keller and D. Roller, "Influence of slicing tools on quality of 3D printed parts," *Computer-Aided Design and Application*, vol. 13, no. 1, pp. 14 - 31, 2015.

- [54] I. Gibson, D. Rosen and B. Stucker, “Software Issues for Additive Manufacturing,” in *Additive Manufacturing Technologies: 3D Printing, Rapid Prototyping and Direct Digital Manufacturing*, New York, Springer, 2015, pp. 351 - 374.
- [55] A. C. Brown and D. de Beer, “Development of a stereolithography (STL) slicing and G-Code generation algorithm for an entry level 3-D printer.,” in *IEEE AFRICON*, 2013.
- [56] B. Hu, G. Jin and L. Sun, “A Novel Adaptive Slicing Method for Additive Manufacturing,” in *Proceedings of the 2018 IEEE 22nd International Conference on Computer Supported Cooperative Work in Design*, Nanjing, China, 2018.
- [57] Q. Li and X. Y. Xu, “Self-adaptive slicing algorithm for 3D printing,” *Materials Research Innovations*, vol. 19, no. sup5, pp. S5-635-S5-641, 2015.
- [58] K. Douglas, “Most Common 3D Printer File Formats in 2021,” All3DP, 20 July 2021. [Online]. Available: <https://all3dp.com/2/3d-file-format-3d-model-types/>. [Accessed 10 August 2021].
- [59] D. Ding , Z. Pan, D. Cuiuri, H. Li and S. van Duin, “Advanced Design for Additive Manufacturing: 3D Slicing and 2D Path Planning,” in *New Trends in 3D Printing*, InTech, 2016, pp. 3 - 23.
- [60] D. A. & C. J. Turner, “An implicit slicing method for additive manufacturing processes,” *Virtual and Physical Prototyping*, vol. 13, no. 1, pp. 2 - 7, 2018.
- [61] V. Carlota, “Top 10 Best Slicer Software For All Levels,” 3Dnatives, 20 March 2019. [Online]. Available: <https://www.3dnatives.com/en/top-10-slicer-software-200520194/#!>. [Accessed 12 January 2021].
- [62] M. Šljivic, A. Pavlovic, M. Krašnik and J. Ilić, “Comparing the accuracy of 3D slicer software in printed enduse parts,” in *IOP Conference Series: Materials Science and Engineering 659*, Serbia, 2019.
- [63] Ultimaker, “Print Settings,” Ultimaker, 10 01 2021. [Online]. Available: <https://support.ultimaker.com/hc/en-us/sections/360003548619-Print-settings>. [Accessed 10 01 2021].
- [64] Natural Resources Leadership Institute, “Multi-Criteria Decision Analysis,” Natural Resources LeadershipInstitute, 21 February 2020. [Online]. Available: <https://projects.ncsu.edu/nrli//decision-making/MCDA.php>. [Accessed 01 April 2022].
- [65] N. Munier, E. Hontoria and F. Jiménez-Sáez, *Strategic Approach in Multi-Criteria Decision Making: A Practical Guide for Complex Scenario*, Switzerland: Springer, 2019.

- [66] D. Sabaei, J. Erkoyuncu and R. Roy, "A review of multi-criteria decision making methods for enhanced maintenance delivery," *Procedia CIRP - Understanding the Life Cycle Implications of Manufacturing*, vol. 37, pp. 30 - 35, 2015.
- [67] K. Ransikarbum and N. Kim, "Multi-Criteria Selection Problem of Part Orientation in 3D Fused Deposition Modeling Based on Analytic Hierarchy Process Model: A Case Study," *IEEE International Conference on Industrial Engineering and Engineering Management (IEEM)*, pp. 1455 - 1459, 2017.
- [68] A. Chaudhuri, H. A. Gerlich, J. Jayaram, A. Ghadge, J. Shack, B. H. Brix, L. H. Hoffbeck and N. Ulriksen, "Selecting spare parts suitable for additive manufacturing: a design science approach," *Production Planning & Control*, vol. 32, pp. 670 - 687, 2020.
- [69] S. U. Sapkal and P. H. Warule, "Application of Multi-attribute Decision Making Methods for Fused Deposition Modelling," in *Sustainability for 3D Printing*, Cham, Switzerland, Springer Tracts in Additive Manufacturing, 2021, pp. 55 - 75.
- [70] X. Yao, S. K. Moon and G. Bi, "A hybrid machine learning approach for additive manufacturing design feature recommendation," *Rapid Prototyping Journal*, vol. 23, no. 6, pp. 983 - 997, 2017.
- [71] H. Bikas, S. Koutsoukos and P. Stavropoulos, "A decision support method for evaluation and process selection of Additive Manufacturing," *52nd CIRP Conference on Manufacturing Systems*, vol. 81, no. 1, pp. 1107 - 1112, 2019.
- [72] J. Tavcar and A. Nordin, "MULTI-CRITERIA ASSESSMENT AND PROCESS SELECTION MODEL FOR ADDITIVE MANUFACTURING IN THE CONCEPTUAL PHASE OF DESIGN.," *Proceedings of the Design Society*, vol. 1, no. 1, pp. 2197 - 2206, 2021.
- [73] W. Liu, Z. Zhu and S. Ye, "A decision-making methodology integrated in product design for additive manufacturing process selection," *Rapid Prototyping Journal*, vol. 26, pp. 895 - 909, 2020.
- [74] S. Kadkhoda-Ahmadi, A. Hassan and E. Asadollahi-Yazdi, "Process and resource selection methodology in design for additive manufacturing," *The International Journal of Advanced Manufacturing Technology*, vol. 104, pp. 2013 - 2029, 2019.
- [75] R. Muvunzi, K. Mpofu and I. Daniyan, "An Evaluation Model for Selecting Part Candidates for Additive Manufacturing in the Transport Sector," *Metals*, vol. 11, no. 765, pp. 1 - 18, 2021.
- [76] C. G. Mancanares, E. d. S. Zancul, J. C. da Silva and P. A. C. Miguel, "Additive Manufacturing Process Selection Based on Parts' Selection Criteria," *The International Journal of Advanced Manufacturing Technology*, vol. 80, pp. 1007 - 1014, 2015.

- [77] P. Ayala and H. F. L. Herrera, "Maintenance Preventive Analysis in Additive Manufacturing Equipment using Analytic Hierarchy Process.," *Research Square*, pp. 1 - 23, 2021.
- [78] N. Wortmann, C. Jurgenhake, T. Seidenberg, R. Dumitrescu and D. Krause, "Methodical Approach for Process Selection in Additive Manufacturing.," in *International Conference on Engineering Design, ICED19*, Delft, Netherlands, 2019.
- [79] S. C. Renjith, K. Park and G. E. Okudan Kremer, "A Design Framework for Additive Manufacturing: Integration of Additive Manufacturing Capabilities in the Early Design Process," *International Journal of Precision Engineering and Manufacturing*, vol. 21, pp. 329 - 345, 2019.
- [80] C. S. Frandsen, M. M. Nielsen, A. Chaudhuri, J. Jayaram and K. Govindan, "In search for classification and selection of spare parts suitable for additive manufacturing: a literature review," *International Journal of Production Research*, vol. 58, pp. 970 - 996, 2020.
- [81] C. Suwanpreecha and A. Manonukul, "A Review on Material Extrusion Additive Manufacturing of Metal and How It Compares with Metal Injection Moulding," *Metals*, vol. 12, no. 429, pp. 1 - 56, 2022.
- [82] J. W. Booth, J. Alperovich, P. Chawla, J. Ma, T. N. Reid and K. Ramani, "The Design for Additive Manufacturing," *Journal of Mechanical Design*, vol. 139, pp. 1 - 18, 2016.
- [83] S. Yang and Y. F. Zhao, "Additive manufacturing-enabled part count reduction: a lifecycle perspective," *Journal of Mechanical Design*, vol. 140, p. 031702, 2018.
- [84] S. Yang, F. Santoro, M. A. Sulthan and Y. F. Zhao, "A numerical-based part consolidation candidate detection approach with modularization considerations," *Research in Engineering Design*, vol. 30, pp. 63 - 83, 2018.
- [85] G. Kazakis, I. Kanellopoulos, S. Sotiropoulos and N. D. Lagaros, "Topology optimization aided structural design: Interpretation, computational aspects and 3D printing," *Heliyon*, vol. 3, no. 10, pp. 1 - 33, 2017.
- [86] Autodesk, "Lightweighting with Shape Optimization," Autodesk, 14 May 2018. [Online]. Available: <https://knowledge.autodesk.com/support/fusion-360/getting-started/caas/simplecontent/content/lightweighting-shape-optimization.html>. [Accessed 06 June 2021].
- [87] Dassault Systems, "Shape Optimization with Abaqus, Ansys, or Msc Nastran," Dassault Systems, 15 May 2015. [Online]. Available: <https://www.3ds.com/products-services/simulia/products/tosca/structure/shape-optimization/>. [Accessed 02 June 2021].

- [88] Y. M. Xie and G. P. Steven, "A simple evolutionary procedure for structural optimization," *Computers & Structures*, vol. 49, no. 5, pp. 885-896, 1993.
- [89] M. P. Bendsoe and O. Sigmund, "Material interpolation schemes in topology optimization," *Archive of Applied Mechanics*, vol. 69, no. 9-10, pp. 635 - 654, 1999.
- [90] J. Zhao and C. Wang, "Robust topology optimization under loading uncertainty based on linear elastic theory and orthogonal diagonalization of symmetric matrices," *Computer Methods Applied Mechanics and Engineering*, vol. 273, pp. 204-218, 2014.
- [91] S. H. Jeong, D.-H. Choi and G. H. Yoon, "Separable stress interpolation scheme for stress-based topology optimization with multiple homogenous materials," *Finite Elements in Analysis and Design*, vol. 82, pp. 16-31, 2014.
- [92] G. Allaire, C. Dapogny and P. Frey, "Shape optimization with a level set based mesh evolution method," *Computer Methods in Applied Mechanics and Engineering*, vol. 282, pp. 22-53, 2014.
- [93] "The parameterized level set method for structural topology optimization with shape sensitivity constraint factor," *Engineering with Computers*, vol. 37, pp. 855-872, 2019.
- [94] B. Bourdin and A. Chambolle, "Design-dependent loads in topology optimisation," *ESAIM: Control, Optimisation and Calculus of Variations*, vol. 9, pp. 19-48, 2003.
- [95] S. I. Valdez, J. L. Marroquin, S. Botello and N. Faurrieta, "A meta-heuristic for topology optimization using probabilistic learning," *Applied Intelligence*, vol. 48, pp. 4267-4287, 2018.
- [96] Y. Xiong, D. Bao, X. Yan, T. Xu and Y. M. Xie, "Lessons Learnt from a National Competition on Structural Optimization and Additive Manufacturing," *Current Chinese Science*, vol. 1, no. 1, pp. 151-159, 2021.
- [97] S. N. Reddy K, I. Ferguson, M. Frecker, T. W. Simpson and C. J. Dickman, "Topology Optimization Software for Additive Manufacturing: A Review of Current Capabilities and a Real-World Example," Charlotte, North Carolina, 2016.
- [98] X. Y. Yang, Y. M. Xie, G. P. Steven and O. M. Querin, "Bidirectional Evolutionary Method for Stiffness Optimisation," *AIAA Journal*, vol. 37, no. 11, pp. 1483-1488, 1999.
- [99] O. M. Querin, V. Young, G. P. Steven and Y. M. Xie, "Computational efficiency and validation of bi-directional evolutionary structural optimization," *Computer Methods in Applied Mechanics and Engineering*, vol. 189, no. 2, pp. 559-573, 2000.
- [100] X. Huang and Y. M. Xie, *Evolutionary Topology Optimization of Continuum Structures: Methods and Applications*, First ed., West Sussex: John Wiley & Sons Ltd, 2010.

- [101] A. Belyaev and Y. Ohtake, "A comparison of mesh smoothing methods," in *Israel-Korea Bi-national conference on geometric modeling and computer graphics*, Tel Aviv University, 2003.
- [102] M. Wei, J. Huang, X. Xie, L. Liu, J. Wang and J. Qin, "Mesh Denoising Guided by Patch Normal Co-filtering via Kernel Low-rank Recovery," *IEEE Transactions on Visualization and Computer Graphics*, vol. 25, no. 10, pp. 2910 - 2926, 2019.
- [103] A. Bacciaglia, A. Ceruti and A. Liverani, "Surface smoothing for topological optimized 3D models," *Structural and Multidisciplinary Optimization*, vol. 64, no. 2021, pp. 3453 - 3472, 2021.
- [104] A. Nealen, T. Igarashi, O. Sorkine and M. Alexa, "Laplacian Mesh Optimization," Kuala Lumpur, 2006.
- [105] K. Yang, Z.-L. Zhao, Y. He, S. Zhou, . Q. Zhou, W. Huang and Y. M. Xie, "Simple and effective strategies for achieving diverse and competitive structural designs," *Extreme Mechanics Letters*, vol. 2019/5, 2019.
- [106] L. Velho and D. Zorin, "4–8 Subdivision," *Computer Aided Geometric Design*, vol. 18, no. 5, pp. 397 - 427, 2001.
- [107] H. I. Medellin-Castillo and J. Zaragoza-Siqueiros, "Design and Manufacturing Strategies for Fused Deposition Modelling in Additive Manufacturing: A Review," *Chinese Journal of Mechanical Engineering*, vol. 32, no. 53, pp. 1 - 16, 2019.
- [108] F. Baumann and D. Roller, "Vision based error detection for 3D printing processes," in *International Conference on Frontiers of Sensors Technologies*, 2016.
- [109] O. Diegel, A. Nordin and D. Motte, "DfAM Strategic Design Considerations," in *A Practical Guide to Design for Additive Manufacturing*, Singapore, Springer, 2020, pp. 41 - 67.
- [110] S. Liedtke, "IHHA conference to 'better equip' Transnet to take advantage of global knowledge, technology," 2019. [Online]. Available: [https://www.miningweekly.com/article/ihha-conference-to-better-equip-transnet-to-take-advantage-of-global-knowledge-technology-2019-05-31/rep\\_id:3650](https://www.miningweekly.com/article/ihha-conference-to-better-equip-transnet-to-take-advantage-of-global-knowledge-technology-2019-05-31/rep_id:3650). [Accessed 17 May 2021].
- [111] W. W. Wits, R. R. García and J. M. J. Becker, "How additive manufacturing enables more sustainable end-user maintenance, repair and overhaul (MRO) strategies," *13th Global Conference on Sustainable Manufacturing - Decoupling Growth from Resource Use*, vol. 40, pp. 694 - 699, 2016.

- [112] S. E. Hoosain, L. Tshabalala, D. Bester, D. Chetty and G. Mukwevho, “ADDITIVE MANUFACTURING CASE STUDY IN THE RAILWAY INDUSTRY,” in *Rapid Product Development Association of South Africa*, Pretoria, 2020.
- [113] J. W. Booth, J. Alperovich, P. Chawla, J. Ma, T. N. Reid and K. Ramani, “The Design for Additive Manufacturing Worksheet,” *Journal of Mechanical Design*, vol. 139, p. 100904, 2016.
- [114] P. Pradel, Z. Zhu, R. Bibb and J. Moultrie, “A framework for mapping design for additive manufacturing knowledge for industrial and product design,” *Journal of Engineering Design*, vol. 29, no. 6, pp. 291 - 326, 2018.
- [115] B. Redwood, F. Schöffner and B. Garret, “Designing of FFF,” in *The 3D Printing Handbook*, Amsterdam, 3D Hubs, 2017, pp. 194 - 215.
- [116] e3D+VET, Transfer of knowledge about basics of 3D printing concepts to the VET teachers, European Union: Erasmus, 2019.
- [117] Teaching Tech, “Teaching Tech 3D Printer Calibration,” Teaching Tech, 14 August 2020. [Online]. Available: <https://teachingtechyt.github.io/calibration.html#intro>. [Accessed 10 October 2021].
- [118] J. Jiang, G. Hu, X. Li, X. Xu, P. Zheng and J. Stringer, “Analysis and Prediction of Printable Bridge Length in Fused Deposition Modelling Based on Back Propagation Neural Network,” *Virtual and Physical Prototyping*, vol. 14, no. 3, pp. 253 - 266, 2019.
- [119] A. D. Toth, J. Padayachee, S. Vilakazi and V. Matjeke, “Multi-Criteria Decision-Making Methodology in Part Selection for Fused Deposition Modelling in the Railway Industry,” *Part F: Journal of Rail and Rapid Transit*, vol. 236, no. 6, pp. 1 - 8, 2022.
- [120] T. L. Saaty, *The Analytic Hierarchy Process: Planning, Priority Setting, Resource Allocation*, United States of America: McGraw-Hill, 1980.
- [121] T. L. Saaty, “How to make a decision: The Analytic Hierarchy Process,” *European Journal of Operational Research*, vol. 48, pp. 9 - 26, 1990.
- [122] M. Brunelli, *Introduction to the Analytic Hierarchy Process*, New York, NY, USA: Springer, 2015.
- [123] A. Ishizaka and P. Nemery, *Multi-Criteria Decision Analysis: Methods and Software*, Hoboken, NJ, USA: John Wiley & Sons, 2013.
- [124] A. D. Toth and S. Vilakazi, “Benefits of reinforced meshing and materials testing of 3D printed parts to assist mechanical design in the railway infrastructure environment,” in *RAPDASA 2019 Conference Proceeding*, Bloemfontein, 2019.

- [125] A. D. Toth and J. Padayachee, "Using topology optimisation to influence the infill placement of fused deposition modelled parts," *R & D Journal of the South African Institution of Mechanical Engineering*, vol. 1, no. 1, pp. 1 - 13, 2022.
- [126] L. M. Dezaki and M. M. Ariffin, "The Effects of Combined Infill Patterns on Mechanical Properties in FDM Process," *Polymers*, vol. 12, no. 12, p. 2792, 2020.
- [127] C. Geuzaine and J.-F. Remacle, "Gmsh: A 3D finite element mesh generator with built-in pre and post-processing facilities," *International Journal for Numerical Methods in Engineering*, vol. 79, no. 11, pp. 1309-1331, 2009.
- [128] K. Wittig, *CalculiX User's Manual: CalculiX GraphiX, Version 2.17.1, 1st ed.*, CalculiX, 2020.
- [129] F. Löffelmann, "Topology optimization, BESO method," 2020. [Online]. Available: <https://github.com/fandaL/beso/wiki/Basic-description>. [Accessed 05 01 2021].
- [130] F. Löffelmann, "Failure Index Based Topology Optimization for Multiple Properties," Svratka, Czech Republic, 2017.
- [131] F. Löffelmann, "beso," GitHub, 03 September 2020. [Online]. Available: <https://github.com/fandaL/beso/wiki/Basic-description>. [Accessed 03 May 2021].
- [132] P. Cignoni, M. Callieri, M. Corsini, M. Dellepiane, F. Ganovelli and G. Ranzuglia, "MeshLab: an Open-Source Mesh Processing Tool," *Eurographics Italian chapter conference*, vol. 2008, pp. 129-136, 2008.
- [133] ASTM International, "ASTM D790-03, Standard Test Methods for Flexural Properties of Unreinforced and Reinforced Plastics and Electrical Insulating Materials," ASTM International, West Conshohocken, PA, 2003.
- [134] A. D. Toth, J. Padayachee and S. Vilakazi, "Additive Manufacturing: Producing functional parts for the South African railway industry," in *International Heavy Haul Association 2022*, China 2022, 2022.
- [135] S. Burge, "The Systems Engineering Tool Box - Pugh Matrix (PM)," National Science Teaching Association, Arlington VA, 2009.
- [136] Airfoil Tools, "Airfoil database search (NACA 4 digit)," Airfoil Tools, 05 10 2020. [Online]. Available: <http://www.airfoiltools.com/airfoil/details?airfoil=n2414-il>. [Accessed 05 10 2020].
- [137] Dielectric Manufacturing, "PETG," Dielectric Manufacturing, 05 10 2020. [Online]. Available: <https://dielectricmfg.com/knowledge-base/petg/>. [Accessed 05 10 2020].



- [138] I. Gibson, D. Rosen and B. Stucker, "Introduction and Basic Principles," in *Additive Manufacturing Technologies: 3D Printing, Rapid Prototyping and Direct Digital Manufacturing*, New York, Springer, 2015, pp. 4 - 6.
- [139] I. Gibson, D. Rosen, B. Stucker and M. Khorasani, "Material Extrusion," in *Additive Manufacturing Technologies Third Edition*, Switzerland, Springer, 2021, pp. 171 - 201.
- [140] I. Gibson, D. Rosen and B. Stucker, "Extrusion-Based Systems," in *Additive Manufacturing Technologies: 3D Printing, Rapid Prototyping and Direct Digital Manufacturing*, New York, Springer, 2015, pp. 147 - 173.
- [141] Creality, "Creality CR10 S Pro V2 3D Printer," Creality, 05 January 2021. [Online]. Available: <https://www.creality3dofficial.com/products/cr-10s-pro-v2-3d-printer>. [Accessed 10 October 2021].
- [142] O. Diegel, A. Nordin and D. Motte, "Material Extrusion," in *A Practical Guide to Design for Additive Manufacturing*, New York, Springer, 2019, pp. 19 - 23.
- [143] B. Redwood, F. Schoffer and B. Garret, "3D Printing Technologies and Materials," in *The 3D Printing Handbook*, Amsterdam, The Netherlands, 3DHubs, 2017, pp. 26 - 179.
- [144] B. Redwood, F. Schoffer and B. Garret, "Material Extrusion," in *The 3D Printing Handbook*, Amsterdam, 3DHub, 2017, p. 50.
- [145] Simplify3D, "Ultimate 3D Printing Materials Guide," 2015. [Online]. Available: <https://www.simplify3d.com/support/materials-guide/>. [Accessed 15 01 2021].
- [146] D. de Beer, W. du Preez, H. Greyling, F. Prinsloo, F. Sciammarella, N. Trollip, M. Vermeulen and T. Wohlers, "A South African Additive Manufacturing Strategy," Department of Science and Technology, Pretoria, 2016.
- [147] S. Rutch, "3D Printing: Replacement on time increases train availability," 2019. [Online]. Available: [https://www.deutschebahn.com/en/Digitalization/DB\\_Digital/productworld/3dprint-1214672](https://www.deutschebahn.com/en/Digitalization/DB_Digital/productworld/3dprint-1214672). [Accessed 14 01 2019].
- [148] L. Griffiths, "Siemens Mobility is 3D printing spare parts at first digital rail maintenance centre," 2018. [Online]. Available: <https://www.tctmagazine.com/3d-printing-news/siemens-mobility-digital-rail-maintenance-3d-print-spare-parts/>. [Accessed 26 October 2018].
- [149] H. Knight, "Run2Rail to investigate carbon fibre and 3D printed parts for trains," theengineer, 18 01 2018. [Online]. Available: <https://www.theengineer.co.uk/run2rail-trains/>. [Accessed 02 06 2019].

- [150] Railway International, "The Growing Role of Additive Manufacturing in the Rail Industry: An Expert Talk," Railway International, 09 10 2020. [Online]. Available: <https://railway-international.com/technical-articles/32101-the-growing-role-of-additive-manufacturing-in-the-rail-industry-an-expert-talk>. [Accessed 13 01 2021].
- [151] A. Killen, L. Fu, S. Coxon and R. Napper, "Exploring the use of Additive Manufacturing in Providing an alternative Approach to the Design, Manufacture and Maintenance of Interior Rail Components," in *Australasian Transport Research Forum 2018*, Darwin, Australia, 2018.
- [152] Transnet Freight Rail, "From MDS to Transnet 4.0," 2018. [Online]. Available: <https://www.transnet-ir-2018.co.za/from-mds-to-transnet-4-0.php>. [Accessed 17 May 2021].
- [153] P. Connor and P. Berkeley, "Rolling Stock Manufacturing," Railway Technical Website, 2017.
- [154] J. Sadeghi and P. Barati, "Evaluation of conventional methods in Analysis and Design of Railway Track System," *International Journal of Civil Engineering*, vol. 8, no. 1, pp. 44 - 56, 2010.
- [155] R. Muvunzi, K. Mpofu, I. Daniyan and F. Fameso, "Analysis of potential materials for local production using Additive Manufacturing. A case for the rail industry.," *SSRN*, 2021.
- [156] O. Abdulhameed, A. Al-Ahmari, W. Ameen and S. H. Mian, "Additive Manufacturing: Challenges, trends, and applications," *Advances in Mechanical Engineering*, vol. 11, no. 2, pp. 1 - 27, 2019.
- [157] Railway Safety Regulator, "National Government of South Africa," Railway Safety Regulator (RSR), 10 January 2012. [Online]. Available: <https://nationalgovernment.co.za/units/view/273/railway-safety-regulator-rsr>. [Accessed 10 August 2021].
- [158] K. Sertoglu, "Kimya 3D prints spare parts for the railway industry with custom PEKK filament," The 3D printing Industry, 25 February 2021. [Online]. Available: <https://3dprintingindustry.com/news/kimya-3d-prints-spare-parts-for-the-railway-industry-with-custom-pekk-filament-185203/>. [Accessed 11 August 2021].
- [159] D. Hohenwarter, C. Fischer and M. Berger, "Influence of 3D-Printing on the Flammability Properties of Railway Applications Using Polycarbonate (PC) and Polylactic acid (PLA)," *IK Instytut Kolejnictwa*, no. 187, pp. 99 - 107, 2020.
- [160] X. Peng, L. Kong, J. Y. Hsi Fuh and H. Wang, "A Review of Post-Processing Technologies in Additive Manufacturing," *Journal of Manufacturing and Material Processing*, vol. 5, no. 38, pp. 1 - 23, 2021.

- [161] G. Schuh, G. Bergweiler, P. Bickendorf, F. Fiedler and C. Colag, "Sheet Metal Forming Using Additively Manufactured Polymer Tools," *53rd CIRP Conference on Manufacturing Systems*, vol. 93, pp. 20-25, 2020.
- [162] P. E. Romero, J. Arribas-Barrios, O. Rodriguez-Alabanda, R. González-Merino and G. Guerrero-Vaca, "Manufacture of polyurethane foam parts for automotive industry using FDM 3D printed molds," *CIRP Journal of Manufacturing Science and Technology*, vol. 32, pp. 396 - 404, 2021.
- [163] M. I. M. Sargini, S. H. Masood, S. Palanisamy, E. Jayamani and A. Kapoor, "Additive manufacturing of an automotive brake pedal by metal fused deposition modelling," *Materials Today: Proceedings*, vol. 45, no. 6, pp. 4601 - 4605, 2021.
- [164] M. Schmitt, R. M. Mehta and I. Y. Kim, "Additive manufacturing infill optimization for automotive 3D-printed ABS components," *Rapid Prototyping Journal*, vol. 26, pp. 89 - 99, 2020.
- [165] A. García-Domínguez, J. Claver and M. A. Sebastián, "Integration of Additive Manufacturing, Parametric Design, and Optimization of Parts Obtained by Fused Deposition Modeling (FDM). A Methodological Approach," *Polymers*, vol. 9, no. 1993, 2020.
- [166] A. Zapciu, G. D. Tasca and C. G. Amza, "Considerations on 3D printing joints parts," *IOP Conference Series: Materials Science and Engineering*, vol. 400, no. 2, 2018.
- [167] A. D. Toth, B. F. du Toit, M. Nethononda and D. Reddy, "Additive Manufacturing: IoT integrated environmental monitoring system for electrified railway lines," in *International Heavy Haul Association 2022*, China, 2022.
- [168] Markforged, "3D Printed Joinery: Simplifying Assembly," Markforged, 12 September 2018. [Online]. Available: <https://markforged.com/resources/blog/joinery-onyx>. [Accessed 11 October 2021].
- [169] A. Samimi, "Using Fasteners with 3D Printed Parts," Fathom, Florida, 2021.

# Appendix A: Fused Deposition Modelling

## 8.1 Fused Deposition Modelling in Additive Manufacturing

“Fused Deposition Modelling (FDM) is a material extrusion 3D printing technology and the most commonly available system. These systems' popularity is due to the low investment costs, large material availability, and ease of use compared to other systems. The FDM method of 3D printing builds parts by heating a thermoplastic filament to a semi-liquid state. The thermoplastic filament is extruded through a small nozzle, turning it into molten plastic, creating the physical part in a bottom-up, layer-by-layer fashion [13], [139], [140].” [3] Figure A - 1-A illustrates a schematic of an FDM 3D printer mechanism, while Figure A - 2-B illustrates the commercially available 3D printer used for this study. The 3D printer specifications are detailed in [141]. All FDM materials, printing parameters and design techniques will be based on the capabilities of the selected printer for this study. “Each FDM printer technology is restricted to its specific printing method and design. Factors related to its design restriction include; build volume, print speed, material type, printer type, feed rate, and printing technology. Some machines also have double nozzles for printing multicolour prints or water-soluble support structures, enclosures or open systems. There are three main FDM machine types: cartesian-based axles, delta-based axles, and some systems built with robotic arms [142]. In all cases, the primary method of 3D printing a part is the same.” [3]

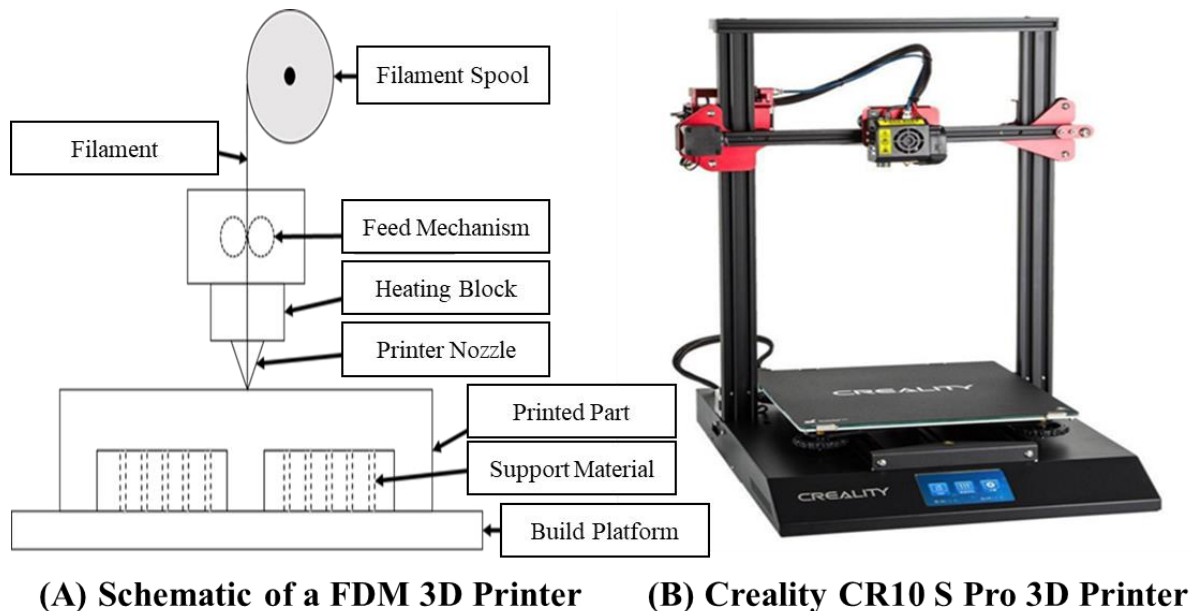


**Figure A - 1 Schematic of a Fused Deposition Modelling 3D Printer (A) and the Creality CR10 S Pro 3D Printer (B)**  
[13], [141]

## 8.2 FDM 3D Printing Materials

The one significant advantage of the FDM technology is the wide range of materials currently available in the market [27]. Given the rapid advancements in AM technologies, materials are also advancing faster than standard material types [1]. Various new composite materials are being developed to improve the mechanical properties of 3D printed parts specific for functional applications. Some of the more common materials used include; Acrylonitrile Butadiene Styrene (ABS), Polylactic Acid (PLA), High Impact Polystyrene (HIPS), Polyethylene Terephthalate (PETG), Polyamide (Nylon), Polyurethane (TPU), Acrylic Styrene (ASA), Polycarbonate (PC), Polypropylene (PP), Polyvinyl Alcohol (PVA) and Polyaryletherkethone (PEEK). These materials can be broken into three main categories: commercial, engineering and high-performance [143]. Figure A - 2 illustrates the 3D printing material categories.

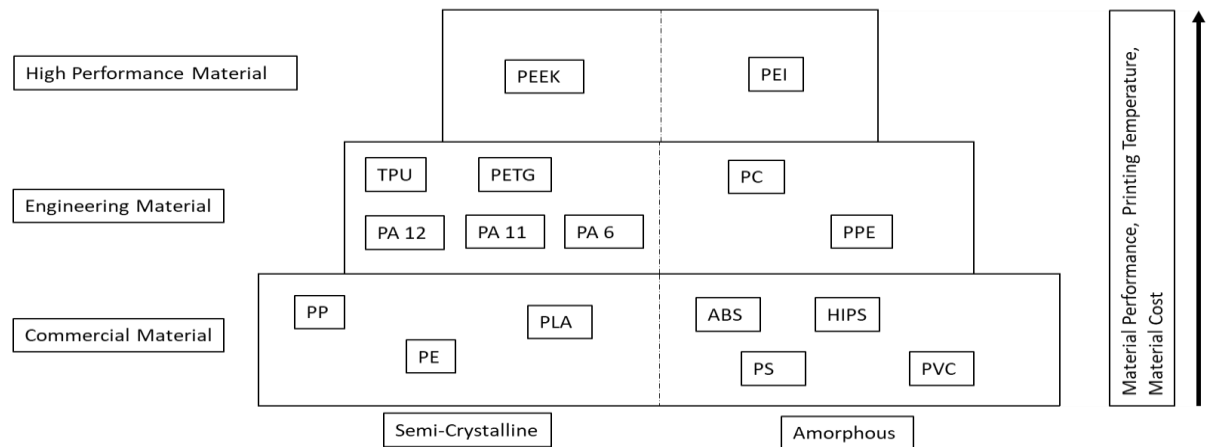


Figure A - 2 illustrates the material types and their respective categories [144].

### 8.2.1 FDM Material Properties

“The FDM printing technology uses thermoplastics, similar to plastics found in traditional manufacturing processes such as injection moulding. The difference lies in the processes used to manufacture the part. The materials available to FDM come in various tolerances, mechanical and chemical properties and environmental stability with specific properties such as translucency, biocompatibility, electrostatic dissipation, chemical resistance, UV stability or flame resistance [1]. A clear understanding of material printing and mechanical properties is needed when selecting the appropriate slicing settings for the 3D print. A significant relationship exists between the printing temperature and the printed part strength. This is due to the dependence on layer adhesion between the build plate and between the print layers. Parts printed at lower glass transition temperatures will result in poor layer adhesion and separation, resulting in weaker parts [1]. Materials in the additive manufacturing space will continue to advance with the advancing technology. A detailed list of FDM materials with their corresponding Ultimate Tensile Strength (UTS), stiffness rating, durability rating, print and build plate temperatures, and some recommended applications are presented in [145].” [3]

# **Appendix B: Additive Manufacturing in the Railway Industry**

## **9.1 The South African Additive Manufacturing Strategy**

In 2016, the South African Department of Science and Technology (DST) commissioned a South African Additive Manufacturing (AM) Strategy. The AM strategy is intended to enable local companies and industry sectors to become global leaders in selected areas of AM by identifying economic opportunities, focusing on development programmes, addressing technology gaps, and informing investment decisions for 2014 – 2023 [146]. The strategy was developed from survey inputs through facilitated stakeholder workshops, desktop studies, international market research, and surveying local capabilities and experts in AM and technology. The survey included industry focus, R&D focus, facilities, certification status, workforce, and infrastructure related to the AM technology capabilities with an industry sample from the automotive, aerospace, consumer goods, creative industries, defence and security, medical, energy and tooling industries [146]. Based on the inputs, a capability matrix for the South African industry was developed with four priority focus areas [146]. To aid the implementation of the South African Additive Manufacturing Strategy, du Preez and de Beer [12] proposed an Additive Manufacturing Centre of Competence (AMCoC). The railway industry is an apparent gap in the capability matrix and the AMCoC framework, likely due to the limited AM expertise within the railway environment at the time of inception [12].

## **9.2 Additive Manufacturing in International Railway Industries**

Research in the additive manufacturing sector for the railway industry has seen more activity in other countries. Various rail operators are already using the manufacturing technology to reduce maintenance cycles, refurbish out-of-service components, or replace railway-related parts. The German railway company, Deutsche Bahn (DB), used this manufacturing technique to build spare parts for the old rolling stock fleet and equipment [147]. 3D printing has also been used to prototype custom designs for customer-facing products across Deutsche Bahn's network and fleet. Parts ranging from ventilation grilles, headrests, coat hooks, and cable boxes have been integrated into the railway industry using the FDM process in additive manufacturing [147]. Another giant in the railway industry, Siemens Mobility, highlights that "The ability to 3D print customised tools and spare parts whenever we need them, with no minimum quantity, has transformed our supply chain" [148]. The company has opened its first digital rail maintenance centre to eliminate the inventory needed for spare parts. They can achieve this using AM and 3D printing techniques. Using this technology, Siemens Mobility has reduced manufacturing lead times by 95% for select railway parts [148].

The 'Run2Rail' project in Europe investigated the feasibility of 3D printing rolling stock parts and components using carbon fibre material to build lighter and quieter trains [149]. Using additive manufacturing allows for on-demand servicing of railway vehicles where obsolete or re-engineered parts can be replaced, reducing the need for upfront tooling costs [150]. Killen et al. [151] investigated the best practices in AM for the Australian railway industry, focusing on manufacturing, designing, and maintaining customer-facing products. The study presented potential cost-saving initiatives, production time savings and the social considerations related to AM parts. The researcher outlined potential AM opportunities within the railway environment being case-dependent with a critical focus on research due to the limited available literature.

### 9.3 AM Challenges for the South African Railway Environment

Table B - 1 illustrates some of the identified challenges experienced in applying additive manufacturing technology within the South African railway environment [10].

**Table B - 1 AM Challenges for the South African Railway Industry [10]**

<b>Challenges</b>	<b>Description</b>
Mass Production [152], [110], [153], [154]	“Low manufacturing volumes benefit the AM technology; however, the low volume of manufactured railway parts is designed to strict design codes to ensure that parts have lifecycles of 30 – 50 years.” [10]
Print Bed Size [155]	“Many load-bearing components on the rolling stock and rail infrastructure are too large to be printed as a single part or component.” [10]
AM Skills Gap [1], [156]	“A significant gap exists between the additive manufacturing technology for industrial applications and the technology's research stages due to limited AM expertise within the railway environment.” [10]
Railway Engineering Standards [5], [157], [158], [159]	“Railway-engineered products are designed and tested to strict design codes and safety regulations based on traditional manufacturing methods. To realise the benefits of additive manufacturing, more research in approving the different material and technology types for railway industry applications is needed.” [10]
Post-Processing Realities [160]	“The additive manufacturing process produces parts that usually require some post-processing method to be applied to the 3D printed part before being used. These methods are dependent on the AM technology used.” [10]

# Appendix C: Part Selection

## 10.1 Application: Weights, Criteria and Decision Matrix

Using Equation 3 - 1, the pairwise matrix is generated, illustrated in Table C - 1 based on the level of importance rating presented in Table 3 - 2, while Table C - 2 illustrates the normalised matrix using Equation 3 - 2. The criteria weights' degree of importance and consistency values are calculated using Equation 3 - 3 and Equation 3 - 4. Table C - 3 presents the criteria weights and consistency measure.

**Table C - 1 Pairwise Comparison Matrix**

Criteria	Design Optimisation	Geometric Complexity	Production Volume	Part Benefit	Material Removal	Part Function	Manufacturing Time
Design Optimisation	1	1/3	1/2	1	4	1/2	3
Geometric Complexity	3	1	4	2	7	3	5
Production Volume	2	1/4	1	1	5	5	3
Part Benefit	1	1/2	1	1	5	1	3
Material Removal	1/4	1/7	1/5	1/5	1	1/5	1
Part Function	2	1/3	1/5	1	5	1	5
Manufacturing	1/3	1/6	1/3	1/3	1	1/5	1

**Table C - 2 Normalized Matrix**

Criteria	Design Optimisation	Geometric Complexity	Production Volume	Part Benefit	Material Removal	Part Function	Manufacturing Time
Design Optimisation	0.104	0.122	0.069	0,153	0,143	0,050	0,143
Geometric Complexity	0.313	0.367	0.553	0,306	0,250	0,280	0,238
Production Volume	0.209	0.092	0.138	0,153	0,179	0,460	0,143
Part Benefit	0.104	0.183	0.138	0,153	0,179	0,090	0,143
Material Removal	0.026	0.052	0.028	0,031	0,036	0,020	0,048
Part Function	0.209	0.122	0.028	0,153	0,179	0,090	0,238
Manufacturing	0.035	0.061	0.046	0,051	0,036	0,020	0,048



**Table C - 3 Criteria Weights and Consistency Measures**

<b>Criteria</b>	<b>Weight</b>	<b>Consistency Measure</b>	<b>Rank</b>
Geometric Complexity	0.317	7.74	1
Production Volume	0.201	8.37	2
Part Function	0.151	7.27	3
Part Benefit	0.148	8.47	4
Design Optimisation	0.104	6.97	5
Manufacturing Time	0.044	6.96	6
Material Removal	0.036	7.19	7

**Table C - 4 Decision Matrix for Selection Potential Railway Parts for AM**

Criteria (a)	Weight (C)	Rating Scale		
Geometric Complexity	0.317	Low	Medium	High
		Parts containing generic shapes like feedstock material.	Parts which require additional operations apart from basic machining operations.	Parts containing complex internal features and contours.
		1	2	3
Production Volume	0.201	Low	Medium	High
		Parts < 1000	$1000 \geq \text{Parts} \leq 5000$	Parts > 5000
		1	2	3
Part Function	0.151	Non-critical	Semi-Critical	Critical
		1	2	3
Part Benefit	0.148	Low	Medium	High
		1	2	3
Design Optimisation: Light-weighting, Assembly-part consolidation and Material change	0.104	Low	Medium	High
		No design optimisation methods needed	< 1 design optimisation method can be applied	> 1 design optimisation methods can be applied
		1	2	3
Manufacturing Time	0.044	Low	Medium	High
		Making a part with traditional methods takes less time than AM	Equal time to produce a part using traditional methods and AM	Making a part with traditional methods takes more time than AM
		1	2	3
Material Removal	0.036	Low	Medium	High
		< 50 % requiring traditional processes	50 % requiring traditional processes	> 50 % using conventional processes
		1	2	3

## **10.2 AHP Model Verification and Validation**

The proposed AHP evaluation model requires verification and validation to be acceptable and used for selecting potential AM parts in the railway environment. Four published additive manufacturing case studies using the FDM technology to produce functional parts are used to validate the proposed AHP MCDM model.

### **10.2.1 Case Study 1: Sheet Metal Forming**

Schuh et al [161] presented a functional design of a custom 3D printable two-sided punch tool for deep-drawn sheet metal parts. The intended tool creates low-quantity, high-value automotive parts with medium geometric complexity. Using the FDM process, the manufacturing time to produce the two-sided punch is considered low based on the recommended print settings. The punch design was evaluated using FEA, and the results were verified using experimental compressive tests, which showed that material removal is not required, but minimal design changes to improve friction was presented.

### **10.2.2 Case Study 2: 3D Printed Moulds**

Romero et al [162] presented a custom design and experimental investigation using FDM 3D printed moulds to create high-value, low-volume polyurethane (PUR) form parts for the automotive industry. The production of PUR foam parts in the automotive industry includes seats, roof insulation and façade panels, which are considered critical functional parts. The experimental investigation recommended print settings for optimal printing time and post-processing methods to improve the demoulding process. Lastly, the design complexity of the 3D printable mould is considered medium, particularly for the interfacing joints with minimal design optimisation method required for the mould. Finally, material removal is not required for the PUR foam parts or the mould.

### **10.2.3 Case Study 3: 3D Printed Metal Brake Pedal**

Sargini et al [163] proposed a new design of an automotive brake pedal printed in metal using the FDM technology. The pedal design incorporated design optimisation techniques such as part consolidation, light-weighting and material optimisation. The design produces low quantity, high value and complex final brake pedals printed in metal-polymer filament material, BASF Ultrafuse 316L. The pedals were experimentally tested, and FEA was performed to verify the results.

### **10.2.4 Case Study 4: 3D Printed Racing Wheel and Automotive Control Arm**

Schmitt et al [164] presented experimental results and custom design considerations for a prototype racing wheel and an automotive control arm printed using the FDM process. The one-off parts are considered high-value components within the automotive environment. Design optimisation, material

removal and part function were performed on the components to improve the strength-to-weight properties and the manufacturing time. The results showed that high-value parts could be optimised using the FDM process to improve manufacturability.

Using the published literature as case studies and the rate scaling (Table C - 4) method for the analytical hierarchy process, the weight criteria derived in Table C - 3 are validated, verifying the proposed model. Table C - 5 presents the qualitative evaluation of the case studies, while Table C - 6 presents the quantitative evaluation.

**Table C - 5 Qualitative Evaluation of Part Candidate Case Studies**

	Geometric Complexity	Production Volume	Part Benefit	Part Function	Design Optimisation	Manufacturing Time	Material Removal
Criteria Weights	0,317	0,201	0,148	0,151	0,104	0,044	0,036
Case 1	Medium	Low	High	Critical	Medium	Low	Low
Case 2	Medium	Medium	Medium	Critical	Medium	Low	Low
Case 3	Medium	Low	Medium	Non-Critical	High	Low	Medium
Case 4	Medium	Low	Medium	Non-Critical	High	Low	Medium

**Table C - 6 Quantitative Evaluation of Part Candidate Case Studies**

	Geometric Complexity	Production Volume	Part Benefit	Part Function	Design Optimisation	Manufacturing Time	Material Removal
Criteria Weights	0,317	0,201	0,148	0,151	0,104	0,044	0,036
Case 1	2	1	3	3	2	1	1
Case 2	2	2	2	3	2	1	1
Case 3	2	1	2	1	3	1	2
Case 4	2	1	2	1	3	1	2

Table C - 7 presents the total weight (R) for each case study and the overall priority by applying the rating scale method and the criteria weights for each criterion.

**Table C - 7 Total Weight and Overall Priority for the Case Study [119]**

Case Studies	Total Weight (R)	Overall Priority	Potential
1	2,020	0,267	Suitable with no design change needed.
2	2.117	0,280	Suitable with no design change needed.
3	1,71	0,226	Suitable after a design change.
4	1.71	0,226	Suitable after a design change.

## 10.3 Functional End-Use 3D Printed Railway Parts

### 10.3.1 Maintenance Tooling

**Table C - 8 Qualitative Evaluation of Part Candidate Case Studies**

	Geometric Complexity	Production Volume	Part Benefit	Function	Design Optimisation	Manufacturing Time	Material Removal
Criteria Weights	0,317	0,201	0,148	0,151	0,104	0,044	0,036
Case 1: Lubricator Tools	Medium	Medium	High	Non-Critical	Low	Low	Low
Case 2: Lubricator Bracket	Medium	Medium	High	Critical	Medium	Low	Low
Case 3: Thermite Welding	Low	Low	Low	Non-Critical	Low	Low	Low

**Table C - 9 Quantitative Evaluation of Part Candidate Case Studies**

	Geometric Complexity	Production Volume	Part Benefit	Function	Design Optimisation	Manufacturing Time	Material Removal
Criteria Weights	0,317	0,201	0,148	0,151	0,104	0,044	0,036
Case 1	2	2	3	1	1	1	1
Case 2	2	2	3	3	2	1	1
Case 3	1	1	1	1	1	1	1

### 10.3.2 Maintenance Measuring

**Table C - 10 Qualitative Evaluation of Part Candidate Case Studies**

	Geometric Complexity	Production Volume	Part Benefit	Function	Design Optimisation	Manufacturing Time	Material Removal
Criteria Weights	0,317	0,201	0,148	0,151	0,104	0,044	0,036
Case 1: Measuring Tool	Medium	Low	Medium	Critical	Medium	Low	Medium

**Table C - 11 Quantitative Evaluation of Part Candidate Case Studies**

	Geometric Complexity	Production Volume	Part Benefit	Function	Design Optimisation	Manufacturing Time	Material Removal
Criteria Weights	0,317	0,201	0,148	0,151	0,104	0,044	0,036
Case 1	2	1	2	3	2	1	2

### 10.3.3 Rolling Stock

**Table C - 12 Qualitative Evaluation of Part Candidate Case Studies**

	Geometric Complexity	Production Volume	Part Benefit	Function	Design Optimisation	Manufacturing Time	Material Removal
Criteria Weights	0,317	0,201	0,148	0,151	0,104	0,044	0,036
Case 1: Mounting Brackets	Low	Medium	High	Critical	Medium	Low	Low
Case 2: Cover	Medium	Medium	High	Critical	Medium	Low	Low

**Table C - 13 Quantitative Evaluation of Part Candidate Case Studies**

	Geometric Complexity	Production Volume	Part Benefit	Function	Design Optimisation	Manufacturing Time	Material Removal
Criteria Weights	0,317	0,201	0,148	0,151	0,104	0,044	0,036
Case 1	1	2	3	3	2	1	1
Case 2	2	2	3	3	2	1	1

### 10.3.4 Prototypes & Light-Weighting

**Table C - 14 Qualitative Evaluation of Part Candidate Case Studies**

	Geometric Complexity	Production Volume	Part Value	Function	Design Optimisation	Manufacturing Time	Material Removal
Criteria Weights	0,317	0,201	0,148	0,151	0,104	0,044	0,036
Case 1: Weather Station	High	Low	High	Critical	Medium	Medium	Low

**Table C - 15 Quantitative Evaluation of Part Candidate Case Studies**

	Geometric Complexity	Production Volume	Part Value	Function	Design Optimisation	Manufacturing Time	Material Removal
Criteria Weights	0,317	0,201	0,148	0,151	0,104	0,044	0,036
Case 1	3	1	3	3	2	2	1

# Appendix D: Custom Infill Placement

## 11.1 Material Properties

There are several 3D printing materials available for the FDM technology. The material selected for this study is Polyethylene Terephthalate (PETG) due to available literature, cost, printing parameters, material properties and the ease of printing on the selected FDM 3D printer [42], [43], [44], [45], [46]. Table D - 1 illustrates the material properties of the PETG test specimens.

**Table D - 1 Polymer Filament Properties Used in the Study [137]**

Properties	PETG
Melting Temperature	81°C - 91°C
Maximum Service Temperature	51°C - 64°C
Surface Quality	Fine
Cool Time	Medium
Moisture Absorption 24 hours	Approx. 0.13%
Shrinkage	1-3 %
Density	1.27 g/cm <sup>3</sup>
Elongation At Break	1.1 % strain
Glass Transition	105°C
Strength at Break (Tensile)	28 MPa
Strength at Yield (Tensile)	50 MPa
Tensile Strength	63 MPa
Youngs Modulus	2.11 GPa
Flexural Modulus	4.1 GPa

## 11.2 Custom Infill Placement

The steps used to create a custom infill placement based on finite element analysis (FEA) and the Bi-directional Evolutionary Structural Optimisation (BESO) technique are presented as a fishbone diagram in Figure 4 - 2.

### 11.2.1 Model Construction (Stage 1)

The digital CAD model of the rectangular test specimens is created using Siemens NX with dimensions presented in Figure 4 - 11. The CAD model is exported as two files, an STL file and a STEP file, in preparation for the custom infill placement. The STL file of the rectangular test specimen will be used during the infill design stage of the process, while the STEP file will be imported into the FreeCAD



software to perform the FEA and BESO techniques. Figure D - 1 illustrates the digital models of the rectangular test specimens.

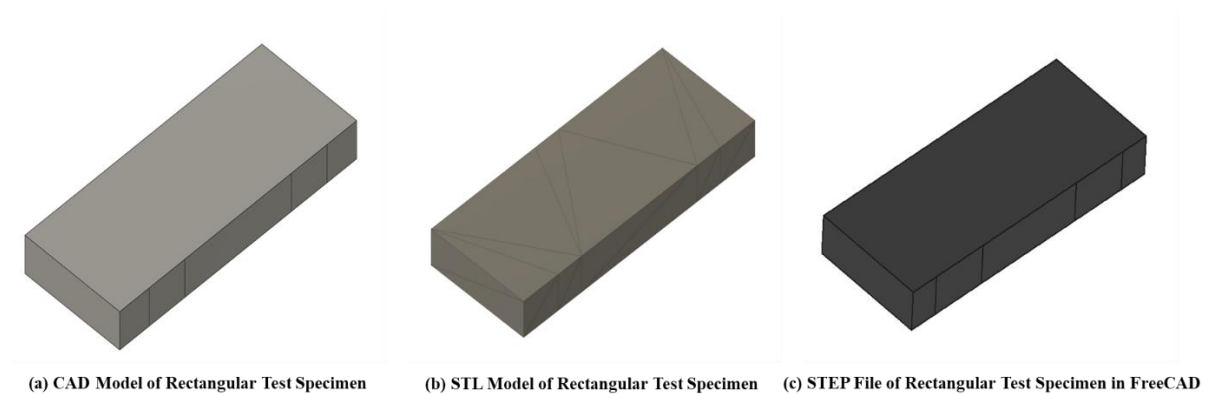


**Figure D - 1 Digital Models of the Rectangular Test Specimen**

### 11.2.2 Mesh Generation (Stage 2)

The finite element mesh is created within FreeCAD's FEM workbench using Gmsh [127]. Since the BESO method adds and removes elements based on a stress criterion, the mesh element size will determine the optimised shape. Table D - 2 illustrates the mesh algorithms used to set up the finite element model for the test specimen. Figure D - 2 illustrates the generated mesh model.

**Table D - 2 Finite Element Mesh Settings for the Rectangular Test Specimens [125]**

FEM Mesh	Gmsh
2D Algorithm	DelQuad
3D Algorithm	Delaunay
Element Size	3 mm
Element Order	Second-order

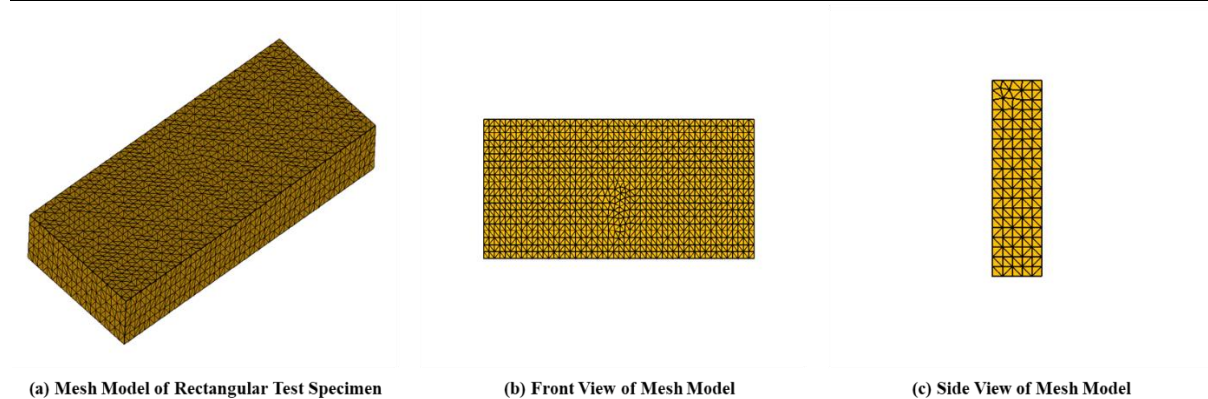


**Figure D - 2 Mesh Generation of the Rectangular Test Specimen Model**

### 11.2.3 Finite Element Analysis (Stage 3)

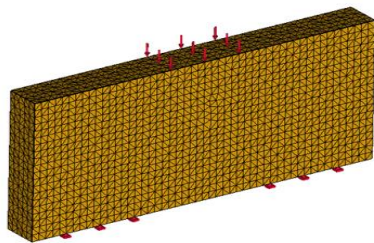
The finite element analysis is done using the CalculiX solver [128], which is required to determine the stress regions of the test specimen. The stress regions are then used in the BESO technique to produce an optimised part. Four types of structural simulations are performed based on the four loading cases required for this study. Figure D - 2 illustrates the mesh applied to the test specimen. Table D - 3 illustrates the boundary and loading conditions used to perform the structural simulation on the rectangular test specimens. The loading force is applied to the surface area section matching the thickness of the roller supports instead of only a tangent. This is due to performing a static analysis on the test specimens. The simulations are performed on the specimen enough to fail due to the applied loading condition. This is done to ensure that the complete stress profile of the body is presented with the corresponding stress values, which will be used when the BESO technique is applied. Table D - 4 presents the final FEA results for the four loading cases, and Figure D - 3 illustrates a graphical representation.

**Table D - 3 Boundary Conditions for Simulation**

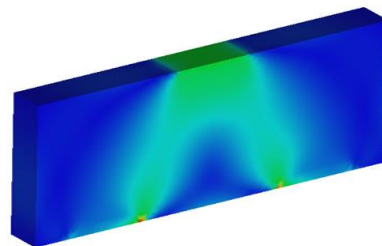
Applied Force	5000 N
Fixed Constraints	0° freedom at the Base of the Test Specimens
Material	PETG Plastic

**Table D - 4 FEA results for the different test cases [125]**

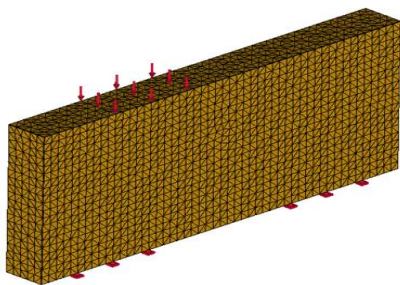
	Three-Point	Off-Centre	Four Point	Inverted
von Mises Stress				
min (kPa)	10.63	8.54	16.13	55.86
max (MPa)	49.08	43.33	45.30	104.75
Displacement				
min (mm)	0	0	0	0
max (mm)	0.33	0.29	0.22	0.56
Shear Stress				
min (kPa)	6.13	4.87	9.25	29.35
max (MPa)	26.26	22.63	24.93	57



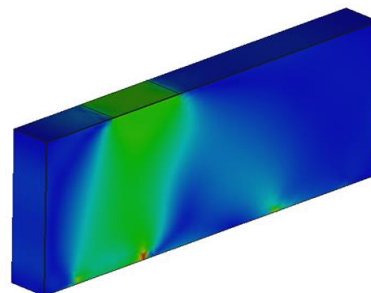
**(A) Three-Point Model Simulation**



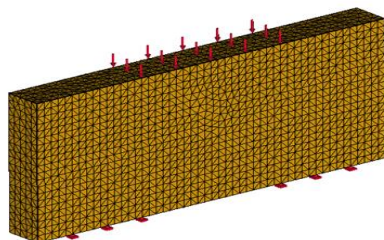
**(B) Three-Point FEA Results**



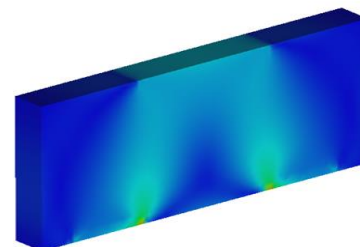
**(C) Offset Three-Point Model Simulation**



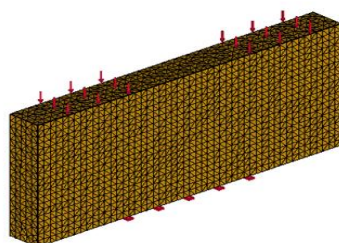
**(D) Offset Three-Point FEA Results**



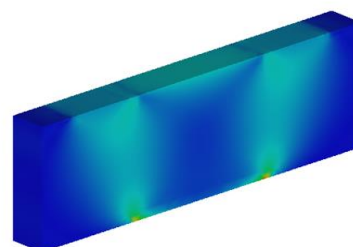
**(E) Four-Point Model Simulation**



**(F) Four-Point FEA Results**



**(G) Four-Point Inverted Model Simulation**



**(H) Four-Point Inverted FEA Results**

**Figure D - 3 Finite Element Analysis Results for the Four Loading Cases**

### 11.2.4 Topology Optimisation using BESO (Stage 4)

In this study, the BESO macro on FreeCAD is used to perform the BESO method with minimal changes to the source code for the current application. Table D - 5 illustrates the changes performed. Figure D - 4 illustrates the final iteration of the BESO method for the different bending tests.

**Table D - 5 BESO Properties for the Rectangular Test Specimens**

Optimisation Base	Stiffness
Mass Goal Ratio	0.4
mass_addition_ratio	0.015
mass_removal_ratio	0.03
Element filter size Limit	4 mm (Twice Element Size)
Number of Iterations	65
Average Run Time	3 minutes 21 seconds

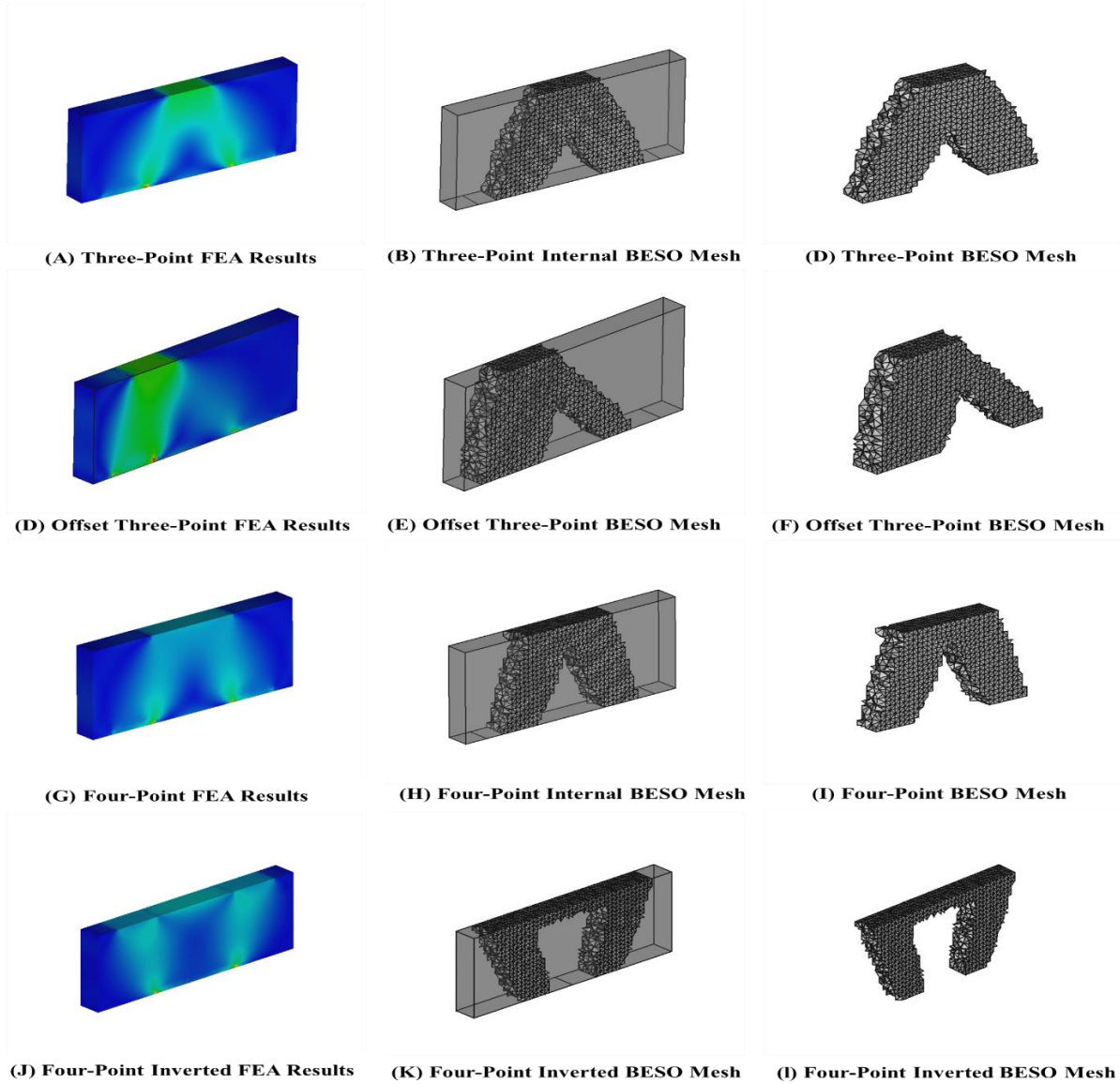


**Figure D - 4 BESO Mesh Results for the Four Loading Cases**

### 11.2.5 Post-Processing Topology Optimised Mesh (Stage 5)

The custom macro converts the FEM mesh created by the BESO method into a mesh geometry natively in FreeCAD. The mesh geometry represented by elements is then converted into quadrilateral elements using the 4-8 subdivision method. Finally, Laplacian smoothing is applied to the quadrant mesh to create a smooth FDM 3D printable model while maintaining the optimised structural shape or size. Figure D - 5 illustrates the graphical representation of the mesh optimisation used to produce an FDM 3D printable body.

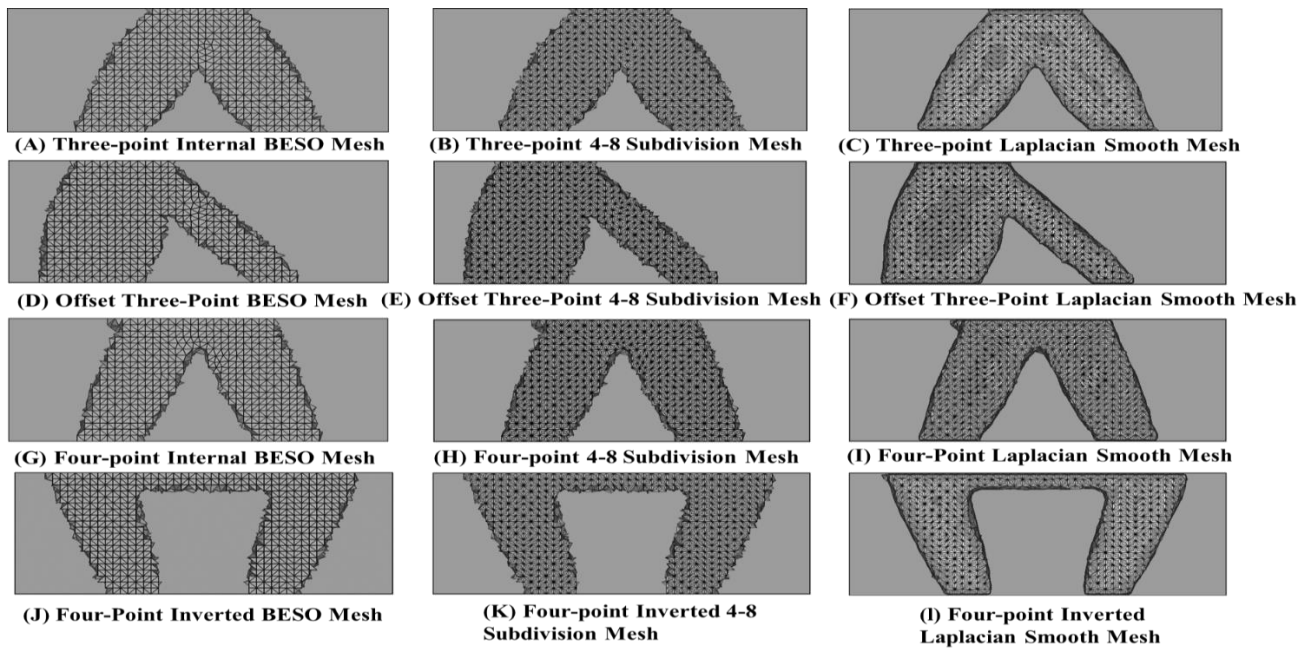


Figure D - 5 Post-Processing the BESO Optimised Mesh of the Rectangular Specimens

### 11.2.6 Infill Design (Stage 6)

The original CAD model and the BESO structure are imported into Cura 4.11 slicer software as STL file formats. The process parameters (infill density, infill patterns, wall thickness, number of walls, material temperature, print speed and extrusion width) are assigned to the BESO optimised structure and the original rectangular test specimen. Both models are merged together with the BESO structure represented as infill and the original rectangular model as the body. Finally, the model is sliced, and the print G-code is created. In this study, two comparisons are performed. The first comparison with test specimens printed with 100 % infill for the reference specimen and the BESO optimised specimen, while the second comparison will test specimens with a multi-infill geometry combination. Each loading case is assigned three infill pattern configurations with the BESO structure containing 3D infill patterns, and the original rectangular model is assigned a rectilinear infill pattern. This approach presents a multi-infill geometry for a 3D printable part.

### 11.3 3D Printed Test Specimens

After the print G-code is created for each test specimen with the optimised infill placement, they are sent to the 3D printer for printing. A total of 20 specimens are printed using PETG material. Table D - 6 illustrates the mass and material extruded lengths for the test specimens for the first test comparison, while Table D - 7 illustrates the printing parameters selected for printing each test specimen in the second test comparison. Table D - 10 through to Table D - 15 presents the dimensional accuracy between the digital models and 3D printed versions. Figure D - 6 and Figure D - 7 illustrates the graphical representation of the internal and external bodies of the test specimens for the first and second test comparisons.

**Table D - 6 3D Printed Test Specimen Details for the First Test Comparison [125]**

Test Specimens	Mass (g)	Material Extruded (mm)	Print Time (minutes)
Reference (100 % Infill)			
Rectilinear	51	16810	195
Optimised (100 % BESO Infill)			
Three-point	35	11490 (- 31.65%)	110 (-43.59%)
Off-centre	35	11590 (- 31.05%)	108 (-44.62%)
Four-point	35	11540 (- 31.35%)	109 (-44.10%)
Inverted	35	11410 (- 32.12%)	112 (-42.56%)
Statistics			
Mean	35 (- 31.4%)	11507.5 (- 31.54%)	126.8 (-34.97%)
Standard deviation	0		

**Table D - 7 3D Printed Test Specimen Details for the Second Test Comparison [125]**

Test Specimens	Mass (g)	Material Extruded (mm)	Print Time (minutes)
Reference (Global Infill)			
Rectilinear	28	8500	170
Optimised (Global & BESO Infill)			
Three-point	28	8510 (+ 0.29%)	173 (+1.76)
Off-centre	28	8530 (+ 0.86%)	176 (+3.53)
Four-point	28	8590 (+ 2.57%)	179 (+5.29)
Inverted	28	8820 (+ 3.76%)	185 (+8.8)
Statistics			
Mean	28	8612.5 (+ 1.32%)	178.25 (+4.85)
Standard deviation	0	0.15	



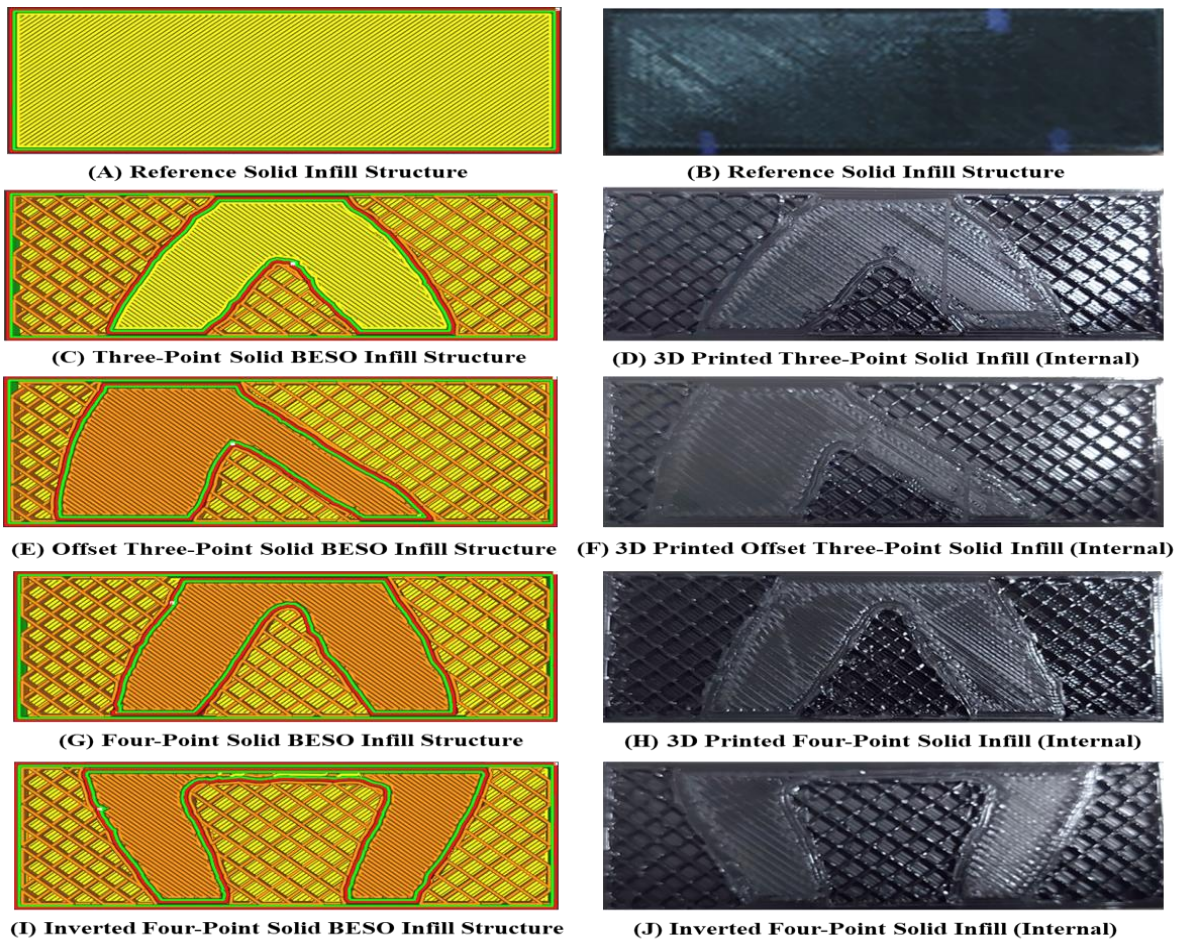


Figure D - 6 3D Printed Internal and External Representation of the Rectangular Test Specimens for the First Test Comparison

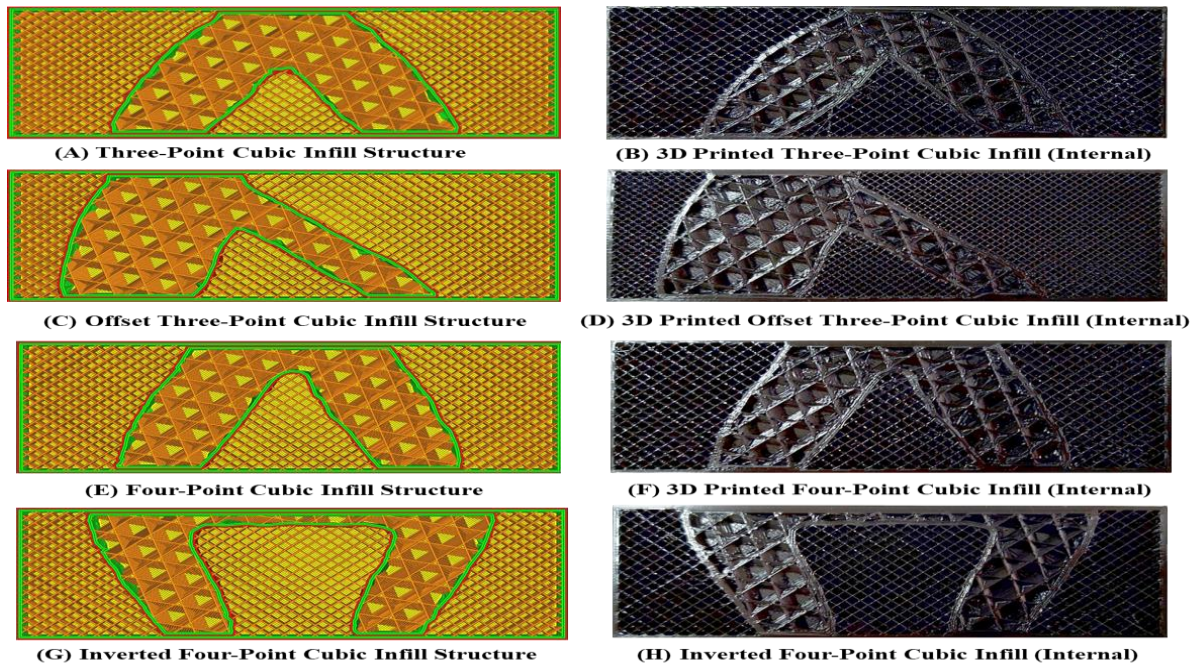
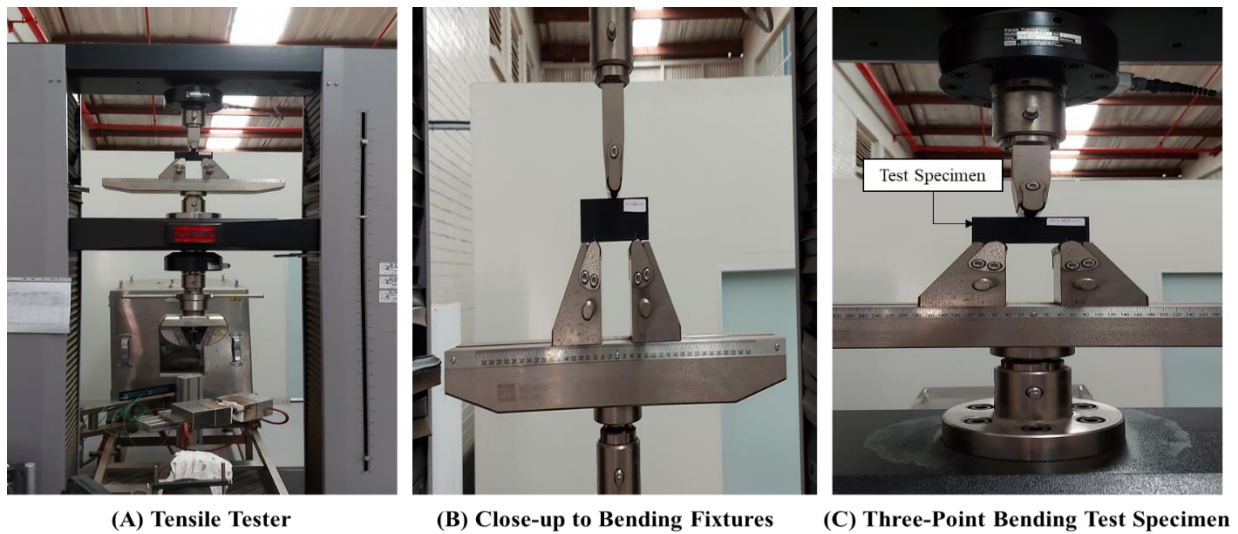


Figure D - 7 3D Printed Internal and External Representation of the Rectangular Test Specimens for the Second Test Comparison

### 11.3.1 Experimental Test Setup and Printing Parameters

The MTS Criterion model C45.105 tensile tester is used to perform all the bending tests. Figure D - 8 illustrates the tensile tester with loaded rectangular test specimens.



**Figure D - 8 Universal Tensile Testing Machine Used in this Investigative Study**

### 11.3.2 First Test Comparison

Table D - 8 illustrates the printing parameters used to compare the 3D printed test specimens for the first test.

**Table D - 8 Printer Parameters Used to 3D Print the Test Specimens for First Test Comparison**

Process Parameters	Global Parameters	Custom Infill Placement	Reference Model
Infill Pattern	Rectilinear	Solid	Solid
Infill Density (%)	20	100	100
Wall Thickness (mm)	1.6	1.6	1.6
Number of Walls	3	3	3
Layer Heights (mm)	0.2	0.2	0.2
Build Plate Direction	XY Plane	XY Plane	XY Plane
Bed Temperature	80 °C		
Nozzle Temperature	245 °C		
Printers	Creality CR10S Pro		
Slicing Softwares	Cura 4.11		
Infill Overlap Percentage (%)	30		
Infill Overlap (mm)	0.243		
Top/Bottom Thickness (mm)	0.92		
Outer Wall Insert (mm)	0.24		
Nozzle Diameter (mm)	0.8		
Cooling	Off		



### 11.3.3 Second Test Comparison

Table D - 9 illustrates the printing parameters for the second test comparison.

**Table D - 9 Printer Parameters Used to 3D Print the Test Specimens for Second Comparison**

Process Parameters	Global Parameters	Custom Infill Placement	Reference Model
Infill Pattern	Rectilinear	Cubic, Octet, and Gyroid	Rectilinear
Infill Density	20 %	20 %	33 %
Wall Thickness	1.6	1.6	1.6
Number of Walls	3	3	3
Layer Heights	0.2	0.2	0.2
Build Plate Direction	XY Plane	XY Plane	XY Plane
Bed Temperature		80 °C	
Nozzle Temperature		245 °C	
Printers		Creality CR10S Pro	
Slicing Softwares		Cura 4.11	
Infill Overlap Percentage (%)		30	
Infill Overlap (mm)		0.12	
Top/Bottom Thickness (mm)		0.8	
Outer Wall Insert (mm)		0.24	
Nozzle Diameter (mm)		0.4	
Cooling		Off	

## 11.4 Print Accuracy

The accuracy of the 3D printed test specimens is compared to the digital 3D model. The most critical dimensions for the 3D print are the specimens' total width, height, and length. The accuracy of all sections was  $\pm 0.1$  mm between the digital design and the 3D printed components. The dimensional accuracy depends on the 3D printer, process parameters and printer calibration [62]. Table D - 10 through to Table D - 15 provides the sections compared for dimensional accuracy.

### 11.4.1 First Test Comparison

Table D - 10 illustrates the dimensional accuracy of the 3D printed test specimens to the 3D digital model.

**Table D - 10 Dimensional Accuracy between Digital Model and 3D Print First Test Comparison**

	Test Specimen	3D Model (mm)			3D Print (mm)			Error (%)		
		Length	Width	Height	Length	Width	Height	Length	Width	Height
First Case (Standard)	Reference	100	40	10	99.60	39.65	10.04	-0.4	-0.35	0.04
					99.40	39.87	9.80	-0.6	-0.13	-0.2
					99.60	39.65	10.02	-0.4	-0.35	0.02
					99.86	39.65	9.86	-0.14	-0.35	-0.14
					99.62	39.71	9.98	-0.38	-0.29	-0.02
	Three-point	100	40	10	99.52	39.92	10.00	-0.48	-0.08	0
					99.50	39.90	10.05	-0.50	-0.10	0.05
					99.51	39.91	10.03	-0.49	-0.09	0.03
	Off-Centre	100	40	10	99.08	39.45	10.09	-0.92	-0.55	0.09
					99.10	39.54	10.07	-0.90	-0.46	0.07
					99.09	39.50	10.08	-0.91	-0.50	0.08
Statistics	Mean	100	40	10	99.44	39.71	10.001	-0.56	-0.30	0.002
	Standard Deviation	0	0	0	0.24	0.16	0.09	0.24	0.16	0.09

### 11.4.2 Second Test Comparison

Table D - 11 to Table D - 15 illustrates the dimensional accuracy of the 3D printed test specimens to the 3D digital models for each multi-infill geometry specimen.

**Table D - 11 Dimensional Accuracy between Digital Model and 3D Print First Case of Second Test Comparison**

	Test Specimen	3D Model (mm)			3D Print (mm)			Error (%)		
		Length	Width	Height	Length	Width	Height	Length	Width	Height
First Case (Standard)	Three-point	100	40	10	99.70	39.98	9.94	-0.3	-0.05	-0.6
	Off-Centre	100	40	10	99.45	40.00	10.02	-0.55	0	0.2
Statistics	Mean	100	40	10	99.58	39.99	9.98	-0.43	-0.043	-0.2
	Standard Deviation	0	0	0	0.13	0.01	0.04	0.13	0.03	0.4

**Table D - 12 Dimensional Accuracy between Digital Model and 3D Print Second Case Cubic Infill of Second Test Comparison**

	Test Specimen	3D Model (mm)			3D Print (mm)			Error (%)		
		Length	Width	Height	Length	Width	Height	Length	Width	Height
Second Case (Standard)	Three-point	100	40	10	99.48	39.70	10.10	-0.52	-0.75	1
	Off-Centre	100	40	10	99.48	39.80	10.00	-0.52	-0.5	0
Statistics	Mean	100	40	10	99.48	39.75	10.05	-0.52	-0.625	0.5
	Standard Deviation	0	0	0	0	0.05	0.05	0	0.13	0.5

**Table D - 13 Dimensional Accuracy between Digital Model and 3D Print Second Case Gyroid Infill of Second Test Comparison**

	Test Specimen	3D Model (mm)			3D Print (mm)			Error (%)		
		Length	Width	Height	Length	Width	Height	Length	Width	Height
Second Case (Standard)	Three-point	100	40	10	99.50	39.98	10.11	-0.5	-0.05	1.1
	Off-Centre	100	40	10	99.45	39.80	9.96	-0.55	-0.5	-0.4
Statistics	Mean	100	40	10	99.48	39.89	10.04	-0.53	-0.28	0.4
	Standard Deviation	0	0	0	0.03	0.09	0.08	0.03	0.23	0.75

**Table D - 14 Dimensional Accuracy between Digital Model and 3D Print Second Case Octet Infill of Second Test Comparison**

	Test Specimen	3D Model (mm)			3D Print (mm)			Error (%)		
		Length	Width	Height	Length	Width	Height	Length	Width	Height
Second Case (Standard)	Three-point	100	40	10	99.50	39.83	10.01	-0.5	-0.425	0.1
	Off-Centre	100	40	10	99.52	40.00	9.94	-0.48	0	-0.6
Statistics	Mean	100	40	10	99.51	39.92	9.98	-0.49	-0.2	-0.25
	Standard Deviation	0	0	0	0.01	0.085	0.035	0.01	0.21	0.35

**Table D - 15 Dimensional Accuracy between Digital Model and 3D Print Second Case Lines Infill of Second Test Comparison**

	Test Specimen	3D Model (mm)			3D Print (mm)			Error (%)		
		Length	Width	Height	Length	Width	Height	Length	Width	Height
Second Case (Standard)	Three-point	100	40	10	99.50	39.75	10.09	-0.5	-0.625	0.9
	Off-Centre	100	40	10	99.44	39.80	10.02	-0.56	-0.5	0.2
Statistics	Mean	100	40	10	99.47	39.78	10.06	-0.53	-0.56	0.6
	Standard Deviation	0	0	0	0.03	0.025	0.035	0.03	0.06	0.35

## 11.5 Test Results

**Table D - 16 Relative Performance Improvement Over Rectilinear Infill Geometry Using Three-Point Bending Test**

	BESO Gyroid-Rectilinear	BESO Cubic-Rectilinear	BESO Octet-Rectilinear
Peak Force (%)	49	25	38
Maximum Extrusion (%)	52	61	65
Flexural Stiffness (%)	9	38	46

**Table D - 17 Summary of Test Results for Three-Point Bending Testing Campaign [125]**

Infill Type	Peak Force (N)	Maximum Force Extrusion (mm)	Tangent Modulus of Elasticity (MPa)	Flexural Stiffness (N/mm)	Strain Energy (Nmm)
Test Comparison 1					
100 % Solid	12116	10.3	251.18	2977	62410.36
	12205	10.15	254.59	3017,4	61957.31
Mean	12160.5	10.23	252.885	2997,2	62183.83
100 % BESO	5636	3.25	219.26	2598,6	9164.86
	6213	3.15	231.74	2746,5	9795.49
Mean	5924.5	3.2	225.5	26725,5	9480.18
Test Comparison 2					
Rectilinear	2680	26.5	91.12	1079,9	25113.44
BESO Gyroid	3985	12.6	99.77	1182,4	25113.44
BESO Cubic	3344	10.25	125.58	1488,4	17143.07
BESO Octet	3693	9.15	133.14	1578	16902.21

Table D - 18 summarises the three-point offset bending test results, while Table D - 19 illustrates the relative performance improvement for the optimised infill placement over the rectilinear infill geometry.

**Table D - 18 Summary of Test Results for Three-Point Offset Bending Testing Campaign [125]**

Infill Type	Peak Force (N)	Maximum Force Extrusion (mm)	Tangent Modulus of Elasticity (MPa)	Flexural Stiffness (N/mm)	Strain Energy (Nmm)
Test Comparison 1					
100 % Solid	9548	5.8	253.05	2999,1	27461.6
	8809	5.6	277.09	3284	24675.0
Mean	9178.5	5.7	265.07	3141,55	26068.3
100 % BESO	9100	9.15	216.68	2568,1	41638.53
	8194	6.4	239.25	2835,5	26228.50
Mean	8647	7.775	228	2701,8	33933.52
Test Comparison 2					
Rectilinear	1678	13.14	95.99	1137,6	11028
	1560	11.45	81.14	961,7	8931
Mean	1619	12.3	88.56	1049,65	9980
BESO Gyroid	5374	7.103	107.83	934,3	13272.27
BESO Cubic	3939	10.05	78.83	1278	19799.57
BESO Octet	4278	9.7	111.73	1324,2	60422.87

**Table D - 19 Relative Performance Improvement Over Rectilinear Infill Geometry Using Three-Point Offset Bending Test**

	BESO Gyroid-Rectilinear	BESO Cubic-Rectilinear	BESO Octet-Rectilinear
Peak Force (%)	143.30	231.93	164.24
Maximum Extrusion (%)	-18.26	-42.24	-21.13
Flexural Stiffness (%)	21.75	-10.99	26.16

**Table D - 20 Simulation Results of the 3D Printed Test Specimen for Three-Point Bending**

	Experimental Results	Simulation Results
Displacement (mm)	10.3	12.76
Stress (MPa)	68.15	84.13
Strain (mm/mm)	0.69	0.223
Strain Energy (N/mm)	62410.36	28.04

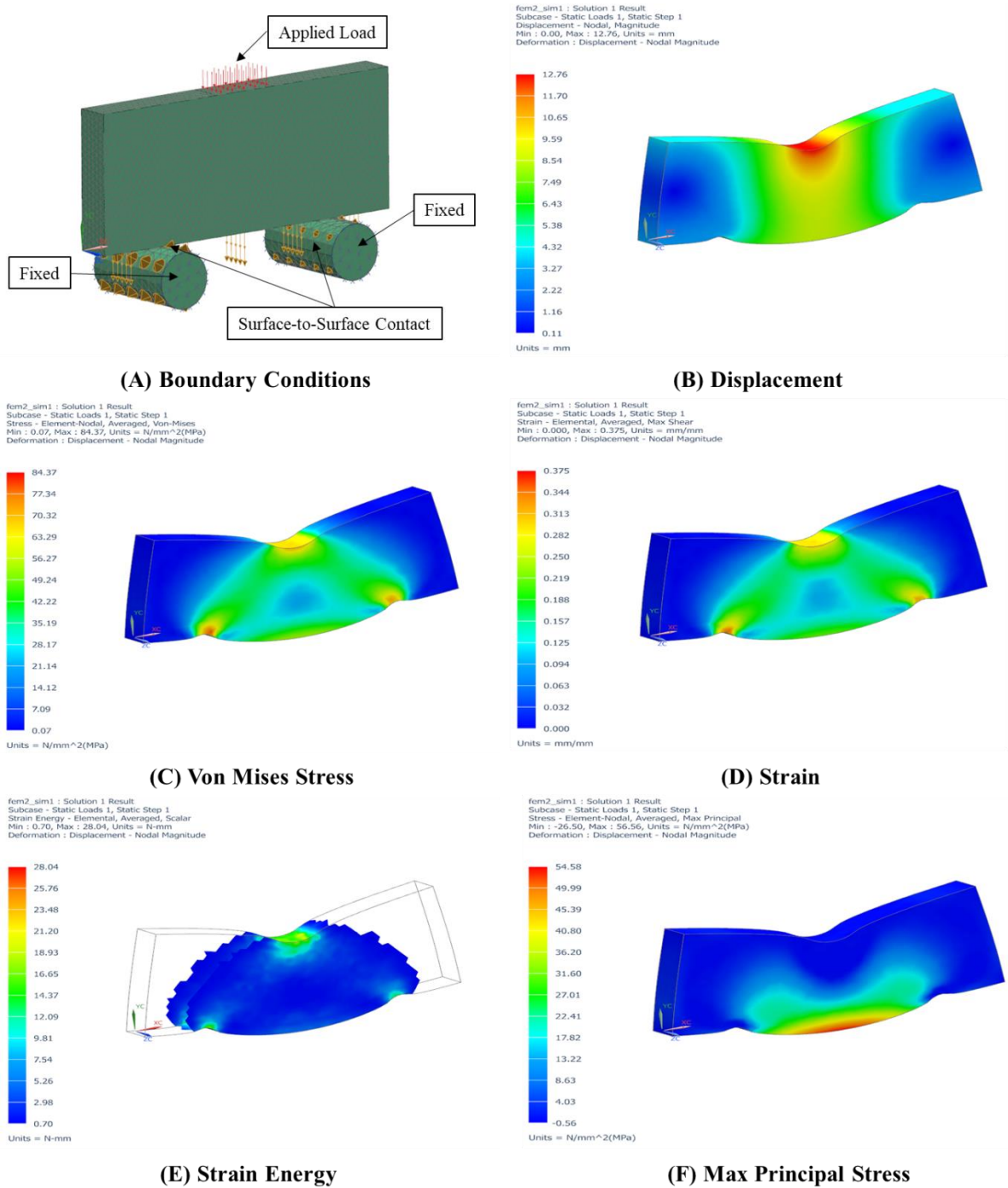


**Figure D - 9 Structural Simulation Results for an Idealised Three-point Bending Test Specimen With An Applied Loading of 12116 N for the PETG material**

# Appendix E: Custom Design Guide <sup>1</sup>

## Abstract

The study in this chapter presents the proposed custom-developed design guide to assist novice rail design engineers in applying the design features to functional 3D printable components to ensure manufacturing repeatability. The design guide incorporates design features for tolerances, layer heights, print orientation, wall thickness, hole diameters, overhang angles and infill density. Furthermore, advanced design techniques are proposed by leveraging standard design features presented in the design guide. These include self-supporting structures, interlocking joints and embedding hardware components into functional FDM 3D printed parts. Finally, the proposed feature design guide and the advanced design techniques are applied to a railway case study: the custom-designed low-cost 3D printable weather station.

---

<sup>1</sup>Elements of this chapter are presented in [10]: Toth AD, Padayachee J, Mahlatiji T, Vilakazi S, 2021, A Report of Case Studies of Additive Manufacturing in the South African Railway Industry, Elsevier, Scientific African Journal, 1 – 16, ISSN 2468-2276.

## 12.1 Introduction

Additive Manufacturing technologies present opportunities in materialising complex shapes and product designs where traditional manufacturing methods struggle. Merging the digital and physical workflows using computational tools for product designs and manufacturing through 3D printing allows the AM technology to develop and achieve unique capabilities that classical manufacturing methods cannot [165], [166]. Some unique capabilities such as 1) weight-mass optimisation, 2) part feature optimisation, 3) infill optimisation, 4) support optimisation, 5) assembly optimisation through interlocking, 6) assembly-part consolidation and 7) hardware integration and embedment into 3D printed parts are capable with the FDM technology. To achieve these unique capabilities using the Fused Deposition Modelling Additive Manufacturing technology, the design considerations and techniques need to be considered at the start of the design cycle phase. Understanding the approach to implementing the design considerations, FDM 3D printed functional parts will further benefit from the AM process. This chapter presents methods and tools to achieve advanced design techniques to produce repeatable 3D printable functional parts.

## 12.2 Custom Design Guide

“The acceptance of new technology by the railway industry depends on the certainty, reliability and economic value associated with the new technology for its application [3], [8], [13], [14]. In most cases, a significant gap exists between transformative technology for industrial applications and the technology's research stages.” [10]. Additive manufacturing technologies, and specifically the FDM process, have shown capabilities in producing new custom measuring and monitoring device housings, spare and replacement parts for legacy systems, new complex designs, jigs, fixtures and tooling [3], [13], [14]. To effectively industrialise the technology, the limitations of the FDM process, design repeatability in design techniques and printing need to be consistent [3]. A custom design aid is developed for rail design engineers to visually understand the limitations and ensure that design and printing repeatability is achieved. The design guide aims to be a definitive guide to assist in the modelling phase to ensure better predictions between the digital design and the 3D printed part. It aims to reduce material waste through iterative design, printing and calibrating to the specific FDM printer. The design guide incorporates all the typical design requirements and considerations presented in the DfAM worksheet [113] and elements from the DfAM conceptual framework [114] to ensure that the first prints are final. The guide covers; 1) tolerances for circular prints, 2) tolerances for square prints, 3) variation in infill density, 4) wall thickness, 5) print orientation, 6) layer height, 7) print angles, and 8) hole diameters. The design requirements are designed specifically for the PETG FDM material with corresponding process parameters presented in Appendix A. Figure E - 1 illustrates the custom design cube guide. The 3D printable design cube is created using snap-fit joints to fix the parts together. This



approach provides greater flexibility in cases where additional design considerations are required. Due to the design, it can be applied to the different FDM material types and the different printer nozzle diameters. This will provide illustrative guides as to the limitations presented for each material and nozzle diameter configuration and will aid in producing final functional parts for the railway environment.

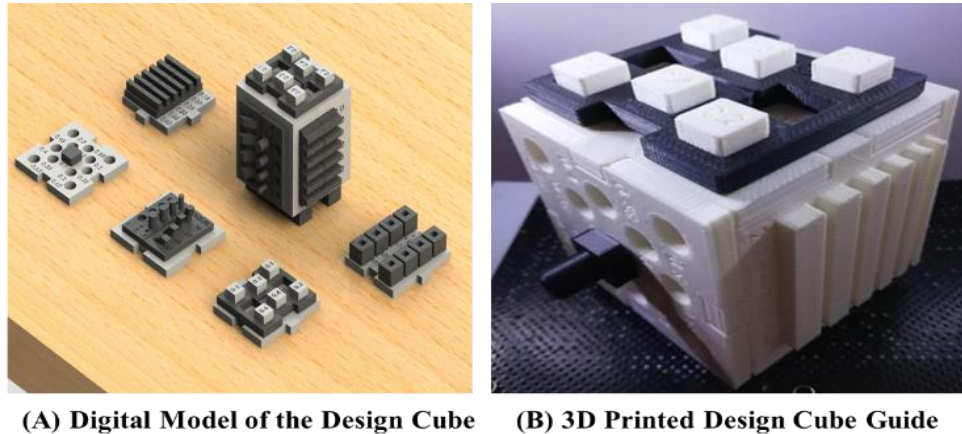


Figure E - 1 Digital Design of the Design Cube

## 12.2.1 Clearance and Interference Guide

The design cube is designed with two types of tolerance variations. The first is square prints, and the second is circular prints. Both are common shapes used when creating snap-fit joints and interfacing components.

### 12.2.1.1 Square Prints

A total of six different tolerance values are designed and printed for the square prints. They range from 0.1 mm – 0.6 mm. The tolerance between the print and the square insert indicates the type of interference experienced for the different tolerances. Figure E - 2 illustrates the digital design and the 3D printed version.

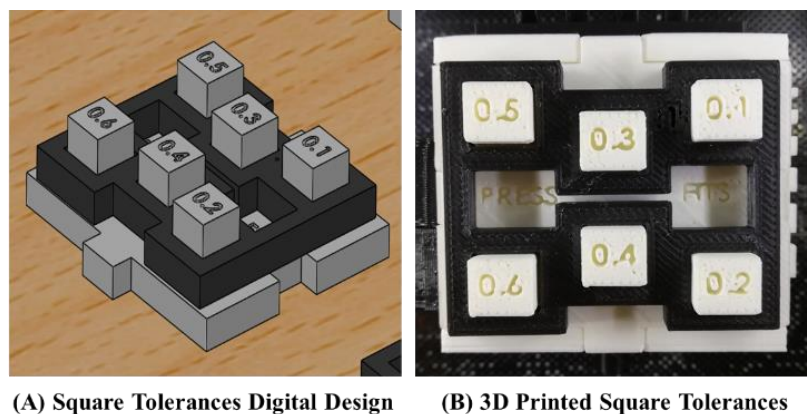
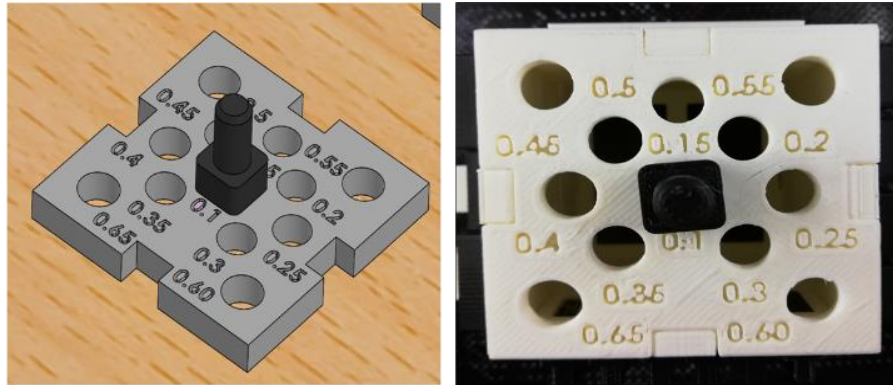


Figure E - 2 Digital Model and 3D Printed Square Tolerance Guide on the Design Cube

### 12.2.1.2 Circular Prints

A total of twelve different tolerance values are designed and printed for the circular holes. They range from 0.1 mm – 0.65 mm in incremental tolerance values of 0.05 mm. The tolerance between the print and the circular insert indicates the type of interface experienced for the different diameters. Figure E - 3 illustrates the digital design and the 3D printed version.

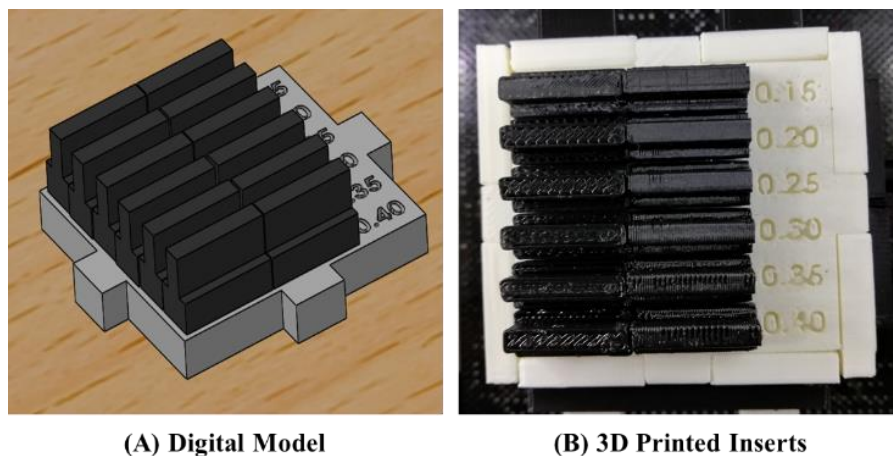


(A) Circular Tolerances Digital Design (B) 3D Printed Circular Hole Tolerances

Figure E - 3 Digital Model and 3D Printed Circular Hole Tolerance Guide on the Design Cube

### 12.2.2 Layer Height and Print Orientation Guide

A total of six different layer height values ranging from 0.15 mm to 0.4 mm are printed in both the vertical and horizontal print orientations. The prints are performed using a stock 0.4 mm nozzle. A total of twelve inserts are printed using the different process parameters and are press-fitted to the design cube. This visual guide presents the potential print quality based on the orientation and the layer height. Apparent differences are presented when these prints are compared to each other. This comparison will inform the operator of the appropriate layer height and print orientation based on the parts application. Figure E - 4 illustrates the digital model and the 3D printed version.



(A) Digital Model

(B) 3D Printed Inserts

Figure E - 4 Digital Model and 3D printed Layer Height and Print Orientation Visual Guide on the Design Guide

### 12.2.3 Wall Thickness Guide

The wall thickness guide is printed with thicknesses varying from 2 mm – 7 mm. These serve as a visual representation of the wall's thickness and the number of walls required to print. The stock 0.4 mm nozzle is used with a wall thickness of 0.4 mm for printing. Understanding the wall thickness provides flexibility in assigning higher values to the slicer software to reduce print time and applying the correct thickness to supported and unsupported walls. These features are commonly used in sliding or press-fit assemblies. Figure E - 5 illustrates the digital model and the 3D printed version of the wall thickness guide, while Figure E - 6 illustrates examples of 3D printed supported and unsupported wall models.

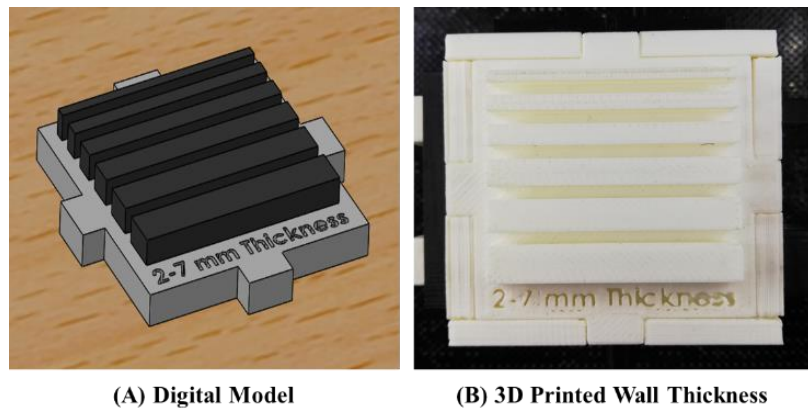


Figure E - 5 Digital Model and 3D Printed Wall Thickness

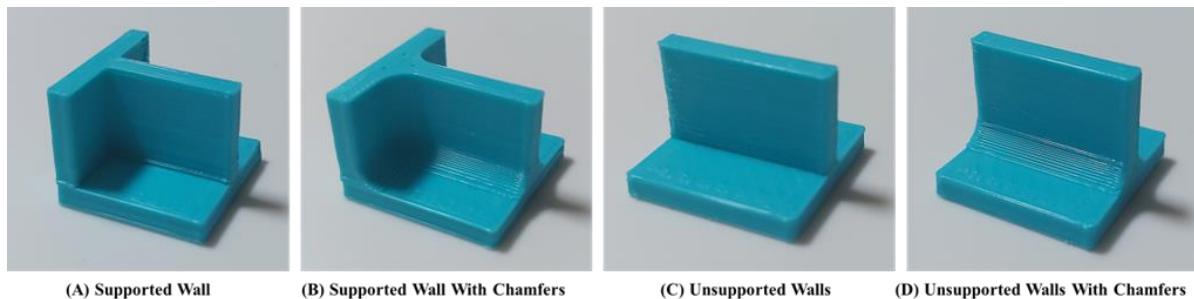
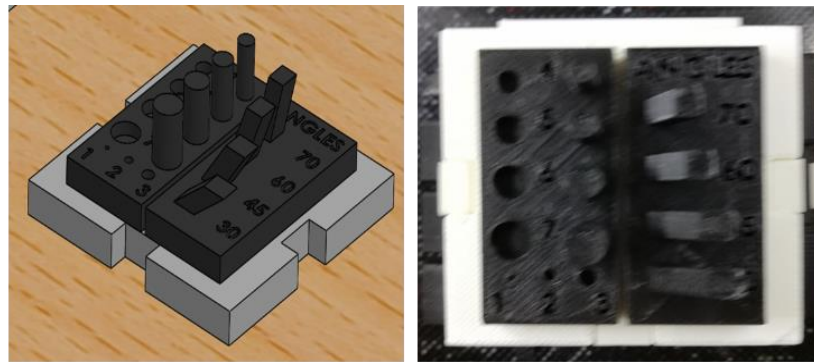


Figure E - 6 3D Printed Versions for Supported Walls (A), Supported Walls with Chamfers (B), Unsupported Walls (C) and Unsupported Walls with Chamfers (D)

### 12.2.4 Holes and Overhangs Guide

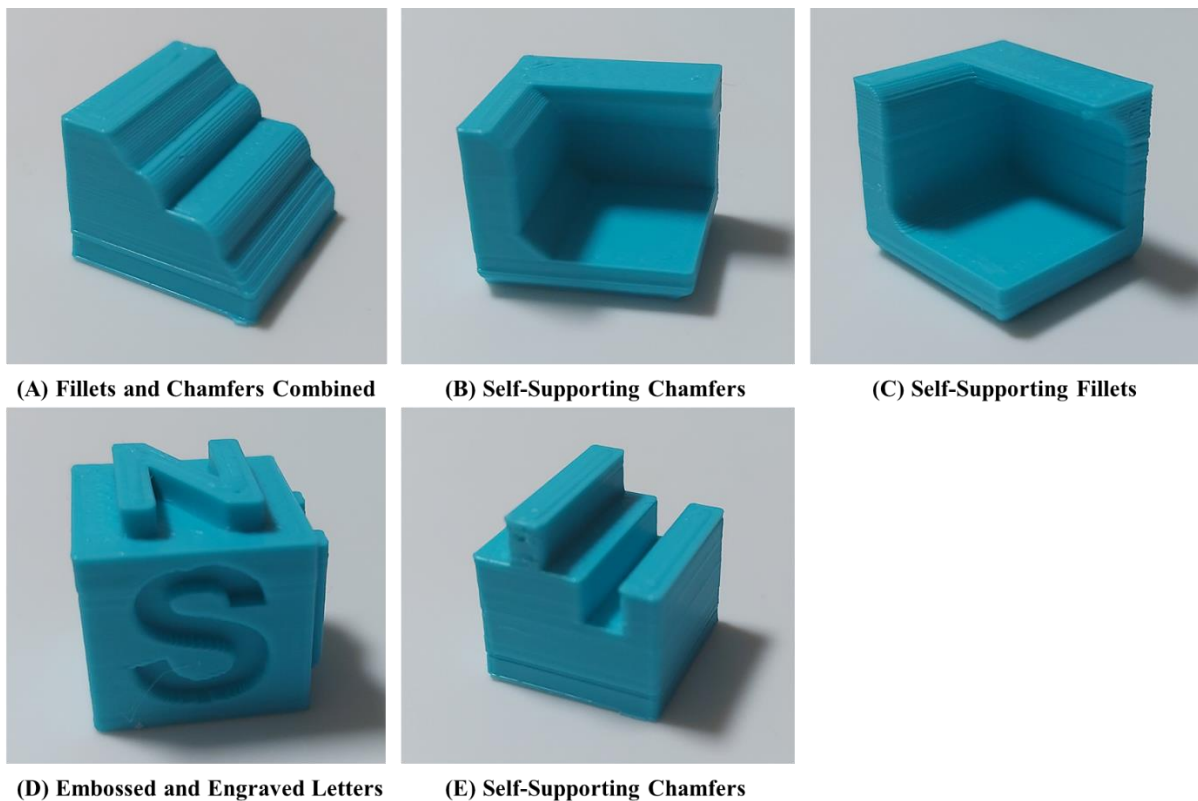
The hole diameters and the printing angles are designed and printed on one side of the design guide cube. The holes vary from 1 mm to 7 mm in diameter, while the printing angles are limited to 30 degrees, 45 degrees, 60 degrees and 70 degrees. Based on the design cube, the initially recommended minimum hole diameter of 3 mm is invalid due to the inconsistency in print. It is also noted that all holes printed were not dimensionally accurate to the intended diameters. In the case of the printing angles, all angles above the self-support angle printed perfectly, while print defects were visible for the 30 degrees angle. Parts designed within the self-supporting angel allow for models to be printed without support material

and reduce overall printing time. Figure E - 7 illustrates the digital model and the 3D printed version of the holes and overhangs guide, while Figure E - 8 3D Printed Versions of Self-Supporting Angles (A-C) and Embossed and Engraved Detail (D) and an Example Using the Emboss and Engrave Details (E) Designed into the Models illustrates examples of 3D printed models with combinations of fillets, chamfers, embossed and engraved detail and angles within the self-supporting angle.



(A) Hole and Print Angle Digital Design (B) 3D Printed Hole and Print Angle

**Figure E - 7 Digital Model and 3D printed Hole Diameters and Printing Angles**



(A) Fillets and Chamfers Combined

(B) Self-Supporting Chamfers

(C) Self-Supporting Fillets

(D) Embossed and Engraved Letters

(E) Self-Supporting Chamfers

**Figure E - 8 3D Printed Versions of Self-Supporting Angles (A-C) and Embossed and Engraved Detail (D) and an Example Using the Emboss and Engrave Details (E) Designed into the Models**



### 12.2.5 Infill Density Guide

The infill density presented in the design cube is purely to determine the amount of material added to the internal model. The selected infill geometry is the rectilinear (grid line) pattern. Infill densities of 0%, 13%, 15%, 20%, 65%, 80% and 99% have been used to print the parts. Figure E - 9 illustrates the digital model and the 3D printed version of the infill guide.

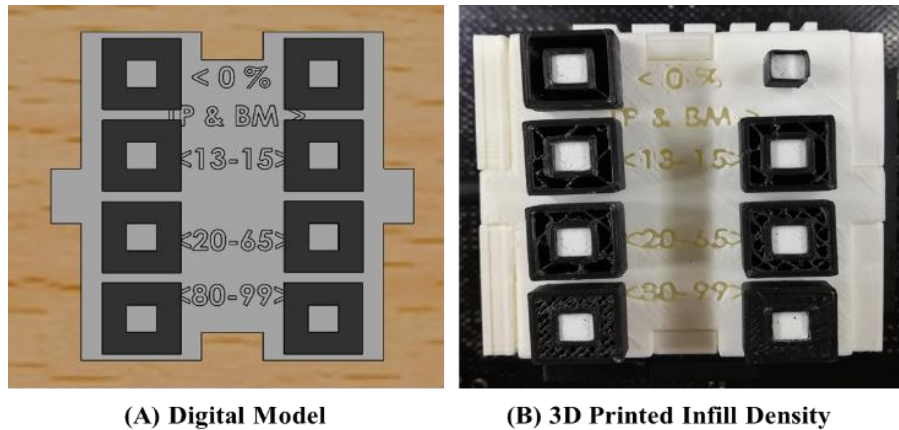


Figure E - 9 Digital Model and 3D printed Infill Density

## 12.3 Advanced Design for Fused Deposition Modelling

Understanding advanced design techniques available to design FDM 3D printable parts will provide a more accessible and cost-effective method to create functional 3D printable parts. Advanced design techniques covered include; 1) self-supporting structures, 2) interlocking joints and 3) embedding hardware components.

### 12.3.1 Self-Supporting Structures

An excellent practice in designing functional parts for the FDM technology is to avoid support material. Advanced design techniques can ensure that support material is avoided in cases where the only option is support material.

#### 12.3.1.1 Sacrificial Bridging

Sacrificial bridging is an advanced design technique that takes advantage of the bridging property of FDM to 3D print regions, which would typically require support material. A single-layer thickness is designed into the model to create a bridge between two supporting walls. This single layer is printed as bridge support or scaffolding for the subsequent layers to print onto. Once the model is 3D printed, the single sacrificial layer can be removed by hand or blade. The disadvantage of this method is the potential drooping that will be experienced due to bridging. Performing the correct calibration steps for the

specific material being printed will reduce the surface defect [117]. Figure E - 10 illustrates a motor bracket utilising the sacrificial bridging design technique. Table E - 1 illustrates the recommended layer thickness for corresponding nozzle diameters.

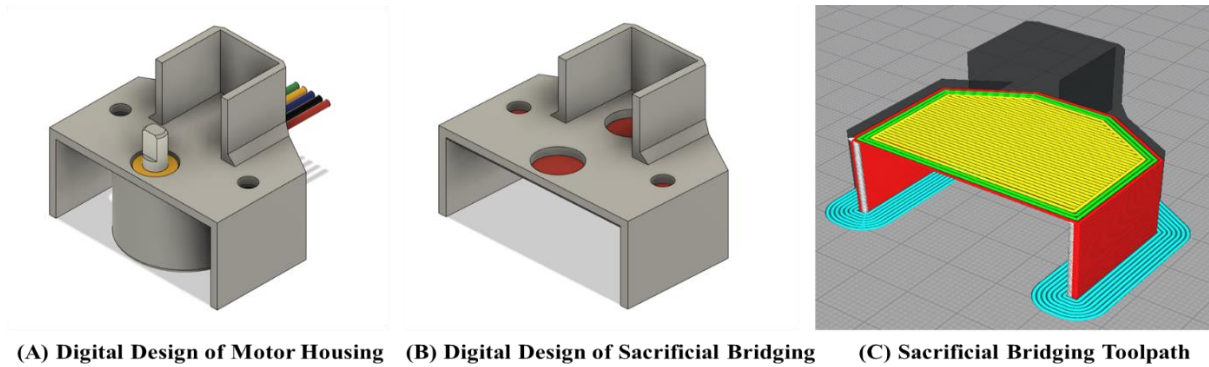


**Figure E - 10 Digital Design of a Stepper Motor Housing Using Sacrificial Bridging**

**Table E - 1 Recommended Single Layer Thickness for PETG Material**

Nozzle Diameter (mm)	Single Layer Thickness (mm)
0.4	0.2
0.6	0.25
0.8	0.28
1.0	0.3

### 12.3.1.2 Design in Supports

By taking advantage of the bridging properties and the printed layers, supports can be intelligently designed into the model in specific regions. This removes the need for pre-generated support material, reduces printing time and allows for easy support material removal. Models with overhang ledge features can be converted into fully supported bridges by designing custom tabs illustrated in Figure E - 11. These tabs can be removed by snapping them along the layer lines. Table E - 2 illustrates the recommended tab thickness for different nozzle diameters.

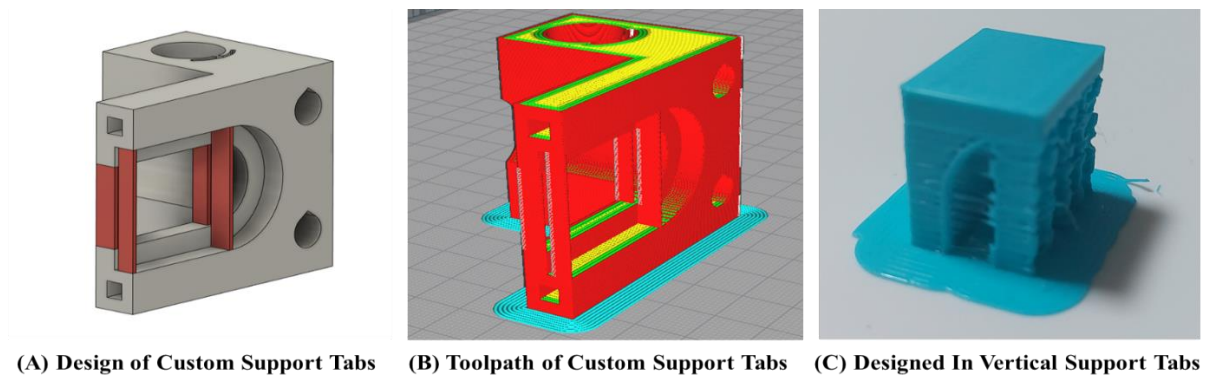


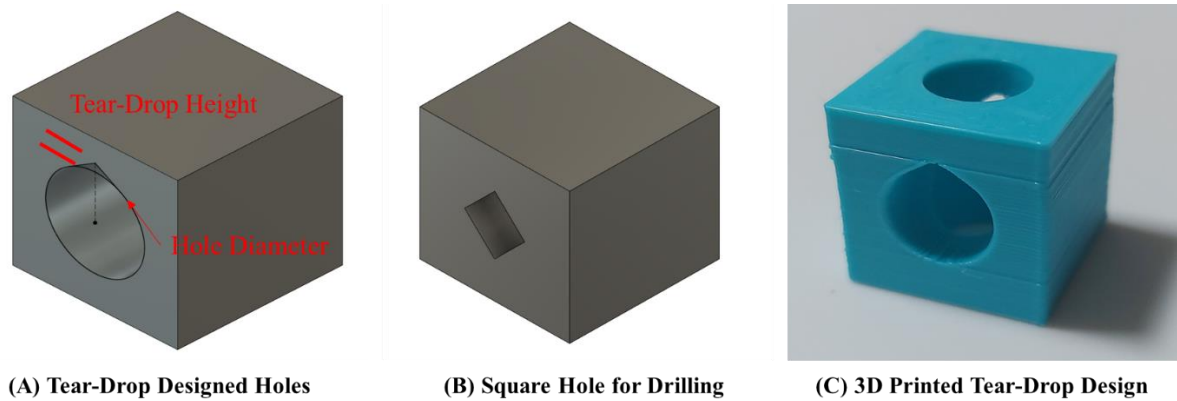
**Figure E - 11 Digital Design of Custom Support Tabs on Motor Housing**

**Table E - 2 Recommended Single Tab Wall Thickness for PETG Material**

Nozzle Diameter (mm)	Custom Wall Thickness (mm)
0.4	0.5
0.6	0.7
0.8	0.8
1.0	1.2

### 12.3.1.3 Vertical Holes

In specific applications, replacement parts are designed with through holes. The FDM technology requires specific design techniques to 3D print vertical holes (in the XY plane). By default, vertical holes greater than 6 mm in diameter will require support material, while holes less than 6 mm can be printed without supports using the unique bridging technique. Designers can influence the design of vertical holes by introducing self-supporting angles within the through-holes. A tear-drop design addition can be applied to a vertical hole in cases where direct use of the 3D printed part is required. The height of the tear-drop is based on the layer height (recommended four layers); the model is 3D printed. Figure E - 12 illustrates the tear-drop design based on a layer height of 0.32 mm. Table E - 3 illustrates the recommended tear-drop distances for different layer heights. A second design technique for 3D printing vertical holes uses a square through profile for applications where the 3D print will be drilled. It provides better drilling guidance than the tear-drop shape and is usually designed at 10 % smaller than the hole [115], [116].

**Figure E - 12 Digital Design of a Tear-Drop and Square through Holes****Table E - 3 Recommended Tear-Drop Height for PETG Models with a 0.4 mm Nozzle**

Tear-Drop Height (mm)	Layer Height (mm)
0.8	0.2
1.28	0.32
1.6	0.4
2.0	0.5

### 12.3.2 Design of Interlocking Joints

FDM 3D printed parts are limited by the printer's build volume, the material type, the print orientation and the process parameters. In specific applications, the 3D printable design must be printed in multiple parts. This might be due to the size or the print orientation. Designing interlocking parts is a standard method used to overcome these limitations.

#### 12.3.2.1 Interlocking Parts

Designing joints for 3D printable parts is an excellent way to connect multiple parts for applications where the part needs to move or is fixed in place. Several types of joints can be designed and printed using the FDM process. The two most common joints used on railway-related 3D parts include [3], [13], [14], [10], [134], [167]; 1) dovetails, and 2) snap-fits. Casing designs commonly use dovetails for the parts to slide, as illustrated in Figure E - 13 - A. Snap-fit joints are common interlocking design techniques predominately used in injection moulded products. As the name suggests, snap-fit connections have parts that bend and snap into place, creating a firm but temporary connection. There are several types of snap-fit connections, with the most common ones being; 1) cantilever joints, 2) annular joints, and 3) ball-and-socket joints. The cantilever snap-fit joint is the most popular joint type for 3D printing due to its design and 3D printing ease. To succeed in designing snap-fit joints, the design clearance and printer tolerances are essential factors [115], [116], [168]. Figure E - 13 - D illustrates a 3D printed snap-fit joint.

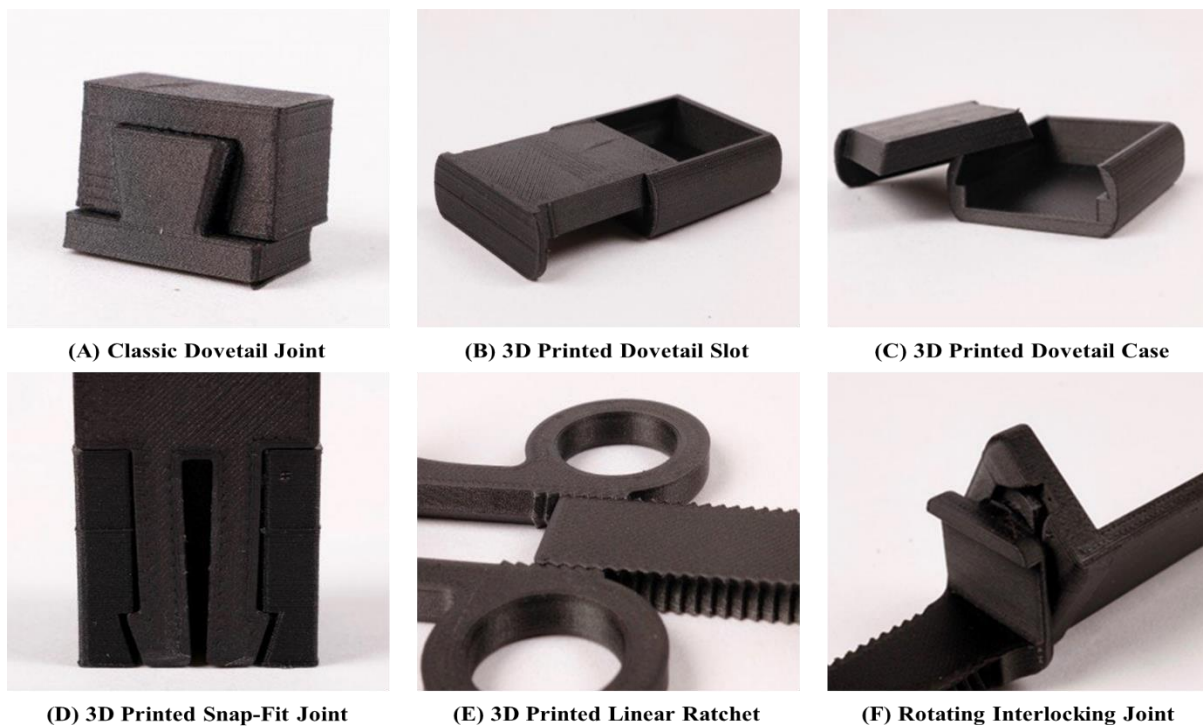
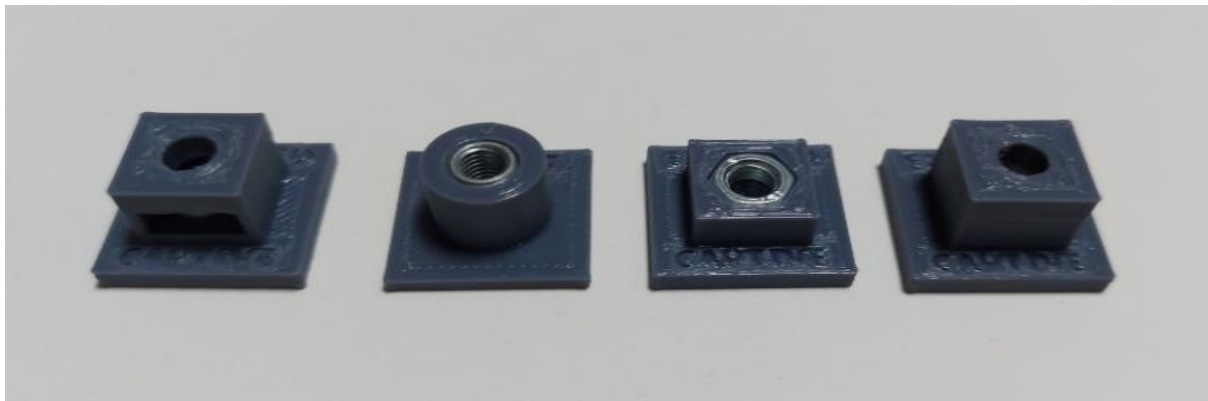


Figure E - 13 3D Printed Case using the Dovetail Joint (A-C) and 3D Printed Snap-Fit Joints (D-F) [168]



### 12.3.3 Hardware Embedment: Fasteners

A standard method to create non-permanent joints between two 3D printed parts is achieved using off-the-shelf fasteners, typically nuts and bolts. A few design considerations are required to achieve a non-permanent joint on FDM 3D printed parts using nuts and bolts. Designing nut inserts for 3D printable parts depends on the application of the part and the surface quality aesthetics. Four standard methods are used in designing fastener inserts in 3D printable parts. These include 1) slot inserts, 2) press-fit inserts, 3) embedded nuts and 4) threaded inserts. Figure E - 14 illustrates these types of fasteners insert methods.



**Figure E - 14 3D Printed Fastener Insert Types**

Designing slot inserts are created when the ease of inserting nuts into functional parts is required. A slot with the appropriate nut clearance is extruded from the 3D printable part to allow the nut to slot into the body of the print. This creates an anchor inside the 3D printed body for the bolt to fasten to. Figure E - 15-A illustrates a digital design with a cross-section on the body and a 3D printed version. Designing press-fit nut inserts are typically performed on the rear-end of the 3D printable part with a corresponding clearance to allow the nut to fit. This design technique exposes the nut at the print surface and is only recommended for rear-end placements to allow the bolt to anchor to the print. Depending on the clearance and tolerances used, the nuts can be press-fitted by hand or heating. Figure E - 15-E illustrates the 3D printed version. Embedding nuts inside the 3D printable design is achieved by pausing the 3D print at the specific layer height (usually two layers above the thickness of the nut). Once the printing process is paused, the nut is manually inserted into the predesigned cavity of the 3D printed body. The additional layers will cover and embed the nut inside the 3D print when the print is resumed. The process creates a permanent joint between the nut and the 3D print, creating a more robust joint than other design methods [169]. Figure E - 15-I illustrates the 3D printed versions of vertical and horizontally embedded nuts. Finally, threaded inserts are another post-processing method that can add a fastener joint to a 3D printed part. The threaded insert is usually heated and press-fitted into position by melting the 3D printed part. The only design consideration required for this method is to ensure the region has adequate material for the threaded insert to melt and grip into [169]. Figure E - 15-J illustrates the

threaded insert on a 3D printed part. When designing nut inserts, it is essential to understand the correct orientation for the predesigned cavities and the appropriate clearances based on the specific FDM printer. A general recommendation is to use a 0.3 mm clearance for nut inserts based on the design guide when printing PETG on an FDM printer with a 0.4 mm nozzle.

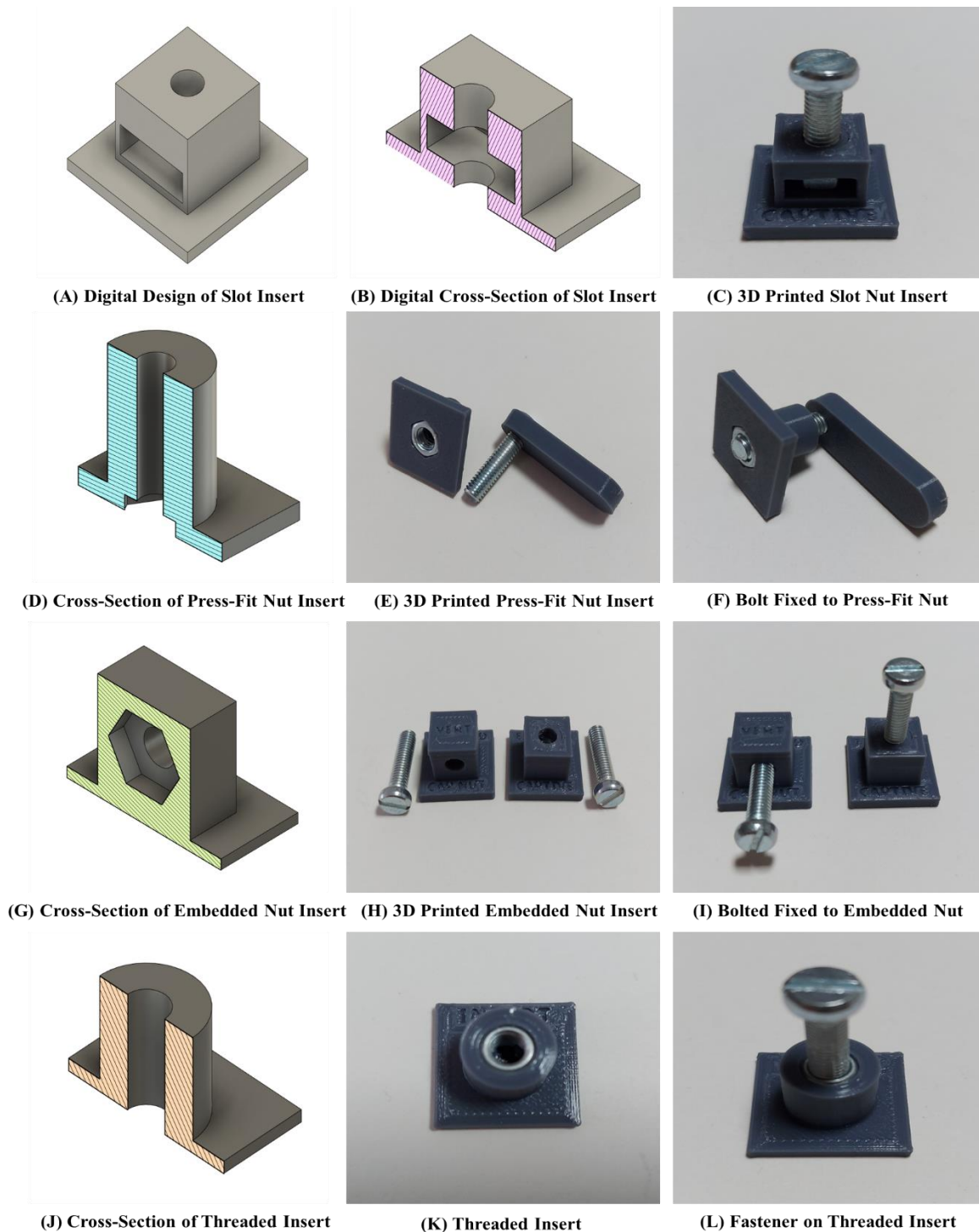


**Figure E - 15 Digital Cross-Section and 3D Printed Slot Insert (A-C), Digital Cross-Section and 3D Printed Press-Fit Nut Insert (D-E), Digital Cross-Section and 3D Printed Embedded Nut Inserts (F-G), and Digital Cross-Section and 3D Printed Threaded Insert**

### 12.3.3.1 Other Embedment's

Stationary fasteners are another set of commonly used fasteners to fix parts together. They are particularly well-suited to creating revolute joints which do not require inserts. Stationary fasteners include self-threading and self-forming screws, commonly used in electronics on injection moulded plastic casings. Thread-forming screws are designed to self-tap into the plastic. The blunt screw threads push plastic material out to form a new thread in a non-threaded hole. These types of screws can be installed and removed into the same hole without damaging the threads. Thread-cutting screws cut permanent threads into a non-threaded hole with the sharp screw thread by removing the material. Thread-forming screws create stronger threads than thread-cutting screws and are recommended for all functional parts [169]. Through-holes for these screws are designed using the recommendation presented in Table E - 4. Additionally, three shell walls are required to ensure that the screws will anchor to the part when the material is cut during the threading process. Figure E - 16 illustrates self-forming, self-threading and a hook screw fixed to 3D printed parts.

Magnets press-fitted into 3D prints can provide a versatile range of practical solutions, including fixing two halves of a part together to create a breakaway hinge. Magnets in 3D printable designs provide an additional, temporary, separable pivot joint. Design considerations for setting magnets into 3D prints include tolerances, material type and adhesives [169]. Figure E - 17-H and Figure E - 17-I illustrate neodymium magnets set into a 3D printed separable arm and base. Several other mechanical parts can be fitted to 3D printed designs based on their intended application. Bearings, rubber seals, shoulder screws, and eyelets are a few mechanical parts fitted to railway-related 3D prints [10]. It is essential that design considerations for tolerances, material types and clearances are factored into the design [115], [116]. The ability to integrate existing mechanical components into 3D printed parts provides numerous potential applications.



Figure E - 16 Self-Threading and Self-Forming Screws



**Figure E - 17 3D Printed Parts that Integrate with Bearings, Rubber Seals, Magnets, Shoulder Screws and Eyelets**

Table E - 4 illustrates the recommended clearance values that could be used to design PETG 3D printable parts with a minimum of three walls with components such as bearings, eyelets, shoulder screws, rubber seals, magnets, thread-forming, and thread-cutting screws. Changes to the recommended clearances can be made based on the interference fit experienced by the design cube.

**Table E - 4 Recommended Clearance Values for Several Components Using PETG**

Components	Nozzle Diameter	Clearance
Bearings, Eyelets and Magnets	0.4	0.20
	0.6	0.30
Rubber Seals and Shoulder Screws	0.4	0.25
	0.6	0.3
Thread-forming and Thread-cutting Screws	0.4	0.2
	0.6	0.25

## 12.4 Railway Application

Understanding the limitations and advanced design techniques available to the FDM AM technology provides new approaches to designing and developing functional railway-related parts, components and products. A railway case study on the custom design of a low-cost 3D printable weather station is presented. The weather station is designed, and 3D printed using the techniques and the design guidelines presented in this chapter.

### 12.4.1 Case Study 1 – Weather Station Prototype

Prototypes, under Chapter 3, of this dissertation, presented a railway case study of a custom prototype weather station design which is 3D printed using the FDM process [10]. To reduce the amount of support material needed to print the weather station base, support sections were designed into the model to reduce the amount of pre-generated supports in the slicing tool. Using the recommendations for design in supports, designing the tear-drop on vertical holes, interlocking joints, using the wall thickness guide to design the connection points to ensure the custom support would be printed and still be easy to be removed and using the overhangs and holes guide to ensure the supports would be 3D printed without failure the custom supports were created. This reduced the print time from 23 hours and 3 minutes to 13 hours and 21 minutes and the overall material usage from 540 grams to 292 grams. Applying the design recommendations saved approximately 248 grams of material, and the part was printed close to 10 hours faster. The part was printed with a 0.32 mm layer height using three shell walls and a 20 % infill density. A 0.6 mm nozzle was used to print the base in PETG. Lastly, the designed-in supports had slits which were 0.6 mm, and the connection points were 1.2 mm. A square support was added to the inside of the base with a 10 mm by 10 mm dimension. Figure E - 18 - A presents the sliced weather station base with pre-generated support material without custom designed-in supports. Figure E - 18 - B illustrates the digital design of the support mounts, and Figure E - 18 - C illustrates the final 3D printed version.

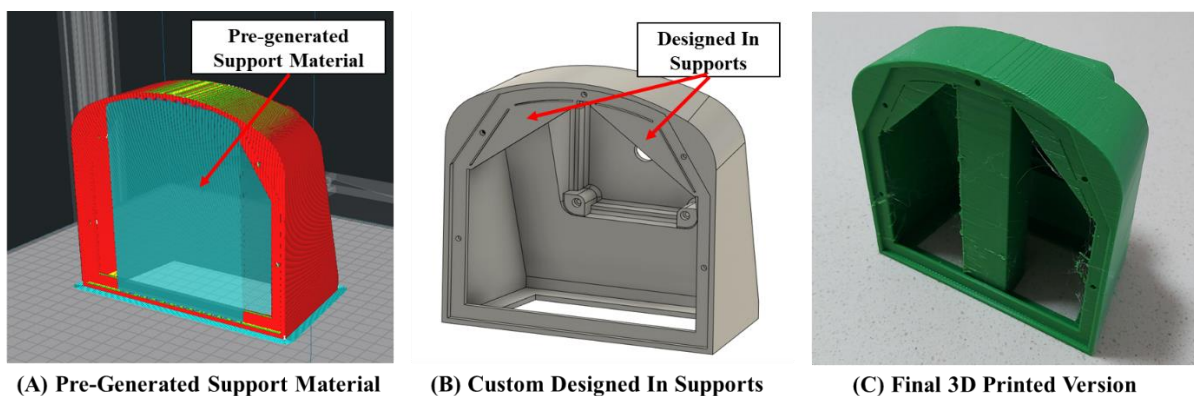
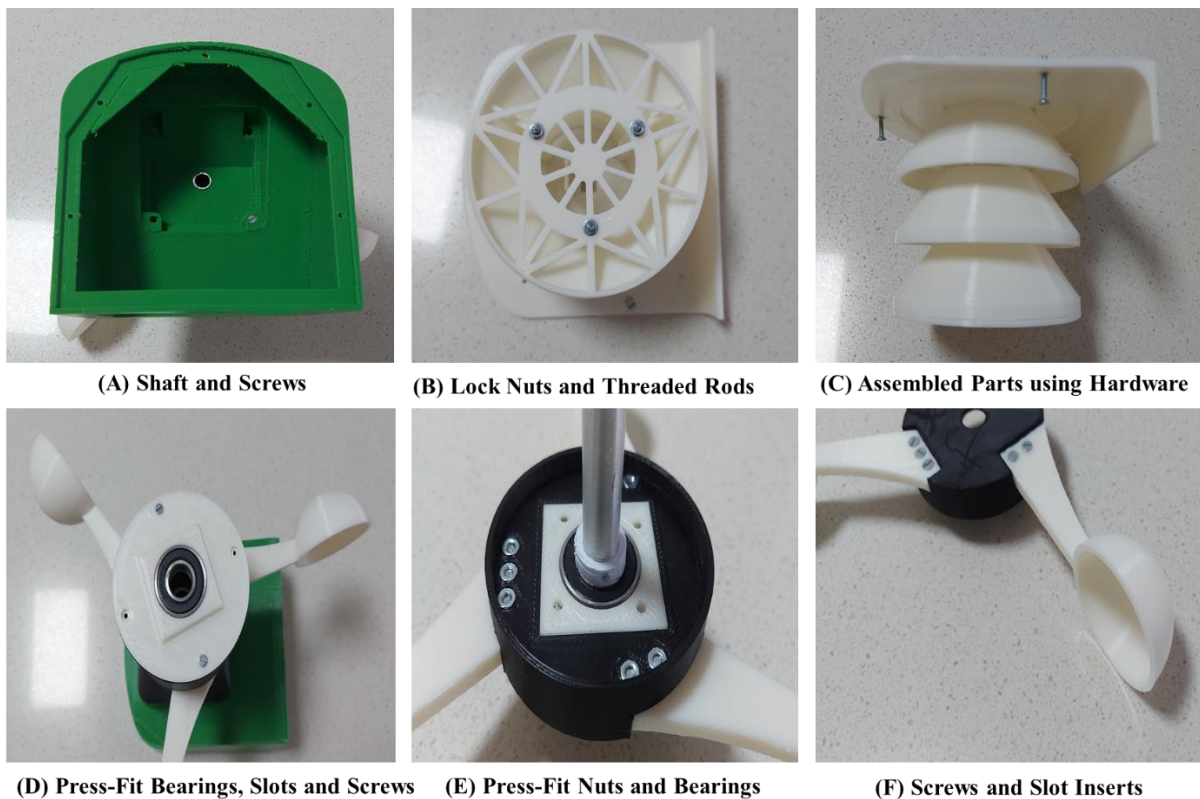


Figure E - 18 Pre-Generated Support Material (A) Custom Designed in Supports (B) and the Final 3D Printed Version



In the case of the metallic embedded components (bearings, nuts, threaded rod, shaft and bolts), the design recommendations for clearance and interference guide, holes and overhangs guide, interlocking joints and hardware embedment has allowed for seamless integration of the hardware components to the 3D printed structure. Lastly, the design guide and the specific recommendations presented in this chapter allowed the weather station to be manufactured using the FDM process and produced a functional end-use product with reduced material wastage and no design iterations due to fit, form and function requirements. Figure E - 19-A illustrates the custom support material placement and designed supports used on the base of the weather station, while Figure E - 19-B and Figure E - 19-C illustrate the embedded threaded rod and lock nuts used to fix the radiation shields together. Figure E - 19-D, Figure E - 19-E and Figure E - 19-F illustrates the press-fitted bearings, nuts, slotted covers and screws, respectively.



**Figure E - 19 Advanced Design Techniques Used to Embed, Fix and Mount Hardware Components to Assemble the Components of the 3D Printed Weather Station [10], [167]**

## 12.5 Chapter Summary

This chapter reviews and analyses design and manufacturing strategies for the Fused Deposition Modelling process. As a result, an advanced set of design strategies for features, self-supporting design techniques, interlocking methods and infill optimisation techniques have been proposed based on the main technical limitations of the FDM process. Furthermore, a custom design guide is presented, integrating all the typical design requirements and considerations for rail design engineers to create functional parts. Since FDM technologies and material types are continuously advancing, the design guide considers the capabilities of specific printers and material types. The illustrative guide and the DfAM strategies are intended to assist rail engineers with decision-making at the design stage to meet the functional needs of the part while ensuring manufacturability is repeatable and consistent using the FDM process. Moreover, the proposed design guide and advanced design strategies can be extended to other FDM printers, materials, and print process parameters.

In consolidating the work presented in this study, several areas of further research were exposed and are summarised as follows:

- Further research in applying different FDM materials, printers and process parameters to the design guide.
- Expand on other potential advanced design techniques for the FDM process.

# **Appendix F: Application Tool**

## **14.4 Introduction**

Additive manufacturing within South African industries has been mainly driven by the medical, automotive and aerospace industries due to research focus and identified high-value parts. Within the South African railway industry, the additive manufacturing technology and research focus are limited due to traditional manufacturing requirements, railway standards and research focus. Several case studies have highlighted the potential benefit of utilising the Fused Deposition Modelling AM technology to produce functional end-use, prototypes and custom tooling for railway-related applications [10]. To further capitalise on the technology for the benefit of producing functional end-use railway-related parts, a structured technical approach detailing the process to guide practising rail design engineers is required. Toth et al. [3] investigated and proposed the procedures for a digital maintenance centre for utilising AM and 3D printing using the FDM process within the South African railway industry. To further advance the centre of excellence, a custom-developed application tool containing recommendations, methodologies, and techniques to succeed in designing and producing functional end-use 3D printable parts related to the railway environment using the FDM process is detailed in this chapter. The application tool is summarised into the generic design process for ease of use and contains 1) the conceptual design stage, 2) the embodiment design stage, and 3) the detailed design stage. Within the conceptual design, the proposed methodologies to evaluate potential railway part selection and conceptual design selections are proposed. Within the embodiment design stage, recommendations to select the appropriate design and manufacturing details for the digital manufacturing workflow, the physical manufacturing workflow, the technique to apply a custom infill placement for optimal internal material allocation and advanced design techniques to improve printing time, support material and hardware embedments are proposed. Lastly, within the detailed design stage, a case study for the identification, selection, redesigning, optimising and manufacturing of a functional 3D printable end-use roof scoop and air vent for the railway inspection trolley is presented. It summarizes the use of the conceptual design and embodiment design stages. The study in this chapter will present the generic design process for traditionally manufactured products and then presents the custom-developed application tool based on the design stages.

## **14.5 Generic Design Process**

Chapter 2 of this dissertation details the general guideline for designing AM parts based on reviewed literature. Several other researchers have proposed and considered multiple methodologies, techniques and design rules that can be adopted into a design framework to produce functional end-use 3D printable parts. Pradel et al. [114] proposed a conceptual framework which organised the growing literature on



DfAM principles. The proposed framework is based on the generic design process model, including 1) conceptual design, 2) embodiment design, 3) detailed design, 4) process planning and 5) process selection. Based on this work, the proposed application tool and the different methodologies, techniques and recommendations will be mapped onto the three stages outlined in the generic design process. This is due to the process planning being merged within the digital and physical manufacturing workflows and the process selection being specific to the Fused Deposition modelling method. Therefore, the research detailed in this dissertation will be categorised into the three generic design stages 1) the conceptual design, 2) the embodiment design, and 3) the detailed design. Figure F - 1 illustrates a fishbone diagram for structuring the application tool in line with the generic design process.

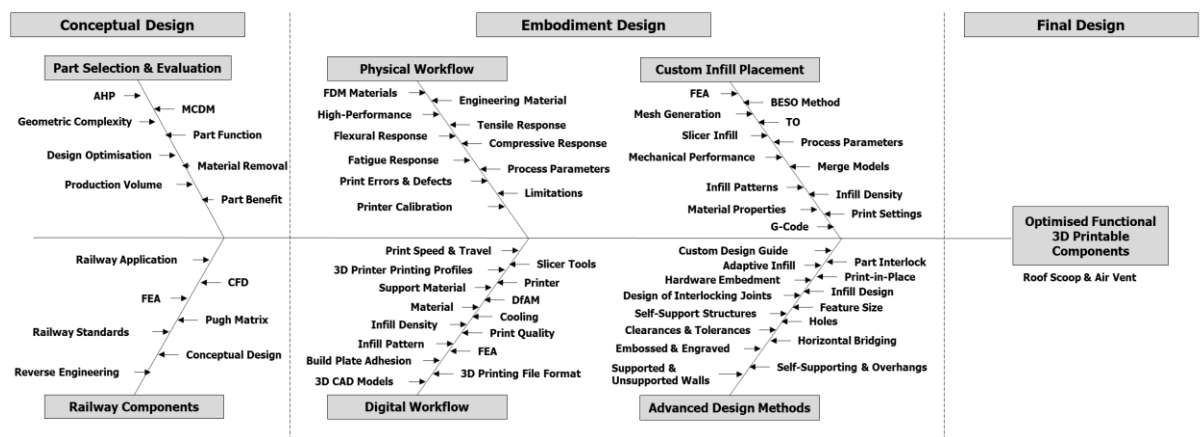


**Figure F - 1 Fishbone Diagram of the Application Tools Structured to the Generic Design Process**

The application is hardcoded using Visual Basic for Application in Microsoft Excel and will mimic the categorised design stages. Each stage is categorised to correspond to a specific generic design process with additional program features contained within the program. The program is hardcoded to ensure easy navigation, recommendations and calculations performed within the application. A total of 38 user forms are built within the application. Figure F - 2 illustrates the main interface program menu.

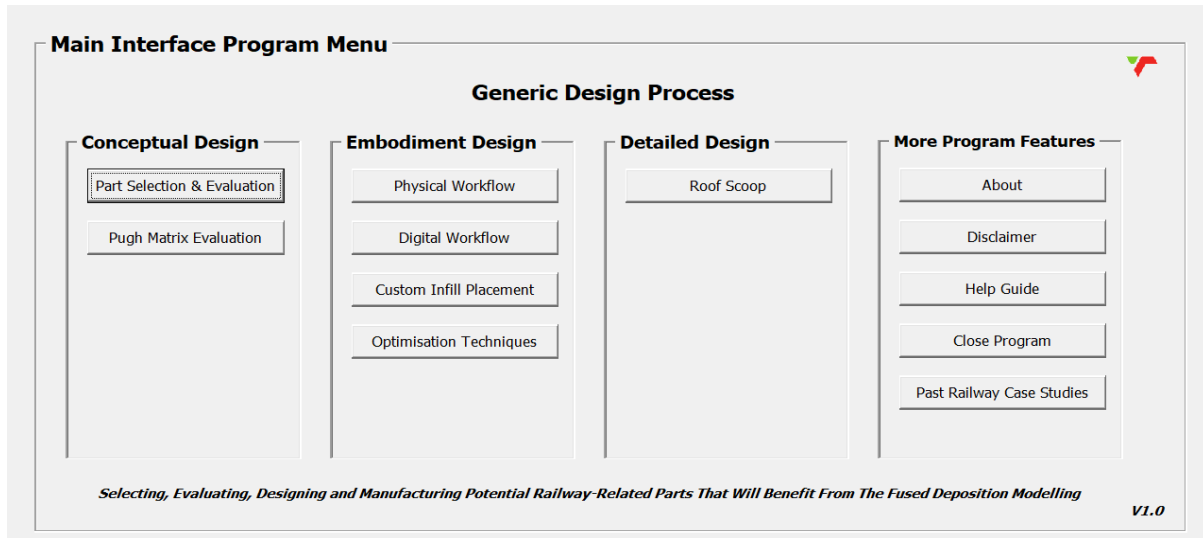


**Figure F - 2 The Main Interface Program Menu for the Application Tool**

### 14.5.1 Conceptual Design

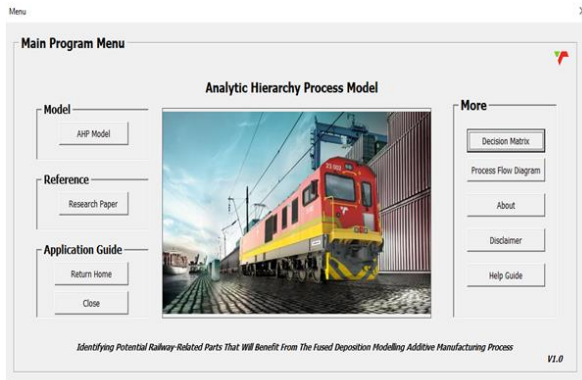
At the conceptual design stage, the program presents an automated calculator to perform the multi-criteria decision-making methodology based on the Analytic Hierarchy Process to identify potential railway-related part candidates illustrated in Figure F - 3 - A and an automated calculator to perform the conceptual design evaluations based on the Pugh Matrix method illustrated in Figure F - 3 - B.

### 14.5.2 Embodiment Design

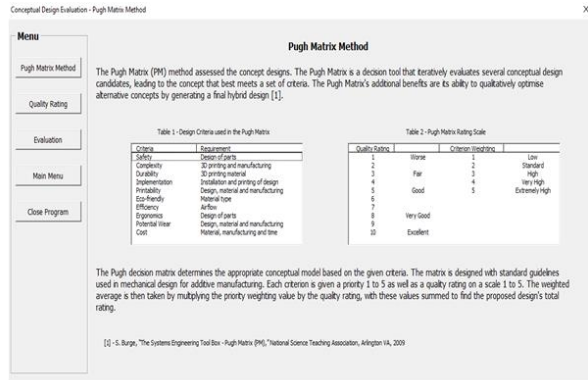
At the embodiment design stage, the digital and physical manufacturing workflow are presented, recommended printing parameters, advanced design techniques for the Fused Deposition Modelling Process and design steps to perform custom infill design placements.

### 14.5.3 Detailed Design

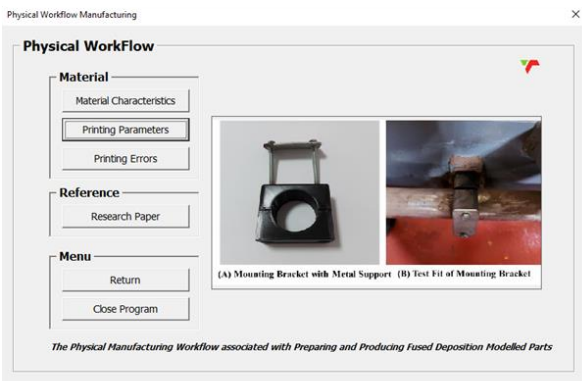
The conceptual and embodiment design stages are summarised at the detailed design stage with a case study on applying them to create a functional railway-related part using the Fused Deposition Modelling Process. The detailed design stage presents the methods of selecting and identifying a potential railway replacement part, evaluating proposed conceptual designs, applying physical and digital manufacturing workflows to ensure the part is 3D printable and suitable for its application, application of the infill allocation to specific regions within the part presents a proposed design cycle and lastly, providing quality control on the final 3D printed part



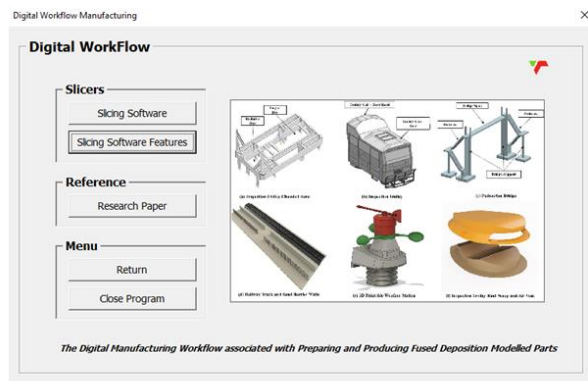
(A) Analytic Hierarchy Model



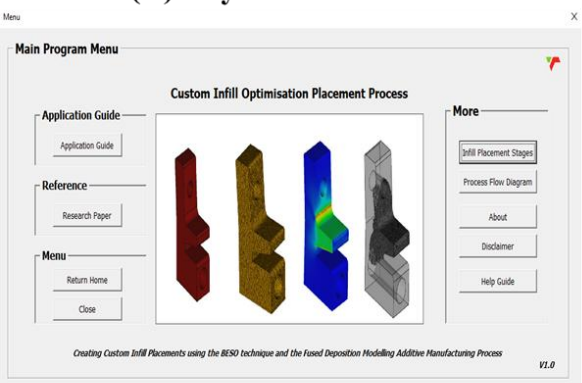
(B) Pugh Matrix Model



(C) Physical Workflow



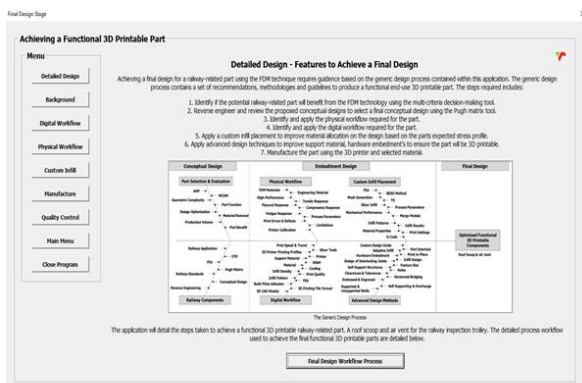
(D) Digital Workflow



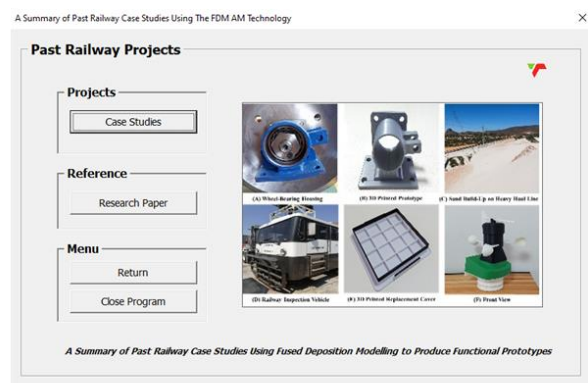
(E) Custom Infill Placement



(F) Design Optimisation Techniques



(G) Detailed Design



(H) Past Railway Projects

Figure F - 3 Conceptual Design Interface Windows (A-B), Embodiment Design Interface Windows (C-F), Detailed Design Interface Window (G) and Past Railway Projects Interface (H)

*Intentionally Left Blank*